Chromosome Nanoscience and Technology

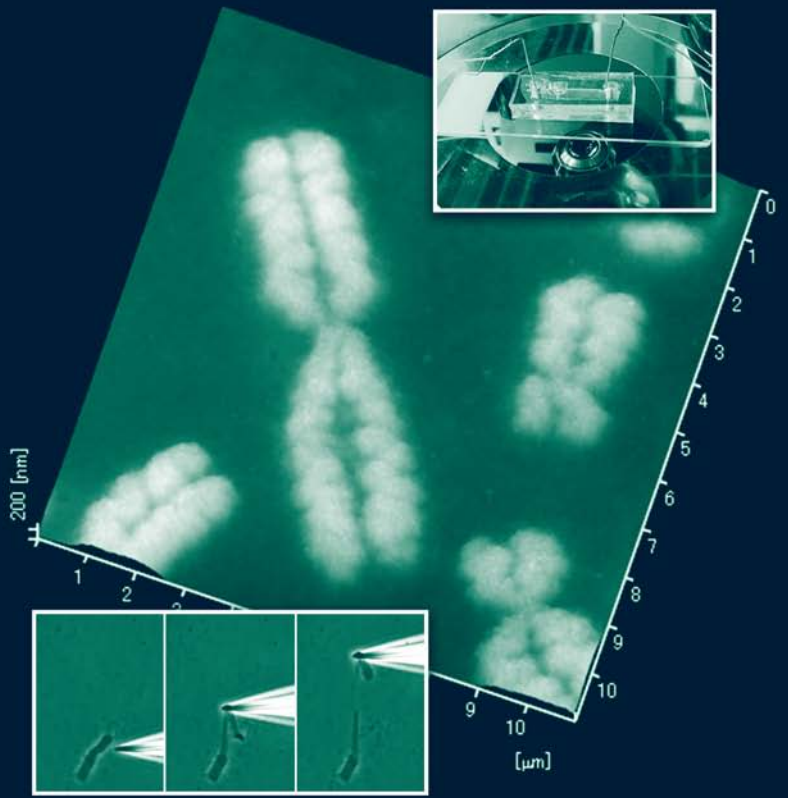

Edited by

Kiichi Fukui
Tatsuo Ushiki

CRC Press
Taylor & Francis Group

Chromosome Nanoscience and Technology

Chromosome Nanoscience and Technology

Edited by
Kiichi Fukui
Tatsuo Ushiki

CRC Press
Taylor & Francis Group
Boca Raton London New York

CRC Press is an imprint of the
Taylor & Francis Group, an informa business

CRC Press
Taylor & Francis Group
6000 Broken Sound Parkway NW, Suite 300
Boca Raton, FL 33487-2742

Printed in the United States of America on acid-free paper
10 9 8 7 6 5 4 3 2 1

International Standard Book Number-13: 978-1-4200-4491-1 (Hardcover)

Library of Congress Cataloging-in-Publication Data

Chromosome nanoscience and technology / editors, Kiichi Fukui and Tatsuo Ushiki.
p. ; cm.
"CRC title."
Includes bibliographical references and index.
ISBN 978-1-4200-4491-1 (alk. paper)
1. Chromosomes. 2. Nanotechnology. I. Fukui, Kiichi. II. Ushiki, Tatsuo, 1957- III. Title.
[DNLM: 1. Chromosomes. 2. Nanotechnology--methods. QU 470 C5565 2008]

QH600.C4943 2008
572.8'7--dc22 2007026618

Visit the Taylor & Francis Web site at
http://www.taylorandfrancis.com

and the CRC Press Web site at
http://www.crcpress.com

Contents

Preface ix
Acknowledgments xi
Editors xiii
Contributors xv

Part I Devices for Chromosome Handling

Chapter 1 Mechanical Approaches to Elucidate Mechanisms of Chromosome Condensation at the Nano- and Microlevels 1

Kazushige Kawabata, Keisuke Nomura, Kensuke Ikeda, Osamu Hoshi, Daisuke Fukushi, Hisashi Haga and Tatsuo Ushiki

Chapter 2 Development of Novel AFM Probes for Chromosome Manipulation 15

Masato Saito, Gen Hashiguchi and Eiichi Tamiya

Chapter 3 Microchamber Array-Based Sequence-Specific DNA Detection from a Single Chromosome via Trace Volume PCR 31

Masato Saito and Eiichi Tamiya

Chapter 4 On-Chip Chromosome Sorter Using Electric and Magnetic Fields 43

Takahito Inoue, Yasuyuki Fujita, Susumu Uchiyama, Tomoyuki Doi, Kiichi Fukui and Hiroshi Yokoyama

Part II Visualization of Chromosomes at the Nano- and Microlevels

Chapter 5 Fluorescence Microscopy for Analysis of Chromosome Dynamics 53

Sachihiro Matsunaga

Chapter 6 Fluorescence *In Situ* Hybridization (FISH) as a Tool for Comparative Genomics: Application of FISH to Studies of Chromosome Evolution in Vertebrates 63

Yoichi Matsuda, Mami Shibusawa, Kazumi Matsubara and Chizuko Nishida-Umehara

Chapter 7 Immunocytochemistry for Analyzing Chromosomes..... 81

Osamu Hoshi, Toru Hirota, Eiji Kimura, Nae Komatsubara and Tatsuo Ushiki

Chapter 8 Transmission and Scanning Electron Microscopy of Mammalian Metaphase Chromosomes..... 93

Sumire Inaga, Keiichi Tanaka and Tatsuo Ushiki

Chapter 9 Atomic Force Microscopy of Human Chromosomes in Relation to Their Higher-Order Structure..... 105

Osamu Hoshi, Daisuke Fukushi and Tatsuo Ushiki

Chapter 10 Mechanism of Higher-Order Chromatin Folding Revealed by AFM Observation of *In Vitro* Reconstituted Chromatin 119

Kohji Hizume, Toshiro Kobori, Shige H. Yoshimura and Kunio Takeyasu

Chapter 11 Scanning Near-Field Optical/Atomic Force Microscopy as a Tool for Simultaneous Specification of Chromosome Topography and Particular Gene Location on the Nanometer Scale 137

Motoharu Shichiri, Tomoyuki Yoshino, Daisuke Fukushi, Shoji Hagiwara, Kohei Akazawa, Toshio Ohtani and Shigeru Sugiyama

Part III Chromosomes as Nanomaterials

Chapter 12 Isolation of Human and Plant Chromosomes as Nanomaterials 155

Susumu Uchiyama, Tomoyuki Doi and Kiichi Fukui

Chapter 13 Proteome Analysis of Human Metaphase Chromosomes..... 167

Kiichi Fukui and Susumu Uchiyama

Chapter 14 Antipeptide Antibodies for Examining the Conformation and Molecular Assembly of an Intracellular Protein 189

Masatoshi Nakagawa, Nobuko Ohmido, Katsumi Ishikawa, Susumu Uchiyama, Kiichi Fukui and Takachika Azuma

Chapter 15 Structure and Interactions of the Imitation SWI-Type Chromatin-Remodeling Complex, ATP-Dependent Chromatin-Assembly Factor 203

Tadayasu Ohkubo, Mariana Petkova-Andonova, Yukiko Kojima, Shota Nakamura, Hiroko Fujita, Yoshinori Nishi, Hiroaki Nakano, Susumu Uchiyama, Kiichi Fukui and Yuji Kobayashi

Chapter 16 Dynamic and Functional Analysis of Chromosomal Proteins.....217

Nobuko Ohmido, Susumu Uchiyama, Sachihiro Matsunaga, Masatoshi Nakagawa, Takachika Azuma and Kiichi Fukui

Part IV Informatics of Chromosome Imaging

Chapter 17 Development of a Sustainable Chromosome Imaging Database 231

Kenji Taniguchi, Chiharu Mitsueda, Naho Okumura and Wakako Miyazaki

Chapter 18 Image Database and Image Analysis of Chromosome Information..... 245

Shin-ichi Toyabe, Takayuki Matsuto, Tatsuo Ushiki and Kohei Akazawa

Index 259

Preface

The chromosome was discovered in the 19th century and even now its structure has not been elucidated, making it one of the main research target materials in the next era of the life sciences. The chromosome has a complex and still largely undefined structure that appears during cell division and that consists of two DNA molecules, histone proteins and nonhistone proteins. Techniques in molecular biology have yielded detailed information on the structure and function of the chromosome; e.g., *in situ* hybridization of fluorescently labeled DNA probes to the complementary DNA in chromosomes enabled the visualization of genes in specific regions of chromosomes. The sequence information of chromosomes of humans and some plants and animals has now been decoded, and has been utilized in numerous biological fields from basic biology to medicine.

Novel analyses beyond the DNA level are, however, now awaited for the further advancement of chromosome science and technology. Recent advances in nanoscience and nanotechnology are casting new light in every biological field. Thus, we developed a national project on nanobiology in the field of chromosome science in the year 2000, supported by the Japanese government as acknowledged at the end of each chapter. Six years cover the academic trend—from when the term "nanobiology" sounded a little bit strange, until the term became fashionable. Without the generous government support for opening of this new biological field, our goals could never have been attained, because the project itself is very multi-disciplinary and the members are a collection of researchers from the disparate backgrounds of molecular biology, biochemistry, protein science, immunology, genetics, cytogenetics, microbiology, anatomy, pharmaceutical science, semiconductor production, polymer chemistry, electronic chemistry, material science, microscopy, biometry, bioinformatics, medical informatics and others.

This book reviews the newest trends in this biological field to which nanoscience and nanotechnology have been very successfully applied and have played various important roles. This book is also the report of our 6-year Japanese national project. The book consists of four main parts with 18 chapters: (1) devices for chromosome handling, (2) visualization of chromosomes at nano- and microlevels, (3) chromosomes as nanomaterials and (4) informatics of chromosome images. In Part I, construction and successful application of various nano- and microdevices, such as a device for microdissection of chromosomes, a microchip for on-chip chromosome sorting and a micromanipulator for measurement of the dynamic properties of chromosomes are introduced and reviewed, based on the results of successful application of these techniques. In Part II, the most advanced methods for allowing simultaneous observation of topological and fluorescent images after FISH at the nanolevel, and for revealing nanolevel folding of chromatin fibers by atomic force microscopy even in a solution, for example,

are reviewed. In Part III, results from proteome analysis of chromosome constituent proteins are described, after successful development of chromosome accumulation and collection methods. Over 200 chromosomal proteins identified and catalogued are presented, in order of the existing quantities of each protein. A new chromosome protein framework is presented based on the results of this localization. Three-dimensional structural analyses of chromosomal proteins and a new antibody production method for chromosomal proteins are also described. In Part IV, chromosome image database systems, both for animal and plant chromosomes, are presented.

We hope that this book will be beneficial to academic staff, researchers, and graduate students needing an introduction to the most advanced nano- and microtechnologies which have enormous potential in the future of the life sciences, especially in chromosome- and genome-related research. Our wish is to help open new doors leading to the nano-era not only for chromosome and genome research, but also for all the life sciences, both in basic and applied facets.

Kiichi Fukui and Tatsuo Ushiki
Osaka and Niigata, Japan

Acknowledgments

We are deeply grateful for the support of the Ministry of Education, Culture, Sports, Science and Technology (MEXT), Japan, which made publication of this book possible. Many interesting results described in this book were obtained by the members of the Research Project on Nano-Devices for Structural and Functional Analyses of Chromosomes, Special Coordination Funds granted by MEXT, Japan. Special thanks to Professors Kazushige Hirosawa (Emeritus professor of the University of Tokyo) and Toshio Yanagida (professor of Osaka University) who, as the heads of the administration committee, guided our project with warm hearts and pioneering scientific minds, taking substantial time from their busy lives.

The contributors to this book reported the essential results that they obtained in this project, making it possible to share throughout the world the most advanced and important results in nanoscience and nanotechnology applied to chromosome science. Contributions by Sachihiko Matsunaga and Sumire Inaga gave this book a more comprehensive overview of this new field.

Finally, we again acknowledge the support from MEXT and the Japan Science and Technology Board, not only for their funding but also for their generosity in allowing us to perform very basic studies for opening up and developing this new field.

K.F. and T.U.

Editors

Kiichi Fukui was born in Kyoto, Japan in 1951. He received a B.S. degree in applied genetics at Kyoto University in 1973 and then M.S. (1978) and Ph.D. (1985) degrees also from Kyoto University in mutation research of higher plants. He extended his research to chromosome engineering at the National Institute of Agricultural Sciences. He then focused on introducing computer imaging methods for identifying individual chromosomes. During his stay in Cambridge (Prof. Collin N. Law, Plant Breeding Institute) in 1985–1986 as a visiting scholar, he also utilized molecular cytology to map and visualize specific genes on specific chromosomes. After he was appointed as a full professor of the Department of Biotechnology, Graduate School of Engineering, Osaka University, Japan, he started analyses of human chromosome proteins and chromosome dynamics in order to reveal chromosome structure and function. Most of his research is directed toward the analysis of higher-order chromosomal structure. He was a project leader of the Research Project on Nano-Devices for Structural and Functional Analyses of Chromosomes, Special Coordination Funds granted by MEXT, Japan, during 2004–2006.

Academic Appointments:

1978–1985 Researcher (Chromosome engineering), National Institute of Agricultural Sciences

1985–1990 Senior researcher (Chromosome imaging), National Institute of Agrobiological Resources

1990–1997 Head of laboratory (Molecular cytology), Hokuriku National Agricultural Experiment Station

1997–Professor (Department of Biotechnology), Graduate School of Engineering, Osaka University, Japan

2005–Dean, Department of Biotechnology

Professional Societies:

Board member of Genetics Society of Japan (Editorial board member, *Genes and Genetic Systems* 2004–)

Board member of Japanese Society for Chromosome Research

Board member of Japanese Society of Biotechnology (Editorial board member, *Journal of Bioscience and Bioengineering* 2002–2006)

Tatsuo Ushiki was born in Niigata, Japan in 1957. He graduated from Niigata University School of Medicine in 1982, and obtained a Ph.D. degree in microscopic anatomy from Niigata University in 1986. Since then, he has engaged in studies on the ultrastructure of mammalian cells, tissues and organs using various microscopic techniques including scanning electron microscopy. In 1990, he was appointed an associate professor of microscopic anatomy, Hokkaido University School of Medicine, when he also extended his research to the application of scanning probe microscopy. In particular, he studied the imaging of various biological samples from DNA to living cells by atomic force microscopy. After he was appointed a full professor of the Department of Microscopic Anatomy, Niigata University School of Medicine, Japan, he focused on studies of the higher-order structure of human metaphase chromosomes using atomic force microscopy; the development of three-dimensional imaging of various biological structures by microscopy has also been one of his interests. He was a project leader of the Research Project on Nano-Devices for Structural and Functional Analyses of Chromosomes, Special Coordination Funds granted by MEXT, Japan, during 2000–2003.

Academic Appointments:

1986–1988 Research assistant (Anatomy), Iwate Medical University, Japan
1988–1989 Lecturer (Anatomy), Iwate Medical University, Japan
1990–1995 Associate professor (Anatomy), Hokkaido University School of Medicine
1995–Professor (Department of Microscopic Anatomy), Niigata University School of Medicine, Japan
2000–Professor (Division of Microscopic Anatomy), Graduate School of Medical and Dental Sciences, Niigata University, Japan

Professional Societies:

Board member of Japanese Association of Anatomists (Editorial board member, *Anatomical Science International*)
Board member of Japan Society of Microscopy (Advisory board member, *Journal of Electron Microscopy*)
Vice-president of International Society of Histology and Cytology (Editor, *Archives of Histology and Cytology* 2000–)
Delegate of International Committee of Symposia on Morphological Sciences (2004–)

Contributors

Kohei Akazawa
Department of Medical Informatics
Niigata University Medical and Dental Hospital
Niigata, Japan

Takachika Azuma
Division of Biosignaling
Research Institute for Biological Sciences
Tokyo University of Science
Noda, Chiba, Japan

Tomoyuki Doi
Department of Biotechnology
Graduate School of Engineering
Osaka University
Suita, Osaka, Japan

Hiroko Fujita
Department of Polymer Chemistry
Graduate School of Pharmaceutical Science
Osaka University
Suita, Osaka, Japan

Yasuyuki Fujita
Nanotechnology Research Institute
National Institute of Advanced Industrial Science and Technology
Tsukuba, Ibaraki, Japan

Kiichi Fukui
Department of Biotechnology
Graduate School of Engineering
Osaka University
Suita, Osaka, Japan

Daisuke Fukushi
Department of Genetics
Institute for Developmental Research
Aichi Human Service Center
Kasugai, Aichi, Japan

Hisashi Haga
Department of Biological Sciences
Faculty of Science
Hokkaido University
Sapporo, Japan

Shoji Hagiwara
Food Engineering Division
National Food Research Institute
Tsukuba, Ibaraki, Japan

Gen Hashiguchi
Faculty of Engineering
Kagawa University
Takamatsu, Kagawa, Japan

Toru Hirota
Department of Experimental Pathology
Cancer Institute of JFCR
Tokyo, Japan

Kohji Hizume
Laboratory of Plasma Membrane and Nuclear Signaling
Graduate School of Biostudies
Kyoto University
Kyoto, Japan

Osamu Hoshi
Division of Microscopic Anatomy
Graduate School of Medical and Dental Sciences
Niigata University
Niigata, Japan

Kensuke Ikeda
Department of Biological Sciences
Faculty of Science
Hokkaido University
Sapporo, Japan

Sumire Inaga
Division of Genome Morphology
Faculty of Medicine
Tottori University
Yonago, Tottori, Japan

Takahito Inoue
Nanotechnology Research Institute
National Institute of Advanced Industrial Science and Technology
Tsukuba, Ibaraki, Japan

Katsumi Ishikawa
Division of Biosignaling
Research Institute for Biological Sciences
Tokyo University of Science
Noda, Chiba, Japan

Kazushige Kawabata
Department of Biological Sciences
Faculty of Science
Hokkaido University
Sapporo, Japan

Eiji Kimura
Department of Anatomy
School of Medicine
Iwate Medical University
Morioka, Iwate, Japan

Yuji Kobayashi
Department of Biotechnology
Graduate School of Engineering
Osaka University
Suita, Osaka, Japan

Toshiro Kobori
Laboratory of Plasma Membrane and Nuclear Signaling
Graduate School of Biostudies
Kyoto University
Kyoto, Japan

Yukiko Kojima
Department of Polymer Chemistry
Graduate School of Pharmaceutical Science
Osaka University
Suita, Osaka, Japan

Nae Komatsubara
Division of Microscopic Anatomy
Graduate School of Medical and Dental Sciences
Niigata University
Niigata, Japan

Kazumi Matsubara
Laboratory of Animal Cytogenetics
Division of Genome Dynamics
Creative Research Initiative "Sousei"
Hokkaido University
Sapporo, Japan

Yoichi Matsuda
Laboratory of Animal Cytogenetics
Division of Genome Dynamics
Creative Research Initiative "Sousei"
Hokkaido University
Sapporo, Japan

Sachihiro Matsunaga
Department of Biotechnology
Graduate School of Engineering
Osaka University
Suita, Osaka, Japan

Takayuki Matsuto
Division of Clinical Preventive Medicine
Graduate School of Medical and Dental Sciences
Niigata University
Niigata, Japan

Chiharu Mitsueda
Laboratory of Plant Chromosome and Gene Stock
Graduate School of Science
Hiroshima University
Higashi-hiroshima, Hiroshima, Japan

Wakako Miyazaki
Laboratory of Plant Chromosome and Gene Stock
Graduate School of Science
Hiroshima University
Higashi-hiroshima, Hiroshima, Japan

Masatoshi Nakagawa
Division of Biosignaling
Research Institute for Biological Sciences
Tokyo University of Science
Noda, Chiba, Japan

Shota Nakamura
Department of Polymer Chemistry
Graduate School of Pharmaceutical Science
Osaka University
Suita, Osaka, Japan

Hiroaki Nakano
Department of Biotechnology
Graduate School of Engineering
Osaka University
Suita, Osaka, Japan

Yoshinori Nishi
Department of Polymer Chemistry
Graduate School of Pharmaceutical Science
Osaka University
Suita, Osaka, Japan

Chizuko Nishida-Umehara
Laboratory of Animal Cytogenetics
Division of Genome Dynamics
Creative Research Initiative "Sousei"
Hokkaido University
Sapporo, Japan

Keisuke Nomura
Department of Biological Sciences
Faculty of Science
Hokkaido University
Sapporo, Japan

Tadayasu Ohkubo
Department of Polymer Chemistry
Graduate School of Pharmaceutical Science
Osaka University
Suita, Osaka, Japan

Nobuko Ohmido
Faculty of Human Development
Kobe University
Kobe, Japan

Toshio Ohtani
Food Engineering Division
National Food Research Institute
Tsukuba, Ibaraki, Japan

Naho Okumura
Laboratory of Plant Chromosome and Gene Stock
Graduate School of Science
Hiroshima University
Higashi-hiroshima, Hiroshima, Japan

Mariana Petkova-Andonova
Department of Polymer Chemistry
Graduate School of Pharmaceutical Science
Osaka University
Suita, Osaka, Japan

Masato Saito
Department of Applied Physics
Graduate School of Engineering
Osaka University
Suita, Osaka, Japan

Mami Shibusawa
Laboratory of Animal Cytogenetics
Division of Genome Dynamics
Creative Research Initiative "Sousei"
Hokkaido University
Sapporo, Japan

Motoharu Shichiri
Nano-Architecture Group
National Institute for Materials Science
Tsukuba, Ibaraki, Japan

Shigeru Sugiyama
Food Engineering Division
National Food Research Institute
Tsukuba, Ibaraki, Japan

Kunio Takeyasu
Laboratory of Plasma Membrane and
Nuclear Signaling
Graduate School of Biostudies
Kyoto University
Kyoto, Japan

Eiichi Tamiya
Department of Applied Physics
Graduate School of Engineering
Osaka University
Suita, Osaka, Japan

Keiichi Tanaka
Tanaka SEM Institute
Yonago, Tottori, Japan

Kenji Taniguchi
Laboratory of Plant Chromosome and
Gene Stock
Graduate School of Science
Hiroshima University
Higashi-hiroshima, Hiroshima, Japan

Shin-ichi Toyabe
Department of Medical Informatics
Niigata University Medical and
Dental Hospital
Niigata, Japan

Susumu Uchiyama
Department of Biotechnology
Graduate School of Engineering
Osaka University
Suita, Osaka, Japan

Tatsuo Ushiki
Division of Microscopic Anatomy
Graduate School of Medical and
Dental Sciences
Niigata University
Niigata, Japan

Hiroshi Yokoyama
Nanotechnology Research Institute
National Institute of Advanced
Industrial Science and Technology
Tsukuba, Ibaraki, Japan

Shige H. Yoshimura
Laboratory of Plasma Membrane and
Nuclear Signaling
Graduate School of Biostudies
Kyoto University
Kyoto, Japan

Tomoyuki Yoshino
Department of Life Sciences
Faculty of Life and Environmental
Sciences
Prefectural University of Hiroshima
Shobara, Hiroshima, Japan

1 Mechanical Approaches to Elucidate Mechanisms of Chromosome Condensation at the Nano- and Microlevels

Kazushige Kawabata[*]*, Keisuke Nomura, Kensuke Ikeda, Osamu Hoshi, Daisuke Fukushi, Hisashi Haga and Tatsuo Ushiki*

CONTENTS

1.1 Introduction 1
1.2 Experimental Design 3
1.2.1 Chromosome Preparation 3
1.2.2 Scanning Probe Microscopy 4
1.2.3 Mechanical Stretching of Chromosomes 5
1.3 Evaluation of Chromosome Elasticity by SPM 7
1.4 Topography and Elasticity Mapping of Human Chromosomes 8
1.5 Mechanical Elongation of Chromosomes 9
1.6 Conclusion 9
Acknowledgments 11
References 11

1.1 INTRODUCTION

Human DNA disperses in the nucleus at the interphase of the cell cycle, and this is essential for transcription. In contrast, the DNA condenses compactly into chromosomes at the M phase, for cell division without entanglement of DNA. Such drastic morphological transformation occurs as a result of the cell cycle.

*To whom correspondence should be addressed.

DNA condensation is due to its hierarchal architecture in that it is wound around histone octamers to form nucleosome cores (see Chapter 10); this appears as a "beads-on-string" structure. These cores are packed regularly and form a chromatin fiber with a 20- to 30-nm diameter [1–4]. The chromatin fiber undergoes further tight condensation to form a chromosome with a 700-nm diameter. Approximately 300 well-stained distinguishable bands, called G-bands, appear on human chromosomes after they are pretreated with trypsin and stained with Giemsa solution. Since this G-band pattern depends on the biological species, the chromosomes inherently have a robust and site-specific higher-order structure on a macroscopic scale. It is very important to study the mechanism of chromatin condensation to understand cell division and genetic diseases that occur due to chromosomal aberrations, such as the deletion of an arm.

Giemsa-dark DNA was reported to be richer than the light R-bands in the base pairs of adenine (A) and thymine (T) [5–8]. This result implies that the site-specific mechanism of chromosomal condensation may be related to nonhomogeneity at the base pair sequence level of DNA. However, the segregation of base pair sequences is too small to directly generate the macroscopic higher-ordered structure [9]. When histone proteins are removed from chromosomes by treatment with dextran sulfate and heparin, the nonhistone proteins remain in the skeleton of the single chromosome. Many loops of DNA are anchored to this scaffold protein. Hence, the nonhistone scaffold protein is considered to be responsible for the morphology of the chromosomes. Since topoisomerase II is distributed along the axis of the chromatid, it is considered that these nonhistone scaffold proteins may be topoisomerase II [10] (see also Chapter 16). Furthermore, from experiments on the stretching of chromosomes from the newt (*Notophthalmus viridescens*) using a micromanipulator, it was observed that digestion with micrococcal nuclease or restriction enzymes reduced the elastic contraction force of the stretched chromosomes. Hence, the morphology of the chromosomes is attributed not only to nonhistone scaffold proteins but also to short DNA chains that have several thousands of base pairs [11]. Since the band width or domain size in a chromosome corresponds to 100,000,000 base pairs of DNA, the chromosomes must have not only this site-specific band structure but also site-specific structures that are of a lower order than the band structure. The chromosomes can be observed by scanning electron microscopy (SEM) [12] (see also Chapter 8) and scanning probe microscopy (SPM) [13] (see also Chapter 9). SPM and SEM images of chromosomal surface morphology reveal a globular structure, and studies indicated that the globular structure has a diameter of 50 to 60 nm. These results suggest that the chromosomes have structures that are of a higher order than chromatin fibers, and of a lower order than the band structure. However, the nature of these structures and how these higher-ordered structures are condensed from a chromatin fiber remains to be elucidated. Recently, since the viscoelastic properties of the chromosome are considered to directly reflect its condensation properties such as the densities of chromatin fibers or cross-link points between chromatin fibers, Newt chromosomes were examined for these properties by suspension with two micropipettes in cell culture medium [14]. Consequently, it was

shown that the single mitotic chromosome showed force relaxation. This result, however, includes no spatial information on the condensation of a single chromosome since the whole chromosome is stretched in this experiment.

SPM enables the high-resolution visualization of the morphology of living samples in liquid environments. It can also measure the adhesive force, frictional force, and electrostatic properties of biomaterials, including lipid membranes, proteins, and other biopolymers. We have developed SPM to visualize the spatial distribution of the local elasticity of samples in liquid environments and we refer to this as mechanical SPM [15]. We succeeded in visualizing the temporal and spatial variation of the local elasticity of single living cells in culture medium by further development of the force mapping mode [16] and the force modulation mode methods [17]. Mechanical SPM is also expected to be a powerful tool for investigating the viscoelastic properties of single chromosomes.

In order to clarify the condensation of the chromatin into chromosomes, we focused on mapping those mechanical properties of the chromosomes that are closely related to their condensation by using micromanipulation and mechanical SPM. To estimate the local elasticity of the chromosomes by mechanical SPM, we adopted a model proposed by Dimitriadis et al. that takes into account the effect of a finite thickness of the sample on its elasticity estimation [18]. We verified that this model is applicable to the elasticity estimation of a single chromosome and visualized the elasticity distribution of the single chromosome.

1.2 EXPERIMENTAL DESIGN

1.2.1 Chromosome Preparation

We used fixed and unfixed human chromosomes. Human lymphocytes obtained from heparinized peripheral blood donated by healthy volunteers were also used. These lymphocytes were cultivated in PB-max medium (Gibco, U.K.) with 10% fetal calf serum for 72 h at 37°C under 5% CO_2 and 95% air. Colcemid was added to the culture medium at a final concentration of 0.005 μg/ml, and incubated for 1 h. The cell suspension was then exposed to 75 m*M* KCl for 30 min at room temperature and fixed with Carnoy's fixative (methanol/acetic acid, 3:1 v/v). One drop of the fixed cell suspension was spread over a slide glass. The sample was then washed with a few drops of Carnoy's fixative and air dried [19]. For the SPM measurements, the sample on the glass slide was placed in a dish and this was filled with phosphate-buffered saline (PBS) solution. We shortened the period of air-drying to reduce the drying effect.

A human cell line, BALL-1 (RCB0256), was used for the unfixed human chromosomes; this was obtained from the RIKEN Cell Bank (Riken, Tsukuba). BALL-1 cells were grown in a 40-ml flask in RPMI 1640 medium (Invitrogen, Tokyo, Japan) at 37°C under an atmosphere of 5% CO_2 and 95% air. After arrest was induced with 0.06 mg/ml colcemide for 12 h, the cells were suspended and centrifuged at 190 *g* for 10 min at 4°C. The cell pellet was resuspended in 10 ml of the culture medium for 20 min, centrifuged again at 190 *g* for 10 min, and then

exposed to 75 m*M* KCl for 15 min. These cells were collected by centrifugation and isolated by the hexylene glycol method according to Wray and Stubblefield [20]; briefly, the cells were gently resuspended in a hexylene glycol buffer composed of 1.0 *M* hexylene glycol (2-methyl-2,4-pentanediol), 0.5 m*M* $CaCl_2$, and 0.1 m*M* PIPES (pH 6.5), and incubated for 10 min at 37°C. The cells were further broken with a Dounce homogenizer (15 ml capacity) by five gentle strokes [12] and centrifuged at 1680 *g* at 4°C for 15 min in order to concentrate the crude chromosome suspension.

1.2.2 Scanning Probe Microscopy

For the SPM measurements, the sample on the slide glass was transferred into a dish and this was filled with PBS. We shortened the period of the air-drying procedure in order to maintain the cells under live conditions. We used a commercial instrument equipped with a piezo scanner with a maximal xy-scan range of 100 µm in each direction and a z range of 10 µm, and a control unit (SPA400 and SPI4000; Seiko Instruments Inc., Chiba, Japan). A schematic representation of SPM for measuring chromosomes is shown in Figure 1.1(a). It should be noted that the spring constant of the cantilevers is chosen such that it is comparable to those of the samples. This is done to reduce the damage to the sample and ensure maximum sensitivity for elasticity measurements. We used commercially available silicon-nitride cantilevers with a length of 85 µm and width of 20 µm; a pyramidal tip with a typical radius of curvature of approximately 50 nm was placed at one end of the cantilever (Microlever; ThermoMicroscopes, Sunnyvale, CA, U.S.A.). According to the calibration by the thermal fluctuation method, the spring constant of the cantilever was 0.5 N/m.

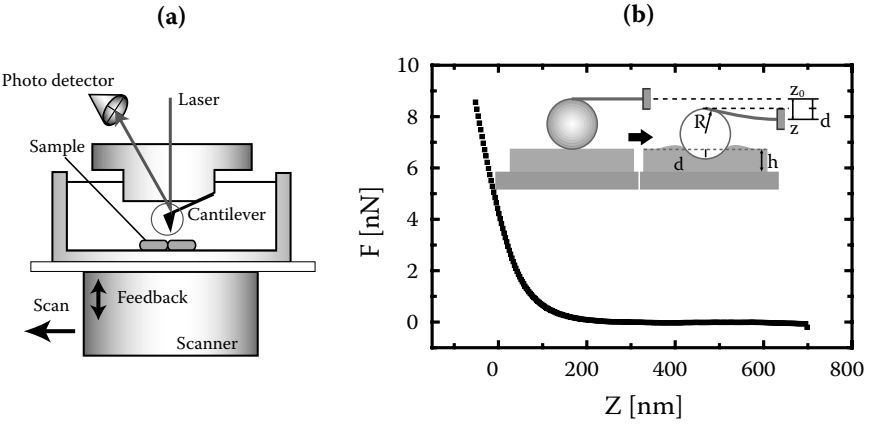

FIGURE 1.1 Mechanical SPM (a). A typical force curve obtained by the force mapping method (b). The inset shows the parameters of Relation (1.1) for the force mapping mode.

The topography and spatial elasticity distribution images of the chromosomes were obtained using the force mapping mode. This mode can simultaneously visualize both the height and elasticity images of the samples by measuring a force-vs.-distance curve (force curve) at each pixel point on the sample. The force mapping mode with SPM is generally used to measure the Young's modulus of soft materials such as cells and gels [21,22]. In this mode, we measured force-vs.-indentation curves (force curves) of a single human chromosome at each pixel point (64 pixels × 64 lines). Figure 1.1(b) shows a typical force curve of a chromosome. The force (F) deflecting the cantilever increases steeply as the cantilever tip indents the sample by piezo-actuator translation (Z). Since the indentation was comparable to the sample thickness, the chromosome was considerably deformed in the present measurements. However, there is no break on the obtained force curves, which means that the measurement was performed within elastic limits. The force curves can be reproduced even when they are measured several times at a point. We estimated the elasticity distribution of a human chromosome by analyzing the force curve with the following method. Under the condition that a single force curve was obtained for 50 ms, each image consisting of 64 × 64 pixels could be obtained in approximately 30 min. In the force mapping mode, a force curve was obtained while a cantilever indented each point on the surface of the sample. By using nonlinear least squares fitting, the force curve obtained at one point on the sample surface was, in general, fitted to Sneddon's model, a theoretical model in which the elastic contact theory of Hertz is applied to the contact between an elastic plane and a rigid cone [23]. This fitting allowed the evaluation of not only the Young's modulus but also the z-position, where the cantilever initially makes contact with the sample (i.e., the height of the sample at that point). However, the chromosome can be as thin as 400 nm in thickness, and consequently we abandoned these models. We instead adopted the model of the contact problem for samples with a finite thickness that has been proposed by Dimitriadis et al. [18]. It should be noted that the spring constant of the cantilevers is chosen such that it is comparable to those of the samples, in order to reduce the damage to the sample and ensure maximum sensitivity for elasticity measurements.

1.2.3 Mechanical Stretching of Chromosomes

Human chromosomes were stretched in the buffer, as shown in Figure 1.2. The chromosome was spread on poly-l-lysine (PLL)-coated glass; PLL has positive electric charges that bind chromosomes. For affirmation, the chromosomes were stained with 1 g/ml 4′,6-diamidino-2-phenylindole and observed by fluorescent microscopy. Micromechanical experiments were performed with an inverted microscope (IX-70, 100×, 1.4 NA; NIKON Instech Co., Kawasaki, Japan) equipped with two micromanipulators (MP-285; Sutter Instruments, Novato, CA, U.S.A.) and a CCD camera (KP-F120; Hitachi). The CCD camera and software

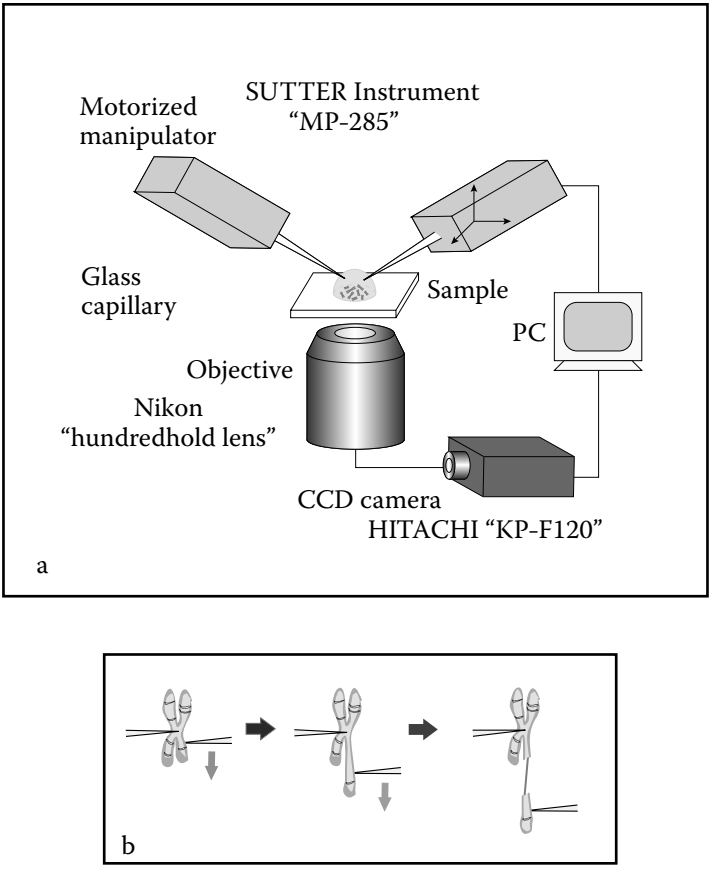

FIGURE 1.2 Setup for the observation of the morphology of the elongating chromosomes in the medium (a). Schematic illustrations of the stretching process of a single chromosome (b).

can acquire phase contrast images at 15 flame/s. This force-measuring micropipette was pulled and cut to have a bending force constant of about 0.1 nN/μm and then mounted directly to the microscope stage to minimize mechanical noise. One glass micropipette holds down this chromosome, while the other hitches, holds up and pulls it in the hexylene glycol buffer. Force-extension experiments were conducted by moving a stiff micropipette at a rate of 0.2 μm/s, while observing the bending of this force-measuring micropipette. After each experiment, the force-measuring micropipette was calibrated by elastic contact with a standard specimen (the cantilever of SPM) that has a known spring constant (0.18 N/m).

1.3 EVALUATION OF CHROMOSOME ELASTICITY BY SPM

When the indentation of the sample by a cantilever tip is set as small as several 10 nm in comparison with the sample thickness, the Hertz contact model is usually adopted for the estimation of elasticity [24]. However, in our case, because the thickness of the chromosomes is comparable to this indentation, this model is no longer applicable. Subsequently, to estimate the local elasticity of the chromosomes, we must take into account the effect of the finite thickness of the sample on its elasticity estimation, which was proposed by Dimitriadis et al. [18]. We first verified that this model is applicable to the estimation of the elasticity of a single chromosome. The indentation depth δ of the sample and F are related as follows:

$$Z - Z_0 = \frac{F}{k} + \delta \tag{1.1}$$

where k is the typical spring constant of the cantilever, and Z_0 is the sample height under zero loading force. The model takes into account the effect of the finite thickness of the sample on the estimation of local elasticity. In this model, the relationship between F and δ is modified as follows:

$$F = \frac{16E}{9} R^{\frac{1}{2}} \delta^{\frac{3}{2}} \left(1 + 1.133 \frac{\sqrt{R\delta}}{h} + 1.283 \frac{R\delta}{h^2} + \cdots \right) \tag{1.2}$$

where E is the elastic modulus of the sample, R is the radius of curvature of the cantilever, and h is the sample thickness. Poisson's ratio is subsumed to the constant in Equation (1.2) by assuming that Poisson's ratio is 0.5. In the present study, we take only the first and second terms in Equation (1.2) to compare the force curve with the model. The obtained force curves are replotted for comparison with the model in Figure 1.3(a). We choose a parameter h to obtain a linear relationship with $\delta^{1.5}$ in a small range of δ, which is expected from the model. The obtained value of h is in agreement with the thickness of the chromosome, which is measured separately by the contact mode of the mechanical SPM. The data deviate from a linear relation when δ becomes comparable to the sample thickness. This means that beyond the correction, the elasticity is affected strongly by the sample thickness, due to the second term of Equation (1.2). Figure 1.3(b) shows the δ-dependence of the elasticity of the sample calculated by Equation (1.1) and (1.2). The elasticity of the sample is independent of δ within the region of $\delta < 60$ nm and increases substantially when $\delta > 100$ nm. When the sample is thinner, the elasticity increases with a smaller value of δ. This result is consistent with the correction of Equation (1.2). The use of this evaluation procedure can successfully eliminate the influence of the sample thickness and is valid for the estimation of the elasticity of thin chromosomes. Therefore, the

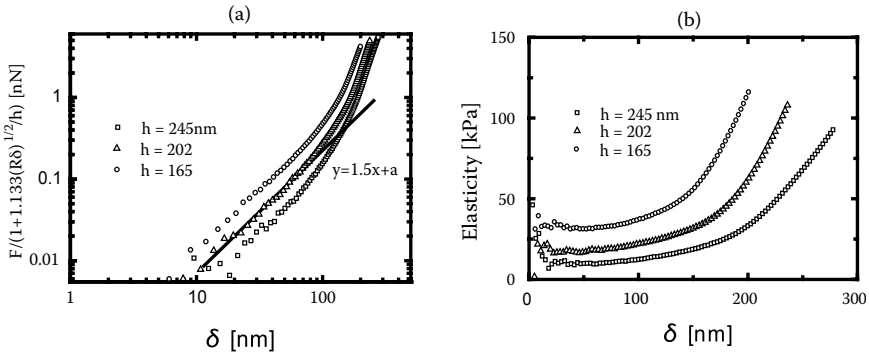

FIGURE 1.3 Comparison of the data set calculated from the force curve with the finite thickness model (a). A straight line is expected from the model (see the text). The δ-dependence of the calculated elasticity (b).

values of elasticity, which are independent of δ, are verified as representing those of the chromosomes.

1.4 TOPOGRAPHY AND ELASTICITY MAPPING OF HUMAN CHROMOSOMES

Figures 1.4(a) and (b) show the topographic and elasticity images of a mitotic human chromosome fixed in PBS solution. In order to obtain the optimal sensitivity, a spring constant of 0.5 N/m is chosen for the cantilever. The height of the chromosome on the substrate is approximately 150 to 360 nm. Morphological observation reveals that the surface is a perceptibly uneven structure with irregularities of approximately 50 to 100 nm. This result agrees qualitatively with a spiral structure of chromosome morphology that was previously reported [13]. The elasticity distribution is not homogeneous over the whole chromosome and some domain-like structure is visible. The values vary considerably from 5 to 50 kPa. This implies that a single chromosome condenses nonhomogeneously. The relationship between the height and the elasticity at each point on a single chromosome is plotted in Figure 1.4(c). The sample is stiffer in the thicker areas; this implies that the chromatin fiber network swells and that the thicker areas correspond to softer areas. We carried out trypsin treatment of the chromosome as shown in Figure 1.5. The chromosomes swelled due to the digestion of cross-linking proteins, and the domain structure became uniform with regard to elasticity. The height increased slightly due to the swelling of the chromosome. The elasticity decreased drastically following treatment with trypsin, indicating that the observed elasticity distribution directly reflects the density of cross-linking points such as scaffold proteins.

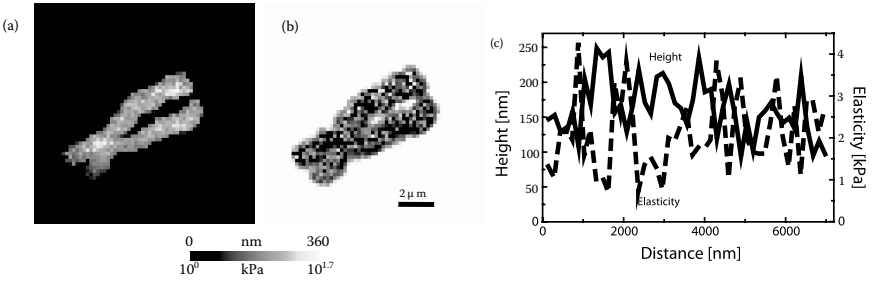

FIGURE 1.4 Topography (a) and elasticity (b) images of a human chromosome visualized by the force mapping method using the model, and taking into account the effect of sample thickness on the estimation of elasticity. Comparison between height and elasticity distribution (c).

A stiffer domain structure is also clearly visible on the different types of human chromosomes. We measured the dependence of domain size on chromosomal type, and found that the domain sizes do not strongly depend on chromosome length. Thus, the domain structure implies that some higher-order structure is common among the different chromosomal types during condensation.

1.5 MECHANICAL ELONGATION OF CHROMOSOMES

Figure 1.6 shows a typical example of the process of mechanical elongation of the unfixed human chromosomes by two glass capillaries moving at constant velocity of 2 μm/s; these are driven by a computer-controlled manipulator. The elongating behavior of the chromosome was recorded through an inverted light microscope by a CCD camera and a computer. The chromosome stretches elastically up to a strain of approximately 2 and then unwinds to form a fiber. The brighter and darker bands are clearly visible on the chromosome in optical phase contrast images. One glass capillary is held at one end of the chromosome and the other is hitched at the other end, and the chromosome is stretched in the hexylene glycol buffer. The stretching experiments revealed that the brighter regions are approximately two or three times softer than the darker regions, and the brighter region abruptly unwinds to form a filament when the strain of the chromosome exceeds approximately 2.

1.6 CONCLUSION

We have presented here two new and powerful methods that have been developed to elucidate the mechanism of condensation of chromatin fibers into single mitotic chromosomes. These are (1) visualization of the spatial distribution of the local elasticity of mitotic chromosomes and (2) observation of the morphology

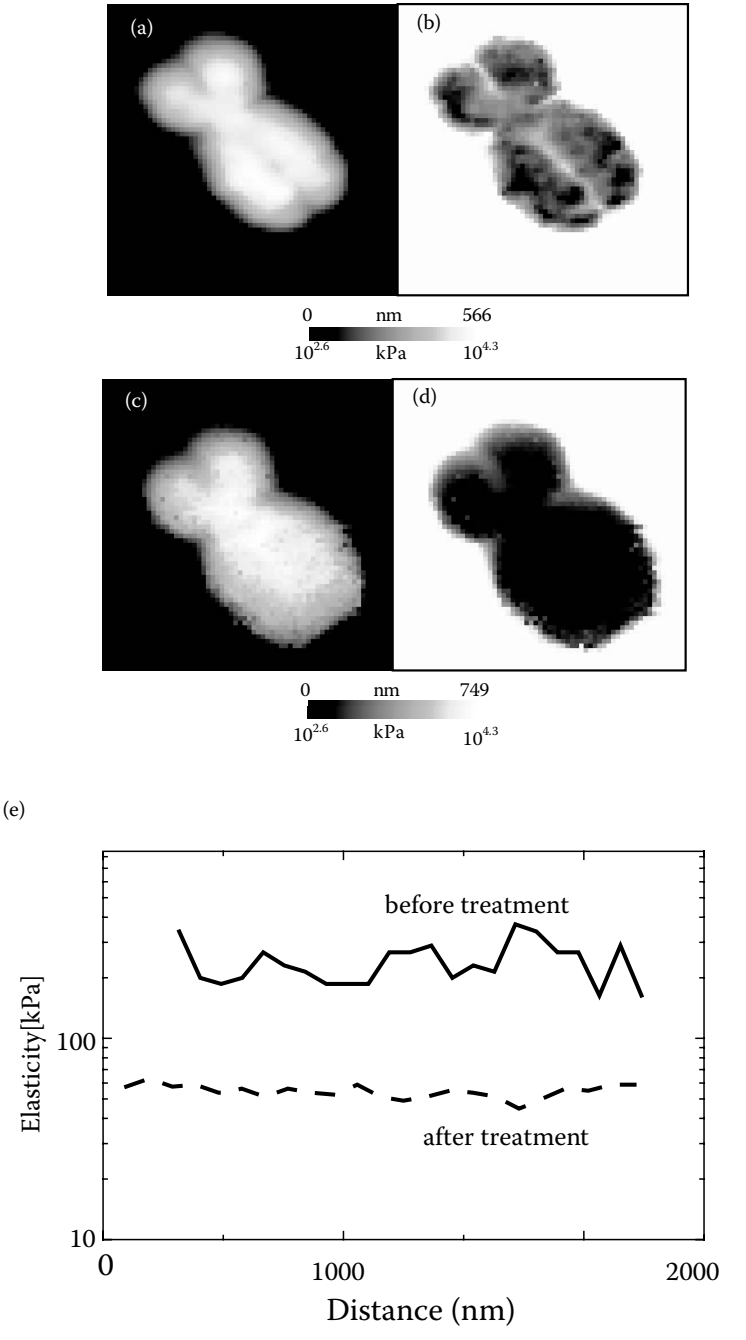

FIGURE 1.5 Topography and elasticity images of a human chromosome before (a, b) and after (c, d) trypsin treatment. Comparison between their respective elasticity distributions (e).

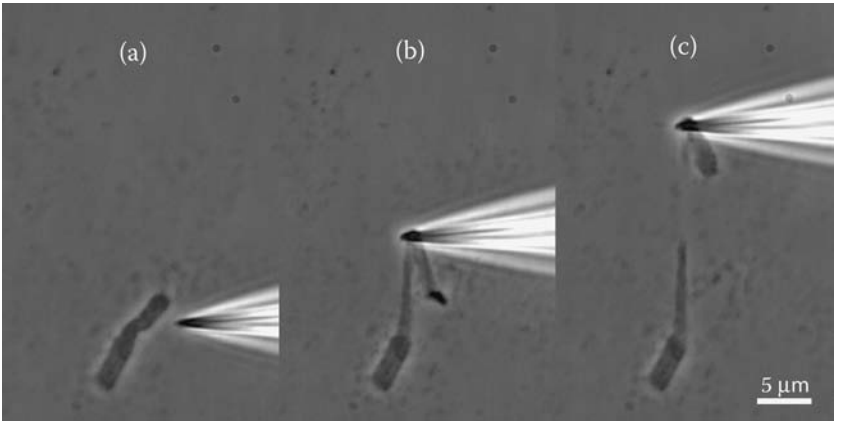

FIGURE 1.6 Time-serial optical phase contrast images of the elongating process of the unfixed human chromosomes in the buffer using two glass capillaries driven by a computer-controlled micromanipulator.

of chromosomes that were stretched with micromanipulators using SPM. In the SPM experiments, the force curves are obtained along whole single human chromosomes in culture medium. This method enables visualization of the topographic and elasticity images of the chromosomes, taking into account the effect of the finite thickness of the samples on the estimation of elasticity. Some ordered structure or a coarse nonhomogeneity is clearly visible in the elasticity image. It is considered that the domain structure reflects a robust higher-ordered structure such as the arrangement of the G-bands. The unfixed human chromosomes were stretched by a micromanipulator in hexylene glycol buffer. This enables, by stretching, elasticity mapping of the chromosome and examination of its morphology of a wound filament.

ACKNOWLEDGMENTS

This study was supported by the Special Coordination Funds of the Ministry of Education, Culture, Sports, Science, and Technology of the Japanese government. This was also supported partially by a Grant-in-Aid from the Ministry of Education, Culture, Sports, Science and Technology of Japan (15650051, 14GS0301 for K.K.).

REFERENCES

1. Carlson RD, Olins DE (1976) Chromatin model calculations: arrays of spherical nu bodies. *Nucleic Acids Res* 3: 89–100.
2. Carpenter BG, Baldwin JP, Bradbury EM, Ibel K (1976) Organisation of subunits in chromatin. *Nucleic Acids Res* 3: 1739–1746.

3. Finch JT, Klug A (1976) Solenoidal model for superstructure in chromatin. *Proc Natl Acad Sci USA* 73: 1897–1901.
4. Hizume K, Yoshimura SH, Takeyasu K (2005) Linker histone H1 per se can induce three-dimensional folding of chromatin fiber. *Biochemistry* 44: 12978–12989.
5. Yokota H, Singer MJ, van den Engh GJ, Trask BJ (1997) Regional differences in the compaction of chromatin in human G0/G1 interphase nuclei. *Chromosome Res* 5: 157–166.
6. Niimura Y, Gojobori T (2002) In silico chromosome staining: reconstruction of Giemsa bands from the whole human genome sequence. *Proc Natl Acad Sci USA* 99: 797-802.
7. Saitoh Y, Laemmli UK (1994) Metaphase chromosome structure: bands arise from a differential folding path of the highly AT-rich scaffold. *Cell* 76: 609–622.
8. Oberringer M, Englisch A, Heinz B, Gao H, Martin T, Hartmann U (2003) Atomic force microscopy and scanning near-field optical microscopy studies on the characterization of human metaphase chromosomes. *Eur Biophys J* 32: 620–627.
9. Paulson JR, Laemmli UK (1977) The structure of histone-depleted metaphase chromosomes. *Cell* 12: 817–828.
10. Sumner AT (1996) The distribution of topoisomerase II on mammalian chromosomes. *Chromosome Res* 4: 5–14.
11. Poirier MG, Marko JF (2002) Mitotic chromosomes are chromatin networks without a mechanically contiguous protein scaffold. *Proc Natl Acad Sci USA* 99: 15393–15397.
12. Marsden MP, Laemmli UK (1979) Metaphase chromosome structure: evidence for a radial loop model. *Cell* 17: 849–858.
13. Ushiki T, Hoshi O, Iwai K, Kimura E, Shigeno M (2002) The structure of human metaphase chromosomes: its histological perspective and new horizons by atomic force microscopy. *Arch Histol Cytol* 65: 377–390.
14. Poirier MG, Nemani A, Gupta P, Eroglu S, Marko JF (2001) Probing chromosome structure with dynamic force relaxation. *Phys Rev Lett* 86: 360–363.
15. Radmacher M, Fritz M, Kacher CM, Cleveland JP, Hansma PK (1996) Measuring the viscoelastic properties of human platelets with the atomic force microscope. *Biophys J* 70: 556–567.
16. Haga H, Sasaki S, Kawabata K, Ito E, Ushiki T, Sambongi T (2000) Elasticity mapping of living fibroblasts by AFM and immunofluorescence observation of the cytoskeleton. *Ultramicroscopy* 82: 253–258.
17. Nagayama M, Haga H, Tanaka Y, Hirai Y, Kabuto M, Kawabata K (2002) Improvement of force modulation mode with scanning probe microscopy for imaging viscoelasticity of living cells. *Jpn J Appl Phys* 41: 4952–4955.
18. Dimitriadis EK, Horkay F, Maresca J, Kachar B, Chadwick RS (2002) Determination of elastic moduli of thin layers of soft material using the atomic force microscope. *Biophys J* 82: 2798–2810.
19. Hoshi O, Owen R, Miles M, Ushiki T (2004) Imaging of human metaphase chromosomes by atomic force microscopy in liquid. *Cytogenet Genome Res* 107: 28–31.
20. Wray W, Stubblefield E (1970) A new method for the rapid isolation of chromosomes, mitotic apparatus, or nuclei from mammalian fibroblasts at near neutral pH. *Exp Cell Res* 59: 469–478.
21. Mizutani T, Haga H, Kawabata K (2004) Cellular stiffness response to external deformation: tensional homeostasis in a single fibroblast. *Cell Motil Cytoskeleton* 59: 242–248.

22. Nitta T, Endo Y, Haga H, Kawabata K (2003) Microdomain structure of agar gels observed by mechanical-scanning probe microscopy. *J Electron Microsc* 52: 277–281.
23. Vinckier A, Semenza G (1998) Measuring elasticity of biological materials by atomic force microscopy. *FEBS Lett* 430: 12–16.
24. Nomura K, Hoshi O, Fukushi D, Ushiki T, Haga H, Kawabata K (2005) Visualization of elasticity distribution of single human chromosomes by scanning probe microscopy. *Jpn J Appl Phys* 44: 5421–5424.

2 Development of Novel AFM Probes for Chromosome Manipulation

*Masato Saito, Gen Hashiguchi and Eiichi Tamiya**

CONTENTS

2.1 Introduction 15
2.2 Design and Fabrication of the Knife-Edged AFM Probe 17
2.3 Design and Fabrication of the Tweezers AFM Probe 18
2.4 Sample Preparation for Manipulation Experiments with the Fabricated AFM Probes 20
2.5 AFM Imaging and Manipulation with the Fabricated AFM Probes 22
2.6 Conclusions 28
Acknowledgment 28
References 28

2.1 INTRODUCTION

The chromosome has a complex structure that consists of DNA and proteins, and the length of DNA sequence reaches about three billion base pairs for the human genome [1]. During cell division, the mitotic chromosome forms a highly condensed structure, and distributes the genetic information to two daughter cells evenly and accurately. Therefore, the formation of a higher order chromosomal structure is an indispensable aspect of its vital activity. However, it has only been possible to observe the macro structure, because chromosome research has been largely carried out by optical or electron microscopy (see also Part II). Recently, genomic research that centers on DNA has advanced prominently. However, the relationships between the structure of the chromosome and the distribution of the

*To whom correspondence should be addressed.

genes and their base sequences have not been determined in detail. Therefore, a new analytical technique that can include these spatially distributed elements is required for advanced research on chromosomes. For example, the chromosome could be finely fractionated by a probe for atomic force microscopy (AFM), then these parts distributed to each chamber of an array, and DNA would be detected by using a suitable method, such as polymerase chain reaction (PCR) amplification (see also Chapter 3).

Since the development of AFM in 1986, it has contributed to research within various fields in physics, chemistry and biology, as a powerful tool that enables the visualization and analysis of a specific region of a molecule, from micrometer to nanometer in scale [2,3]. In addition to collecting surface information of materials, through various improvements AFM is expected to develop as a nanoscale fabrication tool, in connection with dip-pen lithography and anodic oxidation [4]. To mechanically modify solid materials, such as semiconductors and resist films, the dynamic plowing technique using an AFM tip has been reported [5–7]. As an application for biological samples, dissections of chromosomes and DNA using a conventional pyramidal AFM probe have also been reported by several groups [8–15]. Thus, there is no longer any doubt that AFM has become an important device to aid research in nanotechnology.

In our research, we focused on the possibility of nanoscale physical and mechanical operations using AFM. Several dissection and manipulation methods have been developed for analyzing the relationships between three-dimensional structure and chromosomal information. In this report, we attempted the physical dissection of a chromosome through AFM operation, as a first step toward developing our chromosome chip. As an initial step, we were able to achieve the physical dissection of a human metaphase chromosome with the conventional probe, which has a pyramidal wedge-shaped tip [15]. After dissection, the chromosomal inner structures were exposed around the dissected regions and topographic profiles in the section were then obtained with a carbon nanotube probe, under ambient conditions. A cross-sectional analysis revealed that nanoscale globular structures were observed in the gap of the dissected region. However, it has been problematic to apply a conventional probe to chromosome dissection because the chromosome surface was often scarified, with damage by the contact of the wedge-shaped probe tip. The conventional AFM probe limited our range of application as a result of its shape and material properties. Therefore, the development of a suitable and novel probe for AFM manipulation at the nanoscale has been in demand. Additionally, the novel probe would be required to simultaneously have both the functions of imaging and manufacturing. In consideration of these points, we attempted to manufacture a knife-edged probe, as well as perform dissection of DNA and the chromosome [16]. It should be noted that it is desirable to collect the sample selectively after dissection with the knife-edged AFM probe. We made an attempt to develop a tweezer-type AFM probe, which has a high performance in imaging and collecting the biomolecules on the substrate under AFM operation [17,18]. In this chapter, the fabrication of AFM tweezers and their applications will be described [19].

2.2 DESIGN AND FABRICATION OF THE KNIFE-EDGED AFM PROBE

We designed two thick-type (4 and 6 μm) edge-shaped probe devices, which were in the front of the silicon cantilever, as shown in Figure 2.1a. The cantilever length was 200 μm and the knife length was about 20 μm. The thickness of both cantilever and knife was 4 μm (or both 6 μm). The acute angle was 70.54°. The cantilever, which had the knife-edged probe, was joined with a silicon foundation to set on the cantilever holder for AFM operation. Figure 2.1(b) shows a scanning electron microscopic (SEM) photograph of the fabricated knife-edged probe with 4 μm thickness. The theoretical value of the spring constant was 13 N/m. The actual measured values of the resonance frequency, Q value and free amplitude were 103.3 kHz, 100.0 and 28.3 nm, respectively, and the corresponding parameters for the 6-μm probe were 45 N/m, 165.4 kHz, 343.6 and 24.76 nm, respectively.

The fabrication procedure was based on anisotropic etching and local oxidation techniques for silicon, and is shown in Figure 2.2. The starting material was a silicon-on-insulator (SOI) wafer with a 4-μm (or 6-μm)-thick n-type Si(100) layer (SOI layer) and a 2-μm-thick buried SiO_2 layer. First, 50-nm-thick Si_3N_4 was deposited on the top of the SOI wafer by low pressure chemical vapor deposition (LPCVD), and then patterned along the [110] direction by photolithography and reactive ion etching (RIE) (Figure 2.2[a]). The exposed SOI layer was covered with a SiO_2 layer resulting from a process of local oxidation of silicon (LOCOS) (Figure 2.2[b]). A second Si_3N_4 etching was then conducted to open a window for the following Si etching, as shown in Figure 2.2(c). Then, the SOI layer was etched with KOH solution via the opened window, exposing two Si(111) side surfaces at the corner of the opened window (Figure 2.2[d]). After the second LOCOS process, the exposed (111) surfaces were covered in layers of Si_3N_4, then the residual Si_3N_4 layer was removed selectively by RIE (Figure 2.2[e]). The exposed SOI layer was again etched with KOH solution, making a wedged structure that was surrounded by two (111) side surfaces as shown in Figure 2.2f. After removing the LOCOS-formed SiO_2 layer (Figure 2.2[g]), the wedged Si structure was cut to the desired length with deep-RIE apparatus (Figure 2.2[h]) [16].

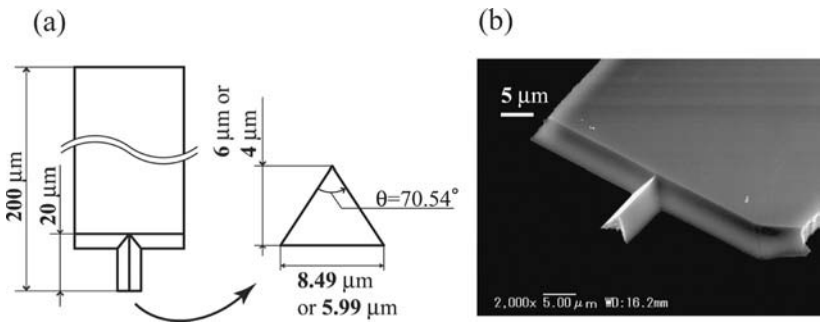

FIGURE 2.1 Design of the knife-edged AFM probe. (a) Illustration of the design of the knife-edged AFM probe. (b) SEM photograph of the fabricated knife-edged AFM probe.

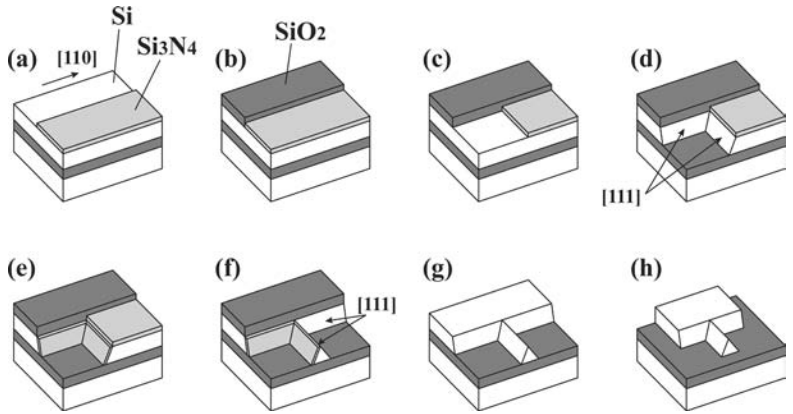

FIGURE 2.2 Schematic of the fabrication process for the knife-edged AFM probe. The fabrication process was as follows: (a) remove Si_3N_4 layer, (b) wet oxidation (~3000 Å), (c) remove Si_3N_4 layer, (d) anisotropic etching of Si, (e) oxidation to protect the Si(111) surface, (f) anisotropic etching of Si, (g) remove SiO_2 layer, (h) arrange the knife-edge length.

2.3 DESIGN AND FABRICATION OF THE TWEEZERS AFM PROBE

We developed a tweezers-type AFM probe, which was designed as shown in Figure 2.3. This device had two thin probes that were formed in the front of the silicon cantilever, with a vertical triangular shape. One functioned as an AFM imaging probe tip for the tapping mode, and was called the sensing probe. The other could be made to work as a tweezer, by closing the vertical face of the probe (the movable probe). The principle of operation for the movable probe was based on the leverage of the thermal expansion actuator, which was assembled in the base of its cantilever and was actuated with DC electricity. Here, we assume the AFM tweezers are used in the tapping mode. If both of the resonance frequencies are the same, it is thought that the sample or substrate surface will be damaged by oscillation of the movable probe during the AFM imaging by the sensing probe. The resonance frequencies were therefore set to different values by making each probe a different length. This means that at the resonance frequency of the sensing probe, the amplitude of the movable probe will be smaller relative to that of the sensing probe. The sample surface can then be scanned using the sensing probe, without damage of the sample surface by contact with the movable probe. We designed the movable probe with a length of 520 μm and the sensing probe with a length of 500 μm. The resonance frequency of the sensing probe was set to be higher than that of the movable probe [17,18].

Figure 2.4 shows a schematic of the fabrication process of the AFM tweezers. The starting material was a SOI wafer (Si[100]: 6 μm/SiO_2: 1 μm/Sub.: 525 μm, n-type, 2–5 Ω cm). First, 25-nm-thick Si_3N_4 was deposited on the top of the SOI wafer by LPCVD (Figure 2.4[a]), and then patterned along the [110] direction by photolithography and RIE (Figure 2.4[b]). The exposed Si layer was covered with a

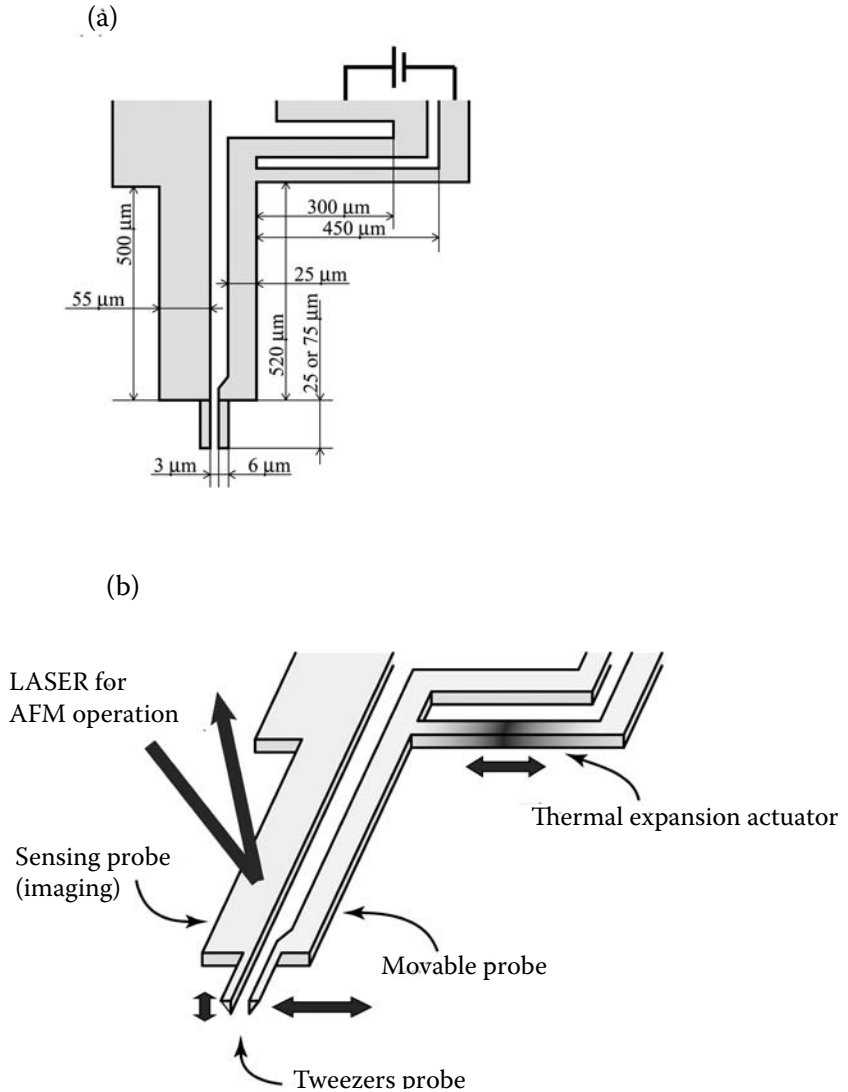

FIGURE 2.3 Design of the AFM tweezers. Illustration of the design (a) and the principle of operation (b) of the AFM tweezers. The AFM image can be taken using the sensing probe. To capture the samples, the movable probe, which had the thermal expansion actuator, was operated by applying voltage.

SiO_2 layer formed by thermal oxidation (Figure 2.4[c]). The thermal expansion actuator and tweezers probe were shaped on the substrate, removing the Si_3N_4 and SiO_2 by lithography (Figure 2.4[d]). A slit was formed between the tweezer probe tips, and the Si_3N_4 layer was removed selectively by RIE (Figure 2.4[e]). Then, the exposed Si layer was etched with KOH solution, making a wedged structure (Figure 2.4[f]).

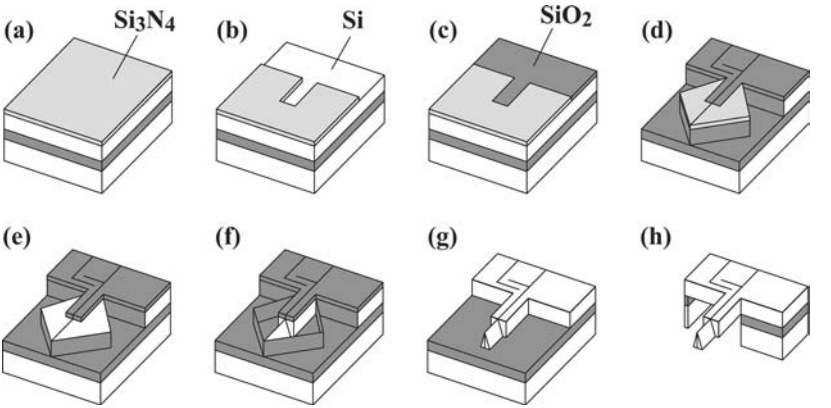

FIGURE 2.4 Schematic of the fabrication process of the AFM tweezers. The fabrication process was as follows: (a) Si_3N_4 deposition on a SOI wafer, (b) remove the Si_3N_4 layer using RIE, (c) thermal oxidation of the Si surface, (d) remove Si_3N_4 and SiO_2 in the shape of tweezers, (e) form the slit between the tweezers' tips and remove the Si_3N_4 layer using RIE, (f) KOH etching of Si, (g) remove SiO_2 and adjust the probe length, (h) remove the substrate using Deep RIE with an Al mask.

After removing the SiO_2 layer and adjusting the probe length (Figure 2.4[g]), the substrate SOI wafer was removed using Deep-RIE apparatus with an Al mask (Figure 2.4[h]). Figure 2.5(a) shows an SEM photograph of the fabricated tweezers probe. The theoretical value of the spring constant of the sensing probe was 3 N/m. The actual measured values of the resonance frequencies of the sensing probe and the movable probe were 148.4 and 134.6 kHz, respectively. The ohmic value of the thermal expansion actuator between the probe electrodes was 4.7 kΩ, and the probe tips were completely closed with 30 V of applied voltage (Figure 2.5[a,b]). In addition, the displacement of the movable probe, which was actuated with the thermal expansion actuator, was magnified approximately 12 times. If this displacement were 2 μm, the gripping force would theoretically be 36 μN [17,18].

2.4 SAMPLE PREPARATION FOR MANIPULATION EXPERIMENTS WITH THE FABRICATED AFM PROBES

Plasmid pBR322 DNA sample was purchased from TAKARA BIO Inc. (Shiga, Japan). An aliquot (10 μL) of 1 ng/μL DNA solution containing 2 m*M* $MgCl_2$ was dropped onto the freshly cleaved mica. After 2 min, the mica was rinsed with ultrapure water and dried using nitrogen gas [20].

Human metaphase chromosomes were prepared from human lymphocytes, which were obtained from whole human peripheral blood according to standard protocols [21]. However, the chromosome samples adsorbed strongly to the substrate, and also included some elements of the cell other than the chromosomes. Therefore, we also used a special kind of chromosome sample that contained

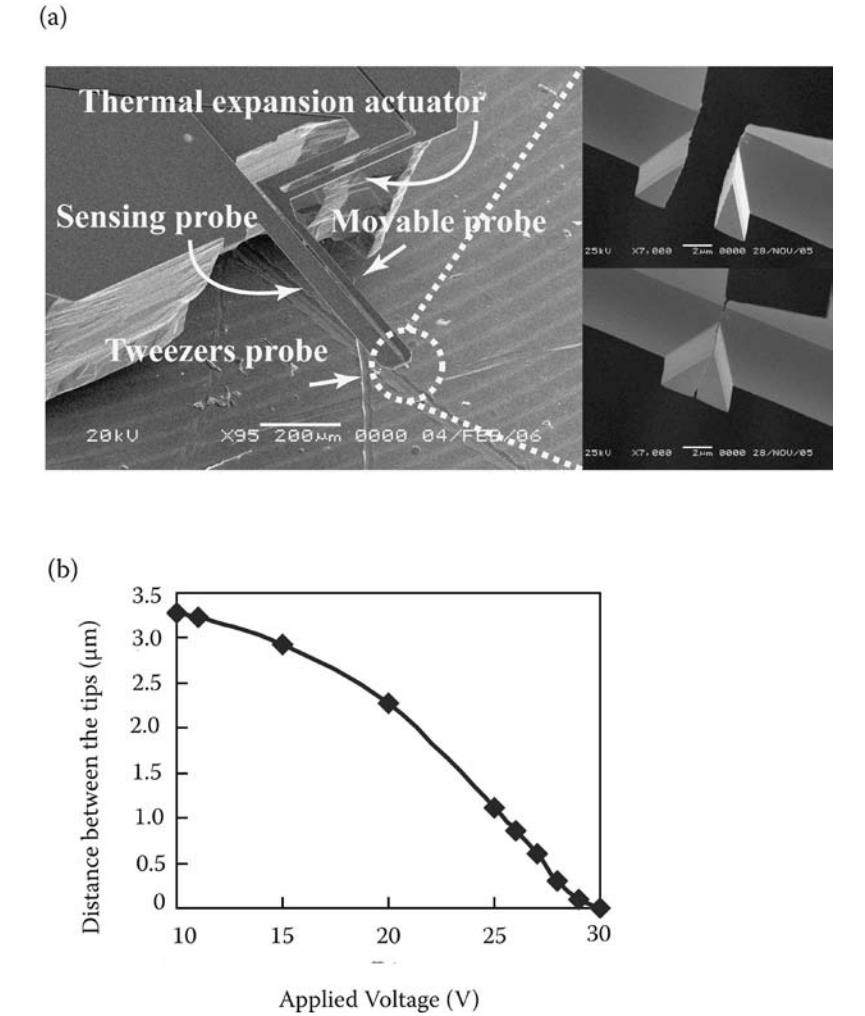

FIGURE 2.5 The fabricated AFM tweezers. (a) SEM photograph of the fabricated AFM tweezers tip with (upper right) and without (lower right) the applied voltage. (b) The plot of the relationship between the distance spanning the tweezers' tips, and the applied voltage.

no cell membrane or cytoplasm [22,23]. This chromosome sample was kindly donated by Prof. K. Fukui and Dr. S. Uchiyama from Osaka University. Cells from a human lymphoblast-like cell line, BALL-1, subcultured once for 24 h, were treated with 50 ng/mL colsemid for 12 h to arrest the cell cycle at metaphase. After collection of the synchronized cells by centrifugation, chromosomes were isolated using a modified polyamine buffer (15 m*M* Tris–HCl, 2 m*M* EDTA, 80 m*M* KCl, 20 m*M* NaCl, 0.5 m*M* EGTA, 1 mg/mL digitonin, 14 m*M* 2-mercaptoethanol, 0.1 m*M* PMSF, 0.2 m*M* spermine, 0.5 m*M* spermidine,

pH 7.2) or citric acid solution (0.1 *M* citric acid, 0.1 *M* sucrose, 0.5% Tween 20, pH 2.7). The chromosome suspension, fixed with Carnoy solution (ethanol/acetic acid, 3:1 v/v), was dropped directly and was adsorbed onto the silicon substrate. After drying, the silicon substrate was rinsed with ultrapure water.

2.5 AFM IMAGING AND MANIPULATION WITH THE FABRICATED AFM PROBES

All AFM experiments were performed using a commercial AFM unit (SPA400-SPI4000; SII NanoTechnology Inc., Chiba, Japan) equipped with a calibrated 20-μm xy-scan and 10-μm z-scan range PZT scanner. Three different types of AFM probes, the conventional cantilever SI-DF40 having a pyramidal-shaped tip (spring constant: 42 N/m; frequency resonance: 300 kHz; SII NanoTechnology Inc.) and the two fabricated knife-edged probes having 4 and 6 μm thickness, were used for imaging and manipulation as described in the following sections.

First, procedures of imaging and dissection of dsDNA were attempted in order to investigate the properties of the knife-edged probe. The dsDNA from pBR322 plasmid was adsorbed onto a freshly cleaved mica surface with Mg^{2+} ion. Before dissection, an AFM image of pBR322 DNA was obtained by using the 4-μm knife-edged probe in the tapping mode (i.e., cyclic contact mode, dynamic force mode) at an optimal force. The probe tip was withdrawn from the sample surface and while maintaining the same location, the operation mode was switched to contact mode without probe oscillation. The probe tip then again approached the same position of the sample surface. For dissection of the DNA molecule, a series of single-line scans was performed at a defined loading force, at a speed of 50 nm/s. For determination of the dissection regions, the AFM probe was positioned using the Seiko vector scanning program. The probe tip was withdrawn once from the surface and again switched to the tapping mode, and the dissected DNA was then imaged. These operations were carried out using the same 4-μm knife-edged probe. As a result, it was possible to image dsDNA using the 4-μm knife-edged probe in the tapping mode at an optimal force, in a similar fashion as with the conventional wedged-shape probe. Several loading forces from 7200 to 0.072 nN that were defined using the vector scanning program, in the contact mode without probe oscillation, were employed in dissection of the DNA along each single-lined scan. A broken line was observed on the mica surface along the scanned line at 7200 nN of loading force (data not shown). From 720 to 0.72 nN, DNA was dissected clearly without any broken lines, and the minimum loading force was found to be 0.72 nN. No dissection was observed at 0.072 nN (data not shown). Figure 2.6(b) shows the DNA dissection, which was carried out along the allowed dotted line as shown in Figure 2.6(a) at a minimum loading force of 0.72 nN. The continuity of the dsDNA is clearly lost, indicating that it was successfully dissected by the 4-μm knife-edged probe. Additionally, it was possible to continue imaging using the same probe after dissection [16].

The knife-edged probe (4 μm) was also applied to dissection of the human chromosome. To examine the dissection conditions, the loading force was

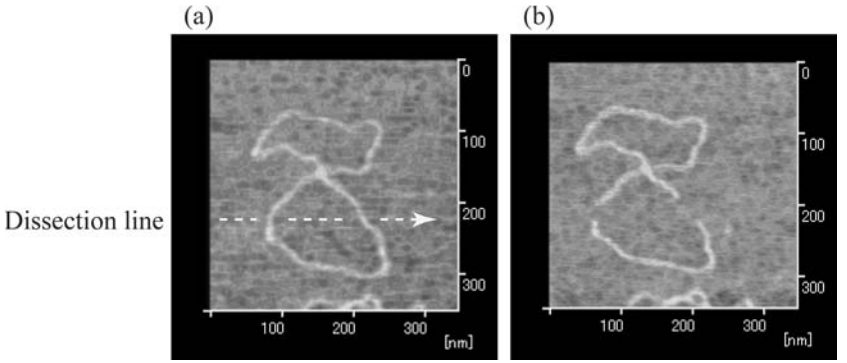

FIGURE 2.6 Dissection of dsDNA from the pBR322 plasmid using the 4-μm-thick knife-edged probe. Before dissection, the AFM image of dsDNA was obtained using the tapping mode (a). After switching to the contact mode without probe oscillation, the dissection was performed at 0.72 nN of loading force along the dotted line as shown in (a). The probe motion was controlled by the Seiko vector scanned program. Dissection speed was set to 50 nm/s. After switching to the tapping mode again, the dissected DNA could be observed (b). The same probe was used for the imaging and dissection procedures throughout this experiment.

increased stepwise by controlling the amplitude reference in the tapping mode. Amplitude reference is a relative indicator of the loading force in a SII™ AFM operation, and is able to be set at any value. This value represents the probe amplitude reduction from the initial amplitude. For example, if the amplitude reference were set to –0.1, the initial amplitude would be reduced by 10%. If the amplitude reference were set to –1.0, the amplitude reduction would become 100%; in other words, the probe amplitude would become 0, and the probe tip would reach and touch the sample surface. The calculation of the loading force in the tapping mode has been previously described by us [16].

To dissect the human chromosome, three types of probes comprising a conventional wedged-shape probe and the two fabricated knife-edged probes (4 and 6 μm thick) were applied. After obtaining an AFM image of the chromosome, a series of single-line scans were performed to allow the use of several amplitude references during the scanning process. For the determination of the dissection regions, the AFM probe was positioned using the Seiko vector scanning program. Figure 2.7 shows the AFM image of the chromosome using the 4-μm knife-edged probe. The dissection, which was operated with a vector scan program in the tapping mode, was carried out by controlling the amplitude references along a series of lines, as shown in Figure 2.7(a). The dissection speed was set to 10 nm/s. The loading forces of $F = 18.22$, 36.71, 367.90, 386.30, 404.69 and 423.09 nN were employed with amplitude references of –0.90, –0.95, –1.00, –1.05, –1.10 and –1.15, respectively. No dissection was observed at amplitude references between –0.90 and –0.95. Below an amplitude reference of –1.00, the dissection

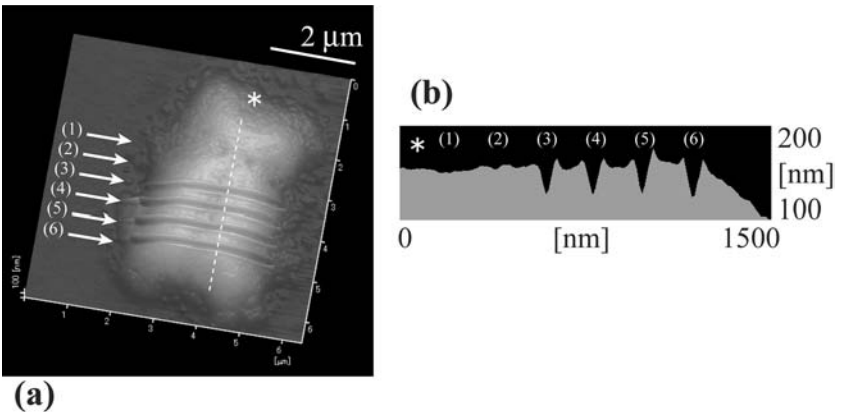

FIGURE 2.7 Chromosome dissection using the 4-μm-thick knife-edged AFM probe in the tapping mode. The dissection was carried out, controlling amplitude reference, along the arrowed lines indicated in (a). The oscillation amplitude of the probe was completely dampened to zero below an amplitude reference of –1.0. Then, the probe tip reached and touched the sample surface. The loading forces of each amplitude reference were (1) –0.90: 18.22 nN; (2) –0.95: 36.71 nN; (3) –1.00: 367.90 nN; (4) –1.05: 386.30 nN; (5) –1.10: 404.69 nN; (6) –1.15: 423.09 nN. The dissection speed was set to 10 nm/s. After dissection, the dissected chromosome was observed with the same knife-edged probe. The cross-sectional analyses are shown in (b).

of the chromosome was achieved similarly to that with the conventional probe. The depth of the dissection area was 31.56 nm at an amplitude reference of –1.00. The dissection depths became greater as the amplitude reference was decreased below –1.00, as follows: –1.05: 33.83 nm; –1.10: 34.11 nm; –1.15: 35.82 nm. Here, chromosome dissection was also achieved with the conventional AFM probe. However, chromosomal debris having a height of 258.6 nm was seen on the right side of the dissection line (see Saito et al. 2006 [16]). This debris, including DNA and several genes, was lost after the manipulation. This problem would be serious when using the dissected chromosome fragments for further analysis with the chromosome chip device. In addition, most of the dissected lines were not linear. Similar results have been reported from previous studies [10,11,14,15], and these reports showed that the dissected regions of the chromosome had jagged lines caused by the wedged-shape probe. Figure 2.8(a) shows a schematic of chromosome dissection with the conventional wedged-shape probe tip. This probe forms a relatively substantial mass facing in the direction of dissecting and scanning, and cuts while digging up the chromosome surface. In this way, a sharp probe tip may easily break. As a result, the conventional cantilevers were not found to be suitable for the precise manipulation of chromosomes. In contrast, the knife-edged probe would form a small mass facing in the scanning and dissecting direction, and would "bump aside" the dissected chromosome on both sides. Therefore, we expected that debris would not arise during dissection, and

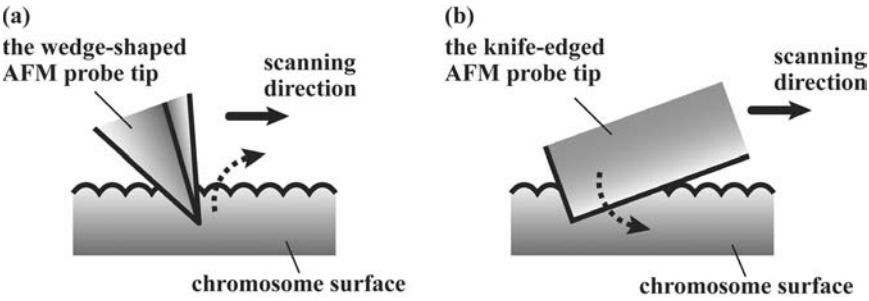

FIGURE 2.8 Schematic of the AFM probe behavior in dissection. The conventional wedge-shaped AFM probe tip may "dig up" the sample surface during scanning (a). The knife-edged AFM probe tip may "bump aside" the sample during scanning.

that the dissection line would be linear. As a result, linear dissections were indeed obtained and debris was not observed on the right side of the dissected area on the chromosome (Figure 2.7).

Thus far, we have clearly demonstrated chromosome dissection using the 4-μm knife-edged probe. However, the height of chromosome was around 167.5 nm and the dissection reached to a depth of only about 35.8 nm; in other words, the dissection area did not reach to the bottom of the chromosome. It may have been that the 4-μm knife-edged probe was weaker than the chromosome and that, therefore, a stronger knife-edged probe was required for deeper dissection. For this reason, we applied the 6-μm knife-edged probe to chromosome dissection, while controlling the amplitude references in the tapping mode. Dissection was also observed below an amplitude reference of –1.00, similarly as for the 4-μm knife-edged probe (data not shown). In order to demonstrate chromosome manipulation using the 6-μm knife-edged probe, chromosome dissection and fragment-moving were attempted in a continuous manner. Figures 2.9(a) and (b) show the AFM images after chromosome dissection and fragment-moving. A loading force of 1.17 μN (amplitude reference of –1.05) and a dissection speed of 10 nm/s were applied in the dissection process. The height of the chromosome was 602.5 nm, and the dissection depth reached 396.9 nm. Thus, a deeper dissection was attained than with the 4-μm probe. The knife-edged probe had a triangular face as the nose of the knife region (Figure 2.1). Therefore, the dissected chromosome fragment was moved by pushing with the nose of the probe, as shown in the schematic (Figure 2.9[c]). Probe behavior was controlled with an amplitude reference of –1.05 and the vector scanning program along the dashed line, as shown in Figure 2.9(b). The dissected portions of the chromosome could be separated on the substrate while retaining their respective shapes (Figure 2.9[b]). We obtained these fine images using a conventional AFM probe, since the chromosome was so high that a fine image could not be obtained with the knife-edged probe. However, the AFM image obtained with the knife-edged probe was clear enough to recognize the chromosome for AFM manipulation.

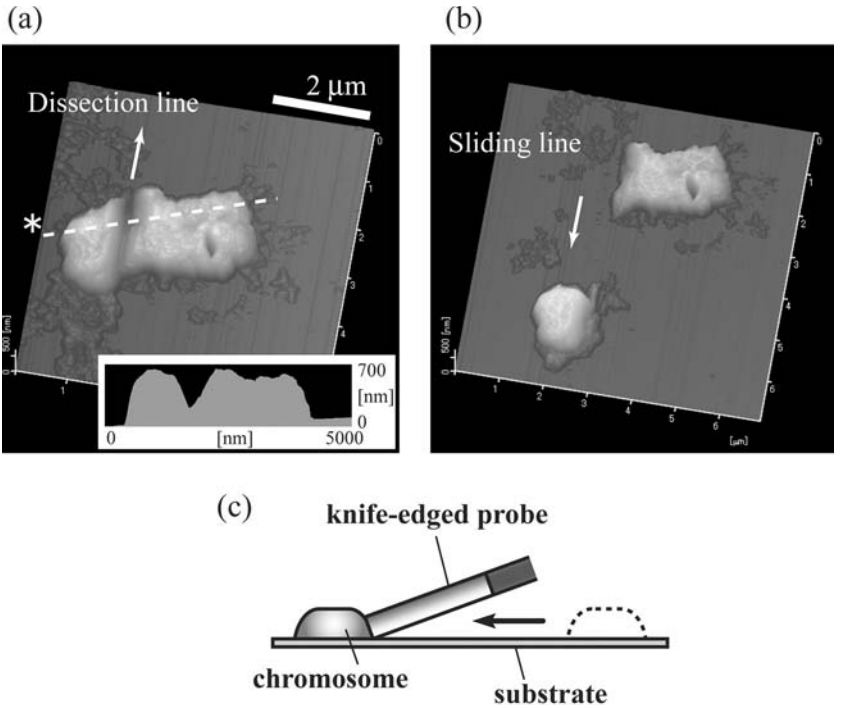

FIGURE 2.9 Chromosome dissection and moving of fragments using the 6-μm-thick knife-edged probe in the tapping mode. AFM images show the dissected (a) and the moved (b) chromosome fragments. The chromosome dissection was conducted with a loading force of 1.17 μN at an amplitude reference of –1.05 in the tapping mode vector scan. The dissection speed was set to 10 nm/s. After dissection, movement of the dissected fragment was performed using the nose of the knife-edged probe as shown in the schematic (c).

We then performed manipulation of the metaphase chromosome using the tweezers AFM probe, to obtain chromosome fragments of a smaller size than those obtained using conventional methods, such as glass microneedles [24]. In this technique, microdissection of specific chromosomal regions is performed under an inverted microscope, using glass microneedles controlled by a micromanipulator. This method has been used to obtain several types of chromosomal probes: either previously known chromosomal probes or chromosomal DNA from an unknown origin. However, the conventional methods are not suitable for the analysis of more than 10 million base pairs, or hundreds to thousands of individual genes, because of the limited size of the microneedles in the process of miniaturization. In this current research, we introduce metaphase chromosome manipulation by novel tweezer-type AFM probes to obtain chromosomal fragments of a smaller size. The metaphase chromosome, which was dissected and translocated with the knife-edged AFM probe as described below, was imaged using the sensing probe of the tweezer-type probe in the tapping mode

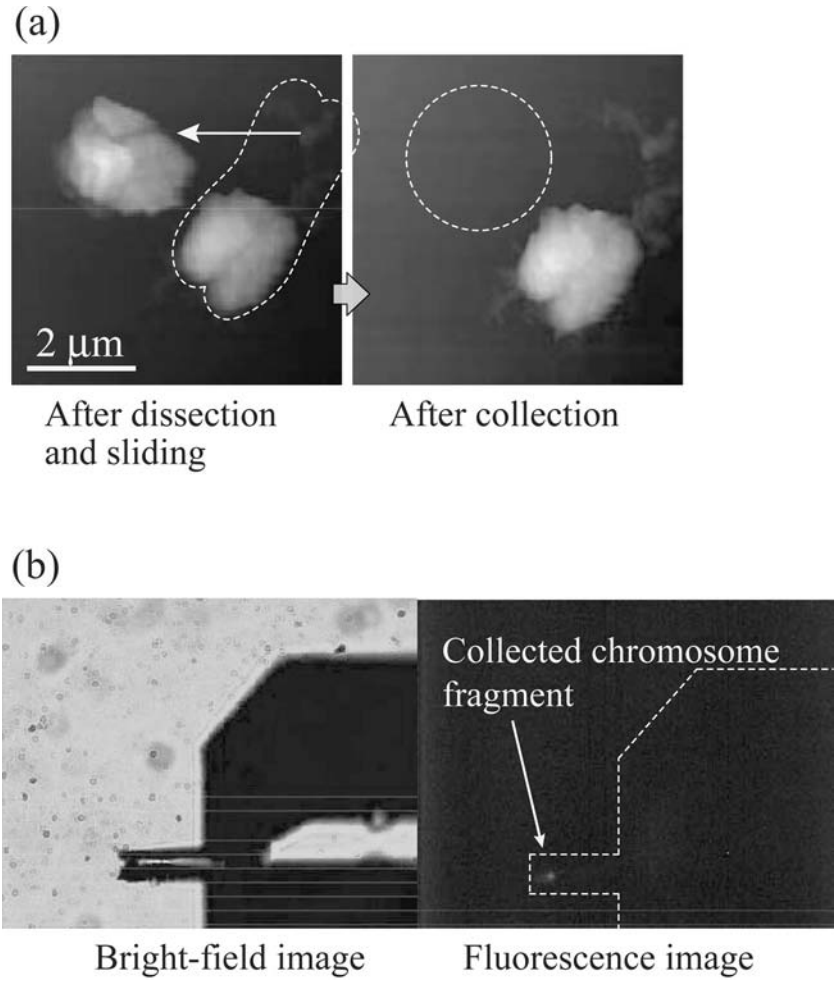

FIGURE 2.10 Collection of the chromosome fragment using the AFM tweezers under AFM operation. After dissection and sliding of the human chromosome using the knife-edged AFM probe (a, left) as shown in Figure 2.10, the dissected portion of chromosome could be collected using the AFM tweezers under AFM operation (a, right). The fluorescence signal of the collected fragment with SYBR Green I staining was observed on the tweezers' tip (b).

(Figure 2.10[a]). The position of the tweezer-type AFM probe was maneuvered so that the dissected fragment of the chromosome was between the sensing probe and the movable probe. Subsequently, in order to make contact between the two probes on the substrate, the loading force was increased while controlling the amplitude reference, which was set at –1.10. As voltage (30 V) was applied to the tweezer-type probe, the movable probe closed and sandwiched the fragment of chromosome.

After the operation of picking up of the fragment, no fragment was observed on the substrate as determined by AFM imaging (Figure 2.10[a]), and fluorescence could be observed at the tip of the tweezer-type probe (Figure 2.10[b]). Additionally, we succeeded in picking up smaller fragments of the order of submicrons [19]. It appears evident that the nanoscale manipulation of biological samples is now possible, especially of chromosomes, and further analysis of a specific portion of a chromosome can be performed using established analytical methods.

2.6 CONCLUSIONS

We have designed and fabricated two novel AFM probes (a knife-edged probe and a tweezer-type probe) for manipulation of biological samples. We have achieved the dissection of DNA and chromosomes using the knife-edged probe under AFM operation. Moreover, the collection of fragments of the metaphase chromosome, which was dissected with the knife-edged probe, was possible using our tweezer-type probe. It is indicated that the nanoscale manipulation of biological samples, especially chromosomes, has become possible, and further analysis of the specific portion of a chromosome can be performed using established analytical methods.

ACKNOWLEDGMENT

The authors gratefully acknowledge that this study was supported in part by a grant from the Special Coordination Funds for Promoting Science and Technology of the Ministry of Education, Culture, Sports, Science and Technology, the Japanese government.

REFERENCES

1. Brown TA (1999) *Genomes 2*. BIOS Scientific Publishers Ltd., Oxford.
2. Horber JK, Miles MJ (2003) Scanning probe evolution in biology. *Science* 302: 1002–1005.
3. Hansma HG, Kasuya K, Oroudjev E (2004) Atomic force microscopy imaging and pulling of nucleic acids. *Curr Opin Struct Biol* 14: 380–385.
4. Piner RD, Zhu J, Xu F, Hong S, Mirkin CA (1999) "Dip-pen" nanolithography. *Science* 29: 661–663.
5. Iwata F, Yamaguchi M, Sasaki A (2003) Nanometer-scale layer modification of polycarbonate surface by scratching with tip oscillation using an atomic force microscope. *Wear* 254: 1050–1055.
6. Hyon CK, Choi SC, Hwang SW, Ahn D, Kim Y, Kim EK (1999) Direct nanometer-scale patterning by the cantilever oscillation of an atomic force microscope. *Appl Phys Lett* 75: 292–294.
7. Heyde M, Rademann K, Cappella B, Geuss M, Sturm H, Spangenberg T, Niehus H (2001) Dynamic plowing nanolithography on polymethylmethacrylate using an atomic force microscope. *Rev Sci Instrum* 72: 136–141.

8. Hansma HG, Vesenka J, Siegerist C, Kelderman G, Morrett H, Sinsheimer RL, Elings V, Bustamante C, Hansma PK (1992) Reproducible imaging and dissection of plasmid DNA under liquid with the atomic force microscope. *Science* 256: 1180–1184.
9. Henderson E (1992) Imaging and nanodissection of individual supercoiled plasmids by atomic force microscopy. *Nucleic Acids Res* 20: 445–447.
10. Jondle DM, Ambrosio L, Vesenka J, Henderson E (1995) Imaging and manipulating chromosomes with the atomic force microscope. *Chromosome Res* 3: 239–244.
11. Stark RW, Thalhammer S, Wienberg J, Heckl WM (1998) The AFM as a tool for chromosomal dissection — the influence of physical parameters. *Appl Phys A* 66: S579–S584.
12. Guthold M, Falvo M, Matthews WG, Paulson S, Mullin J, Lord S, Erie D, Washburn S, Superfine R, Brooks FP Jr, Taylor II RM (1999) Investigation and modification of molecular structures with the nanomanipulator. *J Mol Graph Model* 17: 187–197.
13. Geisler B, Noll F, Hampp N (2000) Nanodissection and noncontact imaging of plasmid DNA with an atomic force microscope. *Scanning* 22: 7.
14. Fotiadisa D, Scheuringa S, Mullera SA, Engela A, Muller DJ (2002) Imaging and manipulation of biological structures with the AFM. *Micron* 33: 385–397.
15. Iwabuchii S, Mori T, Ogawa K, Sato K, Saito M, Morita Y, Ushiki T, Tamiya E (2002) Atomic force microscope-based dissection of human metaphase chromosomes and high resolutional imaging by carbon nanotube tip. *Arch Histol Cytol* 65: 473–479.
16. Saito M, Nakagawa K, Yamanaka K, Takamura Y, Hashiguchi G, Tamiya E (2006) A new design of knife-edged AFM probe for chromosome precision manipulating. *Sens Actuators A* 130–131: 616–624.
17. Takekawa T, Nakagawa K, Hashiguchi G (2005) The AFM tweezers: integration of a tweezers function with an AFM probe, in *Digest Tech Papers Transducers '05*, Sohn BK, Fujita H, Lee DD, Eds. IEEE, NJ: 621–624.
18. Takekawa T, Nakagawa K, Hashiguchi G, Saito M, Yamanaka K, Tamiya E (2005) Development of AFM tweezers for manipulation of nanometer size objects. *IEEJ Trans SM* 125: 448–453.
19. Yamanaka K, Takekawa T, Nakagawa K, Saito M, Takamura Y, Hashiguchi G, Tamiya E (2006) Metaphase chromosome manipulation using newly developed AFM probes, in *Proc Micro Total Analysis System 2006*, Kitamori T, Fujita H, and Hasebe S, Eds. Society for Chemistry and Micro-Nano Systems (CHEMINAS), Tokyo: 1528–1530.
20. Bezanilla M, Manne S, Laney DE, Lyubchenko YL, Hansma HG (1995) Adsorption of DNA to mica, silylated mica, and minerals: characterization by atomic force microscopy. *Langmuir* 11: 655–659.
21. Gosden JR (1994) *Methods in Molecular Biology 29*. Humana Press, NJ: 1–10.
22. Uchiyama S, Kobayashi S, Takata H, Ishihara T, Hori N, Higashi T, Hayashihara K, Sone T, Higo D, Nirasawa T, Takao T, Matsunaga S, Fukui K (2005) Proteome analysis of human metaphase chromosomes. *J Biol Chem* 280: 16994–17004.
23. Sone T, Iwano M, Kobayashi S, Ishihara T, Hori N, Takata H, Ushiki T, Uchiyama S, Fukui K (2002) Changes in chromosome structure by different isolation conditions. *Arch Histol Cytol* 65: 445–455.
24. Bates GP, Wainwright BJ, Williamson R, Brown SD (1986) Microdissection of and microcloning from the short arm of human chromosome 2. *Mol Cell Biol* 6: 3826–3830.

3 Microchamber Array-Based Sequence-Specific DNA Detection from a Single Chromosome via Trace Volume PCR

*Masato Saito and Eiichi Tamiya**

CONTENTS

3.1 Introduction 31
3.2 Design and Fabrication of the Microchamber Array 32
3.3 Reagents and Sample Preparation 33
3.4 Sample Loading into the Microchamber Array Using a Nanoliter Dispenser 35
3.5 Thermal Cycling and Detection of Fluorescence 35
3.6 On-Chip Quantitation of the Initial DNA Concentration 35
3.7 Specific Sequence Detection from a Single Human Chromosome-1 via Nanoliter-Volume PCR 38
3.8 Conclusion 40
Acknowledgment 41
References 41

3.1 INTRODUCTION

The miniaturization of analytical devices by the technique of semiconductor microfabrication is attracting many scientists for its applications in medical and bioanalytical fields, such as genetic analysis [1], clinical diagnostics [2], drug screening [3], and environmental monitoring [4]. The potential advantages of miniaturized analytical devices include reduced consumption of sample volume, high sensitivity, shorter analysis time, portability that allows on-site monitoring,

*To whom correspondence should be addressed.

and disposability [5]. In particular, the sensitivity of detection of amplified DNA in a trace volume polymerase chain reaction (PCR), when compared with the normal scale of reaction, was expected to be substantially higher. If the same amount of DNA were amplified from the same copy template, DNA concentration per unit volume would be higher in the trace volume. Miniaturized on-chip DNA amplification devices have also been reported in the last decade by several investigators [6–9]. However, there are significant problems associated with PCR amplification on chips; for example, cross-talk contamination between chambers and rapid drying of the trace volume PCR solution at nanoscale volumes. Therefore, in order to resolve these problems, we have developed a new method employing an oil layer on the microchamber instead of glass or plastic film covers. The sample DNA mixture to be amplified was introduced into each microchamber of the array, through an oil layer, using a nanoliter dispensing system [10,11]. The feasibility of our microchamber array was further improved by the use of TaqMan PCR [12]. The amplified DNA was detected by a microarray scanner using TaqMan fluorescence chemistry. The quantitation of the initial DNA concentration present in a microchamber was achieved from 0 to 12 copies per chamber, not only by monitoring the real-time fluorescence intensity but also by observing the end-point fluorescence signal [13]. Additionally, target-specific DNA amplification from a single chromosome was also attained using our microchamber [14].

In this chapter, we will introduce the microchamber array chip for DNA amplification, developed by us, and show our results of trace volume PCR amplification of a target gene in the microchamber array chip.

3.2 DESIGN AND FABRICATION OF THE MICROCHAMBER ARRAY

The microchamber array chip for DNA amplification was fabricated using semiconductor microfabrication processes, such as photolithography and anisotropic etching on the optically polished side of a silicon (100) wafer (ShinEtsu, Tokyo, Japan). The chip substrate was designed to be 1 inch × 3 inch (2.54 cm × 7.62 cm) for compatibility with the dispensing system employed. The procedure for fabrication of the silicon microchamber array chip is shown in Figure 3.1. A silicon oxide (SiO_2) layer was formed on the silicon surfaces using wet thermal oxidization for 8 h. After the photolithographic process, the silicon chip substrate was anisotropically etched to a depth of 250 μm with 25% (w/v) tetramethyl ammonium hydroxide (TMAH) in aqueous solution for 8 h at 80°C. The oxide layer was then removed using a solution of HF/NH_4F (1:6 v/v), and a layer of SiO_2 was formed on the surfaces including the etched chamber walls. After spin coating the positive photoresist (OFPR-800; Tokyo Ohka Kogyo, Kanagawa, Japan) on the SiO_2 layer, photolithography was performed in order to leave the SiO_2 layer inside of the microchambers. The oxidized layer outside the microchambers was removed with HF/NH_4F (1:6 v/v) solution. Finally, the remaining photoresist was

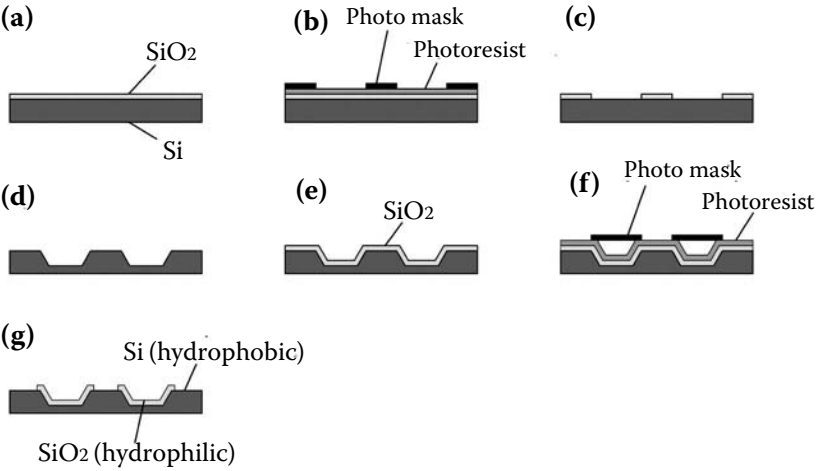

FIGURE 3.1 Schematic illustration of the fabrication process for the microchamber array. The SiO_2 layer was formed on the silicon surfaces using wet thermal oxidization (a). After the photolithographic process to make the pattern of the chamber array on the silicon surface (b–c), the silicon substrate was anisotropically etched with 25% (w/v) TMAH and the SiO_2 layer was removed with HF/NH_4F (1:6 v/v) solution (d). The SiO_2 layer was formed on the surfaces including the etched chamber walls (e). The photolithographic process was performed in order to make the SiO_2 layer in the microchamber walls (f). The oxidized layer that was not covered with the photoresist on the surface was removed using HF/NH_4F (1:6 v/v) solution. Finally, the remaining photoresist was stripped using acetone (g). The fabricated microchamber array has a SiO_2 (hydrophilic) layer in each chamber and a Si (hydrophobic) layer outside of the chambers.

stripped using acetone. The microchamber features were determined using a color laser 3D profile microscope VK-8500 (Keyence, Osaka, Japan) and scanning electron microscope S-3500N (Hitachi, Tokyo, Japan). A top view of the arrayed microchambers is shown in Figure 3.2(a). The dimensions of each chamber were $650 \times 650 \times 200$ μm. Each microchamber accommodated approximately 50 nL, and the total number of chambers on the chip substrate was 1248.

3.3 REAGENTS AND SAMPLE PREPARATION

The sequences of the synthesized primers, which amplified a 74-bp segment of DNA from the human Rhesus D (RhD) gene region on the human chromosome-1 [15], and the probe were as follows: forward primer, 5′-CCT CTC ACT GTT GCC TGC ATT-3′; reverse primer, 5′-AGT GCC TGC GCG AAC ATT-3′; fluorescence probe, 6-carboxyfluorescein (FAM)-5′-TAC GTG AGA AAC GCT CAT GAC AGC AAA GTC T-3′-6-carboxy-*N*,*N*,*N*′,*N*′-tetramethylrhodamine (TAMRA) (FASMAC Co., Japan). The reaction mixture consisted of (final concentration) 1× GeneAmp PCR buffer II, 0.2 m*M* of each dNTP, 4.5 m*M* $MgCl_2$ and 0.1 or 1.25 U/μL of AmpliTaq Gold DNA polymerase (Applied Biosystems, U.S.A.),

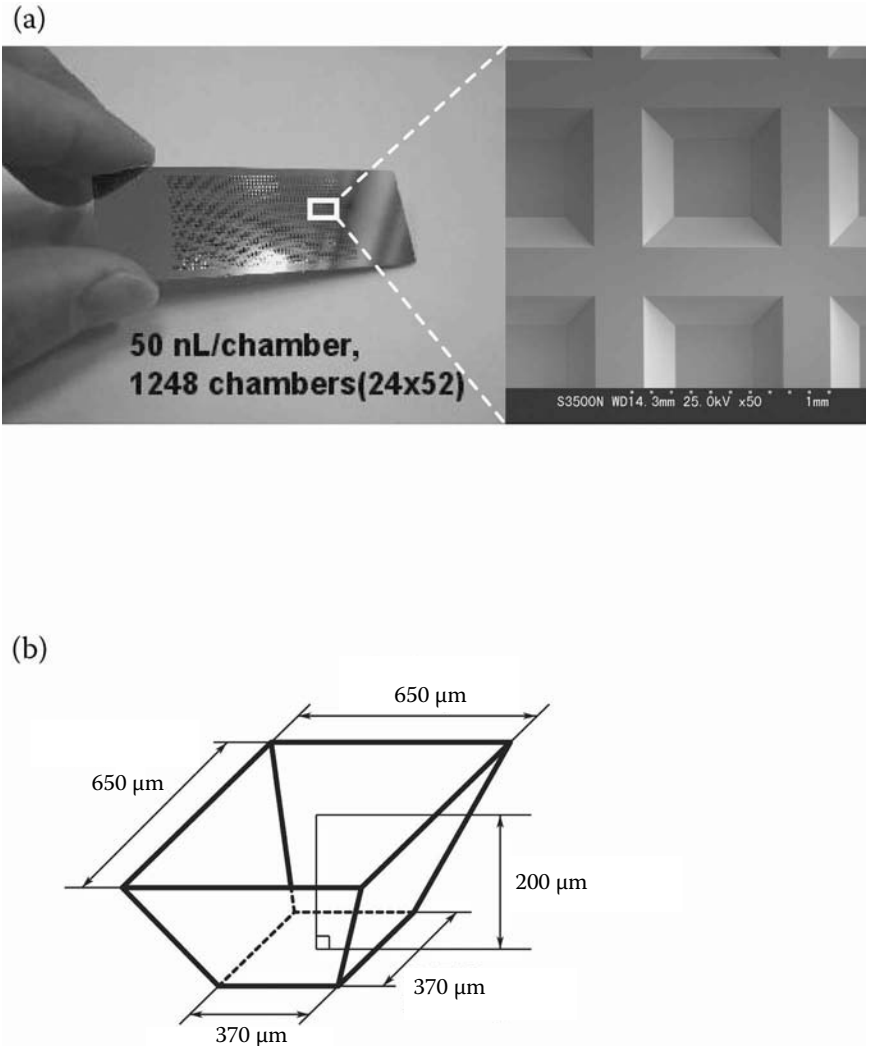

FIGURE 3.2 The fabricated microchamber array. (a) Photograph of a fabricated microchamber array, which has 52×24 (= 1248 in total) chambers in a chip. (b) Schematic illustration of the microchamber. The microchamber was designed with an opening space of 650×650 μm, a bottom space of 370×370 μm, and a depth of 200 μm. The chamber volume was approximately equivalent to 50 nL.

0.5% (w/w) polyvinylpyrrolidone (PVP) (Sigma-Aldrich, Japan), 600 n*M* of the forward and reverse primers, and 400 n*M* of the fluorescence probe. As the template DNA, purified human male genomic DNA, which was purchased from Promega (Japan), and human metaphase chromosome, which was described in the previous section, were used.

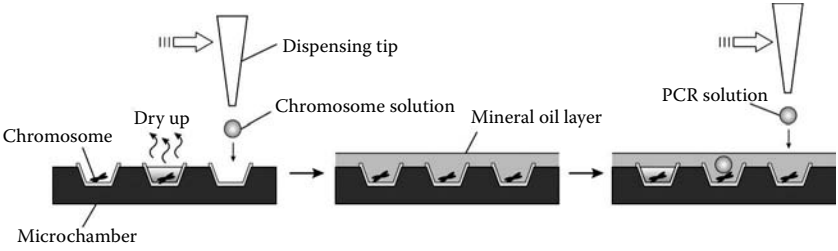

FIGURE 3.3 Schematic illustration of the preparative procedure for microchamber PCR. The chromosome solution was dispensed into the microchambers using the nanoliter dispenser and the chromosomes were adsorbed onto the chamber by drying the solution. Where necessary, purified genomic DNA (instead of chromosomes) and primers were dispensed into the microchamber. The microchamber array chip surface was then coated with mineral oil. The PCR mixture of 40 nL was dispensed into each chamber through the oil layer.

3.4 SAMPLE LOADING INTO THE MICROCHAMBER ARRAY USING A NANOLITER DISPENSER

First, the microchamber array chip was soaked in 1% (w/v) bovine serum albumin solution overnight, then rinsed with Milli Q water and dried; this was done in order to coat the chamber wall and prevent nonspecific adsorption. The precise dispensation of nanoliter volumes of solutions exactly at previously determined locations was found to be relatively straightforward through the use of a nanoliter dispenser from Cartesian Technologies (Michigan, U.S.A.). The volume of dispensed solution in a single microchamber was 40 nL. The mineral oil (Sigma, Tokyo, Japan) used as a cover lid was coated onto the microchamber chip, and 40 nL of PCR mixture, which included RhD gene-specific primers and probe, was dispensed into all of the microchambers through the oil layer as shown in Figure 3.3 [10,11].

3.5 THERMAL CYCLING AND DETECTION OF FLUORESCENCE

After preparing this setup, the chip was placed onto a conventional thermal cycling system for the PCR reaction. Thermal cycling was initiated with a 94°C step which was held for 10 min, followed by 40 cycles of 94°C for 15 s and 60°C for 30 s. After completion of PCR amplification, the amplified DNA was observed using a charge-coupled device (CCD) camera (Zeiss, Germany), which was mounted on a fluorescence microscope (Zeiss).

3.6 ON-CHIP QUANTITATION OF THE INITIAL DNA CONCENTRATION

The quantitation of the initial genomic DNA concentration was performed by using the microchamber array as shown in Figure 3.4. The amplification of the RhD gene was performed by dispensing different concentrations of target DNA

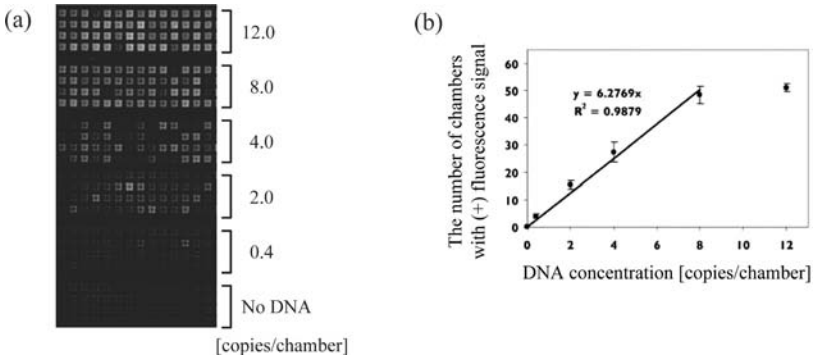

FIGURE 3.4 Quantitative analysis of microchamber array PCR. PCR amplification of the RhD gene from whole purified human genomic DNA as template was performed on the microchamber array. The fluorescence, which was based on TaqMan chemistry, was detected using the DNA microarray scanner (a). The positive chamber releases a high fluorescence signal compared with the negative chamber. As the number of copies of template DNA per microchamber was increased, the number of microchambers which showed a high fluorescence signal also increased. The average number of chambers within a specific fluorescence signal range was plotted against the number of target DNA copies (b). The number of microchambers displaying high fluorescence increased with increasing target DNA copy number. The microchambers which displayed fluorescence below 1000 A.U. were considered to represent negative signals.

into the microchambers. As the number of copies of target DNA was increased from 0 to 12 per chamber, the number of the microchambers with a positive fluorescence signal also increased. PCR amplification in almost the whole block of the chip was achieved by using eight (or 12) copies of the target DNA. When 0.4 copies of the target DNA were used, an average of 2 out of 60 chambers ($n = 3$) showed a signal above the threshold level (the average fluorescence intensity value of 1000 A.U. was determined as the threshold). The relatively high level of fluorescence recorded in these two chambers could also be visually detected. Since 0.4 copies of the target DNA were enough to give a readable signal, this concentration was determined as our limit-of-detection. The chambers with positive fluorescence signals, which indicated successful PCR amplification, showed easily distinguishable fluorescence intensity as shown in Figure 3.4(a). Figure 3.4(b) plots the average number of chambers with positive fluorescence signal vs. input template DNA copy number for the amplification of the RhD gene sequence. In agreement with the image of the chip, Figure 3.4(b) showed an almost linear increase in the number of fluorescence-positive microchambers as the number of target DNA copies increased.

After the amplification of 0.4 copies of target DNA, the fluorescence intensity of the microchambers was much lower in comparison with that for the other copy numbers, and almost all of the microchambers were within 800 to 1000 A.U.

These microchambers with low fluorescence intensity (representing the majority) were accepted as negative results, since they were below the threshold level. When 0.4 copies were dispensed, only two microchambers reached the 1000 to 1200 A.U. level. In agreement with the photograph of the chip block in Figure 3.4(a), where 0.4 copies were dispensed, these two microchambers with visibly high fluorescence were accepted as positive signals. This indicated the achievement of amplification of such a trace amount of DNA, as well as indicating the detection limit of our system. The fluorescence intensity greatly increased as the copy number reached 8 and 12. The number of chambers between 1200 and 1400 A.U. reached its maximum level with 12 copies, as the number of the microchambers with lower intensity decreased. Statistical data for the RhD analysis were also in agreement with the visual observation of the chip. The harmonic mean of the fluorescence data within 95% confidence intervals showed an almost linear form as the number of copies of target DNA increased. The harmonic distribution of the fluorescence data showed a concave bottoming at 4 copies, which was also supported by the plot of the variance vs. target DNA concentration. The highest variance from the mean fluorescence value was obtained when 4 copies of target DNA were used. The variance substantially decreased to 23.88 and 14.34 for 8 and 12 copies, respectively, indicating saturation of the fluorescence signals.

In particular, there were two important factors affecting the efficiency of PCR amplification when using DNA sample levels as low as 0.4 to 4 copies, and thus causing marked variations in the statistical data. First, the biochemical limitations resulting from the TaqMan PCR itself greatly affected the results of the end-point detection. The annealing temperature, $MgCl_2$ and polymerase concentrations, along with the concentrations of the specific primers and TaqMan probes, should be kept under optimal conditions in the 40-nL volume in the microchamber, which was a difficult task. The instrumental limitations also added to the inefficiency of the PCR, when such a small volume was manipulated on the microchamber array.

In order to evaluate the variations in the distribution of DNA samples using the dispensing system, we prepared a human male genomic DNA solution of known concentration, and then diluted it to obtain concentrations ranging from 0.4 to 12 copies per unit of desired volume. These DNA solutions were then interacted with PicoGreen reagent, which is a well-described fluorescent molecule for DNA quantitation. After the dispensation of these DNA samples onto the microchamber array, the fluorescence data indicated that there was still a difference in the mechanical distribution of these ideally prepared samples (data not shown). Although a linear increase in the number of fluorescence-positive microchambers over the threshold value was obtained as the DNA concentration was increased, not all of the microchambers showed the same fluorescence, as had been expected. At all DNA concentration levels, there was a high variance in the distribution of the DNA samples, which indicated our instrumental limitations.

One would have expected to observe 4 out of 10 microchambers to be positive and 6 to be negative if we had an average of 0.4 copies per microchamber and every copy was intact. However, the combined negative effects of biochemical and instrumental limitations along with the inhibitory effects of non-specific adhesion of biomaterials resulted in only 2 microchambers out of 60 displaying positive signals after TaqMan PCR in our system. However, a microchamber array chip provides the strong advantage of being able to increase the trial frequency, by using only specified "areas" of the chip. In order to quantify the DNA concentration, 16 to 60 microchambers were used as one region for only one specific concentration. Increasing the number of microchambers for checking the fluorescence signal of one concentration was not applicable to real-sample analysis, because the required amount of real-sample solution should have also been increased, which was not desirable in terms of cost-effectiveness and sensitivity. Thus, about 16 to 60 microchambers were used to determine the variations in the fluorescence signal for the dispensed target DNA at a specific concentration in our further studies, unless otherwise stated.

3.7 SPECIFIC SEQUENCE DETECTION FROM A SINGLE HUMAN CHROMOSOME-1 VIA NANOLITER-VOLUME PCR

First, the whole human metaphase chromosomes, which contained no cell membrane or cytoplasm, etc. [16,17], were distributed as template DNA into 48 microchambers using a nanoliter dispenser. After staining with SYBR Green I, the number of dispensed chromosomes in the chamber was counted using the fluorescence image (Figure 3.5[a]). The number of the dispensed chromosomes per chamber was 80.7 ± 9.4 (mean ± SD). PCR amplification was performed in each

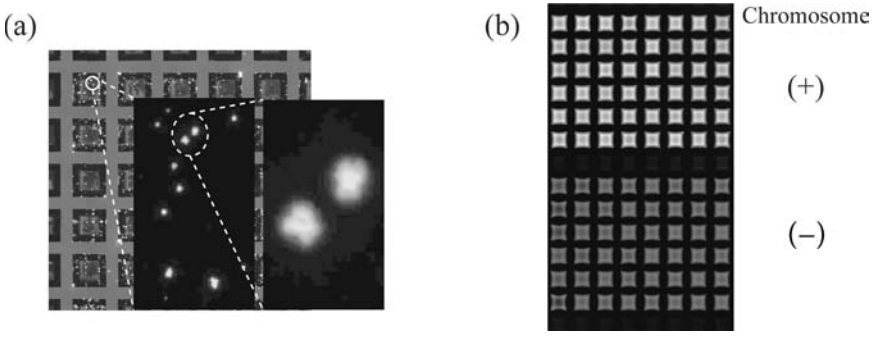

FIGURE 3.5 Microchamber array PCR amplification from whole human chromosomes. Whole human chromosomes as template DNA for PCR were dispensed into the microchambers using the nanoliter dispenser, and were stained with SYBR Green I (a). The number of dispensed chromosomes per microchamber was 80.7 ± 9.4 (mean ± SD). After PCR amplification with RhD gene-specific primers with the addition of fluorescence probe, positive signals were observed on the microchamber array with the chromosomes (b).

microchamber after dispensing the PCR solution including RhD gene-specific primers and fluorescence (TaqMan) probe. The fluorescence was detected using the DNA microarray scanner (Figure 3.5[b]). The chambers with chromosomes displayed high fluorescent signals compared with those without chromosomes. Thus, specific DNA amplification from chromosomes was possible on the microchamber chip.

We then attempted trace volume PCR amplification from a single chromosome using the microchamber. For the certain collection and distribution of a chromosome from the chromosome sample on the substrate to the microchamber, the tweezer-type probe, which was developed for the AFM manipulation described elsewhere (see Chapter 2), was suitable. Initially, chromosome-1 was peeled away from the substrate surface using a glass capillary, and was collected using the tweezer-type probe by closing with the applied voltage (Figure 3.6[a]). The positions of the glass capillary and the tweezer probe tips were controlled using the micromanipulator (Eppendorf, Switzerland), which was attached to the optical or metal surface microscope. The collected chromosome-1 was then released into the microchamber (Figure 3.6[b]) as the template DNA. One chromosome-1 only was placed into each of seven microchambers. After PCR amplification, positive signals were obtained from five microchambers (Figure 3.7). Thus, we had succeeded in the amplification of a specific gene, from a single-chromosome, in the microchamber chip.

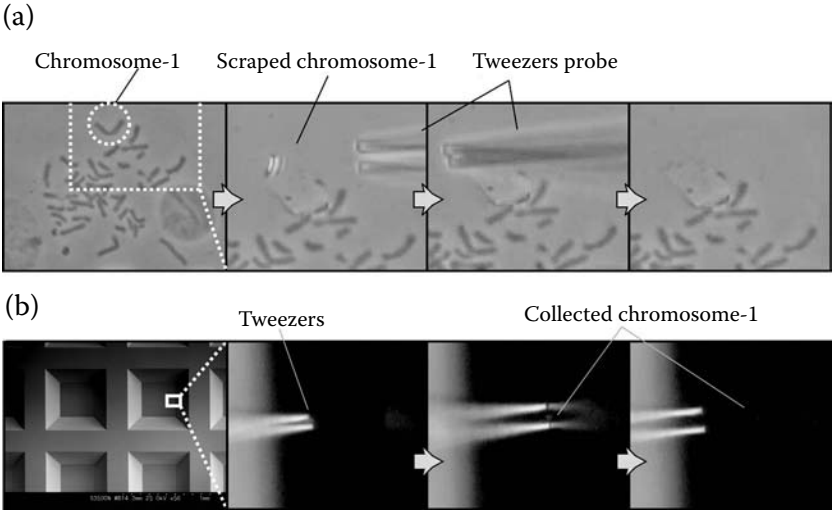

FIGURE 3.6 The collection and the rearrangement of chromosome-1 using the tweezers-type probe. Chromosome-1 was scraped away from the substrate using a glass capillary and was collected with tweezers which were closed by applying voltage (a). The tweezers' tip with the collected chromosome-1 was placed into the microchamber and was pressed onto the side wall of the chamber (b). The collected chromosome-1 was then released into the microchamber.

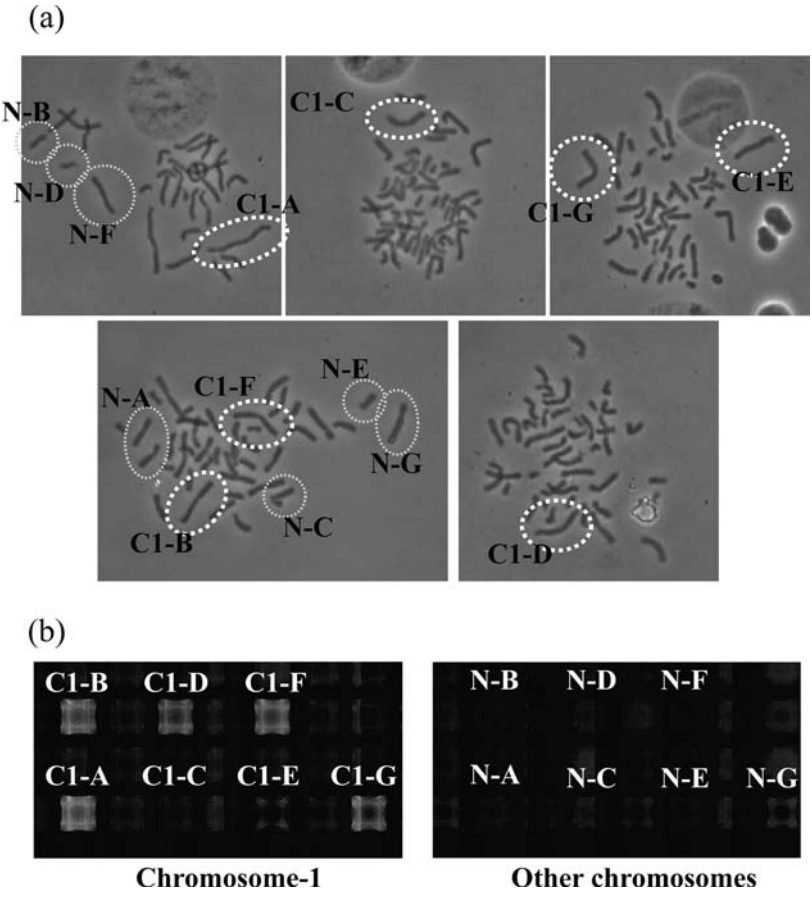

FIGURE 3.7 On-chip DNA amplification from a single chromosome-1. (a) Seven samples of chromosome-1 from C1-A to -G, which are indicated in the dashed circles, were collected with tweezers from the substrate and rearranged into each microchamber as shown in Figure 3.6(a). Other chromosomes from N-A to -G were negative controls. After PCR amplification of the RhD gene from the single chromosome-1, the fluorescence was imaged using an optical microscope with CCD camera (b). As a result, five positive signals in the seven chambers were obtained.

3.8 CONCLUSION

The microchamber array chip presented in this chapter could be used to amplify DNA targets in the RhD gene, in combination with a nanoliter dispenser. The minimum solution volume, which could be dispensed with reliability, was optimized at 40 nL for our experiments. We initially attained DNA amplification from purified human genomic DNA. Subsequently, we reported the successful amplification of a specific gene from a single chromosome, which was collected

and distributed into the microchamber using a tweezer-type probe under an optical microscope. Currently, efforts toward combination of the microchamber array PCR with AFM manipulation are in progress. In the future, it is expected that the analysis of a specific portion of not only a chromosome but also of other biological samples, e.g., cells, DNA, etc., could become possible using our established methods.

ACKNOWLEDGMENT

The authors gratefully acknowledge that this study was supported in part by a grant from the Special Coordination Funds for Promoting Science and Technology of the Ministry of Education, Culture, Sports, Science and Technology, the Japanese government.

REFERENCES

1. Sapolsky RJ, Hsie L, Berno A, Ghandour G, Mittmann M, Fan JB (1999) High-throughput polymorphism screening and genotyping with high-density oligonucleotide arrays. *Genet Anal* 14: 187–192.
2. Robinson WH, DiGennaro C, Hueber W, Haab BB, Kamachi M, Dean EJ, Fournel S, Fong D, Genovese MC, de Vegvar HE, Skriner K, Hirschberg DL, Morris RI, Muller S, Pruijn GJ, van Venrooij WJ, Smolen JS, Brown PO, Steinman L, Utz PJ (2002) Autoantigen microarrays for multiplex characterization of autoantibody responses. *Nat Med* 8: 295–301.
3. Jiang Y, Wang PC, Locascio LE, Lee CS (2001) Integrated plastic microfluidic devices with ESI-MS for drug screening and residue analysis. *Anal Chem* 73: 2048–2053.
4. Rishpon J (2002) Electrochemical biosensors for environmental monitoring. *Rev Environ Health* 17: 219–247.
5. Manz A, Granber N, Widmer HM (1990) Miniaturized total chemical analysis systems: a novel concept for chemical sensing. *Sens Actuators B* 1: 244–248.
6. Cheng J, Shoffner MA, Hvichia GE, Kricka LJ, Wilding P (1996) Chip PCR. II. Investigation of different PCR amplification systems in microfabricated silicon-glass chips. *Nucleic Acid Res* 24: 380–385.
7. Taylor TB, Winn-Deen ES, Picozza E, Woudenberg TM, Albin M (1997) Optimization of the performance of the polymerase chain reaction in silicon-based microstructures. *Nucleic Acid Res* 25: 3164–3168.
8. Daniel JH, Iqbal S, Millington RB, Moore DF, Lowe CR, Leslie DL, Lee MA, Pearce MJ (1998) Silicon microchambers for DNA amplification. *Sens Actuators A* 71: 81–88.
9. Nagai H, Murakami Y, Morita Y, Yokoyama K, Tamiya E (2001) Development of a microchamber array for picoliter PCR. *Anal Chem* 73: 1043–1047.
10. Matsubatra Y, Kobayashi M, Morita Y, Tamiya E (2002) Application of microchamber array for DNA amplification using a novel dispensing method. *Arch Histol Cytol* 65: 481–488.
11. Matsubatra Y, Kerman K, Kobayashi M, Yamamura S, Morita Y, Takamura Y, Tamiya E (2004) On-chip nanoliter-volume multiplex TaqMan polymerase chain reaction from a single copy based on counting fluorescence released microchambers. *Anal Chem* 76: 6434–6439.

12. Livak KJ, Flood SJ, Marmaro J, Giusti W, Deetz K (1995) Oligonucleotides with fluorescent dyes at opposite ends provide a quenched probe system useful for detecting PCR product and nucleic acid hybridization. *PCR Methods Appl* 4: 357–362.
13. Matsubatra Y, Kerman K, Kobayashi M, Yamamura S, Morita Y, Tamiya E (2005) Microchamber array based DNA quantification and specific sequence detection from a single copy via PCR in nanoliter volumes. *Biosens Bioelectron* 20: 1482–1490.
14. Saito M, Nakagawa K, Takekawa T, Yamanaka K, Takamura Y, Hashiguchi G, Tamiya E (2006) A single human chromosome manipulation and gene detection via trace volume PCR amplification using microtweezer probe and microchamber array, in: *Proc Micro Total Analysis System 2006*, Kitamori T, Fujita H, and Hasebe S, Eds. Society for Chemistry and Micro-Nano Systems (CHEMINAS), Tokyo: 1462–1464.
15. Turner MJ, Martin CM, O'Leary JJ (2003) Detection of fetal Rhesus D gene in whole blood of women booking for routine antenatal care. *Eur J Obstet Gynecol Reprod Biol* 108: 29–32.
16. Uchiyama S, Kobayashi S, Takata H, Ishihara T, Hori N, Higashi T, Hayashihara K, Sone T, Higo D, Nirasawa T, Takao T, Matsunaga S, Fukui K (2005) Proteome analysis of human metaphase chromosomes. *J Biol Chem* 280: 16994–17004.
17. Sone T, Iwano M, Kobayashi S, Ishihara T, Hori N, Takata H, Ushiki T, Uchiyama S, Fukui K (2002) Changes in chromosome structure by different isolation conditions. *Arch Histol Cytol* 65: 445–455.

4 On-Chip Chromosome Sorter Using Electric and Magnetic Fields

Takahito Inoue, Yasuyuki Fujita, Susumu Uchiyama, Tomoyuki Doi, Kiichi Fukui and Hiroshi Yokoyama*

CONTENTS

4.1 Introduction 43
4.2 Experimental Design 44
4.2.1 Device Fabrication 44
4.2.2 Human Chromosome Isolation 44
4.2.3 Chemical Treatment of Chromosomes 45
4.2.4 Magnetic Beads and Magnets 45
4.2.5 Instrumentation 46
4.3 Chromosome Sorting Using Voltage Modulation 46
4.4 Chromosome Sorting Using a Magnetic Field 49
4.5 Conclusion 51
Acknowledgment 51
References 51

4.1 INTRODUCTION

DNA from sorted chromosomes is suitable for construction of recombinant DNA libraries and for gene mapping. However, these studies require usable quantities of classified and purified chromosomal DNA. Conventional cell sorters (flow cytometers) have been widely used to study populations and DNA quantities of eukaryotic cells (see Chapter 12). Dual-beam, high-speed sorting based on cell sorters has been developed to facilitate purification of chromosomes by double-staining with two different types of dyes, Hoechst 3325 (Ho) and chromomycin A3 (CA3) [1]. The Ho and CA3 contents of individual chromosomes are determined by measuring the fluorescence intensities, since the water droplets including the double-stained samples pass the focused UV and laser beams in the flow

*To whom correspondence should be addressed.

chamber of the cell sorter. This method is based on measurement of fluorescence properties of the stained sample. However, this instrument is delicate, expensive, mechanically complex, and requires trained technicians for operation.

Recent trends in device miniaturization based on advanced semiconductor fabrication technology have led to the replacement of conventional cell sorters with microfluidic devices that perform sensitive optical detection, with easier setup and operation [2–5]. The potential merits of microfluidic devices include low sample volume, portability, automation, and parallel processing. Therefore, such miniaturized systems can provide economic benefits and reduce energy consumption for their operation. Other research groups have reported microfabricated sorting devices for sorting micron-sized latex beads [3], bacterial cells [4], and magnetic particles [5]. However, separation of chromosomes using such microfabricated sorting devices has not been reported so far. This is because the size distribution of chromosomes is very large, their shape is not spherical and they easily stick to the fluid channel walls due to their "cloggy" surface properties. In previous work, we described the design of microfluidics for chromosome manipulation and analysis of the behavior of chromosomes placed in DC and AC electric fields [6]. We suggested the possibility to realize chromosome sorting in microfluidic devices using a voltage modulation technique without gels or molecular sieving structures. Here, we demonstrate innovative sorting techniques using electric and magnetic fields for chromosome separation in disposable and inexpensive microfluidic devices.

4.2 EXPERIMENTAL DESIGN

4.2.1 Device Fabrication

The fabrication process of the microfluidic device is based on the replica-molding method of polydimethylsiloxane (PDMS) [7–9]. (100) P-type silicon wafers (Shin-Etsu Chemical Co., Japan) were used as substrate. The negative-type thick photoresist (THB120N; JSR Co., Japan) was spin-coated on the substrate. After pre-baking at 90°C for 5 min, optical lithography was carried out with a home-built maskless optical patterning system using a commercially available PC projector. After development, the fluidic mold was post-baked at 130°C for 5 min. Silicon elastomer (Silpot184; Dow Corning Co., U.S.A.) and hardening agent (Sylgard184 Curing Agent; Dow Corning Co., U.S.A.) were mixed at a ratio of 20:1 and poured onto the fluidic mold. After hardening it on a hot plate at 65°C for 1 h, PDMS was peeled off from the fluidic mold. The surface of the PDMS devices was modified by soaking in dilute hydrochloric acid solution (0.01 wt% in water) for 1 h at 70°C. After ultrasonic cleaning of the PDMS device in pure water, it was bonded onto a slide glass.

4.2.2 Human Chromosome Isolation

For human chromosome isolation, cell culture and synchronization of HeLa S3 cells were performed according to the previous report [10], except for the

concentration of fetal calf serum (10% for BALL-1 and 5% for HeLa S3). Chromosome isolation was carried out according to the method previously developed by Laemmli and Uchiyama et al. [11,12]. Cells were harvested at 20°C by centrifugation at 1500 *g* for 10 min, and washed three times at 20°C. Collected cells were hypotonically swollen in wash buffer (7.5 m*M* Tris, 40 m*M* KCl, 1 m*M* EDTA, 0.1 m*M* spermine, 0.25 m*M* spermidine, 1% thiodiglycol, and 0.1 m*M* PMSF) at 20°C. Hereinafter, unless stated otherwise, procedures for Percoll gradient chromosome isolation were performed at 4°C. Subsequently the cells were lysed with ice-cold lysis buffer (15 m*M* Tris, 80 m*M* KCl, 2 m*M* EDTA, 0.2 m*M* spermine, 0.5 m*M* spermidine, 1% thiodiglycol, 0.1 m*M* PMSF, and 0.1% empigen) on ice using a homogenizer, and the chromosomes were readily released. The lysate was layered over the exponential glycerol gradients which were centrifuged in a JS-24.38 rotor for 5 min at 200 *g*, followed by 15 min at 700 *g*. Fractions containing dispersed metaphase chromosomes were placed on the 70% glycerol cushion and centrifuged at 3000 *g* for 15 min to recover chromosomes. Chromosomes partially purified by the procedures described above were stored at –20°C in storage buffer (3.75 m*M* Tris, 20 m*M* KCl, 0.5 m*M* EDTA, 0.05 m*M* spermine, 0.125 m*M* spermidine, 1% thiodiglycol, 0.1 m*M* PMSF, and 0.1% empigen) containing 60% glycerol.

4.2.3 Chemical Treatment of Chromosomes

Isolated chromosomes were stained with the fluorescent dye YOYO-1 (Molecular Probes, U.S.A.). After incubating for 10 min at room temperature, carbobiotin (Seikagaku Co., Japan) solution of 2 μL was added to the chromosome solution. Since carbobiotin used as a biotin marker for nucleic acid has a carbodiimide basis (–N=C=N–), it reacts with thymine (uracil) and guanine in the nucleic acid. After incubating for 30 min at room temperature, the solution was centrifuged for 5 min at 430 *g* and the supernatant was removed. A superparamagnetic bead (see details in the following section) suspension of 2 μL and distilled water of 100 μL were added into the chromosome solution. After incubating for 15 to 30 min at room temperature, the suspension was washed three times with deionized water and was then filtered using a nylon mesh filter (20 μm pore size) to remove aggregates of chromosomes.

4.2.4 Magnetic Beads and Magnets

The superparamagnetic bead suspension (M-PVA SAV1, diameter of 1 μm, streptavidin coated, Chemagen Co., U.S.A.) was filtered using filter paper (No. 2, Advantec Co., Japan) to remove large particles over 2 to 3 μm, and was then filtered again using filter paper (No.5C; Advantec Co.) to remove particles of less than 0.8 μm. Fe_3O_4 superparamagnetic beads used in this study had a magnetic moment of 1.82fAm2 at 100 Oe [13]. Permanent SmCo magnets (cylindrical shape with a diameter of 3 mm and a thickness of 1.5 mm; Edmund Co., U.S.A.) were used to generate the magnetic field in the separation chamber of the microfluidic devices.

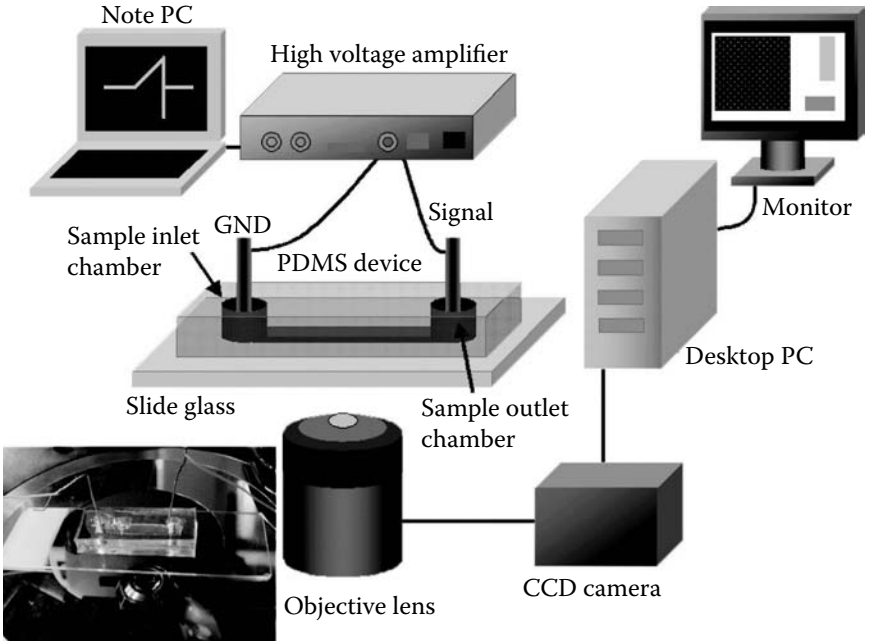

FIGURE 4.1 Schematic representation of the on-chip chromosome sorting apparatus using a voltage modulation technique. See the experimental apparatus section for details.

4.2.5 Instrumentation

A schematic representation of the on-chip chromosome sorting apparatus is shown in Figure 4.1. The chromosome sorting device was mounted on an inverted optical microscope (Axiovert 100; Carl Zeiss, Germany) with a long working distance objective (50×; Nikon Co., Japan). A 70-W Hg lamp (HBO 50; Carl Zeiss) with an excitation filter set was used as an excitation source. Fluorescent images were captured with a cooled CCD camera (iXon DV887 DSC-BV; Andor, U.S.A.) and directly recorded on a PC hard disk. Images were analyzed using the image processing software Image J (NIH, U.S.A.). A modulated voltage was synthesized by a note-style personal computer using a 12-bit digital–analog converter board (KPCMCIA 8AO-B; Keithley Instruments, U.S.A.) and amplified by a high voltage amplifier (M2647; Mess-Tec Co., Japan).

4.3 CHROMOSOME SORTING USING VOLTAGE MODULATION

For DNA separation, polyacrylamide gel electrophoresis is commonly used. In this method DNA molecules are separated by mobility depending on the length of the DNA molecules, since the random long-chain polymers in gels function as a molecular sieving matrix. However, there is no suitable polymer matrix for

sorting chromosomes much larger than DNA molecules. Here, we demonstrate on-chip chromosome sorting in a microfluidic device based on a voltage modulation method, instead of conventional capillary gel electrophoresis.

From a thin double-layer approximation, the electrophoretic mobility of a colloidal particle in steady-state flow can be expressed by Smoluchowski's formula [14],

$$u = \frac{\varepsilon_r \varepsilon_0}{\eta} \xi . \tag{4.1}$$

Here ξ is the zeta potential of the particle and η is the dynamic viscosity of the liquid, while ε_r and ε_0 are, respectively, the relative dielectric permittivity of the liquid and the dielectric permittivity of a vacuum. From this equation, one can see that the particle mobility is proportional to the zeta potential and dielectric properties, but does not depend on its shape and size. Let us now consider the primary moving situation, in which a charged spherical particle of radius R and charge q in a viscous fluid of viscosity η and density ρ now starts to move at time $t = 0$ with a constant acceleration α ($u = \alpha t$). The resistance force F_r exerted on a spherical particle at t can be expressed by [15]

$$F_r = 2\pi R^3 \alpha \left\{ \frac{\rho}{3} + \frac{3\eta t}{R^2} + \frac{6}{R}\sqrt{\frac{\eta \rho t}{\pi}} \right\}. \tag{4.2}$$

When the electric field strength E ($E = E_0 t$) proportional to time is applied to a sphere, the total force F exerted on a sphere is expressed by the sum of F_r and qE. Therefore, we can write

$$F = m\alpha = qE_0 t - 2\pi R^3 \alpha \left\{ \frac{\rho}{3} + \frac{3\eta t}{R^2} + \frac{6}{R}\sqrt{\frac{\eta \rho t}{\pi}} \right\}, \tag{4.3}$$

where m is the mass of a sphere, and we obtain

$$\alpha = \frac{qE_0 t}{m + \frac{2}{3}\pi\rho R^3 + 6\pi\eta R t + 12\pi R^2 \sqrt{\eta \rho t / \pi}} . \tag{4.4}$$

In our experimental conditions, each term from the first to the fourth in the denominator of Equation (4.4) has the order of 10^{-14}, 10^{-15}, 10^{-7}, and 10^{-11}, respectively. Since the third term now has the highest contribution and the other terms can be neglected, α can be expressed by

$$\alpha \sim \frac{qE_0}{6\pi\eta R} . \tag{4.5}$$

From this equation, it is clear that the particle acceleration is proportional to the charge of the particle and inversely proportional to its radius. Since we confirmed that there was no significant correlation between the mobility of a chromosome and its size in the steady electrophoretic flow in our previous experiments, we can expect that there is no significant charge difference among individual chromosomes of different sizes. Therefore, we expect that the chromosome mobility depends on its size when it is placed in a time-dependent electric field. In this study, a saw-tooth voltage pulse of $75V_{pp}$ with a raising time of 0.5 s, a falling time of 1/64 s and a delay time of 31/64 s was applied to two electrodes after sample injection into the sample inlet chamber (Figure 4.1). Chromosome sorting was typically performed for 30 min in a single batch process and we measured the chromosome size and number as a function of the distance from the sample inlet chamber. Chromosomes have their own particular and authentic shapes, which are not spherical. Therefore, in this study we defined the length along the long axis of the molecule as its size. Since the size distribution of human chromosomes is very large, sorted human chromosomes were classified into three groups depending on their size, as seen in the inset of Figure 4.2, in order to simplify the sorting results. The distribution ratio of the classified chromosomes as a function of the distance from the inlet chamber is summarized in Figure 4.2, after sorting about 370 chromosomes for 30 min. At a distance greater than 11 mm from the inlet chamber there are no chromosomes of large size (larger than 8 μm), and these appear at a distance of less than 10 mm. It is clear that the mobility of the smaller chromosomes is greater than that of the larger chromosomes, as expected

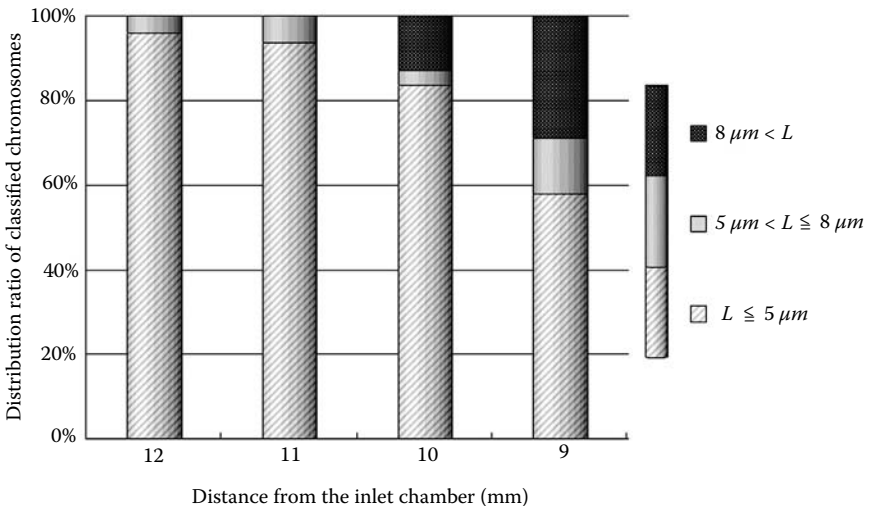

FIGURE 4.2 The distribution ratio of classified chromosomes sorted by voltage modulation as a function of the distance from the inlet chamber after 30 min of operation. The inset shows chromosomes classified into three groups depending on their size.

from Equation (4.5). This tendency seen in Figure 4.2 is highly reproducible, but clogging and aggregation of molecules during operation may reduce reproducibility and accuracy of sorting. To avoid these problems, we reduced the sample density for each run and the adhesive force between molecules and fluid surfaces.

4.4 CHROMOSOME SORTING USING A MAGNETIC FIELD

Here, we demonstrate continuous flow sorting of chromosomes using a magnetic field, which allows increased throughput and higher-speed operation compared to batch process sorting. The design of an on-chip chromosome sorter using a magnetic field is illustrated in Figure 4.3. A laminar flow from the inlet to outlet can be generated in the *x*-direction of the separation chamber, after the buffer and sample inlet reservoirs are filled with water. The permanent SmCo magnet is placed near the separation chamber, which generates a magnetic field gradient in the *y*-direction of the separation chamber (perpendicular to the direction of laminar flow). Chromosomes with superparamagnetic beads can be continuously

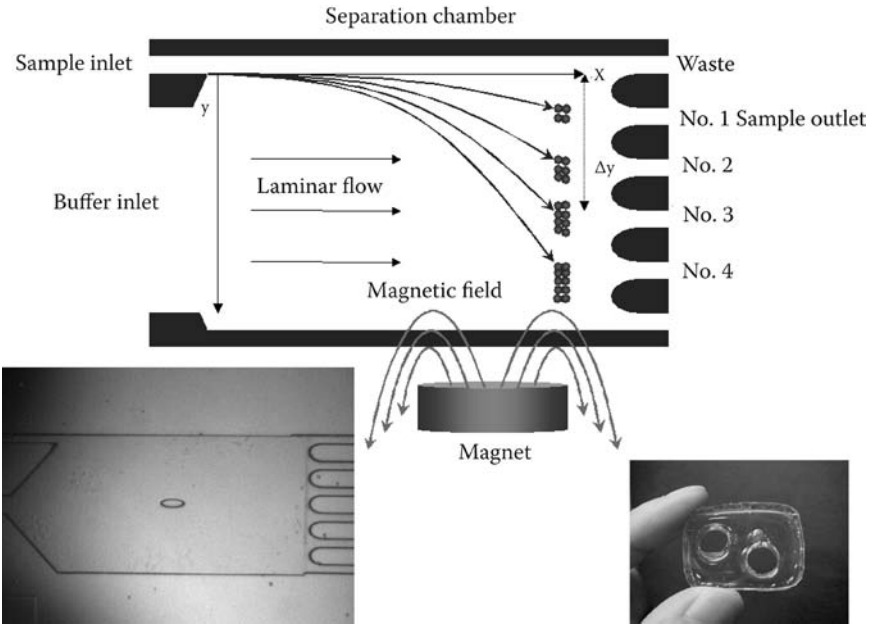

FIGURE 4.3 Principle of an on-chip chromosome sorter using a magnetic field. A laminar flow from the inlet to outlet can be generated in the *x*-direction of the separation chamber. The magnet is placed near the separation chamber and generates a magnetic field in the *y*-direction. Chromosomes with superparamagnetic beads can be continuously injected into the separation chamber and are dragged into the magnetic field against the laminar flow stream.

injected into the separation chamber from the sample inlet. Without the SmCo magnet, chromosomes can be moved straight to the outlet opposite the sample inlet along the laminar flow direction in the microfluidic channels. When the magnet is placed near the separation chamber, the superparamagnetic beads on the chromosomes become magnetized and are dragged into the magnetic field against the laminar flow stream. The magnetic force exerted on the magnetic bead by the external magnetic field is proportional to the magnetic bead volume and the difference in magnetic susceptibility between the bead and the fluid [16]. We confirmed by laser microscopic study that the number of magnetic beads adsorbed onto a chromosome was closely proportional to its size, for example, 10 to 11 beads on a 9-μm chromosome, 7 to 8 beads on a 7-μm chromosome and 3 to 4 beads on a 4-μm chromosome. Therefore, chromosomes of different sizes can be deflected from the direction of laminar flow to different degrees by the magnetic field, and the degree of deflection of a larger chromosome can be expected to be greater than that of a smaller one, as illustrated in Figure 4.3. The distribution ratio of classified chromosomes as a function of the sample outlet number after sorting about 330 chromosomes at a flow rate of 30 μm/s is summarized in Figure 4.4. As expected, chromosomes in the small-sized group (<5 μm) were not deflected, or the degree of deflection was very small, and followed the laminar flow to enter the waste or outlet No. 1, as seen in Figure 4.4. Chromosomes in the large-sized group (>8 μm) were deflected toward outlet No. 1 to No. 4, and the distribution ratio was increased at outlet No. 3 to No. 4, away from the sample waste. Not all the same groups entered the same outlet, but it is clear that the larger-size group tends to exhibit a larger degree of deflection.

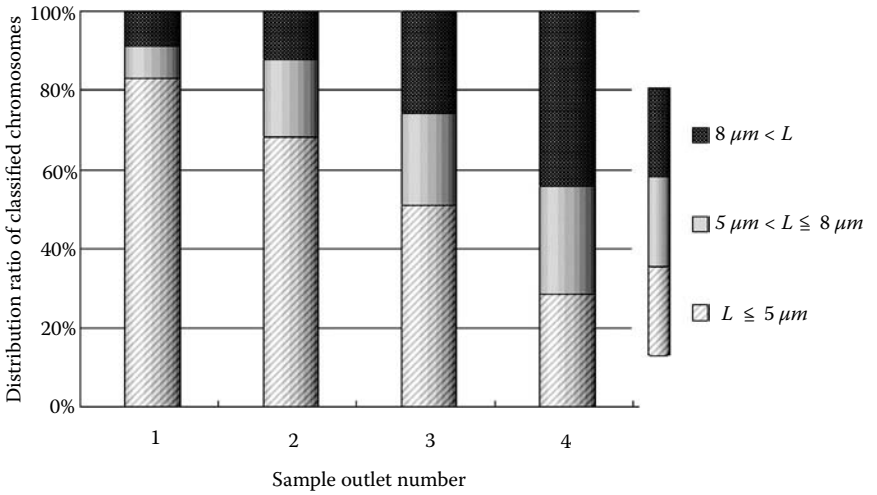

FIGURE 4.4 The distribution ratio of classified chromosomes sorted via the magnetic field as a function of the sample outlet number at a flow rate of 30 μm/s.

4.5 CONCLUSION

In this work, we demonstrated innovative sorting techniques using electric and magnetic fields for chromosome separation, in disposable and inexpensive microfluidic devices. Although further studies to improve sorting accuracy and throughput in these devices are now in progress, we expect that the sorting techniques presented here can be utilized in micro total analytical systems or "lab-on-a-chip" for many areas in biochemical analysis.

ACKNOWLEDGMENT

This study was supported by Special Coordination Funds of the Ministry of Education, Culture Sports, Sciences and Technology of the Japanese government.

REFERENCES

1. Gray JW, Dean P, Fuscoe JC, Peters DC, Trask BJ, van den Engh GJ, van Dilla MA (1987) High-speed chromosome sorting. *Science* 238: 323–329.
2. Chou HP, Spence C, Scherer A, Quake S (1999) A microfabricated device for sizing and sorting DNA molecules. *Proc Natl Acad Sci USA* 96: 11–13.
3. Fu AY, Spence C, Arnold FH, Quake SR (1999) A microfabricated fluorescence-activated cell sorter. *Nat Biotechnol* 17: 1109–1111.
4. Fu AY, Chou HP, Spence C, Arnold FH, Quake SR (2002) An integrated microfabricated cell sorter. *Anal Chem* 74: 2451–2457.
5. Pamme N, Manz A (2004) On-chip free-flow magnetophoresis: continuous flow separation of magnetic particles and agglomerates. *Anal. Chem* 76: 7250–7256.
6. Inoue T, Takahashi K, Yokoyama H (2002) Integrated microfluidics for chromosome engineering — preparation, transportation and manipulation. *Arch Histol Cytol* 65: 465–471.
7. Delamarche E, Bernard A, Schmid H, Michel B, Biebuyck H (1997) Patterned delivery of immunoglobulins to surfaces using microfluidic networks. *Science* 276: 779–781.
8. Effenhauser CS, Bruin GJM, Paulus A, Ehrat M (1997) Integrated capillary electrophoresis on flexible silicone microdevices: analysis of DNA restriction fragments and detection of single DNA molecules on microchips. *Anal Chem* 69: 3451–3457.
9. Duffy DC, McDonald JC, Schueller OJA, Whitesides GM (1998) Rapid prototyping of microfluidic systems in poly(dimethylsiloxane). *Anal Chem* 70: 4974–4984.
10. Uchiyama S, Kobayashi S, Takata H, Ishihara T, Sone T, Matsunaga S, Fukui K (2004) Protein composition of human metaphase chromosomes analyzed by two-dimensional electrophoreses. *Cytogenet Genome Res* 107: 49–54.
11. Lewis C, Laemmli U (1982) Higher order metaphase chromosome structure: evidence for metalloprotein interactions. *Cell* 29: 171–181.
12. Uchiyama S, Kobayashi S, Takata H, Ishihara T, Hori N, Higashi T, Hayashihara K, Sone T, Higo D, Nirasawa T, Takao T, Matsunaga S, Fukui K (2005) Proteome analysis of human metaphase chromosomes. *J Biol Chem* 280: 16994–17004.
13. Panhorst M, Kamp PB, Reiss G, Brückl H (2005) Sensitive bondforce measurements of ligand–receptor pairs with magnetic beads. *Biosens Bioelectron* 20: 1685–1689.

14. Delgado A (2002) Interfacial electrokinetics and electrophoresis. *Surfactant Science Series*, 106. Marcel Dekker, Inc., New York.
15. Landau LD, Lifshitz EM (1987) *Fluid Mechanics*, 2nd ed. Course of Theoretical Physics, Volume 6, Butterworth-Heinemann, Oxford.
16. Hatch GP, Stelter RE (2001) Magnetic design considerations for devices and particles used for biological high-gradient magnetic separation (HGMS) systems. *J Magn Mater* 225: 262–276.

5 Fluorescence Microscopy for Analysis of Chromosome Dynamics

Sachihiro Matsunaga

CONTENTS

5.1 Introduction 53
5.2 Microscopic Systems for Analysis of Chromosome Dynamics 54
5.3 Analysis of Chromosome Dynamics Using Histone H1 Fused with GFP 55
5.4 Analysis of Chromosome Dynamics Using Aurora Kinase Fused with GFP 58
5.5 Conclusion and Perspectives 60
Acknowledgments 61
References 61

5.1 INTRODUCTION

Imaging of chromosomes in fixed cells provides only indirect information on chromosome dynamics. In addition, fixation of cells sometimes causes an artificial distortion of chromosome distribution. Hence, the complex dynamics of chromosomes during cell division can only be addressed through direct analysis of live cells. Two-dimensional time-lapse recordings of live cells have been widely used for the investigation of chromosome dynamics, and recent advances in z-stack projection techniques mean that we can now easily acquire a series of optical sections through the specimen. In particular, confocal microscopy and deconvolution methods have enabled high-speed and automated three-dimensional analyses [1].

One of the best approaches for labeling chromosomes in living cells is the fluorescent tagging of chromosomal proteins. For example, fluorescent labeling of mammalian chromosomes in living cells has been demonstrated using Hoechst 33342; however, the exposure time and concentration of Hoechst 33342 used in

this staining method must be individually optimized in different cell types in order to enable observation. Moreover, a high intensity of ultraviolet (UV)-light irradiation is required for excitation of Hoechst 33342, which often damages living cells and causes cell cycle arrest. In contrast, constitutive expression of green fluorescent protein (GFP) fused with chromosomal proteins enables long-term analyses without perturbing chromosome dynamics. GFP from the jellyfish *Aequorea victoria* retains its fluorescent properties when recombinant GFP fusion proteins are expressed in eukaryotic cells [2], and the blue light for excitation is less damaging than the above-mentioned UV-light excitation needed for Hoechst 33342. Despite the large size of the GFP tag (239 amino acids), GFP-tagged proteins have been shown to be functional and correctly localized in the cells expressing these recombinant proteins [3].

Because GFP and its variant fusion proteins enable observations of chromosomes in their native state without fixation and permeabilization, which causes artificial distortion of chromosomes, they have been widely used to visualize chromosome dynamics in live cells. The use of fluorescent proteins for visualization of chromosome dynamics is also especially useful for evaluating the effects of medicines or chemicals on cell division. This review will introduce our results on dynamic analysis of chromosomes using fluorescent microscopic techniques with fluorescent proteins.

5.2 MICROSCOPIC SYSTEMS FOR ANALYSIS OF CHROMOSOME DYNAMICS

Imaging of chromosomes in dividing cells requires special precautions because the cells must be maintained in a healthy state with normal functioning on the microscope stage, and this is the most critical factor in successful analysis. For this purpose, the environment, including temperature, gas concentration and humidity, must be controlled in the chamber. For example, mammalian cell lines require a carbon dioxide and bicarbonate buffer system for cultivation because they must be kept in an atmosphere containing 5 to 7% carbon dioxide. Accordingly, simple glass slides are not suitable for light microscopy dynamic analysis of live cells because it is difficult to control the environment around the cells. Plastic dishes for cell culture are also not suitable for fluorescent microscopy because of problems related to autofluorescence, the basal thickness and the flat level of dishes. Therefore, a special chamber system which can be equipped on the microscope stage is widely used (Figure 5.1).

It is true that, in short-term dynamic analyses of up to approximately 2 h, 10 to 20 m*M* 4-(2-hydroxyethyl)-1-piperazineethanesulfonic acid (HEPES) buffer can be used to control pH and the observation is usually performed in the absence of a chamber. However, long-term experiments are usually performed using a chamber specifically designed to maintain culture growth conditions close to the optimum for an extended period of time. The imaging chamber used in the present study has a thin glass window, through which chromosome dynamics can be

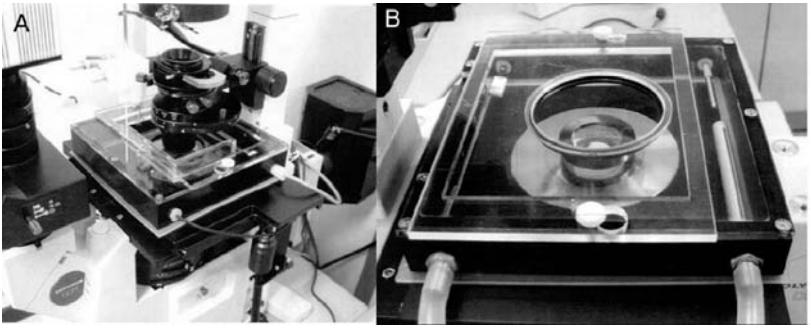

FIGURE 5.1 A microscopic chamber used for dynamic analyses. This chamber is set on the stage of an inverted fluorescent microscope (a). A temperature sensor is present in the upper left corner of the chamber and a gas concentration sensor is in the upper right corner. Two tubes for gas flow originate from the side where a gas concentration sensor is present (b). The samples are placed in a plastic dish which is present in the center of the chamber.

viewed with an objective lens and high numerical aperture (MI-IBC, Olympus, Japan). Temperature control (usually 28 to 37°C) is achieved using a peripheral source of heated air as well as a metal heating plate.

5.3 ANALYSIS OF CHROMOSOME DYNAMICS USING HISTONE H1 FUSED WITH GFP

The first analysis of chromosome dynamics in mammalian cells was performed using HeLa cells expressing a histone H2B-GFP fusion protein [4]. In these cells, H2B-GFP is incorporated into nucleosomes, and this does not inhibit cell cycle progression. The mitotic index and growth rate in this cell line were also similar to those of the original HeLa cells.

To our current knowledge, almost all nucleosomes in most eukaryotes contain at least one molecule of the linker histone H1. Histone H1 binds at the nucleosomal dyad axis and interacts with the linker DNA. However, the precise location of histone H1 in chromatin remains unknown [5]. This is partly because H1 molecules are in constant motion and their nucleosome interactions are temporary. Some researchers have claimed that although histone H1 migrates and redistributes, it is bound to chromosomes for most of the time [6,7]. A recent study also revealed that, although depletion of histone H1 alters the global chromatin structure, the expression of only a small number of genes is affected [8]. The above characteristics indicate that GFP-histone H1 is useful for analysis of chromosome dynamics. In the following paragraphs, I will show examples of analyses of chromosome dynamics in the human cultured HeLa cell line and tobacco cultured BY-2 (*Nicotiana tabacum* cv. Bright Yellow-2) cell line, which were conducted in our laboratory.

HeLa cells were transfected with a plasmid expressing the GFP-histone H1.2 fusion gene under the control of the cytomegalovirus promoter. Approximately 10% of colonies growing in the presence of antibiotic G418 showed GFP autofluorescence, and the brightest clone was selected for further study. Cells were seeded at an average density of 1.7×10^5 cells in a 35-mm glass-bottomed dish (Matsunami, Japan) and incubated for 48 h. Prior to observation, the growth medium was replaced with 50 mL of a time-lapse observation medium composed of phenol red-free Dulbecco's modified Eagle's medium (DMEM) (Gibco 11054-020), 20 m*M* HEPES (Sigma), 4 m*M* l-glutamine, penicillin (100 U/mL), streptomycin (0.1 μg/mL) and 10% fetal bovine serum. The time-lapse observations were performed using a live imaging system consisting of an inverted microscope (Olympus IX71, Japan) equipped with a cooled CCD camera (CoolSnap; Photometrics, Inc., U.S.A.). Metamorph image processing software (v.6.2r6; Universal Imaging Corporation, Inc., U.S.A.) was used, and a microscopic chamber (MI-IBC, Olympus) that kept the ambient temperature of the cells at an optimum of 37°C was also used. At least 100 phase-contrast and GFP fluorescence images (16-bit, 1024 × 860 pixels) were simultaneously obtained for each time-lapse observation. Time-lapse images of dividing cells were then isolated and converted to time-sequential stacks using the Metamorph software.

In the time-lapse images, the GFP-histone H1.2 fusion proteins were colocalized with DNA throughout the cell cycle (Figure 5.2) because the fluorescence was always associated with chromatin and chromosomes. In addition, in our studies using the chromosome spreads, the distribution of the fusion proteins was overlapped with the Hoechst 33342 staining patterns. To ascertain the *in vivo* expression level of the chimera protein, we also performed immunoblotting using an anti-histone H1 monoclonal antibody [9,10] and an anti-GFP polyclonal antibody (Roche, Germany). The GFP-histone H1.2 fusion protein was clearly detected in the lysate of the transfectant, and the immunoblotting analysis revealed that the expression level of the fusion protein was sufficiently lower than that of endogenous histone H1. The results of indirect immunofluorescence staining using the anti-histone H1 monoclonal antibody indicated that the localization and dynamics of GFP-histone H1 protein were the same as those of endogenous histone H1, suggesting that HeLa GFP-histone H1.2 can be used for dynamic analysis of mitotic chromosomes.

In the case of tobacco cultured BY-2 cells, transformation was performed using *Agrobacterium tumefaciens*, EHA101, with a binary vector containing the GFP-histone H1 fusion gene under the control of the 35S cauliflower mosaic virus promoter [11,12]. An aliquot of 3-day-old BY-2 cells was inoculated with an overnight culture of transformants grown on YEB media [13]. After a 3-day incubation at 25°C, the cells were washed three times in 5 mL Linsmaier-Skoog (LS) medium [13], and then transferred to liquid LS medium containing 500 mg/L carbenicillin and 50 mg/L hygromycin. The resulting transformed cell lines were maintained by 33-fold dilutions with culture medium at weekly intervals. For time-lapse observations, 3-day-old BY-2 transformants were transferred to

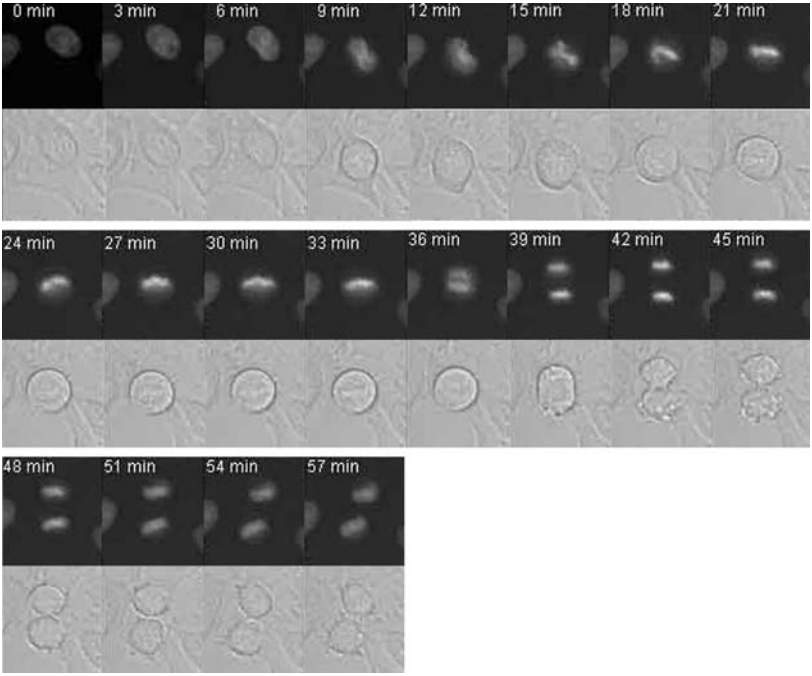

FIGURE 5.2 Dynamic analysis of human mitotic chromosomes by fluorescence microscopy. Nuclei and mitotic chromosomes in a human HeLa cell line were visualized as bright signals by histone H1.2 fused with GFP. Time-lapse fluorescent images, as well as phase-contrast images of the same portion, were obtained every 3 min. Dynamic analyses were performed in DMEM with HEPES at 37°C in 5% CO_2 under the microscopic chamber.

Φ35 mm Petri dishes with Φ14 mm coverslip windows on the bottom (Matsunami). The dishes were placed onto the inverted platform of a fluorescence microscope and cells were examined with a ×20 oil immersion lens. Phase-contrast and GFP images were collected every 3 or 5 min, exported as TIFF files and further processed with Adobe Photoshop (version 7.0). The time-lapse studies of the BY-2 cells also showed that the GFP-histone H1 fusion proteins were expressed throughout the nucleus in interphase and localized in chromosomes during cell division (Figure 5.3).

In plant cells, chromosome dynamic analyses using fluorescent protein have been reported with histone H2B-GFP in *Arabidopsis thaliana* [14]. A previous report suggests that the plant histone H1 is relatively dissimilar to its mammalian counterpart [15]; however, our result shows that plant histone H1 accumulated into chromosomes, and is also suitable for analyzing the dynamic movement of mitotic chromosomes.

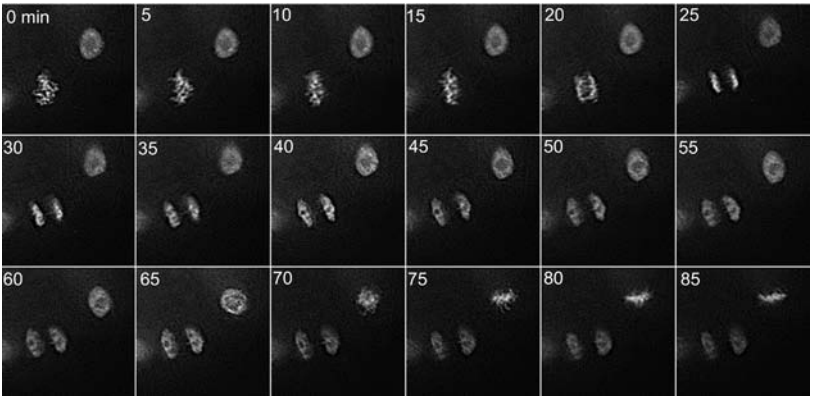

FIGURE 5.3 Dynamic analysis of mitotic chromosomes of plant cells (tobacco BY-2 cell line) by fluorescence microscopy. Nuclei and mitotic chromosomes in two cells were visualized by histone H1 fused with GFP. Time-lapse fluorescent images were obtained every 1 min. Dynamic analyses were performed using BY-2 cells in LS medium at 25°C. The image at 0 min shows a prometaphase cell in the lower left and an interphase cell in the upper right. The lower cell from 20 to 35 min is at anaphase. The upper cell enters mitosis at 65 min.

5.4 ANALYSIS OF CHROMOSOME DYNAMICS USING AURORA KINASE FUSED WITH GFP

Aurora kinases belong to the cell cycle–dependent serine/threonine protein kinase family, which is involved in regulation of several mitotic events [16]. The type and the number of Aurora kinases are known to be different depending on species. For example, while yeast has only one Aurora kinase gene in its genome, animal species have two, Aurora A and B. Moreover, mammalian species such as humans and mice have been shown to have an additional Aurora kinase designated Aurora C, which is specifically expressed in the testis.

Members of the Aurora kinase family show high sequence similarity of more than 60% at the amino acid level, particularly in the kinase domain; however, they differ in their localization and function. Aurora B localizes at the centromeres from prophase to metaphase, then relocates to the spindle midbody during anaphase and until cytokinesis. Aurora B is a chromosomal passenger protein that interacts with INCENP, Survivin, and Borealin/Dasra B to form a chromosomal passenger complex [17]. These proteins are necessary for localization of Aurora B, and consequently for regulation of kinetochore formation, chromosome segregation, and cytokinesis. Aurora-B phosphorylation of histone H3 at Ser10 and Ser28 is considered to be the fundamental role of Aurora B in chromosome segregation and cytokinesis [18].

In the *A. thaliana* genome, three deduced amino acid sequences showed high similarity to those of animal Aurora kinase genes [19,20]. Moreover, the kinase domain of these three deduced proteins showed more than 60% similarity to those of animal and yeast Aurora kinases. These three genes were designated *AtAUR1* (*A. thaliana* Aurora kinase)*/AtAurora1*, *AtAUR2/AtAurora2*, and *AtAUR3/AtAurora3*. Recently, dynamic analysis of GFP-fused AtAUR proteins was performed using tobacco BY-2 cells [19]. We also established BY-2 cells expressing GFP-fused AtAUR proteins and observed the dynamic events of the proteins during cell division. The GFP fusion constructs were prepared using Gateway technology, and vectors expressing the C-terminal GFP fusion protein were constructed. The destination vector was a binary vector designed for producing GFP fusion proteins (pGWB5). The tobacco BY-2 cells were transformed using the constructed binary vectors as described above and transformed cells were selected using hygromycin (final concentration: 7.5 μg/mL). The stable cell lines obtained with GFP-fused proteins were transferred to Petri dishes with poly-l-lysine-coated coverslips on the bottom (Matsunami). The dishes were then placed onto the platform of an inverted fluorescence microscope equipped with a cooled CCD camera system, and time-lapse observations were carried out by taking images at 1-min intervals.

Figure 5.4 shows the results of dynamic analysis of AtAUR3 in tobacco BY-2 cells. Fluorescence for AtAUR3 was localized at the nuclear periphery during interphase, and at prophase, dot-like signals appeared when the chromosomes began to condense. At prometaphase, the signals moved to the metaphase plates

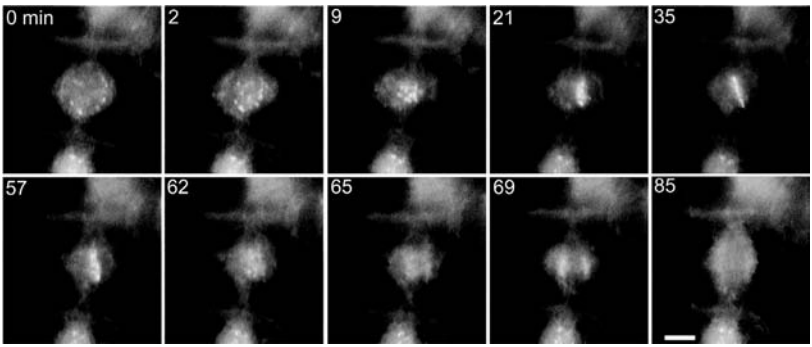

FIGURE 5.4 Dynamic analysis of a plant Aurora kinase in cultured mitotic tobacco BY-2 cells transformed with AtAUR3-GFP. Time-lapse fluorescent images were obtained every 1 min. The numbers indicate time in minutes since the first stage. The scale bar represents 10 μm. The image at 0 min shows a prophase cell in the center. Images at 2 and 9 min indicate prometaphase cells. Images from 21 to 57 min show metaphase cells. After anaphase, the AtAUR3-GFP signals are localized again around the nuclei as shown in the image at 85 min.

along with the condensed chromosomes, and at metaphase, they aligned in the center of the metaphase plates. However, at anaphase, AtAUR3 signals were almost evenly distributed over the entire chromosome, in accordance with chromosome segregation. After cell division, the AtAUR3 signals returned to the nuclear membrane and the cytoplasm around the nucleus. The localization of AtAUR3 we observed during mitosis was the same as that of histone H3 phosphorylated at Ser10 and 28 [21].

Dot-like signals on the chromosomes between prophase and metaphase have also been reported in the case of yeast Aurora kinases and animal Aurora B kinases [22–24]. In these studies, the dot-like signals are located on the centromeres, suggesting that Aurora B regulates the formation and cohesion of kinetochores in animals [23,25]. In our dynamic analysis of BY-2 cells, AtAUR3 was also located along the metaphase plate, strongly suggesting that it is localized on centromeres between prophase and metaphase. When AtAUR3 was limited in distribution at the early mitotic phase, its localization pattern was similar to that of Aurora B. However, after metaphase, AtAUR3 was ubiquitously located on the chromosomes, while animal Aurora B is known to remain at the metaphase plate to regulate cytokinesis [22,26]. In conclusion, our dynamic analyses of a plant Aurora kinase clearly show that Aurora kinase is useful for detecting the centromeric region of mitotic chromosomes.

Although GFP offers significant advantages during dynamic analyses of chromosomal proteins, attention should also be paid to potential artifacts. For example, overexpression of GFP fusion proteins sometimes affects real dynamics or functioning of the target protein during expression using a native promoter. Confirmation of dynamic analyses of chromosomal proteins should therefore be performed with immunostaining using an antibody against the target protein.

5.5 CONCLUSION AND PERSPECTIVES

The recent development of GFP variants — cyan fluorescent protein, yellow fluorescent protein, etc. — and novel fluorescent proteins has resulted in dramatic progress in dynamic analysis of chromosomal proteins. Therefore, dynamic analyses using multiple fluorescent proteins are expected to be successfully applied to analyses of chromosome dynamics. In addition, various advanced methods for fluorescence microscopy have been introduced for analysis of the dynamic events in live cells; they include fluorescence recovery after photobleaching, fluorescence correlation spectroscopy and fluorescence resonance energy transfer. The application of such new techniques to chromosomal research will also provide us with further information important for analyzing the events of chromosome dynamics including chromosome condensation, alignment, segregation and decondensation. In particular, analysis of chromosomal proteins based on these techniques will contribute to the development of quantitative hypotheses or simulation models for the molecular mechanisms, ideally reflecting the *in vivo* dynamics of chromosomes.

ACKNOWLEDGMENTS

This review includes results of studies conducted in collaboration with members of the laboratory of Dynamic Cell Biology, Department of Biotechnology, Graduate School of Engineering, Osaka University. I would like to thank all members of the laboratory for their critical comments, suggestions and assistance.

REFERENCES

1. McNally JG, Karpova T, Cooper J, Conchello JA (1999) Three-dimensional imaging by deconvolution microscopy. *Methods* 19: 373–385.
2. Chalfie M, Tu Y, Euskirchen G, Ward WW, Prasher DC (1994) Green fluorescent protein as a marker for gene expression. *Science* 263: 802–805.
3. Rizzuto R, Carrington W, Tuft, RA (1998) Digital imaging microscopy of living cells. *Trends Cell Biol* 8: 288–292.
4. Kanda T, Sullivan, KF, Wahl, GM (1998) Histone-GFP fusion protein enables sensitive analysis of chromosome dynamics in living mammalian cells. *Curr Biol* 26: 377–385.
5. Thomas JO (1999) Histone H1: location and role. *Curr Opin Cell Biol* 11: 312–317.
6. Bustin M, Catez F, Lim JH (2005) The dynamics of histone H1 function in chromatin. *Mol Cell* 17: 617–620.
7. Catez F, Ueda T, Bustin M (2006) Determinants of histone H1 mobility and chromatin binding in living cells. *Nat Struct Mol Biol* 13: 305–310.
8. Fan Y, Nikitina T, Zhao J, Fleury TJ, Bhattacharyya R, Bouhassira EE, Stein A, Woodcock CL, Skoultchi AI (2005) Histone H1 depletion in mammals alters global chromatin structure but causes specific changes in gene regulation. *Cell* 123: 1199–1212.
9. Higashi T, Miyakawa S, Uchiyama S, Matsunaga S, Takata H, Fujimoto S, Noda M, Terauchi A, Shimizu T, Oda M, Azuma T, Fukui K (2005) Generation of monoclonal antibodies against chromosomal antigens that have a high sequence similarity between human and mouse. *J Biotechnol* 120: 262–272.
10. Uchiyama S, Kobayashi S, Takata H, Ishihara T, Hori N, Higashi T, Hayashihara K, Sone T, Higo D, Nirasawa T, Takao T, Matsunaga S, Fukui K (2005) Proteome analysis of human metaphase chromosomes. *J Biol Chem* 280: 16994–17004.
11. Fujimoto S, Matsunaga S, Yonemura M, Uchiyama S, Azuma T, Fukui K (2004) Identification of a novel plant MAR DNA binding protein localized on chromosomal surfaces. *Plant Mol Biol* 56: 225–239.
12. Fujimoto S, Yonemura M, Matsunaga S, Nakagawa T, Uchiyama S, Fukui K (2005) Characterization and localization analysis of Arabidopsis condensin subunits, AtCAP-H and AtCAP-H2. *Planta* 222: 293–300.
13. Nagata T, Nemoto Y, Hasezawa S (1992) Tobacco BY-2 cell line as the "HeLa" cell in the cell biology of higher plants. *Int Rev Cytol* 132: 1–30.
14. Boisnard-Lorig C, Colon-Carmona A, Bauch M, Hodge S, Doerner P, Bancharel E, Dumas C, Haseloff J, Berger F (2001) Dynamic analyses of the expression of the HISTONE::YFP fusion protein in Arabidopsis show that syncytial endosperm is divided in mitotic domains. *Plant Cell* 13: 495–509.
15. Gantt JS, Lenvik TR (1991) *Arabidopsis thaliana* H1 histones. Analysis of two members of a small gene family. *Eur J Biochem* 202: 1029–1039.

16. Carmena M, Earnshaw WC (2003) The cellular geography of aurora kinases. *Nat Rev Mol Cell Biol* 4: 842–854.
17. Vagnarelli P, Earnshaw WC (2004) Chromosomal passengers: the four-dimensional regulation of mitotic events. *Chromosoma* 113: 211–222.
18. Goto H, Yasui Y, Nigg EA, Inagaki M (2002) Aurora-B phosphorylates Histone H3 at serine28 with regard to the mitotic chromosome condensation. *Genes Cells* 7: 11–17.
19. Kawabe A, Matsunaga S, Nakagawa K, Kurihara D, Yoneda A, Hasezawa S, Uchiyama S, Fukui K (2005) Characterization of plant Aurora kinases during mitosis. *Plant Mol Biol* 58: 1–13.
20. Demidov D, Van Damme D, Geelen D, Blattner FR, Houben A (2005) Identification and dynamics of two classes of aurora-like kinases in Arabidopsis and other plants. *Plant Cell* 17: 836–848.
21. Kurihara D, Matsunaga S, Kawabe A, Fujimoto S, Noda M, Uchiyama S, Fukui K (2006) Aurora kinase is required for chromosome segregation in tobacco BY-2 cells. *Plant J* 48: 572–580.
22. Adams RR, Maiato H, Earnshaw WC, Carmena, M (2006) Essential roles of *Drosophila* inner centromere protein (INCENP) and aurora B in histone H3 phosphorylation, metaphase chromosome alignment, kinetochore disjunction, and chromosome segregation. *J Cell Biol* 153: 865–880.
23. Giet R, Glover DM (2001) *Drosophila* aurora B kinase is required for histone H3 phosphorylation and condensin recruitment during chromosome condensation and to organize the central spindle during cytokinesis. *J Cell Biol* 152: 669–682.
24. Murata-Hori M, Tatsuka M, Wang YL (2002) Probing the dynamics and functions of Aurora B kinase in living cells during mitosis and cytokinesis. *Mol Biol Cell* 13: 1099–1108.
25. Kaitna S, Mendoza M, Jantsch-Plunger V, Glotzer M (2002) The aurora B kinase AIR-2 regulates kinetochores during mitosis and is required for separation of homologous chromosomes during meiosis. *Curr Biol* 12: 798–812.
26. Kaitna S, Pasierbek P, Jantsch M, Loidl J, Glotzer M (2000) INCENP and an aurora-like kinase form a complex essential for chromosome segregation and efficient completion of cytokinesis. *Curr Biol* 10: 1172–1181.

6 Fluorescence *In Situ* Hybridization (FISH) as a Tool for Comparative Genomics: Application of FISH to Studies of Chromosome Evolution in Vertebrates

Yoichi Matsuda, Mami Shibusawa, Kazumi Matsubara and Chizuko Nishida-Umehara*

CONTENTS

6.1 Introduction 64
6.2 Application of Direct R-Banding FISH to Chromosome Mapping 64
6.3 Construction of Comparative Cytogenetic Maps with EST Clones in Map-Poor Animals 65
6.4 Identification of Chromosomal Homology between Different Species by Comparative Chromosome Painting (Zoo-FISH) 69
6.5 Delineation of the Process of Chromosome Rearrangements and of the Ancestral Karyotypes 71
6.6 Investigation of GC Heterogeneity and Genome Compartmentalization Based on Comparative Cytogenetic Maps 73
6.7 Conclusions 75
Acknowledgment 76
References 76

*To whom correspondence should be addressed.

6.1 INTRODUCTION

Fluorescence *in situ* hybridization (FISH) is a powerful technique for localizing cloned DNA probes directly onto metaphase chromosomes and/or interphase nuclei [1,2]. This technique is a prerequisite tool for genome analysis, and the high topographic resolution of FISH has found widespread applications. Genome mapping in vertebrates using FISH has been significantly enhanced by the development of several new techniques, e.g., high-resolution gene mapping with direct R-banding FISH, multi-color FISH, fiber-FISH, comparative genomic hybridization and chromosome painting with chromosome-specific DNA probes. The development of equipment and computer software for digital imaging has also led to rapid progress in the areas of resolution and efficiency of FISH analysis [3–5]. FISH techniques can be applied to genome research not only in species for which genome information and resources are abundant, but also for map-poor species, for which FISH is quite useful for constructing chromosome maps and for investigating their karyotypic evolution. Furthermore, the molecular cytogenetic data on chromosomal homology allow the transfer of genomic information from map-rich species such as humans and mice to a wide variety of other species [6]. We here introduce the application of FISH techniques to comparative genomics of vertebrates, citing examples of our comparative cytogenetic studies of birds and reptiles, which have not been spotlighted for a long period of time in this field.

6.2 APPLICATION OF DIRECT R-BANDING FISH TO CHROMOSOME MAPPING

Use of the FISH method with chromosome banding techniques allows direct visualization of DNA sequences on banded chromosomes, which is required for high resolution and precise chromosome mapping. The direct R-banding FISH method established by Takahashi et al. [7] has accomplished precise sub-chromosomal mapping of DNA clones. With this method, fluorescence hybridization signals can be detected on chromosomes where replication R-bands are produced by incorporating bromodeoxyuridine (BrdU) into cells at the late replication stage (Figure 6.1). There are two great advantages of this method: (1) replication R-banding patterns obtained by BrdU treatment permits simultaneous visualization of FISH signals on banded chromosomes, which are prerequisite for precise sub-chromosomal localization of DNA clones; and (2) fluorescent Hoechst bands, which do not differ from G-bands, are observed on the same metaphase spread using a UV filter, and they enable us to easily identify each chromosome.

The mouse (*Mus musculus*) has a karyotype with 2n = 40 that is composed entirely of acrocentric chromosomes whose size variation is sequential, forming a continuous distribution from the largest to the smallest chromosome. Thus, it is almost impossible to identify each mouse chromosome by conventional chromosome staining. The difficulty and complexity of chromosomal identification have hindered the physical mapping with FISH in a number of vertebrate species. The application of FISH combined with replication R-banding enabled the precise

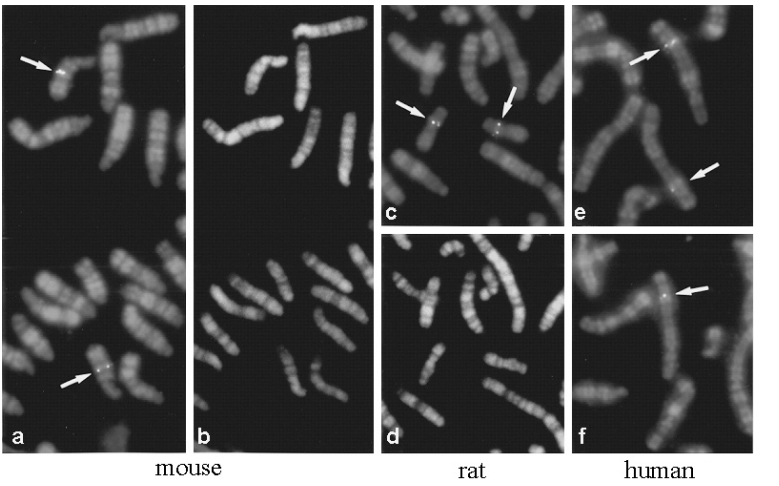

FIGURE 6.1 (**See color insert following page 110**) Comparative chromosome mapping of the *CNR8* gene in mouse (a, b), rat (c, d) and human (e, f) using the direct R-banding FISH method. The 2.3-kb mouse cDNA fragment was used as biotinylated probe, and the fluorescence hybridization signals were directly localized to propidium iodide-stained R-banded mouse chromosome 18C (a), rat chromosome 18q12 (c) and human chromosome 5q31.1 (e, f). Hoechst-stained G-banded patterns of the metaphase spreads of (a) and (c) are demonstrated in (b) and (d), respectively.

localization of DNA clones on R-banded chromosomes in the mouse [8,9]. This system allows rapid and efficient construction of high-density and high-resolution cytogenetic maps in map-poor mammalian species [10–13]. We have also applied this system to avian chromosomes and have constructed high-resolution cytogenetic maps in avian species (Figure 6.2) [14–16].

6.3 CONSTRUCTION OF COMPARATIVE CYTOGENETIC MAPS WITH EST CLONES IN MAP-POOR ANIMALS

Comparative mapping of functional genes makes it possible to identify homologous chromosomal regions between species belonging to different orders or classes, and comparative chromosome maps therefore provide information about the genome architecture and genome evolution. The recent construction of comparative maps of functional genes between chicken and mammalian species provided new insights into the evolution of vertebrate genomes [17–23]. As detailed physical and genetic linkage maps of the chicken have been constructed, extensive chromosomal homology between the chicken and human genomes has been revealed [20,21], whereas much higher rates of chromosome rearrangements have occurred between the mouse and humans [17]. The remaining class of the amniotes, reptiles, has not been the subject of comparative mapping because there are almost no DNA probes for functional genes in this taxon, although comparative mapping between birds and

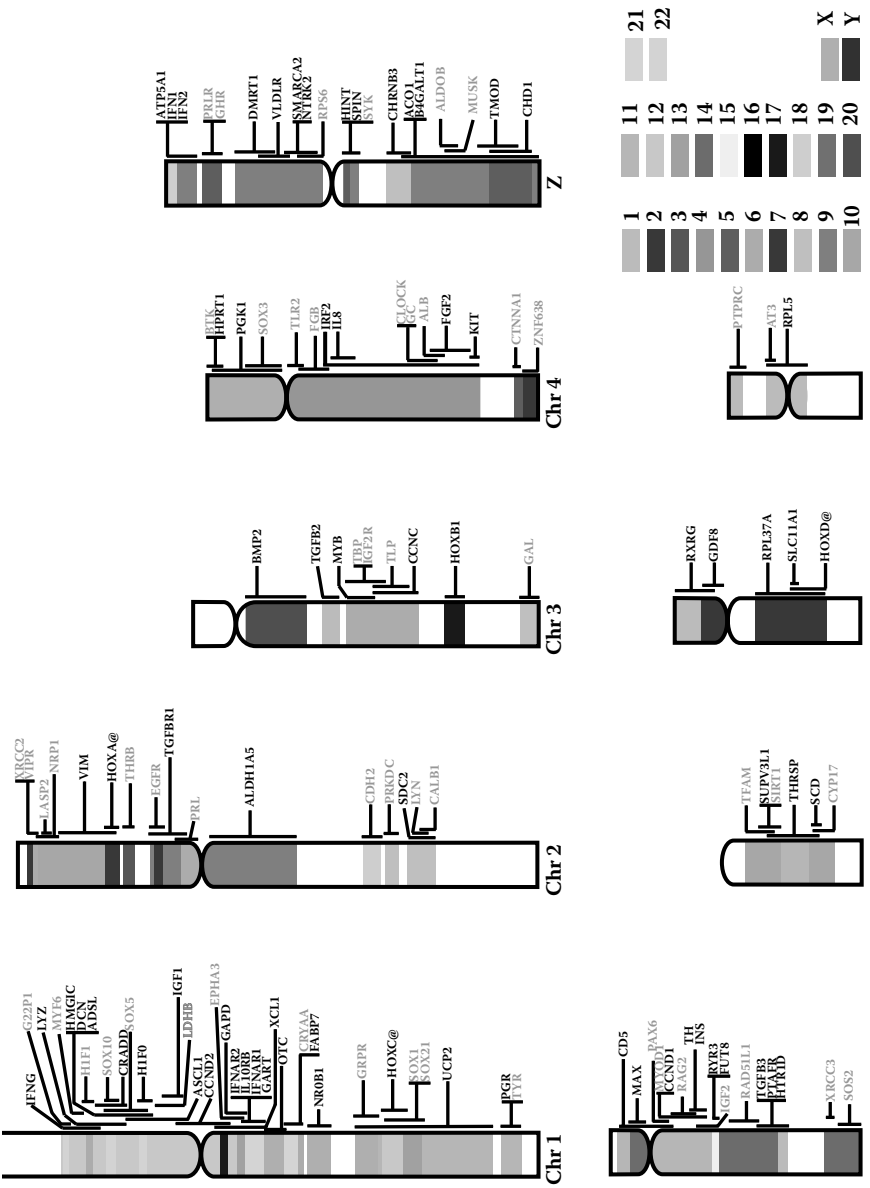

FIGURE 6.2 (**See color insert following page 110**) Cytogenetic map of the chicken constructed with 124 genes using FISH. The chromosomal locations of 54 genes written in green were determined using the direct R-banding FISH method in our laboratory. The chromosomal locations of the other 70 genes were taken from Schmid et al. [21,22]. The conserved regions having homology with particular human chromosomes are sorted by coloring on the chicken chromosomes.

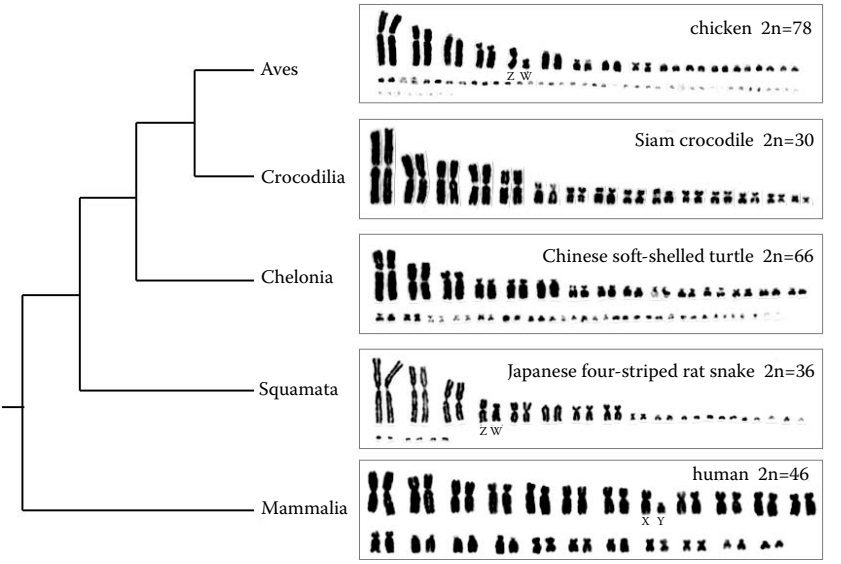

FIGURE 6.3 Phylogenetic relationships and karyotypes of the amniotes. The karyotypes of the chicken (*Gallus gallus*); three reptilian species of different orders: the Siam crocodile (*Crocodylus siamensis*), the Chinese soft-shelled turtle (*Pelodiscus sinensis*) and the Japanese four-striped rat snake (*Elaphe quadrivirgata*); and the human (*Homo sapiens*) are demonstrated as the representatives of three different classes.

reptiles provides essential information about the genome evolution of the amniotes. The karyotypes of birds, turtles and snakes are generally characterized by two major chromosomal components, macrochromosomes and microchromosomes (Figure 6.3). This close karyological relationship between birds and reptiles has long been a topic of speculation among cytogeneticists and evolutionary biologists; however, there is scarcely any evidence for orthology at the molecular level.

Partial sequencing of a large number of cDNAs to develop expressed sequence tags (ESTs) facilitates gene discovery using the EST database (dbEST), and ESTs provide a ready source of DNA probes for comparative gene mapping between any species. Orthologs are homologous genes between different species, which evolved from a common ancestral gene and normally retain the same function during evolution. The identification of orthologous genes using reptilian EST clones facilitates the direct comparison of human, avian and reptilian genomes by comparative gene mapping. The comparative maps of orthologous genes made using EST clones were first constructed between reptiles and chicken by us [24]. We constructed cDNA libraries from the brain tissue and the whole embryos of the Chinese soft-shelled turtle (*Pelodiscus sinensis*) and from the brain tissue of the Japanese four-striped rat snake (*Elaphe quadrivirgata*). We isolated a large number of cDNA clones at random from the turtle and snake cDNA libraries, determined their partial sequences, and then searched for orthologs from the reptilian EST clones for comparative gene mapping.

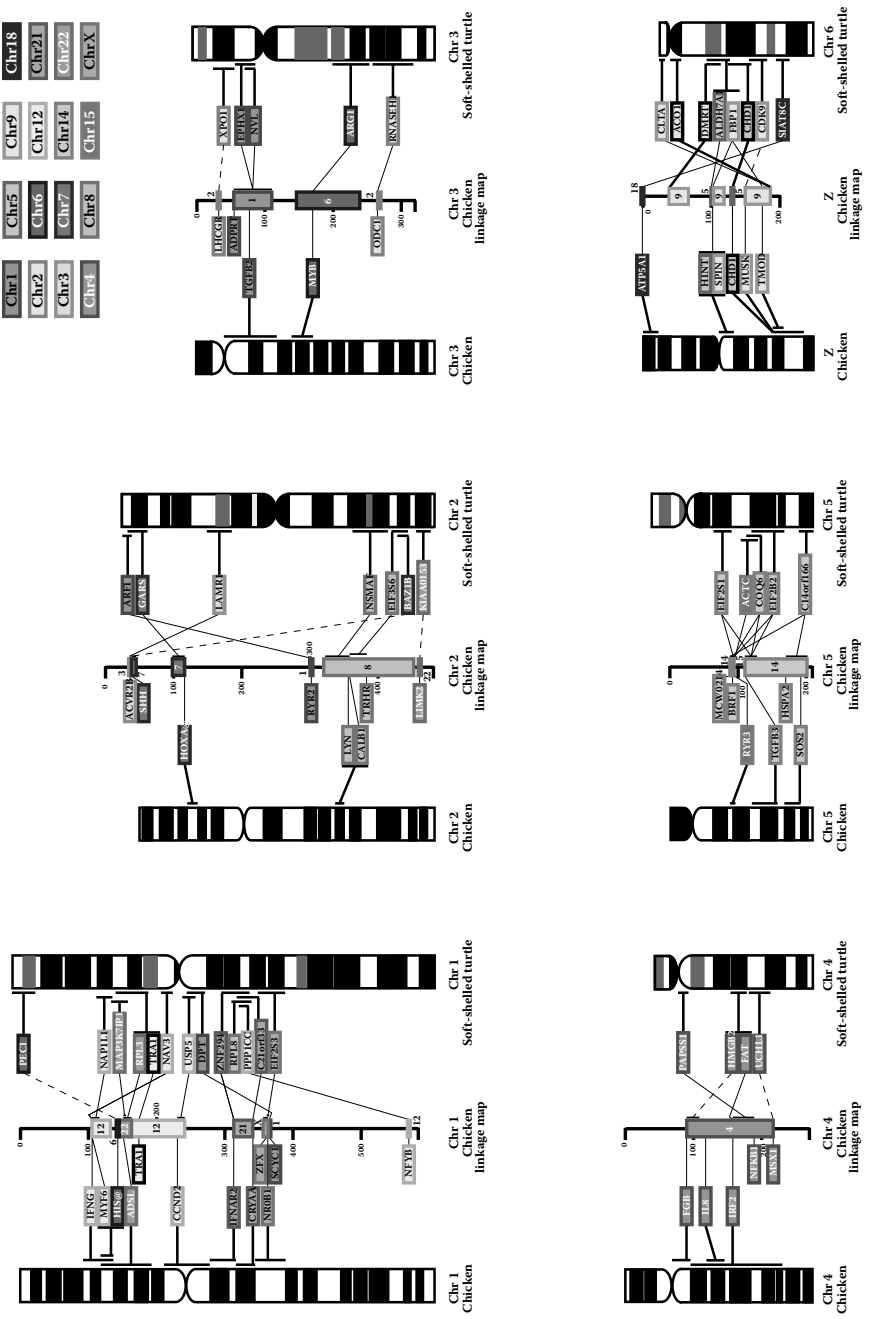
Chr1
Chr2
Chr3
Chr4
Chr5
Chr6
Chr7
Chr8
Chr9
Chr12
Chr14
Chr15
Chr18
Chr21
Chr22
ChrX
Chr 1 Chicken
Chr 1 Chicken linkage map
Chr 1 Soft-shelled turtle
Chr 2 Chicken
Chr 2 Chicken linkage map
Chr 2 Soft-shelled turtle
Chr 3 Chicken
Chr 3 Chicken linkage map
Chr 3 Soft-shelled turtle
Chr 4 Chicken
Chr 4 Chicken linkage map
Chr 4 Soft-shelled turtle
Chr 5 Chicken
Chr 5 Chicken linkage map
Chr 5 Soft-shelled turtle
Z Chicken
Z Chicken linkage map
Chr 6 Soft-shelled turtle

FIGURE 6.4

Figure 6.4 shows the comparative cytogenetic map of the turtle chromosomes 1 to 6 constructed with 42 EST clones [24]. Homology between the turtle and chicken chromosomes is found to be high, with the six largest chromosomes being almost equivalent to each other. On the other hand, homology with chicken chromosomes is much lower in the snake than in the turtle (data not shown), indicating that the avian and turtle genomes have been well conserved during the evolution of the Arcosauromorpha. The turtle chromosome 6q and the snake chromosome 2p represent conserved synteny with the chicken Z chromosome, and the Z chromosomes of the turtle and the snake correspond to chicken autosomes. These results suggest that the avian Z chromosome and the two reptilian Z chromosomes were derived from different autosomes of the common ancestor, and the causative genes of sex determination may be different between birds and the two reptilian species [25,26].

6.4 IDENTIFICATION OF CHROMOSOMAL HOMOLOGY BETWEEN DIFFERENT SPECIES BY COMPARATIVE CHROMOSOME PAINTING (ZOO-FISH)

The karyological relationships between different species have usually been documented by chromosome G-banding analysis. Chromosome banding is an effective method for delineating chromosomal homology between phylogenetically related species, but this approach provides merely indirect information, unsubstantiated at the molecular level. Comparative mapping of functional genes is an ideal method to identify homologous chromosomal regions between different species. However, this approach is not practical for studying karyotypic evolution in map-poor animals because it entails a great deal of time and cost, and skillful techniques for mapping small cDNA clones on chromosomes to construct comparative maps. Advances in flow-sorting of chromosomes became a breakthrough for studies on karyotypic evolution in vertebrates. Cross-species chromosome hybridization with

---

FIGURE 6.4 (**See color insert following page 110**) Comparative cytogenetic maps of the largest six chromosomes between the chicken and the Chinese soft-shelled turtle (*Pelodiscus sinensis*). The gene symbols are described according to human gene nomenclature. The G-band ideogram of chicken chromosomes was taken from the ARKdb-chick Roslin Institute (http://www.thearkdb.org/browser?species=chicken). The chromosomal homology between the two species was indirectly compared according to the current information of the chicken–human comparative map [21,23]. The chicken linkage maps are shown between the cytogenetic chromosome maps of the chicken and turtle. The conserved regions that are homologous with human chromosomes are shown by the colored boxes on the linkage map. The numerical value on the linkage map indicates map position (cM). The solid lines indicate the locations of the genes finely localized to the conserved sub-chromosomal regions of human chromosomes. The dotted lines indicate the locations of the turtle genes that are localized to the vicinity of the sub-chromosomal regions conserved between human and chicken. (Reprinted after modification with permission from Matsuda et al. (2005) *Chromosome Res* 13: 601–615.)

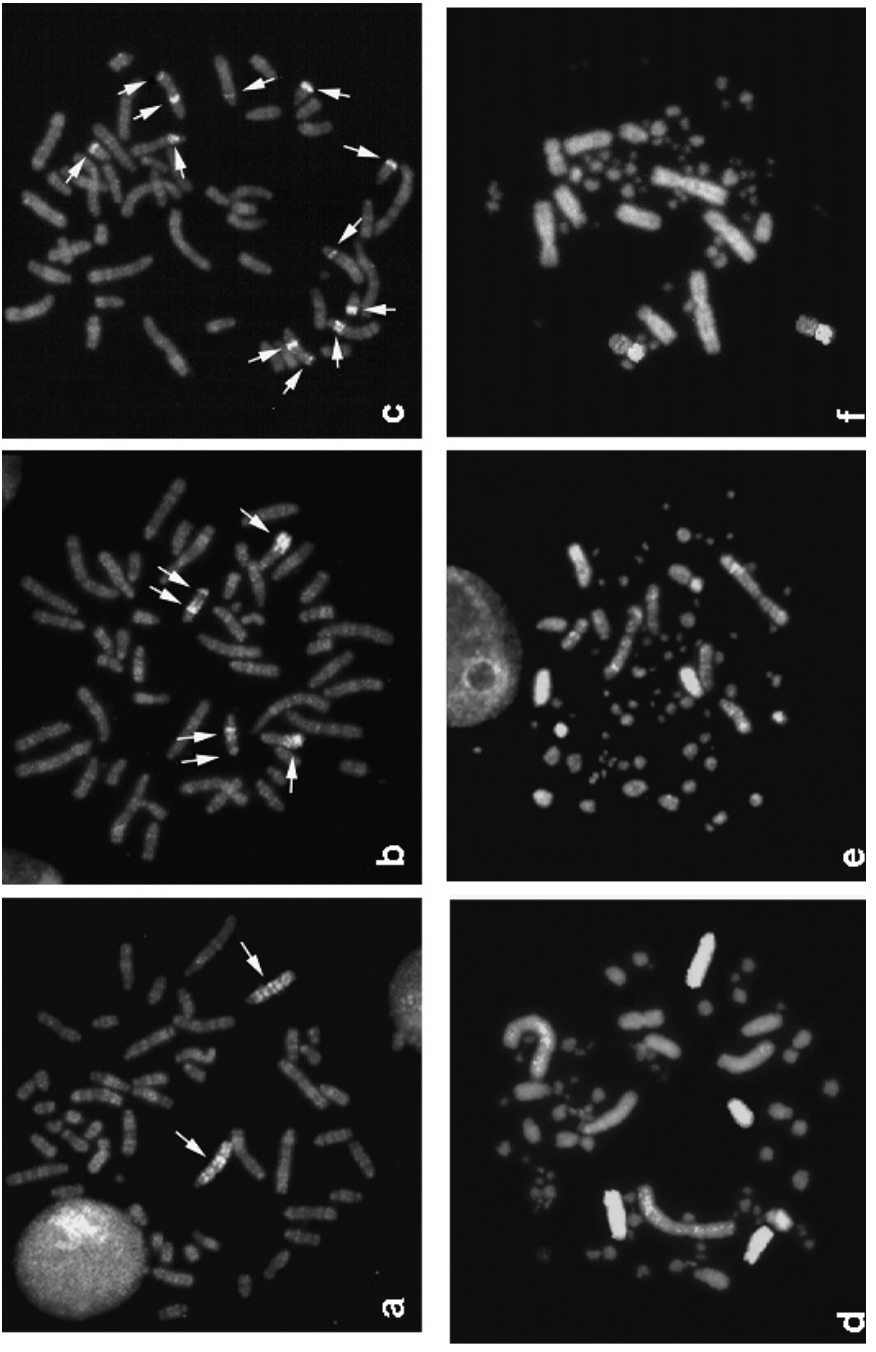

FIGURE 6.5

chromosome-specific DNA probes that were prepared from flow-sorted chromosomes, named Zoo-FISH, is a robust method for delineating chromosomal homology between distantly related species on the whole genome level [27,28]. This approach therefore provides clues for defining the process of the chromosome rearrangements that have occurred during the evolution of species [29,30]. Figure 6.5 shows the Zoo-FISH patterns of *Apodemus peninsulae* (Murinae, Rodentia) with mouse chromosome-specific DNA probes, and of three Galliformes species with chicken DNA probes [31,32]. This cross-species chromosome painting has been extensively performed in mammals [33]. The comparison of the Zoo-FISH data among a wide variety of species makes it possible to identify a set of chromosome segments shared among the species, which made up the karyotypes of the common ancestors. This provides insights into the nature of karyotypic evolution and enables the delineation of ancestral karyotypes across various kinds of taxa [34–37].

This approach has also been applied to many avian species with the chicken probes of chromosomes 1 to 9 and Z [32,38–41]. The Zoo-FISH studies revealed that the avian karyotypes are highly conserved on this molecular basis, with the exception of the cases of the Falconiformes species, in which the numbers of middle-sized chromosomes have increased through fragmentation of macrochromosomes, and the numbers of microchromosomes have decreased through fusions of microchromosomes and their translocation onto larger chromosomes [42]. The reciprocal translocations and interchromosomal rearrangements between macro- and microchromosomes have occurred only rarely in most of the avian species, suggesting that the karyotype that is composed of a small number of macrochromosomes and a large number of microchromosomes is the ancestral type of avian karyotype.

6.5 DELINEATION OF THE PROCESS OF CHROMOSOME REARRANGEMENTS AND OF THE ANCESTRAL KARYOTYPES

Molecular cytogenetic studies on chromosomal homology between different species have been widely performed in mammals and birds [33,40]. To delineate the process of karyotypic evolution by putting the "piecemeal" data together,

FIGURE 6.5 (**See color insert following page 110**) Cross-species comparative painting of *Apodemus peninusulae* (Murinae, Rodentia) chromosomes with mouse (*Mus musculus*) chromosome-specific DNA probes (a–c) and of the chromosomes of three Galliformes species with chicken (*Gallus gallus*) DNA probes (d–f). (a–c) Mouse painting probes of chromosome 3 (a), chromosome 13 (b) and chromosome 17 (c) were hybridized to one pair, two pairs and five pairs, respectively, of *A. peninsulae* chromosomes. (d) Chicken chromosome 2 probe hybridized to chromosomes 3 and 6 in the turkey (*Meleagris gallopavo*). (e) Chicken chromosome 4 probe hybridized to the acrocentric chromosome 4 and a pair of microchromosomes in Lady Amherst's pheasant (*Chrysolophus amherstiae*). (f) Biotin-labeled chicken chromosome 6 (green) and digoxigenin-labeled chicken chromosome 8 (red) probes hybridized to the q and p arms, respectively, of chromosome 5 in the Western capercaillie (*Tetrao urogallus*). The chromosomes are stained with propidium iodide and Hoechst 33258 in (a–c) and (d–f), respectively.

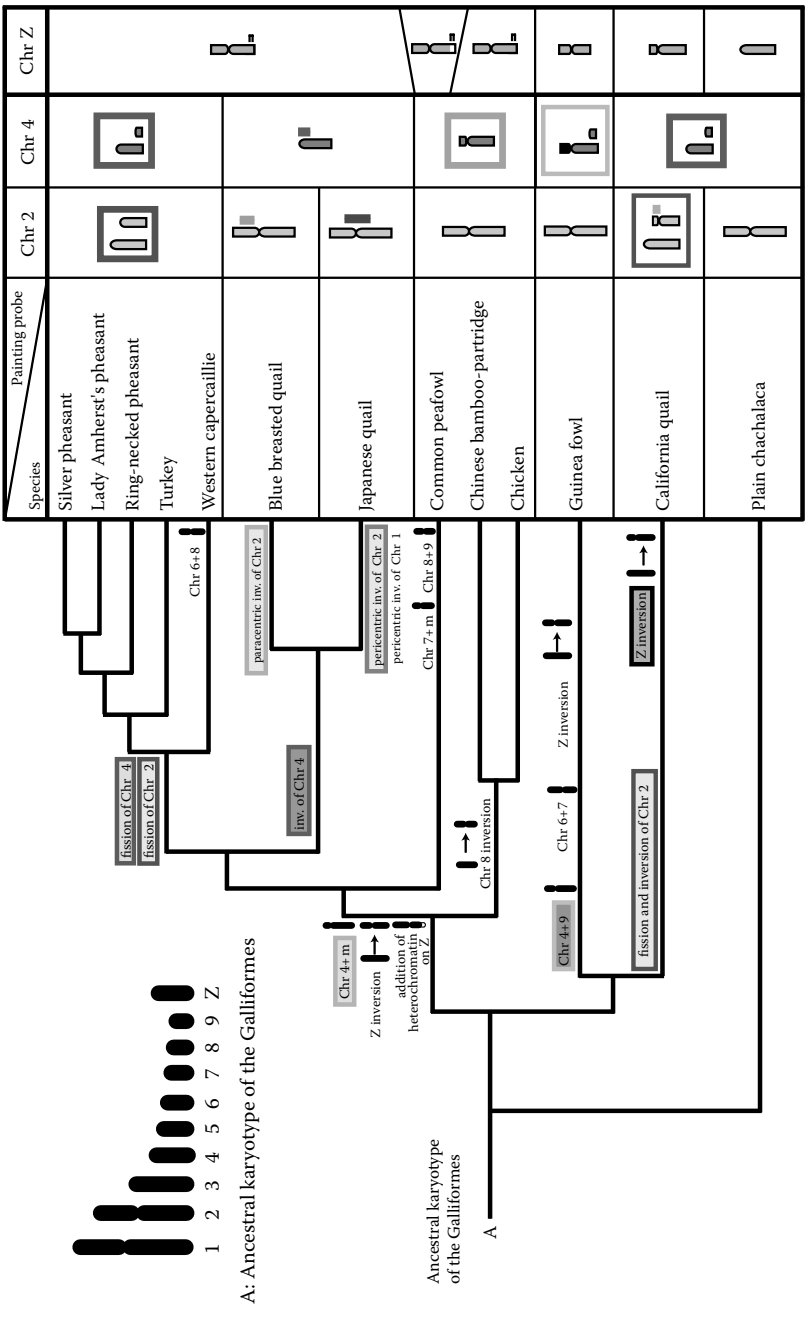
Species
Painting probe
Chr 2
Chr 4
Chr Z
Silver pheasant
Lady Amherst's pheasant
Ring-necked pheasant
Turkey
Western capercaillie
Blue breasted quail
Japanese quail
Common peafowl
Chinese bamboo-partridge
Chicken
Guinea fowl
California quail
Plain chachalaca
fission of Chr 4
fission of Chr 2
Chr 6+8
paracentric inv. of Chr 2
inv. of Chr 4
pericentric inv. of Chr 2
pericentric inv. of Chr 1
Chr 7+m
Chr 8+9
Chr 8 inversion
Chr 4+m
Z inversion
addition of heterochromatin on Z
Chr 6+7
Z inversion
Chr 4+9
fission and inversion of Chr 2
Z inversion
Ancestral karyotype of the Galliformes
A
1 2 3 4 5 6 7 8 9 Z
A: Ancestral karyotype of the Galliformes

FIGURE 6.6

comparison of the cytogenetic data with the molecular phylogeny is a very effective approach. Figure 6.6 shows a schematic representation of the process of chromosome rearrangements in 13 species of the Galliformes, which was inferred by comparing our molecular cytogenetic data with the molecular phylogenetic tree constructed with the nucleotide sequences of the mitochondrial cytochrome b (*Cytb*) gene [32]. The molecular phylogeny of the Galliformes has been constructed for more than 30 species using the nucleotide sequences of the *Cytb* gene [43]. However, the nature of the karyotypic evolution has not yet been proposed by comparing the karyological data with the molecular phylogenetic data. Our approach revealed that the process of the evolutionary changes of macrochromosomes in the 13 Galliformes species was in good accordance with the molecular phylogenetic relationships, and delineated the ancestral karyotype of the Galliformes. The karyotype of the Plain chachalaca was regarded as most closely approaching the ancestral karyotype of the Galliformes, which is similar to the karyotypes of ratites, which are classified as the most primitive birds and have extensively undifferentiated Z and W sex chromosomes [39] (Nishida-Umehara et al., unpublished data). These findings of our studies substantiate the proposal that the comparison of karyological data with the molecular phylogenetic data is very effectual in defining the process of karyotypic evolution in avian species.

6.6 INVESTIGATION OF GC HETEROGENEITY AND GENOME COMPARTMENTALIZATION BASED ON COMPARATIVE CYTOGENETIC MAPS

Mammalian and avian genomes have been revealed, by means of chromosome banding and density gradient centrifugation, to be composed of several classes of chromosomal segments that differ in GC content, which are denoted as "isochores" [44]. Although the evolutionary origin and intrinsic nature of this GC-heterogeneity is still not fully understood [45], the existence of intra-genome GC-heterogeneity has recently been almost certainly confirmed by analyses of whole-genome sequences in the chicken

FIGURE 6.6 Schematic representation of the process of karyotypic evolution in the Galliformes and the ancestral karyotypes of the Galliformes, based on the molecular phylogeny constructed with the nucleotide sequences of the mitochondrial *Cytb* gene. The rearrangements of chromosomes 2, 4 and Z, which were identified by comparative chromosome painting with chicken probes and comparative chromosome mapping, are demonstrated in the right of the molecular phylogenetic tree. The short arm of guinea fowl chromosome 4 hybridized with chicken chromosome 9 probe is painted black. The regions in which inversions were identified by comparative chromosome mapping are indicated by vertical bars on the right of chromosomes. The bracket indicates the region of heterochromatin addition on the Z chromosome of the Phasianidae. Landmark chromosome rearrangements are mapped onto the molecular phylogenetic tree. The ancestral karyotype of the Galliformes is indicated on the top left-hand corner of the figure. (Reprinted after modification with permission from Shibusawa et al. (2004) *Cytogenet Genome Res* 106: 111–119.)

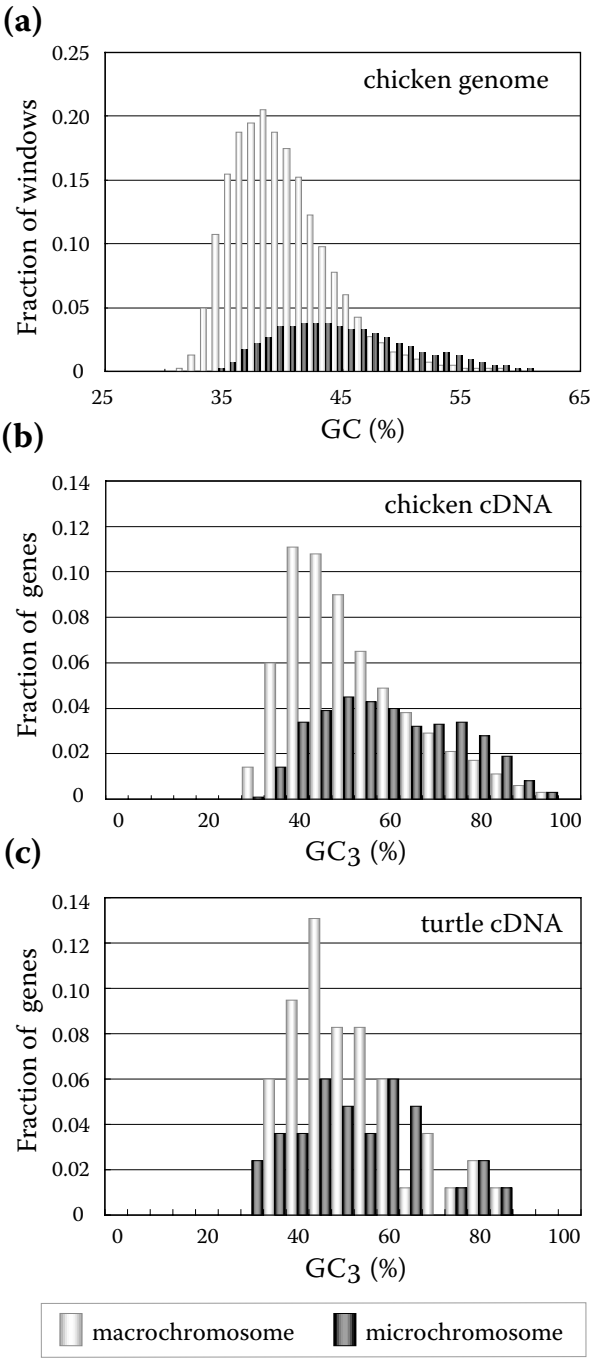
(a)
chicken genome
Fraction of windows
0.25
0.20
0.15
0.10
0.05
0
25
35
45
55
65
GC (%)
(b)
chicken cDNA
Fraction of genes
0.14
0.12
0.10
0.08
0.06
0.04
0.02
0
0
20
40
60
80
100
GC3 (%)
(c)
turtle cDNA
Fraction of genes
0.14
0.12
0.10
0.08
0.06
0.04
0.02
0
0
20
40
60
80
100
GC3 (%)
macrochromosome
microchromosome

FIGURE 6.7

as well as in humans and the mouse [46–48], but not in non-amniotes. Karyotypes of extant sauropsids (reptiles and birds) generally consist of two major components, macrochromosomes and dot-like microchromosomes (Figure 6.3) [23]. In the chicken, cytogenetic observations indicated that microchromosomes exhibit higher gene density [49,50], higher density of CpG islands [51] and higher GC content than macrochromosomes [52]. Examination of the whole genomic sequences of the chicken revealed trends consistent with those above, and moreover suggested that global GC content on chromosomes increases exponentially with reduction in chromosome size [48], whereas this tendency has not been reported in other vertebrates. This feature of the chicken genome suggests that avian microchromosomes might be counterparts of mammalian GC-rich chromosomal segments [52].

The existence of intra-genome GC-heterogeneity in reptiles has not been fully confirmed by chromosome banding studies [53] or density gradient centrifugation [54]. Furthermore, a paucity of sequence information on reptilian species has prevented us from understanding the physical configuration of reptilian genomes and the evolutionary origin of heterogeneity in base composition. The survey of numerous cDNA sequences makes it possible to take an overview of the whole genome of that organism in terms of base composition, as shown previously [55,56], and protein-coding region-based analysis through cDNA-based gene mapping by FISH and GC_3 calculation provides an informative tool for surveying genomic features in non-model organisms with limited amounts of genomic sequence information. We applied this approach to the survey of GC-heterogeneity and chromosomal compartmentalization in reptiles [57]. We determined the chromosomal locations of 90 genes of the Chinese soft-shelled turtle (*Pelodiscus sinensis*) and calculated their GC content at exonic third positions (GC_3). Chromosome mapping of the turtle genes revealed that microchromosomes tend to contain more GC-rich genes than GC-poor genes, as in the chicken (Figure 6.7). These results illustrate two modes of genome evolution in amniotes: in mammals, a sophisticated genomic configuration in which GC-rich and GC-poor regions coexist in individual chromosomes; and in sauropsids, in contrast, a refined chromosome size-dependent GC-compartmentalization in which GC-rich fractions of the genome tend to be confined to microchromosomes.

6.7 CONCLUSIONS

Cross-species chromosome hybridization with chromosome-specific DNA probes (Zoo-FISH) is a robust method for identifying conserved syntenic chromosomal regions between different species. The molecular cytogenetic data obtained using

FIGURE 6.7 Distribution of GC content on macro- and microchromosomes of the chicken and the Chinese soft-shelled turtle (*Pelodiscus sinensis*). (a) Distribution of global GC content of genome sequences on macro- and microchromosomes of the chicken is shown as a histogram in 20-kb non-overlapping windows. (b) Distribution of GC_3 for 1065 chicken cDNAs. (c) Distribution of GC_3 for 90 *P. sinensis* genes. (Reprinted with permission from Kuraku et al. (2006) *Chromosome Res* 14: 187–202.)

this approach provided us clues for delineating the process of karyotypic evolution in vertebrates and the possible karyotypic constitutions of their common ancestors. Zoo-FISH analysis has been extensively performed for many mammalian species, and on the basis of this enormous amount of cytogenetic data regarding chromosomal homology, the ancestral karyotypes have been delineated for several families and/or orders of mammals. The development of chicken chromosome-specific DNA probes has provided a breakthrough for the understanding of the genome organization and the karyotypic evolution in birds. The molecular cytogenetic findings obtained by this cross-species painting revealed a high degree of chromosome homology in avian species, and showed that the ratites have the typical ancestral karyotype of birds. Zoo-FISH is available for chromosomal comparisons between different species within the same order or class, but it fails to work across species of different classes. Comparative chromosome mapping of functional genes is a powerful tool for comparing the chromosomal architecture and genome composition between distantly related species. Construction of chromosome maps with EST clones and/or cDNA clones of the defined functional genes enables the direct comparison of chromosomal homology between the chicken and reptiles on a molecular basis. Furthermore, the recent accomplishment of whole genome sequencing of the chicken facilitates the understanding of the molecular basis of karyological relationships between birds and reptiles, the origin of the reptilian sex chromosomes and the evolution of the genome composition in amniotes based on GC-heterogeneity and genome compartmentalization. These approaches are useful for other map-poor vertebrates including the non-amniotic amphibians and fish, and the characterization of conserved chromosome segments provides clues for clarifying the phylogenetic hierarchy of genome evolution in vertebrates.

ACKNOWLEDGMENT

This study was supported by Special Coordination Funds of the Ministry of Education, Culture Sports, Science and Technology of the Japanese government.

REFERENCES

1. Pinkel D, Straume T, Gray JW (1986) Cytogenetic analysis using quantitative, high-sensitivity, fluorescence hybridization. *Proc Natl Acad Sci USA* 83: 2934–2938.
2. Lawrence JB, Villnave CA, Singer RH (1988) Sensitive, high-resolution chromatin and chromosome mapping in situ: presence and orientation of two closely integrated copies of EBV in a lymphoma line. *Cell* 52: 51–61.
3. Schröck E et al. (1996) Multicolor spectral karyotyping of human chromosomes. *Science* 273: 494–497.
4. Speicher MR, Ballard SG, Ward DC (1996) Karyotyping human chromosomes by combinatorial multi-fluor FISH. *Nat Genet* 12: 368–375.
5. Tanke HJ et al. (1999) New strategy for multi-colour fluorescence *in situ* hybridisation: COBRA: COmbined Binary RAtio labelling. *Eur J Hum Genet* 7: 2–11.
6. O'Brien SJ et al. (1999) The promise of comparative genomics in mammals. *Science* 286: 458–481.

7. Takahashi E, Hori T, O'Connell P, Leppert M, White R (1990) R-banding and non-isotopic in situ hybridization: precise localization of the human type II collagen gene (COL2A1). *Hum Genet* 86: 14–16.
8. Matsuda Y et al. (1992) Location of the mouse complement factor H gene (*cfh*) by FISH analysis and replication R-banding. *Cytogenet Cell Genet* 61: 282–285.
9. Matsuda Y, Chapman VM (1995) Application of fluorescence in situ hybridization in genome analysis of the mouse. *Electrophoresis* 16: 261–272.
10. Kuroiwa A, Tsuchiya K, Matsubara K, Namikawa T, Matsuda Y (2001) Construction of comparative cytogenetic maps of Chinese hamster to mouse, rat and human. *Chromosome Res* 9: 641–648.
11. Matsubara K et al. (2001) Comparative FISH mapping of human cDNA clones to chromosomes of the musk shrew (*Suncus murinus*, Insectivora). *Cytogenet Cell Genet* 93: 258–262.
12. Iannuzzi L et al. (2003) The river buffalo (*Bubalus bubalus*, 2n=50) cytogenetic map: assignment of 64 loci by fluorescence in situ hybridization and R-banding. *Cytogenet Genome Res* 102: 65–75.
13. Iannuzzi L et al. (2003) Chromosomal localization of sixty autosomal loci in sheep (*Ovis aries*, 2n=54) by fluorescence in situ hybridization and R-banding. *Cytogenet Genome Res* 102: 135–138.
14. Suzuki T et al. (1999) Cytogenetic mapping of 31 functional genes on chicken chromosomes by direct R-banding FISH. *Cytogenet Cell Genet* 87: 32–40.
15. Shibusawa M et al. (2001) A comparative cytogenetic study of chromosome homology between chicken and Japanese quail. *Cytogenet Cell Genet* 95: 103–109.
16. Shibusawa M et al. (2002) Chromosome rearrangements between chicken and guinea fowl defined by comparative chromosome painting and FISH mapping of DNA clones. *Cytogenet Genome Res* 98: 225–230.
17. Burt DW et al. (1999) The dynamics of chromosome evolution in birds and mammals. *Nature* 402: 411–413.
18. Nanda I et al. (1999) 300 million years of conserved synteny between chicken Z and human chromosome 9. *Nature Genet* 21: 258–259.
19. Nanda I et al. (2000) Conserved synteny between the chicken Z sex chromosome and human chromosome 9 includes the male regulatory gene *DMRT*1: a comparative (re)view on avian sex determination. *Cytogenet Cell Genet* 89: 67–78.
20. Groenen MAM et al. (2000) A consensus linkage map of the chicken genome. *Genome Res* 10: 137–147.
21. Schmid M et al. (2000) First report on chicken genes and chromosomes 2000. *Cytogenet Cell Genet* 90: 169–218.
22. Schmid M et al. (2005) Second report on chicken genes and chromosomes 2005. *Cytogenet Genome Res* 109: 415–479.
23. Burt DW (2002) Origin and evolution of avian microchromosomes. *Cytogenet Genome Res* 96: 97–112.
24. Matsuda Y et al. (2005) Highly conserved linkage homology between birds and turtles: bird and turtle chromosomes are precise counterparts of each other. *Chromosome Res* 13: 601–615.
25. Kawai A et al. (2007) Different origins of bird and reptile sex chromosomes inferred from comparative mapping of chicken Z-linked genes. *Cytogenet Genome Res* (in press).
26. Matsubara K et al. (2006) Evidence for different origin of sex chromosomes in snakes, birds and mammals, and stepwise differentiation of snake sex chromosomes. *Proc Natl Acad Sci USA* 103: 18190–18195.

27. Scherthan H et al. (1994) Comparative chromosome painting discloses homologous segments in distantly related mammals. *Nat Genet* 6: 342–347.
28. Ferguson-Smith MA, Yang F, Rens W, O'Brien PCM (2005) The impact of chromosome sorting and painting on the comparative analysis of primate genomes. *Cytogenet Genome Res* 108: 112–121.
29. Wienberg J, Frönicke L, Stanyon R (2001) Insights into mammalian genome organization and evolution by molecular cytogenetics, in *Comparative Genomics*, Clark M ed. Kluwer Academic Publishers, Boston: 207–244.
30. Wienberg J (2004) The evolution of eutherian chromosomes. *Curr Opin Genet Dev* 14: 657–666.
31. Matsubara K, Nishida-Umehara C, Tsuchiya K, Nukaya D, Matsuda Y (2004) Karyotypic evolution of *Apodemus* (Muridae, Rodentia) inferred from comparative FISH analyses. *Chromosome Res* 12: 383–395.
32. Shibusawa M et al. (2004) Karyotypic evolution in the Galliformes: an examination of the process of karyotypic evolution by comparison of the molecular cytogenetic findings with the molecular phylogeny. *Cytogenet Genome Res* 106: 111–119.
33. Chowdhary BP, Raudsepp T (2001) Chromosome painting in farm, pet and wild animal species. *Methods Cell Sci* 23: 37–55.
34. Murphy WJ, Stanyon R, O'Brien SJ (2001) Evolution of mammalian genome organization inferred from comparative gene mapping. *Genome Biol* 2: R0005.1–R0005.8.
35. Richard F, Lombard M, Dutrillaux B (2003) Reconstruction of the ancestral karyotypes of eutherian mammals. *Chromosome Res* 11: 605–618.
36. Froenicke L (2005) Origins of primate chromosomes — as delineated by Zoo-FISH and alignments of human and mouse draft genome sequences. *Cytogenet Genome Res* 108: 122–138.
37. Chowdhary BP, Raudsepp T, Frönicke L, Scherthan H (2006) Emerging patterns of comparative genome organization in some mammalian species as revealed by Zoo-FISH. *Genome Res* 8: 577–589.
38. Griffin DK et al. (1999) Micro- and macrochromosome paints generated by flow cytometry and microdissection: tools for mapping the chicken genome. *Cytogenet Cell Genet* 87: 278–281.
39. Shetty S, Griffin DK, Graves JAM (1999) Comparative painting reveals strong chromosome homology over 80 million years of bird evolution. *Chromosome Res* 7: 289–295.
40. Guttenbach M et al. (2003) Comparative chromosome painting of chicken autosomal paints 1–9 in nine different bird species. *Cytogenet Genome Res* 103: 173–184.
41. Shibusawa M et al. (2004) A comparative karyological study of the blue-breasted quail (*Coturnix chinensis*, Phasianidae) and California quail (*Callipepla californica*, Odontophoridae). *Cytogenet Genome Res* 106: 82–90.
42. de Oliveira EHC et al. (2005) Chromosome reshuffling in birds of prey: the karyotype of the world's largest eagle (Harpy eagle, *Harpia harpyja*) compared to that of the chicken (*Gallus gallus*). *Chromosoma* 114: 338–343.
43. Kimball RT, Braun EL, Zwartjes PW, Crowe TM, Ligon JD (1999) A molecular phylogeny of the pheasants and partridges suggests that these lineages are not monophyletic. *Mol Phylogenet Evol* 11: 38–54.
44. Bernardi G (2000) Isochores and the evolutionary genomics of vertebrates. *Gene* 241: 3–17.
45. Eyre-Walker A, Hurst LD (2001) The evolution of isochors. *Nat Rev Genet* 2: 549–555.

46. International Human Genome Sequencing Consortium (IHGSC) (2001) Initial sequencing and analysis of the human genome. *Nature* 409: 860–921.
47. Mouse Genome Sequencing Consortium (MGSC) (2002) Initial sequencing and comparative analysis of the mouse genome. *Nature* 420: 520–562.
48. International Chicken Genome Sequencing Consortium (ICGSC) (2004) Sequence and comparative analysis of the chicken genome provide unique perspectives on vertebrate evolution. *Nature* 432: 695–716.
49. McQueen HA, Siriaco G, Bird AP (1998) Chicken microchromosomes are hyperacetylated, early replicating, and gene rich. *Genome Res* 8: 621–630.
50. Smith J et al. (2000) Differences in gene density on chicken macrochromosomes and microchromosomes. *Anim Genet* 31: 96–103.
51. McQueen HA et al. (1996) CpG islands of chicken are concentrated on microchromosomes. *Nat Genet* 12: 321–324.
52. Andreozzi L et al. (2001) Compositional mapping of chicken chromosomes and identification of the gene-richest regions. *Chromosome Res* 9: 521–532.
53. Holmquist GP (1989) Evolution of chromosome bands: molecular ecology of noncoding DNA. *J Mol Evol* 28: 469–486.
54. Hughes S, Clay O, Bernardi G (2002) Compositional patterns in reptilian genomes. *Gene* 295: 323–329.
55. Clay O, Caccio S, Zoubak S, Mouchiroud D, Bernardi G (1996) Human coding and noncoding DNA: compositional correlations. *Mol Phylogenet Evol* 5: 2–12.
56. Musto H, Romero H, Zavala A, Bernardi G (1999) Compositional correlations in the chicken genome. *J Mol Evol* 49: 325–329.
57. Kuraku S et al. (2006) cDNA-based gene mapping and GC_3 profiling in the softshelled turtle suggest a chromosomal size-dependent GC-bias shared by sauropsids. *Chromosome Res* 14: 187–202.

7 Immunocytochemistry for Analyzing Chromosomes

Osamu Hoshi, Toru Hirota, Eiji Kimura, Nae Komatsubara and Tatsuo Ushiki*

CONTENTS

7.1 Introduction 81
7.2 Methodological Remarks 82
7.2.1 Cells 82
7.2.2 Chromosome Spreading 83
7.2.3 Immunocytochemistry 83
7.3 Studying Chromosomal Proteins 83
7.4 Studying Histone Modifications 84
7.5 Differential Staining of Chromosomes 86
7.6 Conclusion 89
Acknowledgments 89
References 89

7.1 INTRODUCTION

Immunocytochemistry, based on the specific interaction between antigens and antibodies, has been widely applied in recent decades to studies of the localization of specific proteins in cells. In this technique, cells (or tissue sections, in immunohistochemistry) to be studied are incubated in a solution containing an antibody to the protein of interest. If the protein is present in the cells and the incubation conditions are suitable, the antibody binds specifically to the targeted protein. Subsequently, its location can be detected using a light or electron microscope depending on the type of compound (fluorescent substance, enzyme or gold particles) used for antibody labeling. This immunocytochemical procedure requires the development of antibodies specific for the proteins being examined (i.e., primary antibodies), and techniques for labeling the antibodies. In fact, various techniques for producing the antibodies, both polyclonal and monoclonal,

*To whom correspondence should be addressed.

have been developed for the specific and sensitive detection of antigens by immunocytochemistry. Two labeling methods — direct and indirect — have also been introduced for immunocytochemistry. In the direct method, primary antibodies are directly labeled with a fluorescent dye, which enables visualization of the protein of interest with a fluorescent microscope. In the indirect method, primary antibodies are unlabeled but are visualized using labeled secondary antibodies that can bind to the corresponding primary antibodies.

Employing immunocytochemical techniques, previous investigators have identified numerous chromosomal proteins that contributed significantly to the analysis of chromosomal structure and function (see Chapter 16) [1,2]. In this chapter, we provide brief technical notes for immunocytochemistry, specifically when it is applied to the study of chromosomes. We will also discuss advantages and disadvantages of immunocytochemistry in this research field.

7.2 METHODOLOGICAL REMARKS

7.2.1 Cells

Choice of cell type for the study of chromosomes is important, because the overall morphology of chromosomes and their total number per cell varies among cell types, and may be altered depending on the condition of the cells employed. Cell lines derived from tumors, such as HeLa cells, are frequently used for mammalian chromosome studies because they are easier to grow and it is easier to synchronize the cell cycle, but they are often associated with numerical and structural chromosomal aberrations. On the other hand, cell lines derived from normal tissue, such as human retinal pigment epithelium cells, are diploid and thought to be free from structural abnormalities. Another commonly used material in the study of chromosomes is lymphocytes cultured from peripheral blood from human or animals.

Cells are often treated with a spindle poison such as colchicine or nocodazole before fixation. This treatment is useful for obtaining a large number of mitotic cells, because this class of drug activates the spindle checkpoint and thus cells are arrested in a prometaphase-like state due to disruption of the spindle microtubules. However, it must be remembered that chromosomes obtained from cells that have been arrested in mitosis by colchicine (known as C-mitosis) are morphologically different from those from unperturbed mitotic cells. During spindle checkpoint arrest induced by colchicine, chromosomes become progressively condensed and extremely shortened, while chromosome arms, but not centromeres, dissociate from each other. This results in small X-shaped chromosomes, or C-pairs [3]. By contrast, chromosomes in prometaphase or metaphase in unperturbed mitosis are much longer and less compacted. Their sister chromatids are physically connected not only at the centromeres but also along the length of the arms, until they segregate at onset of anaphase [4]. Thus, to study chromosome behavior in physiological conditions, cell synchronization methods that do not perturb mitotic progression (e.g., double thymidine arrest and release regimen [5]) should be used to enrich mitotic cells.

7.2.2 Chromosome Spreading

There are various methods for chromosome spreading. A conventional method for chromosome spreading is to swell cells by hypotonic treatment (e.g., 75 m*M* KCl for 30 min), fix them with Carnoy's solution (methanol/acetic acid = 3:1), drop the cell suspension onto glass slides and leave these to dry in air. This conventional method is useful for studying chromosome behavior, including the position or overall shape of chromosomes in the cell. A disadvantage of this procedure is that many proteins in chromosomes (i.e., antigens for immunohistochemistry) are lost by the acid treatment with Carnoy's solution, although some can be recovered by neutralization.

To avoid the loss of proteins in chromosomes, the cytospin spreading method is often used; cells with/without hypotonic treatment are attached to glass slides using cytospin centrifugation followed by fixation [6]. Treatment of the cytospun cells with a detergent (e.g., 0.1% Triton-X 100 in phosphate buffered saline) may also be helpful for obtaining clearer signals in immunostaining of chromosomal proteins, because cytoplasmic proteins are washed out during this treatment.

7.2.3 Immunocytochemistry

Immunocytochemistry of chromosomes is generally no different to that of other biological targets. However, in some cases, including bromodeoxyuridine (BrdU) antibody staining, the specimens must be denatured by acid or alkaline solution before incubation of antibodies (see below). Immunofluorescence microscopy is commonly used for detection of binding of antibody to its antigen in chromosomes, because the bright fluorescence stands out in strong contrast to the background of the specimens. Counterstaining of DNA with nucleic acid-binding fluorescent dyes is helpful for visualizing the overall morphology of chromosomes. These fluorochromes include intercalating dyes such as ethidium bromide, propidium iodide and acridine orange, and minor groove binders such as 4′,6-diamidino-2-phenylindole (DAPI) and Hoechst dyes.

7.3 STUDYING CHROMOSOMAL PROTEINS

A large number of studies to date have identified numerous chromosomal proteins (see Chapter 13). Studying the behavior of these proteins provides insight into the function of chromosomes, and immunocytochemical analysis of these proteins has been widely used for this purpose (see Chapter 16).

Very little is known as yet about how chromosomes are assembled in mitosis, although the proteinaceous structure in chromosome axes is thought to have relevant functions [7]. Studies using immunofluorescence microscopy have shown in particular that the protein complex known as condensin and the decatenation enzyme, topoisomearase IIα, are enriched in the chromosome axes [1,2,8,9]. It is therefore reasonable to hypothesize that these proteins are essential for assembly of chromosomes, either structurally or enzymatically (i.e., for winding or unwinding of DNA strands).

In mammalian cells, two classes of condensin complexes have been identified; they share two ATPases called Smc subunits but contain a different set of non-Smc subunits. Immunocytochemical studies using antibodies for the condensin I- or II-specific subunit revealed that the behavior is very different between the two condensins [2,8,9]. First, the timing of chromosome association is different; condensin II is loaded onto chromosomes in prophase, and condensin I in prometaphase. Second, condensin I and II locate in different domains on the chromosome arms. These results obtained by immunocytochemistry have already implied that the regulation and function of these two complexes are distinct, even before this is addressed using other molecular biological approaches.

Immunocytochemistry for topoisomerase IIα also shows that this enzyme becomes enriched in the chromosome axis in prophase [1,10]. The axial localization becomes much clearer in prometaphase and metaphase (Figure 7.1). It is interesting that the fluorescence intensity of topoisomerase IIα is not uniform but is "spotted" along the chromosome axes, although the biological significance of this is still unknown [1]. The pattern of these intense spots in the chromosome arms seems to overlap with the banding pattern of Q-banded chromosomes. In late metaphase, the topoisomerase IIα-positive axis is observed as a zigzag structure, presumably reflecting that the chromosomes become highly folded at this mitotic stage.

In contrast to condensins or topoisomerase IIα, which are incorporated into chromosomes in mitosis, there are several chromosomal proteins that are removed during chromosome assembly; these include the cohesin complex and heterochromatin protein 1 (HP1). Immunocytochemical studies have been useful for revealing that cohesin is located in the interchromatid space, although this is not discernible with a standard fixation protocol; for this purpose, the "pre-extraction" protocol is required in order to wash out the abundant cytoplasmic fraction of cohesin that does not associate tightly with chromosomes [11,12]. Even after the pre-extraction of cytoplasmic cohesin, many antibodies to cohesin may still fail to bind to their antigen in the chromosomes. This phenomenon is commonly seen for many other molecules that bind to DNA, presumably because nucleic acids hinder the access of antibodies. Indeed, endogenous cohesin and HP1 are scarcely detectable using their specific antibodies in mitotic chromosomes. Thus, an alternative approach in such a case is to tag the protein and express it stably in cells, followed by detection with antibodies to the tag [13].

7.4 STUDYING HISTONE MODIFICATIONS

Core histones form another group of protein that is found in chromosomes, in addition to the chromosomal proteins discussed above (thus the latter are sometimes grouped as "non-histone proteins"). The amino-terminal tails of core histones undergo a range of post-translational modifications including phosphorylation, methylation and acetylation [14]. These epigenetic marks affect the structure and function of chromatin, thereby controlling gene expression

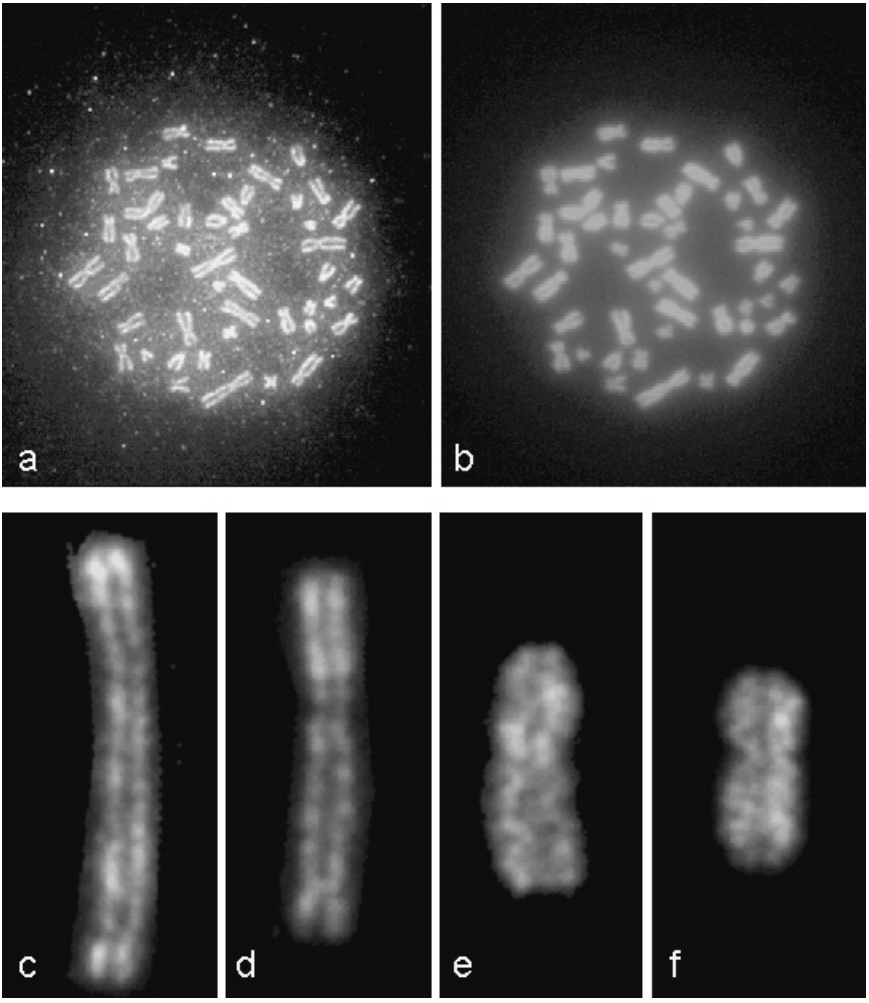

FIGURE 7.1 Human chromosomes stained with an anti-topoisomerase IIα antibody. Chromosomes derived from lymphocytes were first fixed with Carnoy's solution, spread on glass slides and additionally fixed with acetone. After being blocked with 10% fetal bovine serum (FBS) in 0.1% Triton X-PBS for 30 min, chromosomes were incubated with an anti-topoisomerase IIα antibody (Calbiochem, U.S.A.) for 24 h and then with a fluorescence-labeled secondary antibody (Alexa Fluor 488 goat anti-mouse IgG [H+L]; Molecular Probes, Oregon, U.S.A.) for 12 h. Some specimens were counterstained with YOYO3. They were observed with a fluorescence microscope (ECLIPSE TE2000-U; Nikon, Tokyo, Japan) and photographed using a digital image acquisition system (Pixcera; Pixcera, Kawasaki, Japan). (a, b) Metaphase chromosomes stained with the anti-topoisomerase IIα antibody (a) and YOYO3 (b). (c–d) Chromosomes from prometaphase to late metaphase immunostained for topoisomerase IIα.

and mitotic chromosome segregation. Like many other proteins in mitosis, histone tails are subject to phosphorylation, and it has been assumed that histone phosphorylation has a significant impact on chromosome assembly and/or structure.

To date, four residues in the amino terminus of histone H3—Thr3, Ser10, Thr11 and Ser28—are known to be phosphorylated in mitosis [15–18]. The development of antibodies to the phosphorylated residues at these specific sites made it possible to study immunocytochemically how these phosphosites are regulated. For instance, phosphorylation of these four residues on H3 generally appears simultaneously, initiated in the prophase nuclei and maintained through metaphase, but attenuated in anaphase and disappearing in telophase. Interestingly, these phosphorylations are detected in different chromosomal domains: phosphorylation of Ser10 and Ser28 is found ubiquitously throughout chromosomes, but Thr3 or Thr11 phosphorylation is enhanced in centromeres [15–18]. Furthermore, recent experiments using RNA interference have also suggested that each of these phosphorylation sites on H3 is catalyzed by different mitotic kinases [15–18]. All of these results are based on immunocytochemical analyses.

It should be borne in mind that any quantitative measurement of fluorescence intensities gives relative, not absolute, quantification. This means that the strength of signals is not comparable when different antibodies are used, because the antibody avidity — the strength of the interaction between an antibody and its antigen — varies from antibody to antibody.

Antibodies associated with human autoimmune disease, against mitotic chromosomes, have also been used to identify novel chromosomal proteins [19]. A number of proteins that reside at kinetochores or centromeres were found by this approach. Furthermore, mitotic-specific protein modifications can also be identified by characterizing these antibodies. One example is the discovery of a H3 modification, doubly modified by trimethylation of Lys9 and phosphorylation of Ser10, which indicates that these two modifications can take place on a single H3 molecule [20]. This was in dramatic contrast with the previous finding by biochemical analysis, which suggested that only one or the other of these modifications could occur. Immunocytochemical analysis further showed that this double modification on Lys9 and Ser10 is distributed predominantly in pericentromeric heterochromatin (Figure 7.2). A consequence of mitotic Ser10 phosphorylation at these chromosomal domains is thought to be the removal of HP1 proteins that had been bound to H3 Lys9 in interphase.

7.5 DIFFERENTIAL STAINING OF CHROMOSOMES

BrdU is a thymidine analog and is incorporated into DNA in place of thymine during S phase. Use of antibodies to BrdU enabled the immunocytochemical detection of DNA strands that had incorporated BrdU [21]. This technique has been traditionally used to examine the population of proliferating cells in normal

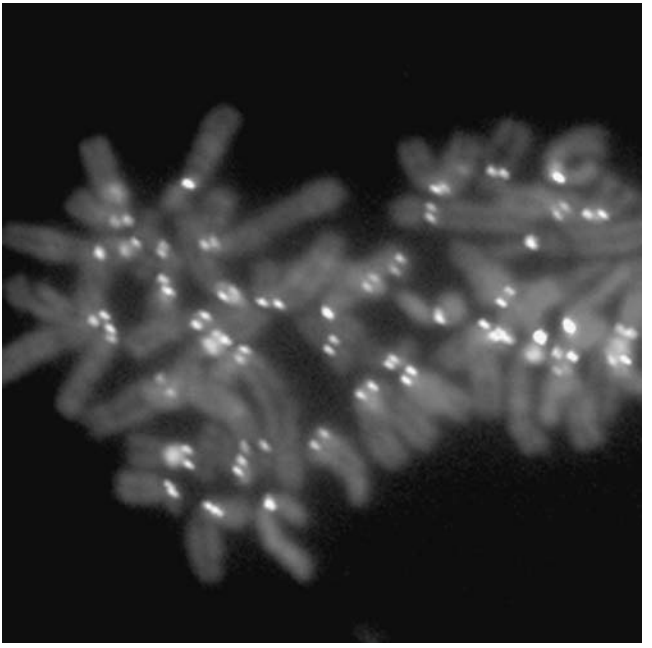

FIGURE 7.2 (**See color insert following page 110**) Immunofluorescence microscopy of human chromosomes using antibodies that selectively react with H3 doubly modified by trimethylation of Lys9 and phosphorylation of Ser10 (red). The kinetochores were labeled with green fluorescence protein fused to the centromere protein CENP-A (green). DNA was counterstained with DAPI (blue).

or pathological tissues, including neoplastic tumors. If animals or cells are treated with BrdU shortly before fixation, the nuclear DNA of cells undergoing mitotic cell division incorporates BrdU in S phase, whereas this does not occur in non-proliferating resting cells.

The BrdU incorporation assay has been also used to study chromosomal structure. For example, differential staining of sister chromatids in the chromosome was performed by immunocytochemistry of BrdU-incorporated chromosomes. Cells are incubated in the presence of BrdU for 72 h to complete two rounds of S phase (in the case of lymphocytes). This treatment produces a sister chromatid pair with different concentrations of BrdU; one sister chromatid contains a BrdU-labeled and an unlabeled DNA strand, while the other sister chromatid contains two BrdU-labeled DNA strands. Immunocytochemical staining with the BrdU antibodies gives a relatively weak signal from the former sister chromatid, while the latter sister chromatid is more intensely stained, resulting in differently stained sister chromatids in each chromosome [22]. An example of a metaphase chromosome spread prepared using this method is shown in Figure 7.3. The sister chromatid exchange (SCE) points

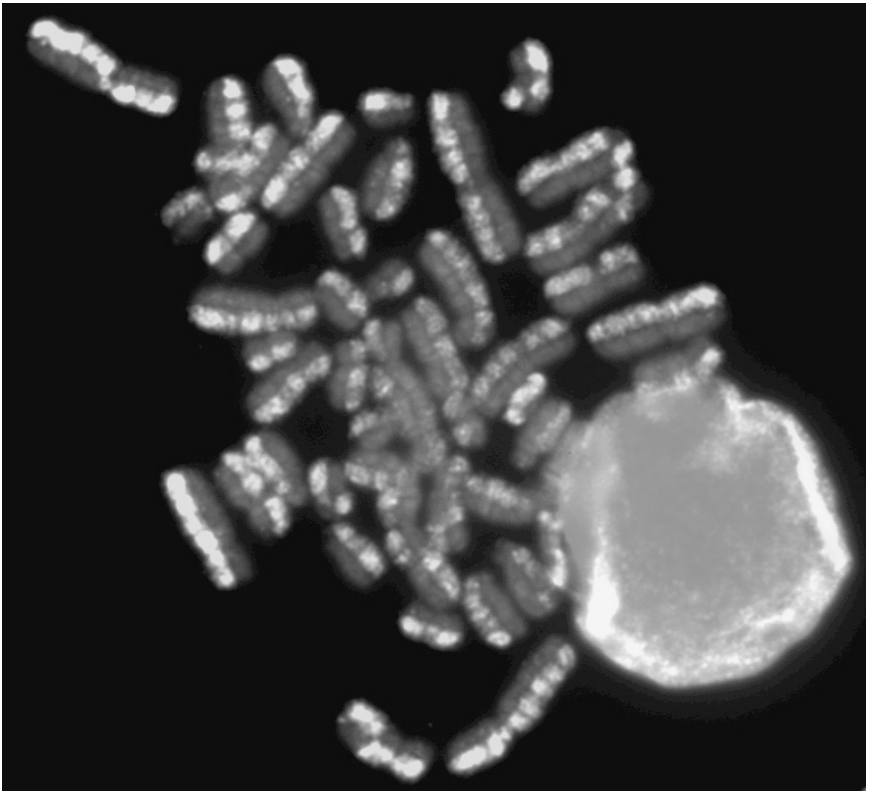

FIGURE 7.3 (**See color insert following page 110**) Differential staining of sister chromatids. Isolated human lymphocytes were cultured at 37°C for 72 h in karyotyping medium (Gibco BRL), containing 5-bromo-2′-deoxyuridine (BrdU) (Wako, Osaka, Japan). Growth of the lymphocytes was arrested with 0.05 μg/mL colcemid (Demecolcine, Wako) for 60 min. The cell suspension was exposed to 0.075 *M* KCl hypotonic treatment and fixed with methanol-acetic acid (3:1). Spreads of metaphase chromosomes were made by dropping the cell suspension onto cover-slips, followed by air-drying. After additional fixation with 15% formalin, the specimens were denatured with HCl and reacted with an anti-BrdU antibody (Becton Dickinson Immunocytometry Systems, San Jose, U.S.A.). The immunostained specimens were further treated with YOYO-3 (Molecular Probes) for DNA staining and observed with a fluorescence microscope. The sister chromatids with two BrdU-labelled strands are intensely stained bright green for the anti-BrdU immunostaining, while those with one native and one BrdU-labelled strand are stained dark red with YOYO-3.

are unambiguously recognizable in some chromosomes of this chromosome spread. It may be possible to extend the use of differential staining of sister chromatids to address more challenging questions; it would be interesting to study, for example, if there are any differences in SCEs between differentiated cells and stem cells, or between normal cells and cancer cells under various conditions including x-ray or ultraviolet irradiation.

7.6 CONCLUSION

In this chapter, we showed that immunocytochemistry is useful for analyzing the localization of specific molecules in chromosomes. Recently, live cell imaging using chromosome labeling methods has also been introduced for analysis of chromosome dynamics (see Chapter 5). For example, chromosomes in living cells can be labeled with Hoechst 33342, since this fluorescent dye can permeate the cell membrane and is retained in DNA. On the other hand, labeling of chromosomes with green fluorescent protein fused to chromosomal proteins has also been performed by several investigators [23–25]. Immunohistochemistry is complementary to live cell imaging, even though the chromosomes are fixed with chemicals. In particular, immunocytochemistry is a powerful tool for analyzing post-translational modifications of histone tails, because antibodies against different antigens such as phosphorylated and non-phosphorylated histones can be produced for this technique. Labeling of BrdU-incorporated DNA is useful not only for differential staining of sister chromatids in the metaphase chromosome, but also for analyzing the structure of chromosomes in relation to the timing of DNA replication in the S phase.

Recently, we succeeded in obtaining images of chromosomes using atomic force microscopy (AFM) in a buffer solution, and showed the usefulness of AFM for analyzing the structure of chromosomes three-dimensionally in liquid conditions [26,27]. AFM observation of chromosomes followed by immunohistochemistry for chromosomal proteins is expected to be highly useful for investigating the higher-order structure of chromosomes in relation to the roles of chromosomal proteins.

ACKNOWLEDGMENTS

This study was supported by Special Coordination Funds of the Ministry of Education, Culture, Sports, Sciences and Technology of the Japanese government (TU), and partly by a Grant-in-Aid for Scientific Research (No. 18390058) from the same ministry (TU).

REFERENCES

1. Maeshima K, Laemmli UK (2003) A two-step scaffolding model for mitotic chromosome assembly. *Dev Cell* 4: 467–480.
2. Ono T, Losada A, Hirano M, Myers MP, Neuwald AF, Hirano T (2003) Differential contributions of condensin I and condensin II to mitotic chromosome architecture in vertebrate cells. *Cell* 115: 109–121.
3. Rieder CL, Palazzo RE (1992) Colcemid and the mitotic cycle. *J Cell Sci* 102: 387–392.
4. Rieder CL, Cole R (1999) Chromatid cohesion during mitosis: lessons from meiosis. *J Cell Sci* 112: 2607–2613.
5. Bootsma D, Budke L, Vos O (1964) Studies on synchronous division of tissue culture cells initiated by excess thymidine. *Exp Cell Res* 33: 301–309.

6. Hladilova R, Siroky J, Vyskot B (1998) A cytospin technique for spreading plant metaphases suitable for immunofluorescence studies. *Biotech Histochem* 73: 150–156.
7. Laemmli UK, Cheng SM, Adolph KW, Paulson JR, Brown JA, Baumbach WR (1978) Metaphase chromosome structure: the role of nonhistone proteins. *Cold Spring Harb Symp Quant Biol* 42: 351–360.
8. Hirota T, Gerlich D, Koch B, Ellenberg J, Peters J-M (2004) Distinct functions of condensin I and condensin II in mitotic chromosome assembly. *J Cell Sci* 117: 6435–6445.
9. Ono T, Fang Y, Spector DL, Hirano T (2004) Spatial and temporal regulation of condensin I and II in mitotic chromosome assembly in human cells. *Mol Biol Cell* 15: 3296–3308.
10. Earnshaw WC, Heck MMS (1985) Localization of topoisomerase II in mitotic chromosomes. *J Cell Biol* 100: 1716–1725.
11. Sumara I, Vorlaufer E, Gieffers C, Peters BH, Peters JM (2000) Characterization of vertebrate cohesin complexes and their regulation in prophase. *J Cell Biol* 151: 749–762.
12. Hoque MT, Ishikawa F (2001) Human chromatid cohesin component hRad21 is phosphorylated in M phase and associated with metaphase centromeres. *J Biol Chem* 276: 5059–5067.
13. Waizenegger IC, Hauf S, Meinke A, Peters JM (2000) Two distinct pathways remove mammalian cohesin from chromosome arms in prophase and from centromeres in anaphase. *Cell* 103: 399–410.
14. Jenuwein T, Allis CD (2001) Translating the histone code. *Science* 293: 1074–1080.
15. Dai J, Sultan S, Taylor SS, Higgins JM (2005) The kinase haspin is required for mitotic histone H3 Thr 3 phosphorylation and normal metaphase chromosome alignment. *Genes Dev* 19: 472–488.
16. Hsu JY, Sun ZW, Li X, Reuben M, Tatchell K, Bishop DK, Grushcow JM, Brame CJ, Caldwell JA, Hunt DF, Lin R, Smith MM, Allis CD (2000) Mitotic phosphorylation of histone H3 is governed by Ipl1/aurora kinase and Glc7/PP1 phosphatase in budding yeast and nematodes. *Cell* 102: 279–291.
17. Preuss U, Landsberg G, Scheidtmann KH (2003) Novel mitosis-specific phosphorylation of histone H3 at Thr11 mediated by Dlk/ZIP kinase. *Nucleic Acids Res* 31: 878–885.
18. Goto H, Yasui Y, Nigg EA, Inagaki M (2002) Aurora-B phosphorylates Histone H3 at serine28 with regard to the mitotic chromosome condensation. *Genes Cells* 7: 11–17.
19. Gitlits VM, Macaulay SL, Toh BH, Sentry JW (2002) Novel human autoantibodies to phosphoepitopes on mitotic chromosomal autoantigens (MCAs). *J Investig Med* 48: 172–182.
20. Hirota T, Lipp JJ, Tho BH, Peters JM (2005) Histone H3 serine 10 phosphorylation by Aurora b causes HP1 dissociation from heterochromatin. *Nature* 438: 1176–1180.
21. Latt SA (1973) Microfluorometric detection of deoxyribonucleic acid replication in human metaphase chromosomes. *Proc Natl Acad Sci USA* 70: 3395–3399.
22. Kimura E, Hitomi J, Ushiki T (2002) Scanning near field optical/atomic force microscopy of bromodeoxyuridine-incorporated human chromosomes. *Arch Histol Cytol* 65: 435–444.
23. Mo YY, Beck WT (1999) Association of human DNA topoisomerase IIα with mitotic chromosomes in mammalian cells is independent of its catalytic activity. *Exp Cell Res* 252: 50–62.

24. Tavormina PA, Come MG, Hudson JR, Mo YY, Beck WT, Gorbsky GJ (2002) Rapid exchange of mammalian topoisomerase IIα at kinetochores and chromosome arms in mitosis. *J Cell Biol* 158: 23–29.
25. Christensen MO, Larsen MK, Barthelmes HU, Hock R, Andersen CL, Kjeldsen E, Knudsen BR, Westergaard O, Boege F, Mielke C (2002) Dynamics of human DNA topoisomerase IIα and IIβ in living cells. *J Cell Biol* 157: 31–44.
26. Hoshi O, Owen R, Miles M, Ushiki T (2004) Imaging of human metaphase chromosomes by atomic force microscopy in liquid. *Cytogenet Genome Res* 107: 28–31.
27. Hoshi O, Shigeno M, Ushiki T (2006) Atomic force microscopy of native human metaphase chromosomes in a liquid. *Arch Histol Cytol* 69: 73–78.

8 Transmission and Scanning Electron Microscopy of Mammalian Metaphase Chromosomes

Sumire Inaga, Keiichi Tanaka and Tatsuo Ushiki*

CONTENTS

8.1 Introduction 93
8.2 Transmission Electron Microscopy of Metaphase Chromosomes 94
8.2.1 TEM of Ultrathin Sections 94
8.2.2 TEM of a Whole-Mount Preparation of Chromosomes 96
8.3 Scanning Electron Microscopy of Metaphase Chromosomes 97
8.3.1 High-Resolution SEM of Dried and Metal-Coated Chromosomes 97
8.3.2 Hydrous Chromosomes Observed by Low-Vacuum SEM 100
8.4 Conclusion 102
Acknowledgment 103
References 103

8.1 INTRODUCTION

Understanding the structure of chromosomes is important for recognizing the behavior of chromosomes during cell division. To our current knowledge, chromosomes consist of DNA and various (i.e., histone and nonhistone) proteins, which are assembled and compacted in a complex manner, resulting in the 10,000-fold packing of the DNA molecule in each chromosome. The arrangement of DNA and proteins in the chromosome has been studied using electron microscopy, since the resolution needed for visualizing these structures is far

*To whom correspondence should be addressed.

beyond that of light microscopy. These electron microscopic studies revealed the presence of fibrous structures in various orders of the packing of DNA molecules into chromosomes.

At the lowest level, the DNA fiber forms nucleosomes with histone octamers and is observed as a "beads-on-a-string" fiber, about 10 nm in thickness, as viewed by transmission electron microscopy (TEM) of dispersed chromatin. This fiber is, in turn, packed into a 30-nm chromatin fiber, which is also revealed by TEM. Previous TEM studies have further shown that the 30-nm fiber is packed into a chromosome in a particular manner. However, the higher-order structure of the chromosome is rather complicated, and it is difficult to reveal the three-dimensional arrangement of the chromatin fiber in a chromosome by conventional TEM of ultrathin sections. To overcome this difficulty, some investigators proposed the observation of whole-mount chromosomes by TEM [1,2]. On the other hand, scanning electron microscopy (SEM) has also been applied to the study of chromosomes, because it can reveal the three-dimensional surface structure of samples with high resolution. These studies have contributed toward the proposal of several models for the higher-order structure of the chromosome, such as a folded fiber model [3], a coiled coil model [4,5], a scaffold and radial loop model [6], and a helical coiling of radial loops model [7]. However, a definite conclusion has not yet been reached, probably because of the presence of some artifacts during sample preparation for TEM and SEM, making the interpretation of the findings complicated and disputable. In this respect, it may be worthwhile to verify the previous TEM and SEM studies of chromosomal structure, paying special attention to the preparation techniques for chromosome imaging.

Thus, in this chapter, we will review the previous TEM and SEM studies on the structure of chromosomes. In the course of this, we will introduce several techniques which we consider to be suitable for analyzing the higher-order structure of chromosomes by TEM and/or SEM. We will also discuss our results on the higher-order structure of mammalian metaphase chromosomes which were obtained using these techniques.

8.2 TRANSMISSION ELECTRON MICROSCOPY OF METAPHASE CHROMOSOMES

8.2.1 TEM of Ultrathin Sections

The study of ultrathin sections of mitotic cells by TEM is useful for analyzing the ultrastructure of chromosomes within cells. For this purpose, mitotic cells are usually fixed with glutaraldehyde and embedded in epoxy resin, in the same way as for conventional TEM. The ultrathin sections are also stained with uranyl acetate and lead citrate to enhance the imaging contrast. In portions where chromosomes are cut transversely, chromosomes are observed as a dark mass of fine granular material with a somewhat irregular outline (Figure 8.1). Because the relationship of chromosomes with the surrounding structures can be analyzed,

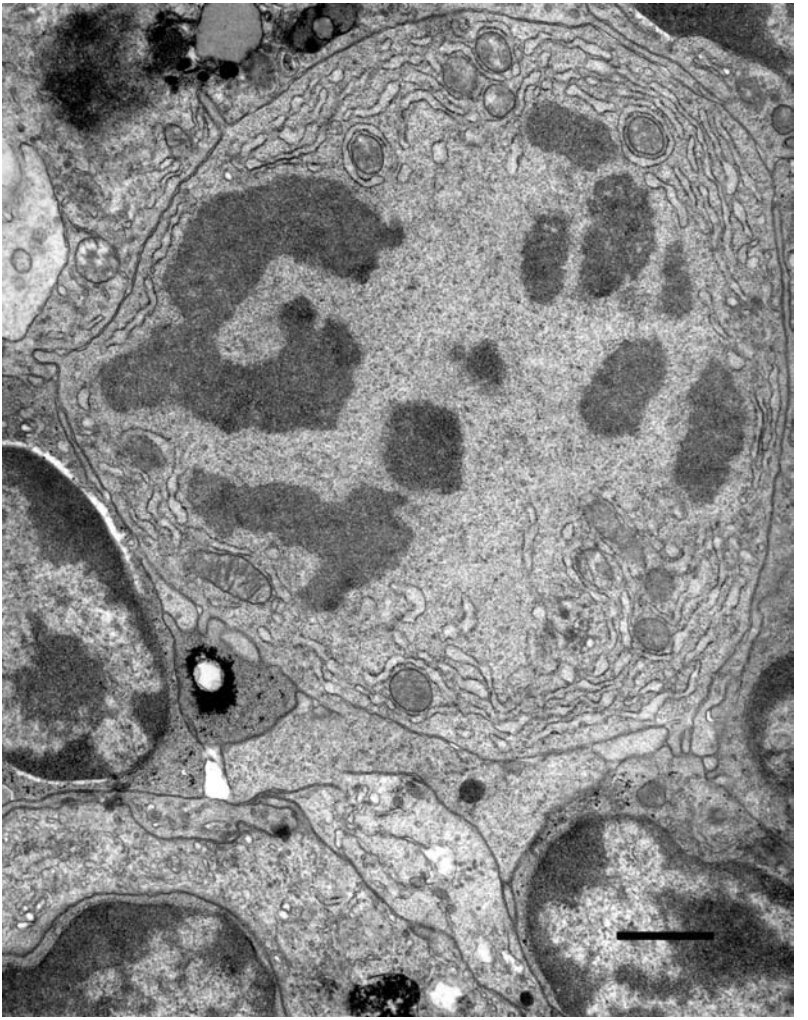

FIGURE 8.1 Transmission electron micrograph of an ultrathin section of a mitotic thymocyte in the adult rat thymus. The tissues were fixed with 2% glutaraldehyde in 0.1 *M* phosphate buffer (pH 7.4), postfixed with 1% OsO_4 in the same buffer, dehydrated in a graded ethanol series, and embedded in epoxy resin. The ultrathin section, made with an ultramicrotome, was stained with uranyl acetate and lead citrate. Chromosomes are observed as a dark mass of fine granular materials.

the ultrastructure of kinetochores was revealed most convincingly by TEM of ultrathin sections [8,9]. However, this method is not suitable for investigating the three-dimensional ultrastructure of chromosomes, although there may be a possibility for three-dimensional observation of thicker sections stereoscopically or tomographically with high-voltage TEM.

8.2.2 TEM of a Whole-Mount Preparation of Chromosomes

In order to observe the higher-order structure of chromosomes by TEM, several investigators have performed a whole-mount preparation method for chromosomes [1,2]. In this method, cultivated cells (such as leukocytes or cells of a cell line) are treated with colchicines in order to arrest cell division, and a

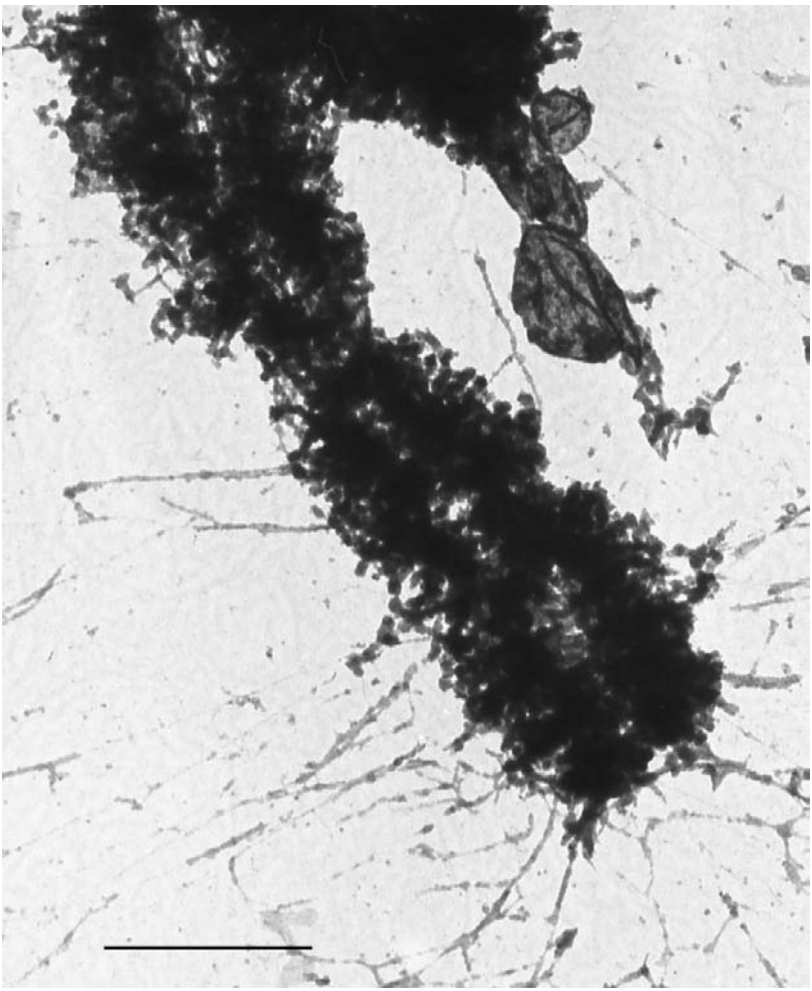

FIGURE 8.2 Transmission electron micrograph of a Chinese hamster metaphase chromosome prepared with a whole-mount preparation method. The chromosome spread on the water was picked up on a grid, dehydrated in ethanol and dried in a critical point dryer using liquid CO_2. A silhouette of the unsectioned chromosome showing thin chromatin fibers is observed in this method. Bar: 1 μm.

suspension of these cells is dropped into water. This treatment induces bursting of mitotic cells on the water surface due to the surface tension, resulting in the spread of chromosomes on the water. These chromosomes are then picked up on a grid and observed by TEM. To avoid artifacts from air-drying, chromosomes mounted on the grid are usually dehydrated in ethanol and dried in a critical point dryer using liquid CO_2. TEM of whole-mount chromosomes using this method enables us to show a silhouette of unsectioned chromosomes at a resolution much higher than that of light microscopy (Figure 8.2). The micrograph clearly shows that the chromatid of each chromosome appears to consist of a long fiber, about 20 to 50 nm thick, that is irregularly and tightly packed along its length. From TEM studies using this method, DuPraw [2] proposed the folded-fiber model of chromosome structure. However, the images obtained with this method are still two-dimensional, and the tight packing and high density of chromosomes with a relatively appreciable thickness only allow the details of chromatin fibers at the margin of the chromosome to be resolved by TEM.

8.3 SCANNING ELECTRON MICROSCOPY OF METAPHASE CHROMOSOMES

8.3.1 High-Resolution SEM of Dried and Metal-Coated Chromosomes

SEM is a powerful tool for revealing the three-dimensional surface structure of biological samples. Thus, a great number of previous investigators have been interested in the observation of chromosomes by SEM [10–13]. For these SEM studies, chromosome spreads have been commonly prepared as follows: after cultivated cells are treated with a hypotonic solution and fixed with methanol/acetic acid (3:1), a cell suspension is dropped onto a glass slide or coverslip followed by simply drying in air. However, when these chromosome spreads are metal-coated and observed by SEM, the chromosomes are strongly flattened and appear to be covered with a thin felt-like layer (Figure 8.3). The flattening of chromosomes is apparently due to air-drying, while the covering substances are considered to be cytoplasmic debris. In order to avoid the production of these preparation artifacts, various preparation methods have been proposed by previous SEM researchers. These studies showed that the ultrastructure of chromosomes is easily and drastically altered depending on the preparation method.

Among these methods, short trypsin treatment of the chromosome spread has been commonly used by previous SEM investigators [13,14]. In this method, chromosomes fixed with methanol/acetic acid and dried in air are briefly digested (e.g., for 5 s) with trypsin. After the action of trypsin is stopped with glutaraldehyde, the chromosomes are conductive-stained, critical-point dried, metal-coated and observed by SEM.

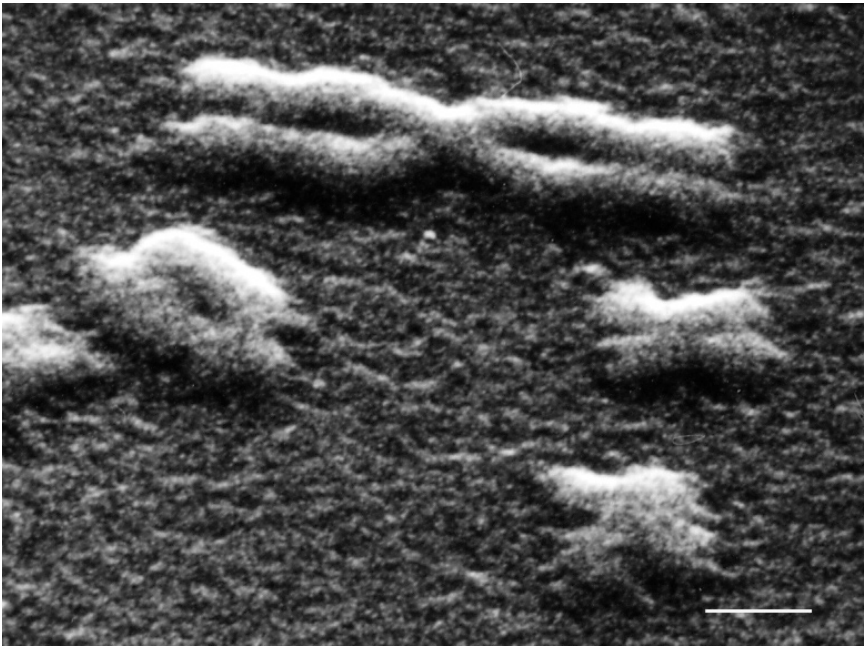

FIGURE 8.3 Scanning electron micrograph of human chromosomes prepared with a standard spreading method for light microscopy. A cell suspension, which was treated with 75 m*M* KCl and fixed with methanol/acetic acid (3:1), was dropped onto a glass slide *or coverslip*, followed by simply drying in air. The specimen was metal-coated and observed by SEM. Chromosomes are strongly flattened and appear to be covered with a thin felt-like layer. Bar: 1 μm.

Another reliable method we have recommended for chromosome study is an acetic acid-heating method [15] in which the chromosomes fixed with methanol/acetic acid are placed in a mixture of 1% aceto-orcein and 45% acetic acid on a glass slide, covered with a glass coverslip, and heated for 1 to 2 s over the flame of an alcohol lamp to remove the cytoplasm adhered to the chromosome surface. They are then dehydrated in a graded ethanol series, critical-point dried in liquid CO_2, metal-coated and observed by SEM. Using this method, chromatin fibers of 25 to 35 nm in diameter are clearly observed in the chromosomes. These chromatin fibers are strongly twisted and entangled along the length of each chromatid, and their arrangement is rather irregular in these specimens (Figure 8.4).

The surface-spread method introduced above for TEM studies has been also applied to SEM studies of chromosomes [16]. This method is useful for revealing chromatin fibers in the chromosomes, because these fibers are apparently artificially unraveled during this treatment. It is also interesting that the surface-spread chromosomes sometimes appear to be composed of chromatin fibers of different

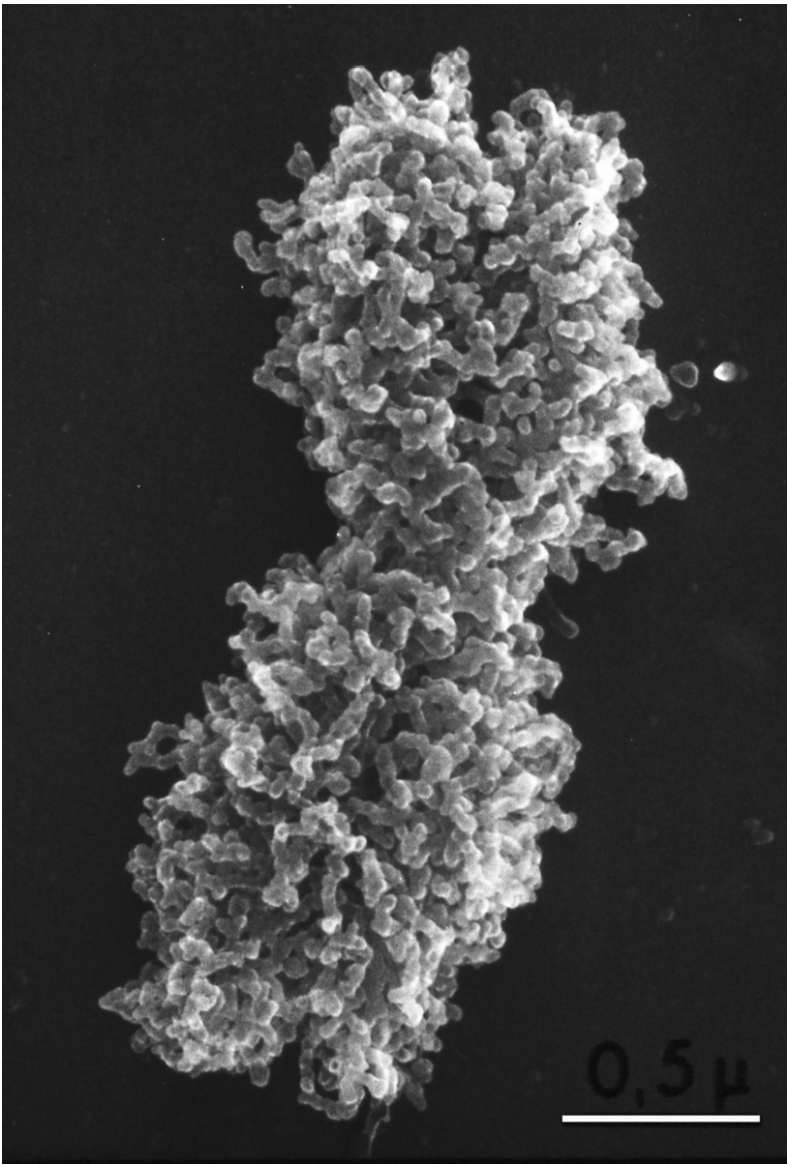

FIGURE 8.4 Scanning electron micrograph of a human metaphase chromosome prepared using an acetic acid-heating method. Human mitotic lymphocytes fixed with methanol/acetic acid were placed in a mixture of 1% aceto-orcein and 45% acetic acid on a glass slide, covered with a glass coverslip, and heated for 1 to 2 s over the flame of an alcohol lamp. They were then dehydrated in a graded ethanol series, critical-point dried in liquid CO_2, metal-coated and observed by SEM. This chromosome appears to be composed of chromatin fibers, 25 to 35 nm in diameter, that are strongly twisted and entangled in each chromatid. Bar: 0.5 µm.

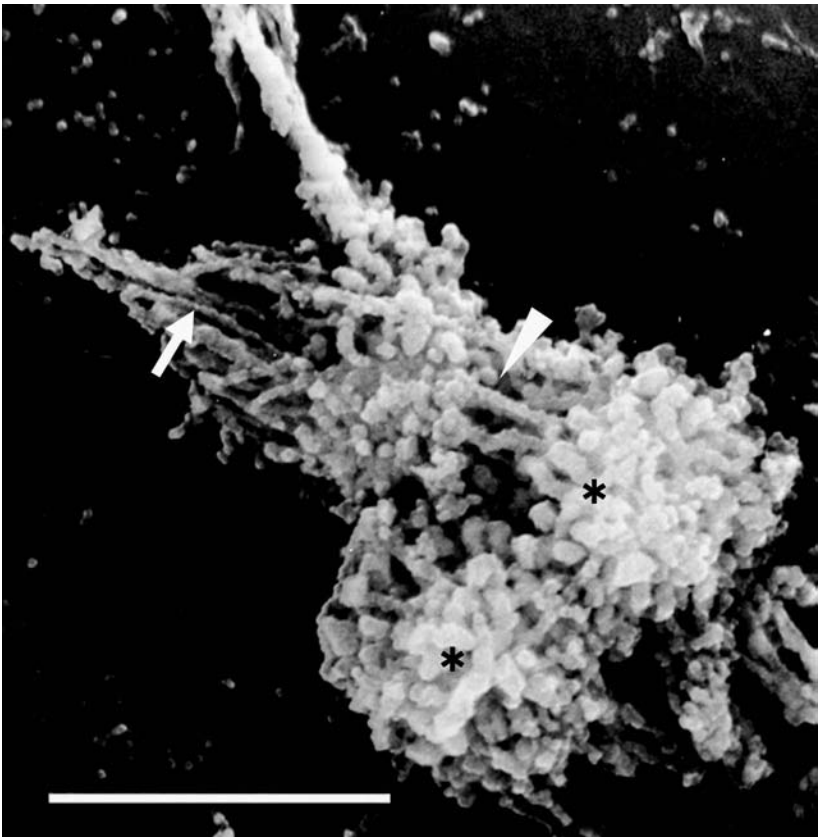

FIGURE 8.5 Scanning electron micrograph of a human metaphase chromosome prepared using a whole-mount preparation method. Chromosomes spread on the water were mounted on a grid, dehydrated in ethanol, dried in a critical point dryer using liquid CO_2, metal-coated and observed by SEM. Because the chromosome was artificially unraveled during the preparation, chromatin fibers having a thickness of 10 nm (arrow), 20 to 30 nm (arrowhead), and 60 nm (asterisks) are observed in this micrograph. Bar: 1 μm.

(10, 20–30, and 60 nm) thicknesses (Figure 8.5), suggesting the presence of a hierarchical packing order in the metaphase chromosome [5].

8.3.2 Hydrous Chromosomes Observed by Low-Vacuum SEM

Recent advances in technology have led to the production of a new type of SEM with a low-vacuum chamber, or a low-vacuum SEM. This instrument has the advantage of being free from charging artifacts even in nonconductive materials; residual gas molecules are ionized in the specimen chamber and neutralize the

negative charge forming on the nonconductive specimens. The low-vacuum SEM also has the potential for observing biological samples in a hydrous state, if the samples are maintained in an atmosphere below the saturated vapor pressure of water. Thus, we can omit drying and metal-coating of samples by using low-vacuum SEM. However, conductive staining of the samples is practically very important, because the signal intensity of unstained biological samples is too weak to obtain high-resolution images in low-vacuum SEM. Our studies on conductive staining for low-vacuum SEM showed that the most suitable technique is Pt blue staining [17]. Because Pt blue has a relatively high affinity for DNA, the chromatin fibers can be strongly stained with it, which is very useful for SEM observation of chromosomes.

Our recommended method for chromosome study by low-vacuum SEM is as follows [17]: isolated chromosomes are placed on a glass slide previously treated with 0.1% poly-L-lysine, are stained with 3% Pt blue aqueous solution for 15 min, immersed in 20% dimethyl sulfoxide (DMSO) solution for 20 min and observed using low-vacuum SEM. Treatment of chromosomes with DMSO is used to avoid ice crystal damage during SEM observation below 0°C. Observations are usually made in a back-scattered electron (BSE) mode at −10°C with a vacuum grade from 90 to 270 Pa; in these conditions, chromosomes can be kept in the hydrous state during observation, because the saturated vapor pressure of the water is 270 Pa at −10°C.

When the samples are observed in a low-vacuum SEM equipped with a highly sensitive BSE detector, BSE images of hydrous chromosomes are obtained with high resolution [17,18]. The choice of the accelerating voltage is important for obtaining BSE images of chromosomes. When fixed chromosomes are observed by low-vacuum SEM, perichromosomal substances are mainly seen at an accelerating voltage of 5 kV or less, while chromatin fibers under perichromosomal substances are clearly observed with good contrast at a higher accelerating voltage of 20 kV. This is probably due to the high affinity of the Pt blue for chromatin fibers, in contrast to its poor affinity for perichromosomal substances; the high voltage BSE imaging concerns the composition (average atomic number) of samples, while low voltage BSE imaging is useful for observing the surface topography of samples.

Low-vacuum SEM of hydrous chromosomes revealed that metaphase chromosomes consist of highly twisted chromatin fibers, about 80 nm in thickness (Figure 8.6). The coiled appearance of chromatids was sometimes apparent in these specimens, probably due to loosening of the final level of the higher-order structure of compact metaphase chromosomes. When unfixed chromosomes were compared with fixed chromosomes, it was found that chromatin fibers were arranged more compactly and tightly in unfixed chromosomes than in fixed chromosomes. The perichromosomal matrix was more apparent in unfixed chromosomes than in fixed chromosomes, suggesting that the perichromosomal matrix may play an important role in maintaining the higher-order structure of chromosomes.

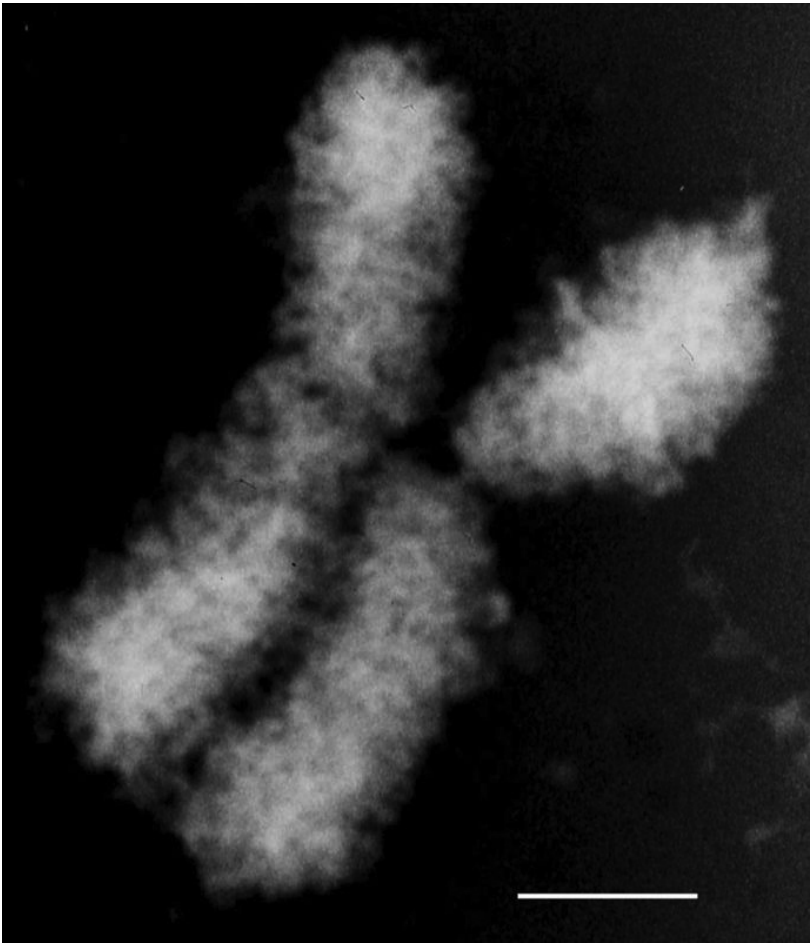

FIGURE 8.6 Hydrous chromosome observed by low-vacuum SEM. Chinese hamster chromosomes fixed with 1% paraformaldehyde are placed on a glass slide, stained with 3% Pt blue aqueous solution, immersed in 20% dimethyl sulfoxide (DMSO) solution and observed in a low-vacuum SEM at −10°C with a vacuum grade from 90 to 270 Pa. Highly twisted chromatin fibers, about 80 nm in thickness, are observed as bright structures. Bar: 1 μm. (From Tanaka et. al. [17]. With permission.)

8.4 CONCLUSION

This chapter has introduced various methods of preparation and observation using TEM and SEM. We have discussed the merits and demerits of each technique, and also pointed out that the ultrastructure of chromosomes can be easily and drastically altered depending on the preparation method. However, based on the results of our studies, we have introduced suitable methods for observing the

three-dimensional ultrastructure of metaphase chromosomes, especially using SEM. Our findings have also demonstrated the utility of three-dimensional observation of chromosomes by low-vacuum SEM, and have indicated that native or unfixed chromosomes maintain a compact arrangement of the helical chromatid covered with the perichromosomal matrix. The instrumentation of TEM and SEM is still improving, and soon it may be possible to analyze the higher-order structure of chromosomes three-dimensionally using TEM tomography more clearly than at present. In the near future, studies of chromosomes by low-vacuum SEM at higher magnification are also expected to provide additional novel findings on the higher-order structure of unfixed chromosomes.

ACKNOWLEDGMENT

This study was partly supported by a Grant-in-Aid for Scientific Research (No. 18390058) from the Ministry of Education, Culture Sports, Sciences and Technology of the Japanese government (TU).

REFERENCES

1. Gall J (1963) Chromosome fibers from an interphase nucleus. *Science* 139: 120–121.
2. DuPraw EJ (1970) *DNA and Chromosomes*. Holt, Rinehart and Winston, New York.
3. DuPraw EJ (1966) Evidence for a 'folded-fibre' organization in human chromosomes. *Nature* 209: 577–581.
4. Sedat J, Manuelidis L (1978) A direct approach to the structure of eukaryotic chromosomes. *Cold Spring Harb Symp Quant Biol* 42: 331–350.
5. Inaga S, Osatake H, Katsumoto T, Kameie T, Yan YL, Naguro T, Iino A (1994) Chromatin structure and hierarchy of metaphase chromosome studied by ultrahigh-resolution SEM and TEM, in *Electron Microscopy 1994 (Proceedings of 13th International Congress on Electron Microscopy)*, Hernandez-Verdun D, Schrevel J, Thomas D, Eds. Les editions de physique, Ulis Cedex A, Paris: Vol. 3A, 433–434.
6. Laemmli UK, Cheng SM, Adolph KW, Paulson JR, Brown JA, Baumbach WR (1978) Metaphase chromosome structure: the role of nonhistone proteins. *Cold Spring Harbor Symp Quant Biol* 42: 351–360.
7. Rattner JB, Lin CC (1985) Radial loops and helical coils coexist in metaphase chromosomes. *Cell* 42: 291–296.
8. Harris P (1961) Electron microscope study of mitosis in sea urchin blastomeres. *J Biophys Biochem Cytol* 11: 419–431.
9. Rieder CL (2005) Kinetochore fiber formation in animal somatic cells: dueling mechanisms come to a draw. *Chromosoma* 114(5): 310–318.
10. Pease RF, Hayes TL (1966) Some biological applications of the scanning electron microscope, in *Electron Microscopy 1966 (Proceedings of 6th International Congress on Electron Microscopy)*, Ueda R, Ed. Marzen, Tokyo: 19–20.
11. Tanaka K, Makino R, Iino A (1970) The fine structure of human somatic chromosomes studied by scanning electron microscopy and the replica method. *Arch Histol Jpn* 32: 203–211.
12. Harrison CJ, Jack EM, Allen TD, Harris R (1985) Light and scanning electron microscopy of the same human metaphase chromosomes. *J Cell Sci* 77: 143–153.

13. Sumner AT (1991) Scanning electron microscopy of mammalian chromosomes from prophase to telophase. *Chromosoma* 100: 410–418.
14. Kättström PO, Nilsson BO (1992) Preparation of human chromosomes for high resolution scanning electron microscopy. *Arch Histol Cytol* 55(Suppl.): 53–56.
15. Nagai S, Inoue T, Iino A (1982) Fibrous structures of human chromosomes observed by scanning electron microscopy. *Cytobios* 34: 35–43.
16. Utsumi KR (1982) Scanning electron microscopy of Giemsa-stained chromosomes and surface-spread chromosomes. *Chromosoma* 86: 683–702.
17. Tanaka K, Inaga S, Iino A, Ushiki T, Saito S (1998) Fine structure of hydrous chromosomes observed by low vacuum scanning electron microscopy. *Arch Histol Cytol* 61: 337–342.
18. Inaga S, Tanaka K, Iino A (2002) Three-dimensional helical coiling structures and band patterns of hydrous metaphase chromosomes observed by low vacuum scanning electron microscopy. *Arch Histol Cytol* 65: 415–423.

9 Atomic Force Microscopy of Human Chromosomes in Relation to Their Higher-Order Structure

*Osamu Hoshi, Daisuke Fukushi and Tatsuo Ushiki**

CONTENTS

9.1 Introduction 105
9.2 Atomic Force Microscopy (AFM) 107
9.3 Sample Preparation 108
9.3.1 Chromosome Spreads 108
9.3.2 Isolated Chromosomes 108
9.4 AFM of Dried Chromosomes 109
9.5 AFM of Wet Chromosomes 111
9.6 Proposed Model of the Higher-Order Structure of Human Metaphase Chromosomes 113
9.7 Dynamic Changes in the Structure of the Chromosome during Cell Division 115
9.8 Conclusion 116
Acknowledgments 116
References 116

9.1 INTRODUCTION

Chromosomes are the intracellular structures that appear as the devices for segregating genetic material during cell division. Biochemical studies have revealed that chromosomes are composed of DNA, histones and nonhistone proteins (see Chapter 13). The structure of the chromosomes has been most often studied at

*To whom correspondence should be addressed.

mitotic metaphase, because the chromosomes are shortest and most condensed in this stage. Morphologically, each metaphase chromosome consists of a pair of sister chromatids that are arranged in parallel along their axes and are joined at their centromeres. The tips of the chromosomes are also referred as the telomeres, which are formed by the end of the DNA molecule. At the most condensed state of mitosis, the packing ratio of DNA in the chromosome is estimated to be 7000 [1]; for example, the smallest human chromosome with a length of 2 μm contains about 4.6×10^7 base pairs of DNA, which is equivalent to about 14 mm of extended DNA. Because the high degree of compaction can be interpreted as being the result of a hierarchal arrangement of DNA packing during the cell cycle, previous investigators have been interested in the ultrastructure of metaphase chromosomes in relation to this subject.

As is well known, at the lowest level, DNA is wound around the histone octamer to form a nucleosome core of about 10 nm in diameter. Thus, the DNA fiber with a large number of nucleosomes is observed as a continuous string of beads, which can be observed by transmission electron microscopy (TEM). This "beads-on-a-string" fiber is condensed into a fiber about 30 nm in thickness (see Chapter 10), which is considered to be a basic form of chromatin in the interphase nucleus. During mitosis, the chromatin fiber is further condensed to form the chromosome. In this sense, the manner of compaction of the chromatin fiber is the most important in clarifying the mechanism of chromosome condensation and chromatid separation during mitosis, and various models of the higher-order structure of the chromosome have been proposed by investigators who observed the chromosome by TEM and/or scanning electron microscopy (SEM). These include the folded fiber model [2], the successive helical coiling fiber model [3,4], the scaffold and radial loop model [5], and the helical coiling of radial loops model [6,7]. However, the issue is still unresolved, probably partly due to the difficulty of conducting preparations which preserve the native chromosome structure, and also due to the technical limitations for precise investigation of chromosomes by conventional TEM and SEM; whole chromosomes are too thick and condensed to be observed using TEM, while drying and metal-coating are required for SEM.

The atomic force microscope (AFM) was invented in 1986 as an offspring of the scanning tunneling microscope [8]. This microscope can create topographic images of the solid surface that are similar to those obtained by SEM. However, the AFM has an advantage in observing samples without metal-coating, because it can obtain images of both conductive and nonconductive structures. It is also attractive for biologists that the AFM can be used not only in a vacuum but also in an air or liquid environment, indicating that samples can be directly observed under wet conditions at a resolution comparable to that of SEM. Thus, the AFM has been recently applied to studies on the surface structure of various kinds of biological samples [9–11] including chromosomes [12–14].

In this chapter, we will first briefly introduce the principle of AFM; second, we will review our AFM studies on the structure of human chromosomes; and finally provide some comments on the higher-order structure of chromosomes.

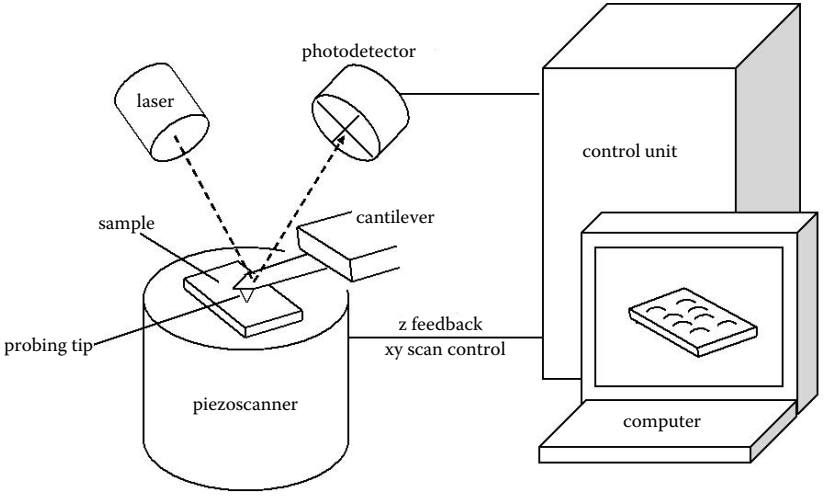

FIGURE 9.1 The schematic illustration of the atomic force microscope (AFM). The AFM has a sharp probing tip which scans over a sample while measuring the tiny interaction force between the tip and the sample surface. The tip is commonly attached to the end of a cantilever which serves as a force sensor. A piezoelectronic *xyz*-scanner is usually used both to control the vertical position of the sample (*z*) and to raster-scan the sample in the *xy*-plane.

9.2 ATOMIC FORCE MICROSCOPY

The basic concept of AFM is the measurement of forces between a sharp probing tip and a sample surface [15]. The tip is commonly attached to the end of a cantilever which serves as a force sensor; when the tip approaches the sample surface, a tiny interaction force occurs between the tip and the sample, which influences the position of the cantilever (Figure 9.1). The positional change is usually monitored by a beam-deflection method; the laser beam is reflected at the rear side of the cantilever and its deflection is monitored by a position-sensitive photodetector. Thus, the force between the tip and sample can be accurately detected as the deflection of the cantilever. For AFM imaging, the sample is scanned by the tip in the *xy*-plane, while the interaction force between them is monitored as above and regulated by changing the height of the sample using a feedback system. A piezoelectronic *xyz*-scanner is usually used both to control the vertical position of the sample (*z*) and to raster-scan the sample in the *xy*-plane.

Several operation modes of AFM have been introduced according to the method of cantilever operation, but can be broadly divided into the static and dynamic modes. In the static mode, the tip is simply dragged across the sample surface, measuring the deformation of the cantilever, and thus is also called the contact mode. In the dynamic mode, the sample surface is scanned with a vibrating cantilever, and the tip–sample interaction force is monitored by alteration of the resonance frequency or oscillation amplitude of the cantilever. The most

commonly used dynamic mode measures a reduction of the oscillation amplitude as feedback amplitude and is also referred to the intermittent contact mode. The advantage of the dynamic mode is to reduce the effect of lateral forces exerted on the cantilever, and the vertical interaction force can also be controlled more finely in the dynamic mode (10^{-9} to 10^{-10} N) than in the contact mode (about 10^{-8} N). In this regard, the dynamic mode is commonly used for AFM imaging of chromosomes, because the sample is very soft and easily deformed by the external force.

AFM has several imaging modes. The AFM image produced by the feedback voltage to the *z*-scanner is called the "constant force image" (or height image), which contains the height of the sample. On the other hand, the image displaying the change in cantilever deflection (in contact mode AFM) or the oscillation frequency (in dynamic mode AFM) is called the "variable deflection image," which is useful for detection of the height change of the sample.

9.3 SAMPLE PREPARATION

9.3.1 Chromosome Spreads

Human lymphocytes collected from heparinized peripheral blood of healthy male donors were cultivated in the karyotyping culture medium (PB-max; Gibco, BRL, U.K.) with 10% fetal calf serum for 72 h at 37°C, under 5% CO_2 and 95% air. In some cases, lymphocytes after cultivation were arrested in metaphase by adding colcemid to the culture medium at a final concentration of 0.05 μg/mL for 1 h. The cell suspension was then exposed to 75 m*M* KCl for 30 min at room temperature and fixed with Carnoy's solution (methanol/acetic acid = 3:1, v/v). Chromosome spreads were then formed by dropping the cell suspension onto glass slides, and leaving in a humid atmosphere.

9.3.2 Isolated Chromosomes

Cells from the human cell line BALL-1 (RCB0256), obtained from RIKEN Cell Bank (Riken, Tsukuba, Japan), were grown in a 40-mL flask in culture medium (RPMI 1640; Invitrogen, Tokyo, Japan) at 37°C under an atmosphere containing 5% CO_2 and 95% air. After arrest with 0.06 μg/mL colcemide for 12 h, the cells were suspended and centrifuged at 190 *g* for 10 min at 4°C, resuspended as a pellet in 10 mL of the culture medium for 20 min, centrifuged again at 190 *g* for 10 min, and then exposed to 75 m*M* KCl for 15 min. These cells were collected by centrifugation at 190 *g* and isolated using the hexylene glycol method [16]; briefly, the cells were gently resuspended in hexylene glycol buffer composed of 1.0 *M* hexylene glycol (2-methyl-2,4-pentanediol), 0.5 m*M* $CaCl_2$ and 0.1 m*M* PIPES (pH 6.5), and incubated in the same buffer for 10 min at 37°C. The cells were further broken with a Dounce homogenizer (15 mL capacity) by five gentle strokes [17] and centrifuged at 1680 *g* at 4°C for 15 min for concentration of the crude chromosome suspension.

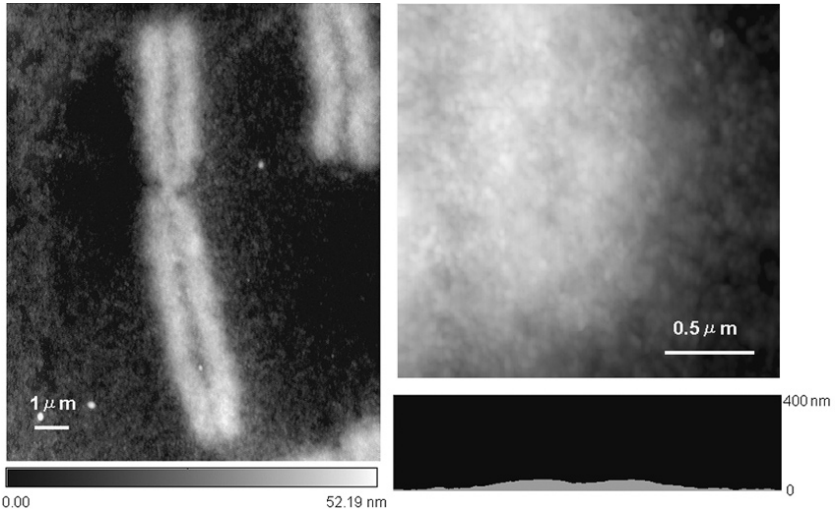

FIGURE 9.2 AFM images of the air-dried chromosomes. Human chromosomes were fixed with the Carnoy's solution, air-dried onto a glass slide and observed in air with a dynamic mode AFM. The chromosome is characterized by the presence of the chromosome arms separated by the centromere. The chromosome arm is composed of a pair of chromatids that are arranged parallel along the axis of the arm. Each chromatid is generally uniform in structure and its surface appeared smooth with a fluffy texture. The profile of the chromosome arm (below right) shows that the height is about 50 nm (below right). At high magnification, the chromatid only shows a granular appearance. (For AFM imaging, commercially available rectangular silicon cantilevers with a nominal spring constant of 42 N/m were used for AFM imaging in air; the resonance frequency was normally 300 kHz in air.)

9.4 AFM OF DRIED CHROMOSOMES

AFM is commonly used for imaging dried samples in ambient conditions. When the chromosome spread was simply dried in air and observed in the dynamic mode, each chromatid of the metaphase chromosome was usually about 1 μm in width and about 50 to 200 nm in height (Figure 9.2). The chromosome arms were rather uniform in structure and the surface appeared smooth, with a fluffy texture [18]. Even at high magnification, they showed only a granular appearance and no fibrous structures could be detected in these specimens. This is probably mainly due to the deformation artifact caused by surface tension during air-drying, as well as the presence of a blanket-like layer of cytoplasmic debris draped over the chromosome during the standard method for preparation of the chromosome spread.

To minimize these artifacts, the chromosome spreads produced by dropping the cell suspension onto the glass slide were dried for a few minutes, and hydrated again by immersion in phosphate buffer for 30 min or more. They were then treated with a 1% tannic acid solution for 15 min, washed in the buffer for 15 min (three changes, 5 min each), and treated with a 1% OsO_4 solution for hardening of chromosomes. These samples were dehydrated in a graded series of ethanol baths,

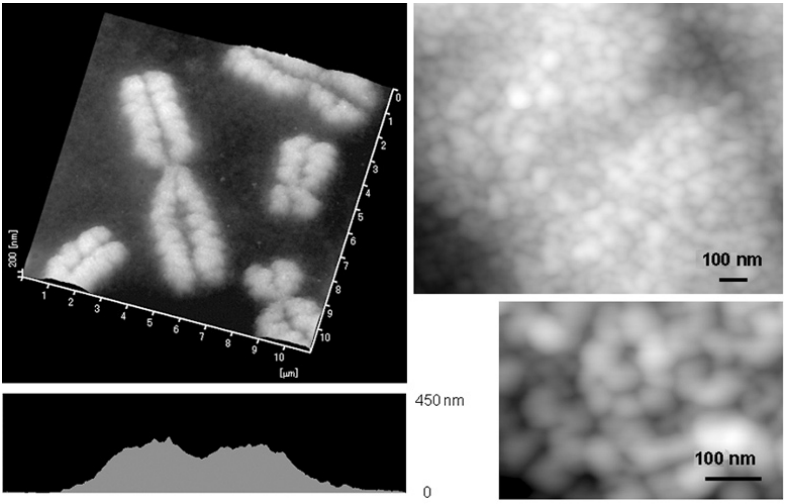

FIGURE 9.3 AFM images of the critical-point dried chromosomes. Spreads of human metaphase chromosomes were immersed in a buffer, treated with a 1% tannic acid solution and 1% OsO_4, critical-point dried in liquid CO_2, and observed in air with a dynamic mode AFM. The operation condition is almost the same as that of Figure 9.2. Ridges and grooves are clearly observed in the sister chromatids of the chromosomes. The profile of the chromosome arm (below left) shows that the height is about 200 nm. At higher magnification, globular structures about 50 to 60 nm thick are observed in the surface of the chromatid. There are also fibrous structures suggesting the presence of highly twisted chromatin fibers.

and critical-point dried in CO_2 to avoid the deformation artifact from air-drying. In these specimens, chromosomes were measured to be about 200 to 350 nm in height, and often showed circumstantial grooves and ridges on the surface of the chromatid arms (Figure 9.3) [13]. The arrangement of the grooves and ridges was roughly symmetrical with the counterpart of the paired sister chromatids, and the ridges are considered to correspond to the positive bands of G/Q-banded chromosomes observed by light microscopy. The grooves and ridges can also be related to the zigzag or spiral arrangement of the chromatids in the metaphase chromosome, as proposed by previous investigators [6,13,19].

At high magnification, the surface of the critical-point dried chromosome was clearly observed, when the chromosome spread with low quantities of cytoplasmic debris was carefully selected by light microscopy prior to AFM examination. The surface of the chromosome had a globular appearance, but careful studies suggested that they were produced by strongly twisted fibrous structures about 50 nm thick. The condensation of the twisted fibers was marked in the ridged portions, while it was weaker in the grooved portions. AFM of the chromosomes further revealed that a pair of sister chromatids was not completely separated even in late metaphase, but was connected by fibrous structures of about 50 to 60 nm in thickness, suggesting catenation of chromatin fibers between the chromatids. The catenation was especially found in regions between the ridges of the chromosome.

9.5 AFM OF WET CHROMOSOMES

AFM has the potential for obtaining images of samples in liquid conditions. For imaging wet chromosomes by AFM, chromosome spreads were briefly dried in air in order to fix them onto the glass slides, and were then immersed in phosphate-buffered saline. After a chromosome spread with little cytoplasmic debris was selected by phase contrast microscopy, the chromosomes in the spread were observed in the phosphate-buffered saline in the dynamic mode of AFM. Because of the extreme softness of chromosomes in liquid environments, the operation conditions were important for the quality of AFM imaging; in particular, the interaction force between the tip and sample should be carefully adjusted to the minimum possible; otherwise chromosomes are easily deformed during scanning.

In the appropriate operating conditions, the height of the chromosomes was generally about 200 to 300 nm, but sometimes ranged up to 600 nm (Figure 9.4) [20]. The surface of chromatids in these chromosomes was characterized by the presence of alternating ridges and grooves, the arrangement of which was roughly symmetrical with the counterpart of the paired sister chromatids. These features were almost the same as those found in the critical-point dried chromosomes, but the patterns of ridges and grooves were more apparent in the wet chromosomes than in the critical-point dried chromosomes. As a result, the pattern of ridges and grooves in the chromosomes was able to be precisely investigated in these specimens, and this revealed that the number and arrangement of the ridges and

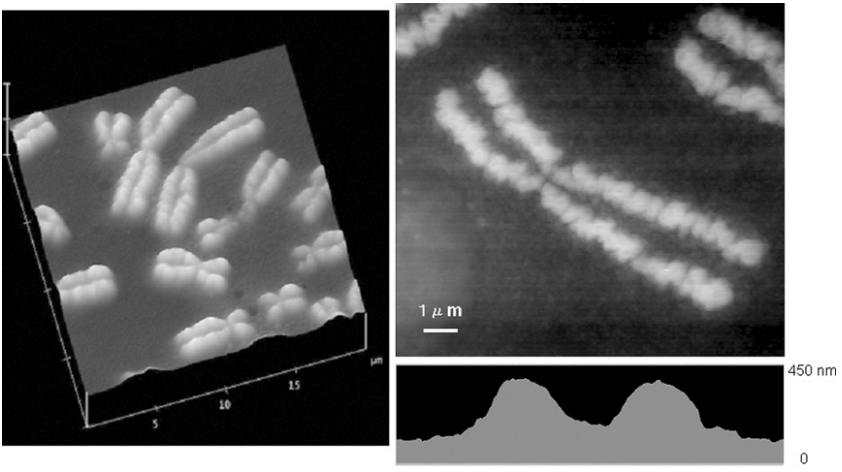

FIGURE 9.4 AFM images of fixed chromosomes in a liquid condition. Spreads of human metaphase chromosomes were immersed in a phosphate-buffered saline and observed in the same solution with a dynamic mode AFM. Ridges and grooves are evident in the sister chromatids of the chromosomes. The profile of the chromosome arm (below right) shows that the height is about 250 nm. (V-shaped silicon nitride cantilevers with oxide-sharpened tips with nominal spring constant of 0.37 N/m were used for imaging in liquid; the resonance frequency was normally about 12.5 kHz in liquid.)

grooves appeared to be specific to the type of chromosome; for example, the number of ridges was usually 17 for chromosome 1, and 16 for chromosome 2. The ridges and grooves in the chromatid arm were not strictly aligned along the chromosome axis, but sometimes showed a slightly zigzag arrangement because some ridges were connected with those of the counterpart of the paired chromatids and they closely associated with each other.

For studying the structure of unfixed, or native, chromosomes in a liquid environment, the chromosome spread described above cannot be used because chromosomes must be fixed in this preparation method. Thus, isolated human metaphase chromosomes were prepared as introduced in Section 3.2. These chromosomes were adsorbed onto a silane-coated glass slide by dropping the chromosome suspension onto the slide. The chromosomes to be studied were selected in the hexylene glycol buffer with a phase contrast microscope, and were observed in a dynamic mode AFM in the same buffer solution [21].

The native chromosomes were about 1 μm in width and ranged from 400 to 800 nm in height (Figure 9.5). At high magnification, globular or fibrous structures about 50 nm thick were observed on the surface of each chromatid, although they

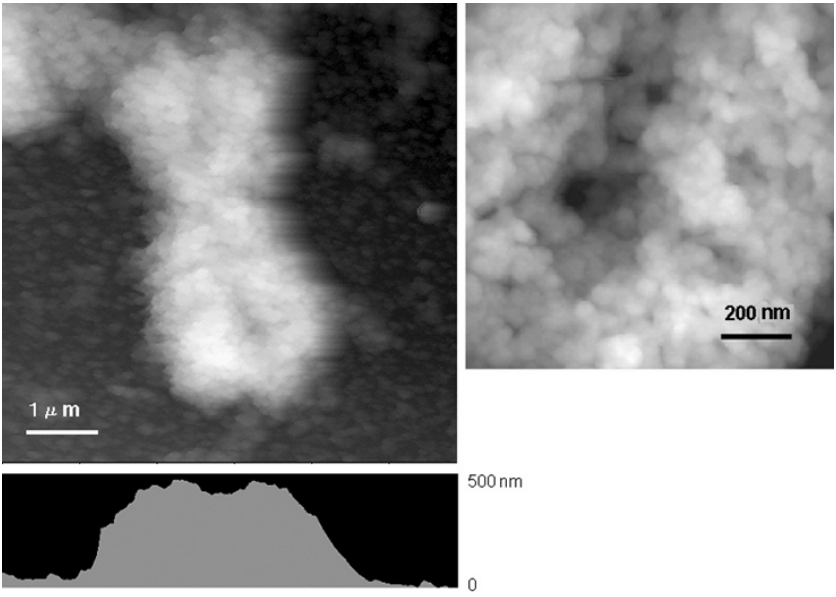

FIGURE 9.5 AFM images of unfixed chromosomes in a liquid condition. Chromosomes of the human cell line BALL-1 were isolated by the hexylene glycol method, mounted on a glass slide and observed in a hexylene glycol buffer solution with a dynamic mode AFM. The operation condition is almost the same as that of Figure 9.4. The profile of the chromosome arm (below left) shows that the height is nearly 500 nm. At high magnification, chromatids are observed as an aggregation of globular or fibrous structures. The right image is reproduced with permission from Hoshi et al. [21].

were arranged without any apparent regularity. The partial connection of paired sister chromatids with entangled chromatin fibers was also observed in these chromosomes. These findings correspond well to those obtained in the critical-point dried chromosomes and wet fixed chromosomes.

9.6 PROPOSED MODEL OF THE HIGHER-ORDER STRUCTURE OF HUMAN METAPHASE CHROMOSOMES

The three-dimensional surface structure of human metaphase chromosomes revealed by our AFM studies is summarized as follows:

1. The chromatid arm of the metaphase chromosome is not uniform in structure but has ridges and grooves along its length. The arrangement of these ridges and grooves is roughly symmetrical with the counterpart of the paired sister chromatids. The number and arrangement of the ridges and grooves also appear to be specific to the type of the chromosome.
2. The chromatid is filled with granular and/or fibrous structures about 50 to 60 nm in diameter on its surface, suggesting that the chromatid is produced by the compaction of highly twisted chromatin fibers about 50 to 60 nm thick.
3. The compaction of the chromatin fibers is stronger in the ridged regions of the chromosomes than in the grooved regions.
4. The paired chromatids are usually connected to each other by chromatin fibers about 50 nm thick. These connections are especially apparent in the ridged regions of the chromatids of the metaphase chromosomes.

These features indicate that the structure of the chromosome arm is not uniform but heterogeneous because of the presence of highly condensed and less condensed regions in the chromosome; the highly condensed portions are observed as ridged regions of the chromatid, while less condensed portions are observed as grooved regions. These ridges and grooves are also considered to be related to the G/Q-positive and G/Q-negative bands, respectively, in G/Q banded chromosomes [13].

Several investigators pointed out the spiral arrangement of the sister chromatid in the chromosomes of various species [22,23]. With regard to human chromosomes, Ohnuki [19] treated samples with a special hypotonic solution and showed the sister chromatid of the metaphase chromosome as a spiral or zigzag fiber. We observed by AFM these chromosomes with the zigzag arrangement after the special hypotonic treatment, and showed that the zigzag arrangement is closely related to the arrangement of ridges and grooves in the metaphase chromosome [13].

Taking these results together, we consider that the chromatid of the metaphase chromosome is not uniform in structure but is composed of zigzag fibers with ridges and grooves. The ridge regions are probably related to the positive bands of the G/Q banded chromosome, which also suggests a difference in structure between the ridges and grooves. This model of the structure of the metaphase chromosome may be also accord with the immunocytochemical findings on the

distribution of topoisomerase IIα, which is known to be a scaffold protein of the chromosome; the immunofluorescence of topoisomerase IIα is not uniform but is spotted along the chromosome axis, and the pattern of these intense spots in the chromosome arms seems to overlap with the banding pattern of G/Q-banded chromosomes (see Chapter 7). It is also interesting that the topoisomerase IIα-positive axis is observed as a zigzag structure at late metaphase. The basic structure of the human metaphase chromosome is illustrated in Figure 9.6.

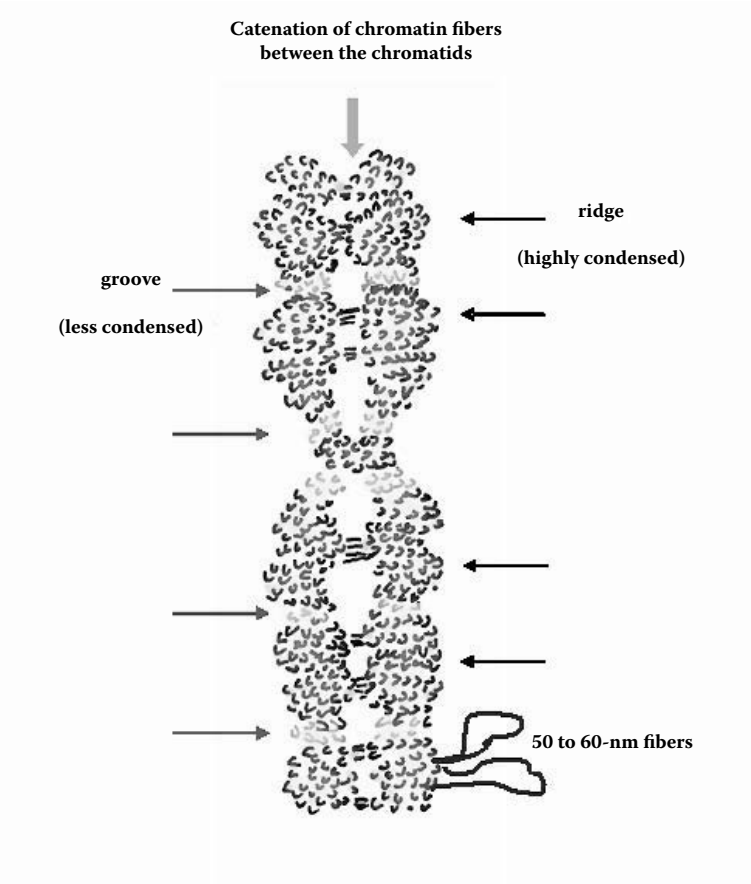

FIGURE 9.6 (See color insert following page 110) Schematic representation of the higher-order structure of the human metaphase chromosome. The chromosome is composed of a pair of the sister chromatids with ridges and grooves. The chromatid is filled with granular and/or fibrous structures about 50 to 60 nm in diameter on its surface, suggesting that the chromatid is produced by the compaction of highly twisted chromatin fibers about 50 to 60 nm thick. The compaction of the chromatin fibers appears stronger in the ridged regions than in the grooved regions. The paired chromatids are often connected with entangled chromatin fibers, suggesting the presence of the catenation even in the metaphase chromosome.

9.7 DYNAMIC CHANGES IN THE STRUCTURE OF THE CHROMOSOME DURING CELL DIVISION

The change in higher-order structure of the chromosome during mitosis is also an important subject for understanding the mechanism of chromosome condensation and chromatid separation. For observing chromosomes in different mitotic stages, chromosome spreads were obtained from cultured human lymphocytes without any anti-mitotic agents and were observed by AFM (Figure 9.7). In these specimens, chromatin fibers about 50 nm thick were observed inside the prophase nucleus, suggesting the beginning of condensation in this stage (micrograph not shown). During prometaphase, chromatin fibers apparently took the shape of the chromosomes, though the length was substantial and the degree of condensation was not uniform in the chromosome, in that highly condensed portions were present as a banded pattern along the axis of each chromosome. In metaphase, the condensation of chromatin fibers was most marked, and each sister chromatid became clearly distinguishable. The sister chromatids began to split in the chromosomal arms, although they still adhered to each other in the centromere as well as partially in the arms. In anaphase, the sister chromatids were completely separated, forming two groups of chromatids, but they were still relatively short. During telophase, two nuclei of each daughter cell were produced by raveled chromatin fibers.

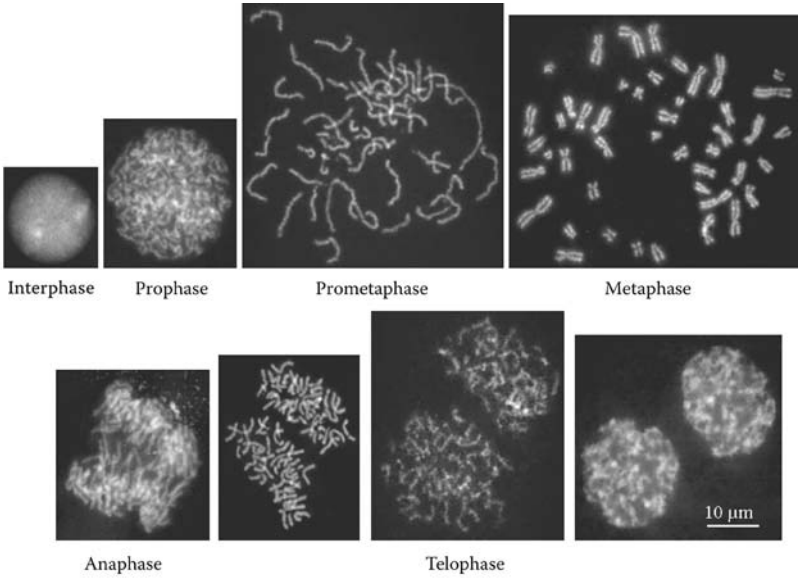

FIGURE 9.7 AFM images of human metaphase chromosomes in different mitotic stages. Chromosome spreads were obtained from cultured human lymphocytes without any anti-mitotic agents and were observed in air with a dynamic mode AFM. The operation mode is the same as that of Figure 9.2.

9.8 CONCLUSION

In this chapter we have introduced AFM for obtaining images of the three-dimensional surface topography of chromosomes, and have presented our AFM results on the structure of human chromosomes. AFM is useful for observing the surface structure of the samples without the metal-coating necessary for SEM. Thus, we succeeded in clarifying the three-dimensional structure of human chromosomes in relation to their higher-order structure.

As shown in this chapter, AFM has the characteristic of being amenable to obtaining images of samples not only in vacuum but also in air and liquid. AFM imaging of chromosomes in liquid is very attractive because sample preparation can be minimized, resulting in the prevention of artifacts arising during the complicated preparation methods hitherto employed. After AFM imaging, the samples can be also used for various purposes including fluorescence *in situ* hybridization, chromosome banding and immunocytochemistry. Thus, using this technique, information on the structure of chromosomes can be directly compared with that obtained by various biological techniques. On the other hand, AFM imaging of dried samples is also still useful because images can be easily and constantly obtained in the standard dynamic mode. However, as described in this chapter, the sample preparation method is very important for avoiding the deformation artifact.

Recent advances in AFM have enabled the development of high-speed AFM, in which topographic images of samples can be obtained at video rate [24]. In the near future, it may be possible to use this type of AFM to study changes in the structure of chromosomes through direct observation of native chromosomes in liquid conditions.

ACKNOWLEDGMENTS

This study was supported by Special Coordination Funds of the Ministry of Education, Culture, Sports, Science and Technology of the Japanese government (TU) and was supported in part by Grant-in Aids for Scientific Research (No. 18390058) from the Japan Society for Promotion of Science, Japan (to TU).

REFERENCES

1. Lewin B (2000) *Genes VII*. Oxford University Press, Oxford.
2. Dupraw EJ (1965) Macromolecular organization of nuclei and chromosomes: a folded fiber model based on whole-mount electron microscopy. *Nature* 206: 338–343.
3. Bak AL, Zeuthen J, Crick FH (1977) Higher-order structure of human mitotic chromosomes. *Proc Natl Acad Sci USA* 74: 1595–1599.
4. Sedat J, Manuelidis L (1978) A direct approach to the structure of eukaryotic chromosomes. *Cold Spring Harb Symp Quant Biol* 42: 331–350.

5. Laemmli UK, Cheng SM, Adolph KW, Paulson JA, Browns JA, Baubach WR (1978) Metaphase chromosome structure and the role of non-histone proteins. *Cold Spring Harb Symp Quant Biol* 42: 351–360.
6. Rattner JB, Lin CC (1985) Radial loops and helical coils coexist in metaphase chromosomes. *Cell* 42: 291–295.
7. Rattner JB (1992) Integrating chromosome structure with function. *Chromosoma* 101: 259–264.
8. Binnig G, Quate CF, Gerber C (1986) Atomic force microscope. *Phys Rev Lett* 56: 930–933.
9. Engel A, Lyubchenko Y, Müller DJ (1999) Atomic force microscopy: a powerful tool to observe biomolecules at work. *Trends Cell Biol* 9: 77–80.
10. Ushiki T (2003) Atomic force microscopy for imaging living organism: from DNA to cell motion, in *Micromachines as Toos for Nanotechnology*, Fujita H, Ed. Springer, Berlin/Heidelberg/New York: 121–130.
11. Hörber JK, Miles MJ (2003) Scanning probe evolution in biology. *Science* 302: 1002–1005.
12. Tamayo J, Miles M (2002) Scanning probe microscopy for chromosomal research. *Arch Histol Cytol* 65: 369–376.
13. Ushiki T, Hoshi O, Iwai K, Kimura E, Shigeno M (2002) The structure of human metaphase chromosomes: its histological perspective and new horizons by atomic force microscopy. *Arch Histol Cytol* 65: 377–390.
14. Thalhammer S, Heckl WM (2003) Atomic force microscopy in cytogenetics, in *Force Microscopy: Application in Biology and Medicine*, Jena BP, Hörber JKH, Eds. John Wiley & Sons, New York: 249–266.
15. Meyer E, Hans JH, Roland B (2004) *Scanning Probe Microscopy: The Lab on a Tip*. Springer, Berlin.
16. Wray W, Stubblefield E (1970) A new method for the rapid isolation of chromosomes, mitotic apparatus, or nuclei from mammalian fibroblasts at near neutral pH. *Exp Cell Res* 59: 469–478.
17. Marsden MPF, Laemmli UK (1979) Metaphase chromosome structure: evidence for a radial loop model. *Cell* 17: 849–868.
18. Hoshi O, Ushiki T (2001) Three-dimensional structure of G-banded human metaphase chromosomes observed by atomic force microscopy. *Arch Histol Cytol* 64: 475–482.
19. Ohnuki Y (1968) Structure of chromosomes. I. Morphological studies of the spiral structure of human somatic chromosomes. *Chromosoma* 25: 402–428.
20. Hoshi O, Owen R, Miles M, Ushiki T (2004) Imaging of human metaphase chromosomes by atomic force microscopy in liquid. *Cytogenet Genome Res* 107: 28–31.
21. Hoshi O, Shigeno M, Ushiki T (2006) Atomic force microscopy of native human metaphase chromosomes in a liquid. *Arch Histol Cytol* 69: 73–78.
22. Makino S (1936) The spiral structure of chromosomes in meiotic division of Podisma (Orthopetera). *J Fac Sci Hokkaido Imp Univ Ser VI* 3: 29–40.
23. White MJD (1940) The heteropycnosis of sex chromosomes and its interpretation in terms of spiral structure. *J Genet* 40: 67–82.
24. Picco LM, Bozec L, Ulcinas A, Engledew DJ, Antognozzi M, Horton MA, Miles MJ (2006) Breaking the speed limit with atomic force microscopy. *Nanotechnology* 18: 1–4.

10 Mechanism of Higher-Order Chromatin Folding Revealed by AFM Observation of *In Vitro* Reconstituted Chromatin

*Kohji Hizume, Toshiro Kobori, Shige H. Yoshimura and Kunio Takeyasu**

CONTENTS

10.1 Introduction 120
10.2 Current Understanding of Higher-Order Chromatin Structure 121
10.2.1 The Nucleosome as the Most Fundamental Unit in Chromosome Folding 121
10.2.2 Linker Histones and Other Nonhistone Proteins Involved in Higher-Order Chromatin Folding 121
10.2.3 Use of an *In Vitro* Chromatin Reconstitution System for Chromosome Study 122
10.2.4 The Importance of *In Vitro* Chromatin Reconstitution Studies 122
10.3 Establishment of an *In Vitro* Reconstitution System for a Long Nucleosome Array 123
10.3.1 Materials for the Reconstitution 123
10.3.2 Salt-Dialysis-Reconstitution and AFM Observation of Nucleosomes 123
10.3.3 Frequency of the Nucleosomes in Relation to Plasmid Length 124
10.3.4 DNA Negative Supercoiling Affects Nucleosome Formation 126
10.3.5 Chromatin Salt-Dependent Conformational Changes 127

*To whom correspondence should be addressed.

10.4 Role of Linker Histone H1 in Nucleosome Compaction 128
10.4.1 Addition of Linker Histone H1 to Reconstituted 100-kb Chromatin 128
10.4.2 Dose-Dependency of Linker Histone H1 for Formation of Thicker Fibers 129
10.4.3 Physiological Ionic Strength Is Critical for the Formation of 30-nm Fibers 129
10.5 Nonhistone Chromosome Proteins also Induced Chromatin Compaction 130
10.5.1 Contribution of Matrix/Scaffold Proteins 131
10.5.2 Nonhistone Chromosomal Protein PC4 Induced Chromatin Compaction by a Mechanism Different from the Histone H1-Induced Compaction 133
10.6 Conclusion 133
Acknowledgment 133
References 134

10.1 INTRODUCTION

In eukaryotic cells, genomic DNA is packaged into the nucleus in a well-organized manner. The ultimate goal of chromosome researchers is to understand the molecular mechanisms underlying the process in which DNA is folded up and packed, together with a number of associated proteins, into the nucleus. For years, researchers have known that the chromosome is built up from DNA and protein, and also that the chromosome condenses to form an "X" shape in mitosis [1]. Although the precise number of steps is not known, it has generally been believed that there are at least several steps on the path from DNA to the chromosome [1,2].

To clarify the steps between DNA and the chromosome, researchers have taken two different approaches. One is to start from DNA and step upward the chromosome. This so-called "reconstitution" approach proved that the first step is the formation of a nucleosome structure in which the DNA strand wraps around a core histone octamer. It is now accepted that the nucleosome is formed by electrostatic interaction between DNA and histone [3]. The other approach is to start from the chromosome (or nucleus) and step down toward DNA (see Chapter 9). Using this procedure, it was elucidated that chromosomes contain fibers of several different widths (30, 100 and 300 nm) [4–8]. Although these fibers exist somewhere on the path between DNA and the chromosome, it is still controversial exactly where these different fiber types are located along this path.

The development of various new imaging techniques in recent years, together with the proteomic and biochemical analyses of chromosomal proteins, is making large contributions toward elucidating the "gap" between the nucleosome and the chromosome. In this chapter, we will first survey the current understanding of the higher-order structure of chromatin and the chromosome, and we will then review our results regarding the *in vitro* reconstitution of chromosomal structures.

10.2 CURRENT UNDERSTANDING OF HIGHER-ORDER CHROMATIN STRUCTURE

10.2.1 The Nucleosome as the Most Fundamental Unit in Chromosome Folding

The most fundamental and well-known structural unit of the chromosome is the nucleosome [9,10]. The nucleosome is composed of 146 bp of DNA wrapped around a core histone octamer (two of each the subunits H2A, H2B, H3 and H4) for ~1.65 turns [3]. These subunits of the core histones have relatively low molecular weights, ranging from 11 to 15 kDa, and have 17 to 20 positive charges at pH 7.0, as calculated from the amino acid composition. In a single nucleosome, two molecules each of H3 and H4 form a tetramer, and H2A and H2B form two dimers [11]. More specifically, two dimers of H2A/H2B bind to one tetramer of H3/H4, and as a result, a histone octamer with a diameter of 6.5 nm is formed. The basic histone octamer makes a tight complex with the acidic DNA strand, and therefore the dissociation of the histone octamer from DNA requires high-salt treatment (2 *M* NaCl) [12].

10.2.2 Linker Histones and Other Nonhistone Proteins Involved in Higher-Order Chromatin Folding

Although a number of biochemical and microscopic studies have demonstrated that linker histones play an important role in the higher-order folding of chromatin fibers, the details of the folding mechanism are still a matter of controversy. Histone H1 (composed of 210 to 220 amino acid residues) has a globular domain in the middle region [13], through which it binds to linker DNA; in particular, the region where DNA enters into and exits from the nucleosome core particle [9,14]. The removal of histone H1 results in the unfolding of a 30-nm fiber into a "beads-on-a-string" fiber [4,15]. The depletion of H1- and H3-tail from chromatin fiber by trypsin treatment induces a loss of the "zigzag" arrangement of nucleosomes and deforms the 30-nm fiber [14]. Therefore, the role of histone H1 seems to be to tighten the nucleosome–nucleosome interaction. As such, it is important for the chromatin architecture, although this is still controversial in some species. (e.g., *Schizosaccharomyces pombe*) lacks histone H1 [16], and the results of several studies have indicated that histone H1 is not essential for chromosome condensation (see below).

In addition to histone H1, a number of proteins are known to be involved in the maintenance of chromosome structure. The chromosomal associated proteins (CAPs) [17] interact with nucleosomes and are involved in transcriptional regulation. The high mobility group (HMG) proteins participate in the regulation of chromatin structure as well as being involved in transcriptional regulation [18–20]. On the other hand, heterochromatin protein 1 localizes to the heterochromatin region, suggesting that it is involved in transcriptional silencing. Some of the CAPs, for example, HMGN, are thought to compete with H1 [21].

Other CAPs, such as MENT (Myeloid and Erythroid Nuclear Termination stage-specific protein), are thought to bind to nucleosomes in association with H1 [22].

Another group of nonhistone proteins has been identified as being essential for the formation of highly condensed chromosomes. It has been shown that topoisomerase II exists in the fraction of the so-called nuclear matrix of interphase cells [23] and in the scaffold fraction of the mitotic chromosome [24]. The condensin complex has been reported to be localized in the same scaffold fraction [24] and to be essential for mitotic chromosome condensation [25]. The frog condensin complex exhibits ATP-dependent DNA supercoiling activity [26], and topoisomerase II has an activity allowing DNA strands to pass through each other [27]. Thus, these two factors are thought to be critical for chromatin condensation, although the precise molecular mechanisms have not yet been resolved [2].

10.2.3 Use of an *In Vitro* Chromatin Reconstitution System for Chromosome Study

In addition to various microscopic observations, *in vitro* chromatin reconstitution techniques have also been used in the study of chromatin structure and function. High-efficiency reconstitution can be achieved when *Drosophila* embryo extract is used; the nucleosomes are formed efficiently and are evenly spaced (one nucleosome per every ~200 bp) [28]. The most recently established method utilizes the chromatin assembly factors (NAP-1 protein and the ACF complex), with which the correct spacing of the nucleosome can also be obtained [29]. However, these reconstitution systems are still rather complicated, and more well-defined systems are preferable.

The purest reconstitution system requires only core histones and naked DNA [30], but no other protein. The histone octamer and DNA are mixed in a high-salt environment (2 *M* NaCl) and then dialyzed against a salt-free buffer to slowly reduce the salt concentration. This simple procedure, called salt-dialysis, can produce a nucleosome array without the input of any other proteins, and is independent of the nucleotide sequence of the template DNA (nucleosomes can be formed even on bacterial DNA). Although the efficiency of the reconstitution is not as high as with the crude extract system, the effectiveness of the salt-dialysis procedure, by itself, indicates that the underlying mechanism of nucleosome formation is a simple electrostatic interaction between DNA and histone.

10.2.4 The Importance of *In Vitro* Chromatin Reconstitution Studies

As mentioned above, the stability of the nucleosome is predominantly governed by electrostatic interaction between negatively charged DNA and positively charged core histones. What, then, causes this nucleosome to fold into a thick chromatin fiber, such as the 30-nm fiber? A set of proteins might be involved in such higher-order chromatin folding, in addition to the fundamental histone–DNA interactions. Biochemical and microscopic analyses have suggested that other

proteins (especially linker histones) might play an important role [2,17,31]. However, so far none of the reconstitution systems (including the crude extract system) can produce chromatin fibers thicker than the zigzag array of nucleosomes, suggesting that other unknown factor(s) may be missing in these systems.

In a series of reconstitution experiments, our group has found (as shown in this chapter) that the efficiency of chromatin reconstitution using the salt-dialysis method was dramatically increased simply by using long (100 kb) and supercoiled DNA. This result suggested that the physical properties of DNA might be the "missing factor" necessary for higher-order chromatin folding. Since double-stranded DNA, like other polymer chains, carries a certain elasticity and flexibility, the length of DNA could affect the stability of nucleosomes and the chromatin fiber. Furthermore, it can be speculated that the nucleosome stability could be tightly coupled with the superhelical strain of the DNA, because the formation of nucleosomes introduces positive supercoiling into the neighboring DNA. In the following chapters, we will explain how chromatin reconstitution with a long DNA contributes to the elucidation of fundamental chromosome packing mechanisms.

10.3 ESTABLISHMENT OF AN *IN VITRO* RECONSTITUTION SYSTEM FOR A LONG NUCLEOSOME ARRAY

10.3.1 Materials for the Reconstitution

The overall goal of our research is to understand the packing mechanisms of the chromosome through *in vitro* reconstitution and observation of the chromosome structure. For this purpose, it was necessary to construct a longer nucleosome fiber from DNA and core histones, because the higher-order chromosome structure should be composed of at least hundreds of nucleosomes as the basic units. In order to assemble a long nucleosome array, we prepared plasmids as follows: the human centromere-specific repetitive sequences (alphoid DNA) [32,33] with various lengths (2, 25, 50 and 100 kb) were subcloned into either pUC119 (for the 2-kb fragment) or a bacterial artificial chromosome vector (BAC, for the 25-, 50- and 100-kb fragments) [34], to stably maintain the long repetitive DNA fragments. Thus, the total lengths of the template DNAs are 5, 31, 56 and 106 kb. Noncentromeric DNA of 3 kb in length (pBlueScript) was also prepared. As shown in Figure 10.1(a), all (i.e., 3, 31 and 106 kb) plasmids observed by atomic force microscopy (AFM) were highly twisted and tangled because of the negative supercoiling introduced in *Escherichia coli* cells. Histone octamers were purified from HeLa cells by hydroxylapatite chromatography followed by gel-filtration. The AFM image of the histone octamer is shown in Figure 10.1(b).

10.3.2 Salt-Dialysis-Reconstitution and AFM Observation of Nucleosomes

The chromatin was reconstituted using the salt-dialysis method [30]. Equal amounts (0.5 μg) of purified DNA and histone octamer were mixed in Hi-buffer

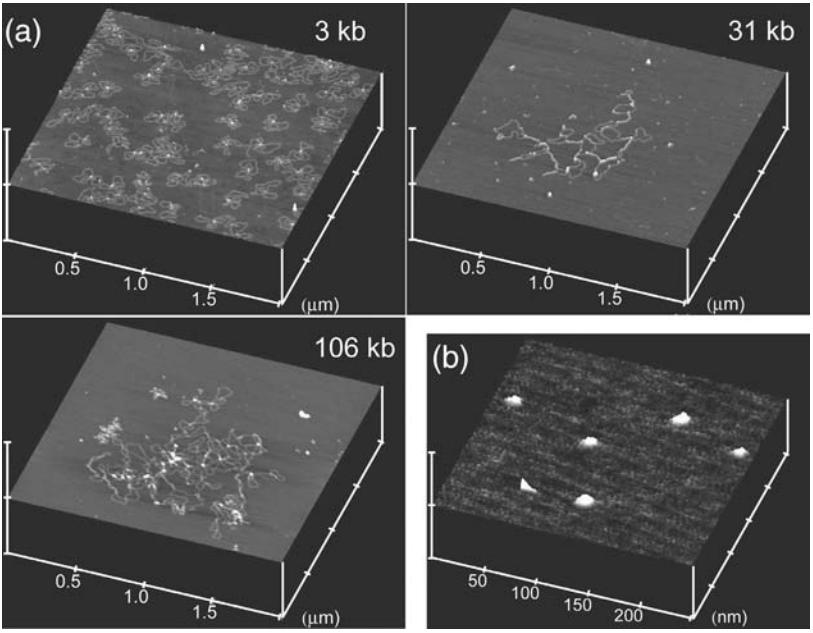

FIGURE 10.1 Materials for the chromatin reconstitution. (a) The 3-, 31- and 106-kb plasmids were purified from *E. coli* and imaged by AFM. AFM data are shown as a surface plot view. All plasmids were twisted and tangled because of the negative supercoiling introduced in *E. coli* cells. (b) The core histone octamer was purified from HeLa cells and imaged by AFM. The histone octamers were applied onto a freshly cleaved mica surface without spermidine treatment.

(10 m*M* Tris–Cl [pH 7.5], 2 *M* NaCl, 1 m*M* EDTA, 0.05% NP-40, 5 m*M* 2-mercaptoethanol) and were transferred into a dialysis tube (total volume 50 μL). The dialysis was started with 150 mL of Hi-buffer, with stirring at 4°C. Lo-buffer (10 m*M* Tris–Cl [pH 7.5], 1 m*M* EDTA, 0.05% NP-40, 5 m*M* 2-mercaptoethanol) was added to the dialysis buffer at 0.46 mL/min, and simultaneously, the dialysis buffer was pumped out at the same speed with a peristaltic pump, so that the dialysis buffer contained 50 m*M* NaCl after 20 h.

The reconstituted samples were visualized by AFM. The "beads-on-a-string" structure was clearly identified in all chromatin fibers with different lengths (Figure 10.2). The average numbers of nucleosomes formed in a single chromatin fiber were 4.3, 7.8, 85.4, 184 and 371 for the 3-, 5-, 31-, 56- and 106-kb plasmids, respectively.

10.3.3 Frequency of the Nucleosomes in Relation to Plasmid Length

The individual internucleosomal distance was also measured. Interestingly, as the plasmid became longer, the average internucleosomal distance became shorter; the distance was about 170 nm in the 3-kb chromatin but about 50 nm in the

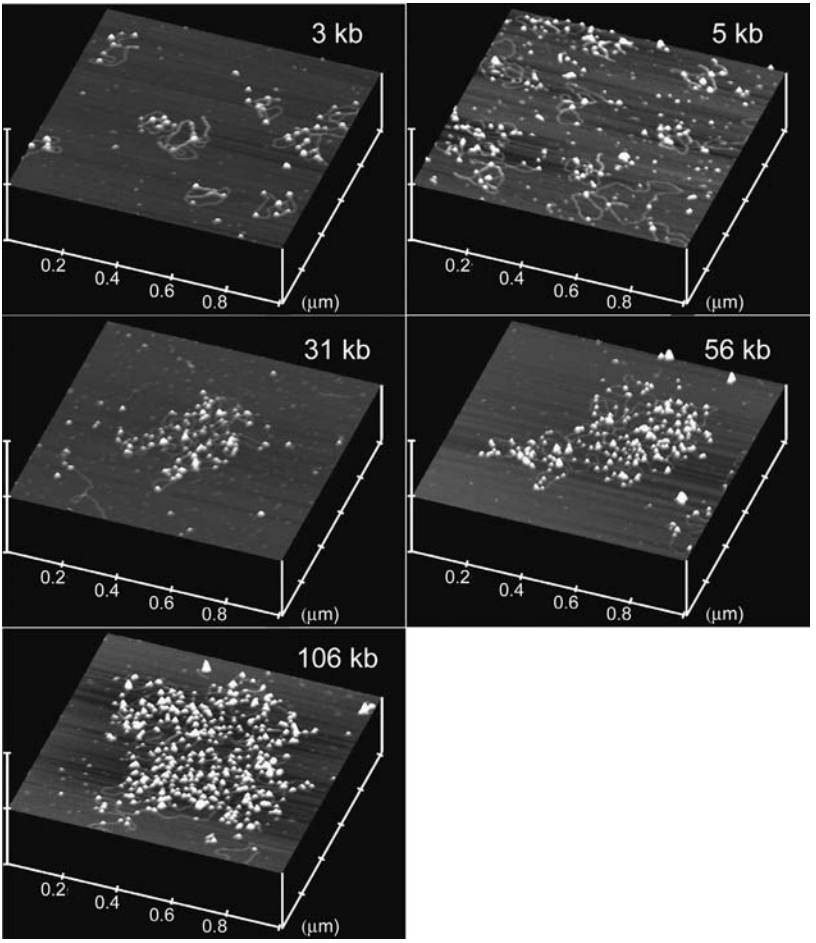

FIGURE 10.2 AFM images of reconstituted chromatin fibers. The chromatin fibers were reconstituted using the purified plasmids and histone octamers by a salt-dialysis method, and observed under AFM. The 3-, 5-, 31-, 56- or 106-kb DNA was used as a template. Normally, free histone octamers that are not incorporated into nucleosomes cannot bind to the spermidine-coated mica surface, since the histones have strong positive charges. The spermidine coating is necessary for the adsorption of DNA. Thus, free histones can hardly be detected in the same frame as chromatin, even if they exist in the reconstitution mixture.

106-kb chromatin. In other words, the efficiency of the reconstitution became higher as the length of DNA used became longer. This tendency was characterized by the length of DNA per formation of one nucleosome. In the 3-kb chromatin, one nucleosome was formed on average in every 826 bp of DNA, while in the 31-, 56- and 106-kb chromatin fibers, one nucleosome was formed in every 413, 308 and 260 bp of DNA, respectively.

As expected, the same tendency was observed when the maximum number of nucleosomes on the plasmids of each length was counted. The most efficiently reconstituted chromatin fiber contained 7, 12, 100, 213 and 436 nucleosomes for the 3-, 5-, 31-, 56- and 106-kb plasmids, respectively, which corresponded to one nucleosome in every 428, 416, 310, 263 and 243 bp of DNA. When the "100% efficiency" of nucleosome formation is defined as one nucleosome per 200 bp (in living cells, one nucleosome is formed per 200 bp on average [9]), the average (and maximum) efficiencies of chromatin reconstitution for the 3-, 5-, 31-, 56- and 106-kb plasmids were estimated to be 29 (47), 31 (48), 48 (65), 65 (76) and 69 (82)%, respectively.

10.3.4 DNA Negative Supercoiling Affects Nucleosome Formation

The higher-order architectural structures of DNA/protein complexes are achieved on the balance of the physical properties of DNA and the interactive forces of DNA-binding proteins [35,36]. In our *in vitro* reconstruction system, only DNA and histones, but not other DNA-binding proteins, are involved in the reconstitution. Therefore, the superhelical strain of the template DNA should be the only possible force that affects the efficiency of nucleosome formation. The superhelical strain of the DNA has been suggested to play a critical role in a variety of genome events such as transcriptional regulation and DNA replication [37]. However, its effect on chromatin formation has not as yet been directly investigated in detail. We thus examined the effect of the superhelical strain of the DNA template on nucleosome reconstitution. For this purpose, the 3- and 56-kb plasmids were linearized by a restriction enzyme. In the chromatin reconstituted on the linearized 56-kb plasmid, the plasmid contained approximately 89 ± 6.7 (mean $\pm$ SD, $n = 11$) nucleosomes (Figure 10.3[a]), indicating that the efficiency of reconstitution was about 32%. On the other hand, the average nucleosome number on the linearized 3-kb plasmid was 4.5 ± 1.2 ($n = 38$) (efficiency of ~30%). These results indicate that, in contrast to the circular plasmid, the efficiency of nucleosome reconstitution on the linearized DNA was not affected by the length of the DNA.

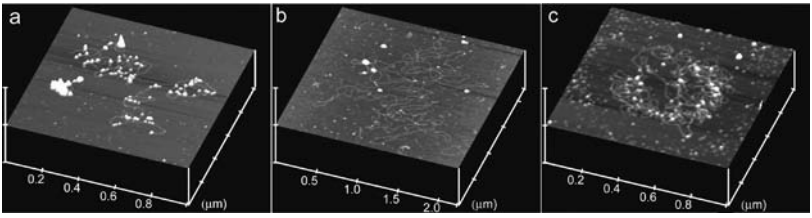

FIGURE 10.3 Effects of the superhelical strain of the template DNA on chromatin reconstitution. (a) The 56-kb plasmid was linearized by a restriction enzyme and used for the chromatin reconstitution. (b) Plasmids were treated with topoisomerase I to remove the superhelical strain and were observed by AFM. (c) AFM image of the chromatin fiber reconstituted on the relaxed plasmid.

Treatment of the plasmids with topoisomerase I completely removed the superhelical strain [38]. Figure 10.3(b) shows the AFM image of the relaxed 106-kb plasmid. Compared to the supercoiled plasmid (Figure 10.1[a]), DNA twisting was diminished in the relaxed plasmid. When the relaxed 106-kb plasmid was used for chromatin reconstitution, it was found to contain only 30 nucleosomes (Figure 10.3[c]). The efficiency was as low as 5.6%, much lower than the linearized plasmid. It should be noted that the reconstituted chromatin fiber was highly tangled on the mica surface with a number of DNA loops (Figure 10.3[c]). This is probably due to accumulation of the positive supercoiling in the closed circular DNA upon nucleosome formation.

10.3.5 Chromatin Salt-Dependent Conformational Changes

The higher-order structure of the nucleosome array is affected by the salt environment [15]. A clear beads-on-a-string structure could be seen in 50 m*M* NaCl (Figure 10.4[a]). Under these conditions, every nucleosome formed on the 106-kb circular plasmid can be seen as a bead in the beads-on-a-string structure. When the dialysis was stopped at a NaCl concentration of 100 m*M* (Figure 10.5[b]), the distance between nucleosomes [19.2 ± 10.1 nm; mean ± SD ($n = 190$)] became much shorter than that in 50 m*M* NaCl [24.4 ± 11.1 nm ($n = 292$)]. In addition, partial aggregation of nucleosomes was observed. This salt-dependent aggregation of nucleosomes can be explained by interaction between the nucleosomes induced by a high salt concentration [39].

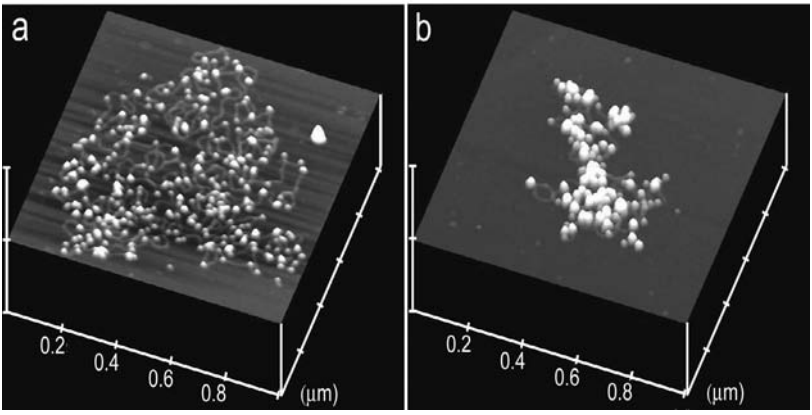

FIGURE 10.4 The effect of salt on the reconstituted chromatin. The chromatin was reconstituted using the salt-dialysis procedure and was observed by AFM. The final NaCl concentration of the dialysis was either 50 m*M* (a) or 100 m*M* (b).

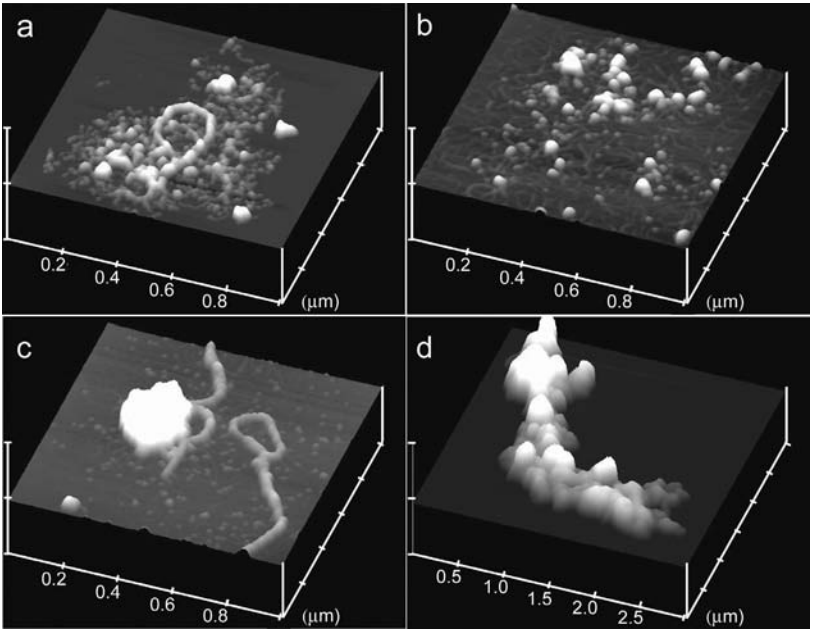

FIGURE 10.5 Reconstitution of chromatin with varying amounts of linker histone H1. Various amounts of H1 were added to the reconstituted chromatin after the salt dialysis was stopped at 50 m*M* NaCl. Histone H1 and histone octamer were added at molar ratios of 1:1 (a), 1:4 (b), 2:1 (c) or 4:1 (d).

10.4 ROLE OF LINKER HISTONE H1 IN NUCLEOSOME COMPACTION

10.4.1 Addition of Linker Histone H1 to Reconstituted 100-kb Chromatin

Linker histone H1 was purified from HeLa cells and added to the reconstituted nucleosomes formed on the 106-kb supercoiled plasmid after salt dialysis was completed at 50-m*M* NaCl. Micrococcal nuclease treatment of this H1-containing chromatin produced an ~170-bp band, whereas that of the chromatin fiber not containing H1 produced an ~150-bp fragment, indicating that histone H1 was incorporated into the linker DNA.

When the H1-containing chromatin fiber was observed by AFM, some portions were found to have formed thick fibers (Figure 10.5[a]). The average length and width of this thick fiber was 395 ± 261 nm [mean ± SD (n = 79)] and 21.2 ± 5.13 nm [mean ± SD (n = 164)], respectively. This fiber was made up of solenoid-like repetitive turns along the fiber axis. The peak-to-peak distance between adjacent solenoid turns was 23.8 ± 7.77 nm [mean ± SD (n = 104)]. The height

of the fiber measured 10.1 ± 2.25 nm [mean ± SD (n = 164)], which is ~4 times greater than that of a single nucleosome [2.71 ± 0.280 nm, mean ± SD (n = 86)], indicating that these thick chromatin fibers resulted from a three-dimensional arrangement of a nucleosomal array, and are not from a mere two-dimensional association of neighboring nucleosomes.

10.4.2 Dose-Dependency of Linker Histone H1 for Formation of Thicker Fibers

In the experiments shown in Figure 10.5, the 20-nm fibers were formed with the greatest efficiency when the molar ratio of histone H1 to the core histone octamer was 1:1 (Figure 10.5[a]). When this ratio was reduced to 1:4, the nucleosome particles could still be seen over the plasmid, but thick chromatin fibers were hardly detected (Figure 10.5[b]). Although some portions did form 20-nm fibers, the lengths were significantly less than in Figure 10.5[a]. This result suggests that the 20-nm fibers represent the first and thinnest unit which is formed above the level of nucleosomes for construction of the higher-order architecture.

On the other hand, the addition of an increased amount of H1 tended to induce thicker chromatin structures. When the ratio of histone H1 to the core histone octamer equaled 2, thick bead-like structures were formed in addition to the 20-nm fibers (Figure 10.5[c]). When histone H1 and the core histone octamer were added at a ratio of 4:1, the 20-nm fiber was no longer observed (Figure 10.5[d]), and the entire chromatin was compacted into a single, relatively large structure composed of many beads, which had a diameter of 93.8 ± 27.3 nm [mean ± SD (n = 176)]. Thus, the amount of H1 in the reconstitution system was found to be critical for the formation of thicker fibers.

10.4.3 Physiological Ionic Strength Is Critical for the Formation of 30-nm Fibers

As discussed above, we did observe three-dimensionally folded thick chromatin fibers following the addition of linker histone H1 alone to the reconstituted chromatin fiber. However, most of the subsequent fiber had a width of 20 nm. The 30-nm fiber was previously observed by EM and AFM after being isolated from the nucleus. To elucidate the difference between these fibers and the present reconstituted fibers, the H1-containing chromatin fibers were exposed to solutions of different ionic strengths.

Histone H1 was added to the reconstituted chromatin fibers at a NaCl concentration of 50 m*M*, and the NaCl concentration was then slowly increased to 100 m*M*. AFM observation revealed that the width of the fiber was relatively uniform and measured around 30 nm. The height was 12.5 nm, which is larger than that of the 20-nm fiber (10.1 nm). The appearance of the 30-nm fiber was similar to that of the 20-nm fiber, i.e., solenoid-like repetitive turns. However,

the peak-to-peak distance of the solenoid turn was 21.6 ± 6.28 nm [mean ± SD ($n = 89$)] and was significantly ($p = 0.028$) shorter than that of the 20-nm fiber. When the salt concentration was reduced back to 50 m*M*, the 20-nm fibers again became dominant, indicating that the salt-induced conformational change between the 20- and 30-nm fibers is a reversible process.

When histone H1 was added to the reconstituted chromatin at 100 m*M* NaCl, the 30-nm fiber was also observed. However, 80% of the thick fiber had a width of 20 nm, suggesting that the higher-order folding of the chromatin fiber depends not only on the final salt concentration, but also on the ionic environment when histone H1 is added. The incorporation of H1 into the chromatin fiber and/or the intermolecular interactions of histone H1 might be affected by the salt concentration.

To further investigate the effects of salt, histone H1 was added during the reconstitution. In this procedure, histone H1 was added to the reconstitution reaction mixture at a NaCl concentration of 600 m*M*, when the nucleosome structure has already been formed [12]. After the addition of H1, dialysis of the reaction mixture was continued to a final NaCl concentration of 50 or 100 m*M*. When the dialysis was continued to 50 m*M*, only a small fraction of the chromatin formed the 30-nm fiber. However, the average length of the fiber was 179 ± 94 nm [mean ± SD (n = 44)], approximately one-half of the length of that formed after salt dialysis alone, without H1 addition. When the dialysis was stopped at 100 m*M* NaCl, the thick fibers could hardly be seen, but large aggregations of the nucleosomes were found. The incorporation of histone H1 into linker DNA could be seen in the micrococcus nuclease assay, but the signal was slightly weaker than when the 20-nm fiber was formed. All of these results indicate that not only the final salt concentration but also the timing of H1 addition substantially affects the higher-order folding of the chromatin fiber.

10.5 NONHISTONE CHROMOSOME PROTEINS ALSO INDUCED CHROMATIN COMPACTION

As a structure of higher order than the 30-nm fiber, ~90-nm beaded structures were detected in the presence of a four-times-greater number of histone H1 molecules relative to the histone octamer (Figure 10.5[d]). This reconstitution condition may not represent physiological conditions, because the linker histone H1 exists in the cell at a ratio of one or two molecules per nucleosome [40]. However, the formation of 90-nm beads itself is interesting, because 80- to 100-nm beaded structures have been observed in HeLa cells [7,41]. Although the 80- to 100-nm beaded structures may be formed with help from other chromosomal proteins, it is intriguing that such beaded structures can be formed with DNA and histones alone. At the same time, it is necessary, of course, to determine and compare the structural effects of the nonhistone chromosomal proteins using this reconstitution system.

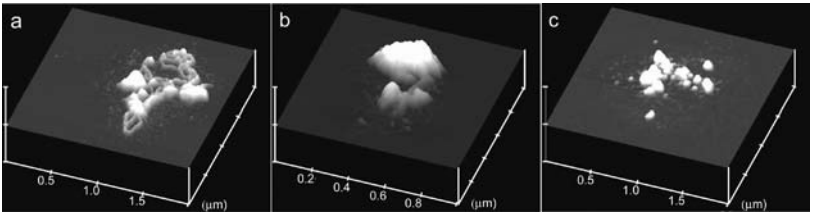

FIGURE 10.6 Effects of topoisomerase II and PC4 on the structure of the reconstituted chromatin. The H1-induced fiber was reconstituted as shown in Figure 9.5(a), and topoisomerase II was then added to the sample at a molar ratio of 1:50 (a) or 1:5 (b) relative to the histone octamer. (c) AFM images of reconstituted nucleosomes to which PC4 had been added at the same molar ratio as the histone octamer, and kept on ice for 1 h.

10.5.1 Contribution of Matrix/Scaffold Proteins

The matrix and scaffold are the additional important concepts of chromosomal architecture. In order to understand structures of much higher order than the 30-nm fiber, analysis of the effects of scaffold components on the H1-induced thicker fibers will be useful. In our preliminary experiment, the reconstituted H1-induced thicker fibers were mixed with topoisomerase II (a major component of the matrix/scaffold) for 30 min at 37°C and subjected to AFM (Figure 10.6). When topoisomerase II was added at a ratio of 1:50 relative to the histone octamer, the H1-induced fibers were locally tangled (Figure 10.6[a]). When topoisomerase II was added at a ratio of 1:5 relative to the histone octamer, the chromatin complex was further aggregated (Figure 10.6[b]) with 30-nm beaded structures. These data support the idea that a large-scale structural change of chromatin fibers can be achieved by local protein binding.

The molecular mechanisms of condensation of the mitotic chromosomes are still mysterious. Only topoisomerase II and subunits of condensin have been identified as proteins essential for mitotic condensation, and it was reported that topoisomerase II appears on the chromosome earlier than condensin [24]. This suggests that topoisomerase II has a role in the initial step of mitotic condensation. An *in vitro* analysis of the molecular function of topoisomerase II would help us to understand the entry mechanism of condensation.

The intranuclear arrangement of the chromosomes during interphase is also an interesting topic of genome dynamics. It has been thought that chromatin fibers are attached to the nuclear matrix inside the nucleus, and that the nuclear matrix is connected to the nuclear envelope [23,42]. The reconstitution techniques of the nuclear envelope have been developed using frog extract [43–46]. The development of a total reconstitution system of chromatin attached to the nuclear lamina (the nuclear envelope) would be expected to be very useful toward an understanding of the nuclear architecture.

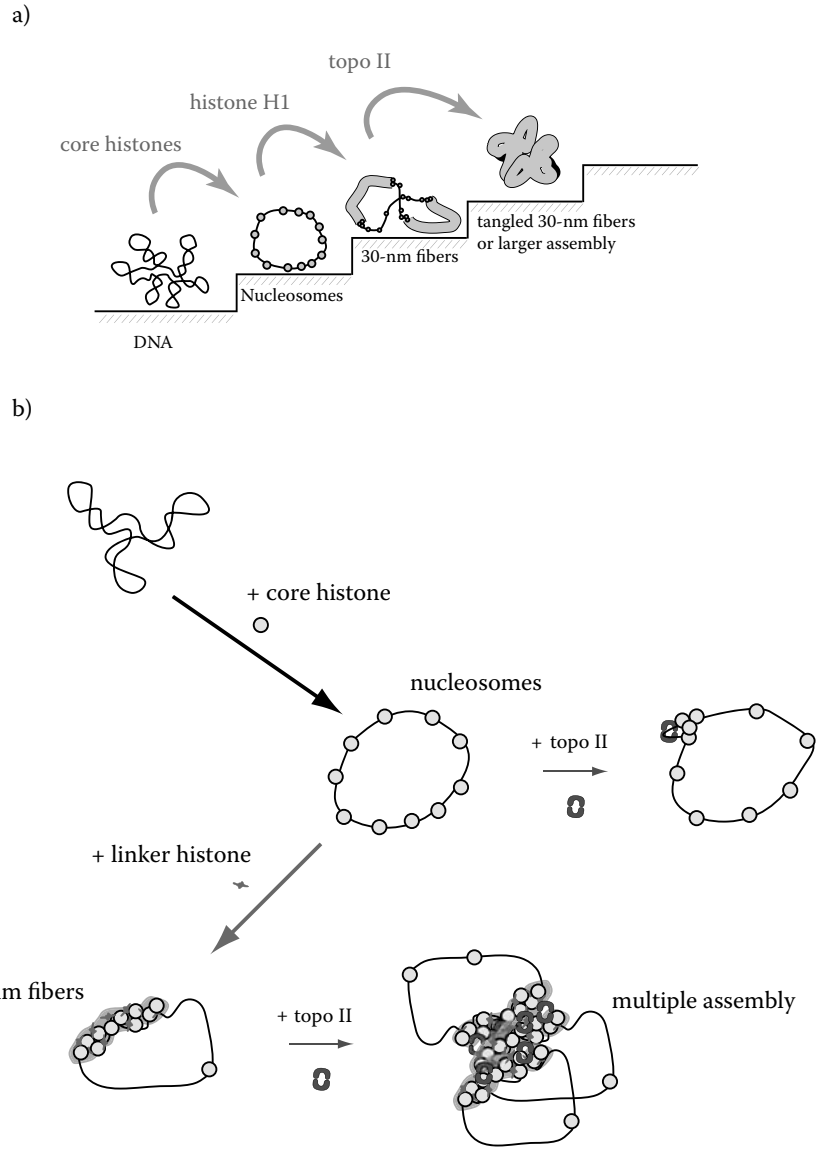

FIGURE 10.7 (See color insert following page 110) Current model of higher-order chromatin folding. a) Nucleosomes are reconstituted using histone octamer and supercoiled DNA. The linker histone H1 is important for formation of the 30-nm chromatin fiber from a beads-on-a-string structure. Nonhistone chromosome proteins such as topoisomerase II also induce chromatin compaction. b) The 30-nm fibers are formed when the linker histone H1 is mixed with the reconstituted nucleosomes. Topoisomerase II is essential for multiple assembly of the H1-induced fibers, while this protein only produces local entanglement of the beads-on-a-string fibers.

10.5.2 Nonhistone Chromosomal Protein PC4 Induced Chromatin Compaction by a Mechanism Different from the Histone H1-Induced Compaction

In addition to histone H1, the chromosomal fraction contains several kinds of low molecular weight proteins that are associated with chromatin directly. For example, positive coactivator 4 (PC4) is abundant in the cell, however, only 5% of the total cellular PC4 is active [47]. The other 95% is speculated to play different roles, including transcriptional inhibition. CD spectroscopic analysis has shown that recombinant PC4 induces chromatin compaction as histone H1 does (Chandrima et al., personal communication). Therefore, we conducted structural analyses of the PC4-induced chromatin compaction.

As shown in Figure 10.6(c), reconstituted structures were induced by PC4. PC4 induced ball-shaped aggregation, with varying sizes of 30 to 250 nm in diameter. This PC4-induced aggregation was different from the H1-induced fibers (Figure 10.5[a]). This compaction depended on the histone-binding activity of PC4, because mutated PC4 lacking the histone-binding region, Δ62–87 PC4, did not induce nucleosome aggregation. It should also be noted that the full-length PC4 did not induce such aggregation of naked DNA, suggesting that the interaction between DNA and PC4 is not the mechanism for the PC4-induced chromatin aggregation.

Post-transcriptional modifications of PC4 result in a drastic alteration of its activity as a transcriptional coactivator. For example, phosphorylation of PC4 causes inactivation [47], and acetylation of PC4 stimulates its DNA-binding activity [48]. These biochemical data imply the physiological significance of PC4 and should be combined with structural analyses for further understanding of nuclear dynamics.

10.6 CONCLUSION

In this chapter, we reviewed how the higher-order architecture of the chromosome has been studied and described how we established a highly efficient *in vitro* chromatin reconstitution system combined with a single-molecule observation technique to help understand the molecular mechanisms of higher-order chromatin folding. Based on our results, our current model of chromatin folding is depicted in Figure 10.7.

ACKNOWLEDGMENT

This study was supported by Special Coordination Funds of the Ministry of Education, Culture Sports, Sciences and Technology of the Japanese government.

REFERENCES

1. Ushiki T, Hoshi O, Iwai K, Kimura E, Shigeno M (2002) The structure of human metaphase chromosomes: its histological perspective and new horizons by atomic force microscopy. *Arch Histol Cytol* 65: 377–390.
2. Swedlow JR, Hirano T (2003) The making of the mitotic chromosome: modern insights into classical questions. *Mol Cell* 11: 557–569.
3. Luger K, Mader AW, Richmond RK, Sargent DF, Richmond TJ (1997) Crystal structure of the nucleosome core particle at 2.8 Å resolution. *Nature* 389: 251–260.
4. Thoma F, Koller T (1977) Influence of histone H1 on chromatin structure. *Cell* 12: 101–107.
5. Widom J, Klug A (1985) Structure of the 300 Å chromatin filament: X-ray diffraction from oriented samples. *Cell* 43: 207–213.
6. Tamayo J, Miles M (2000) Human chromosome structure studied by scanning force microscopy after an enzymatic digestion of the covering cell material. *Ultramicroscopy* 82: 245–251.
7. Allen MJ, Lee C, Lee JD, Pogany GC, Balooch M, Siekhaus WJ, Balhorn R (1993) Atomic force microscopy of mammalian sperm chromatin. *Chromosoma* 102: 623–630.
8. Belmont AS, Sedat JW, Agard DA (1987) A three-dimensional approach to mitotic chromosome structure: evidence for a complex hierarchical organization. *J Cell Biol* 105: 77–92.
9. McGhee JD, Felsenfeld G (1980) Nucleosome structure. *Annu Rev Biochem* 49: 1115–1156.
10. Kornberg RD (1974) Chromatin structure: a repeating unit of histones and DNA. *Science* 184: 868–871.
11. Arents G, Burlingame RW, Wang BC, Love WE, Moudrianakis EN (1991) The nucleosomal core histone octamer at 3.1 Å resolution: a tripartite protein assembly and a left-handed superhelix. *Proc Natl Acad Sci USA* 88: 10148–10152.
12. Tatchell K, van Holde KE (1977) Reconstitution of chromatin core particles. *Biochemistry* 16: 5295–5303.
13. von Holt C, Strickland WN, Brandt WF, Strickland MS (1979) More histone structures. *FEBS Lett* 100: 201–218.
14. Zlatanova J, Leuba SH, van Holde K (1999) Chromatin structure revisited. *Crit Rev Eukaryot Gene Exp* 9: 245–255.
15. Thoma F, Koller T, Klug A (1979) Involvement of histone H1 in the organization of the nucleosome and of the salt-dependent superstructures of chromatin. *J Cell Biol* 83: 403–427.
16. Wood V, Gwilliam R, Rajandream MA, Lyne M, Lyne R, Stewart A, Sgouros J, Peat N, Hayles J, Baker S, et al. (2002) The genome sequence of *Schizosaccharomyces pombe*. *Nature* 415: 871–880.
17. Adkins NL, Watts M, Georgel PT (2004) To the 30-nm chromatin fiber and beyond. *Biochim Biophys Acta* 1677: 12–23.
18. Agresti A, Bianchi ME (2003) HMGB proteins and gene expression. *Curr Opin Genet Dev* 13: 170–178.
19. Bustin M (2001) Chromatin unfolding and activation by HMGN(*) chromosomal proteins. *Trends Biochem Sci* 26: 431–437.
20. Ellwood KB, Yen YM, Johnson RC, Carey M (2000) Mechanism for specificity by HMG-1 in enhanceosome assembly. *Mol Cell Biol* 20: 4359–4370.

21. Catez F, Brown DT, Misteli T, Bustin M (2002) Competition between histone H1 and HMGN proteins for chromatin binding sites. *EMBO Rep* 3: 760–766.
22. Springhetti EM, Istomina NE, Whisstock JC, Nikitina T, Woodcock CL, Grigoryev SA (2003) Role of the M-loop and reactive center loop domains in the folding and bridging of nucleosome arrays by MENT. *J Biol Chem* 278: 43384–43393.
23. Berrios M, Osheroff N, Fisher PA (1985) In situ localization of DNA topoisomerase II, a major polypeptide component of the Drosophila nuclear matrix fraction. *Proc Natl Acad Sci USA* 82: 4142–4146.
24. Maeshima K, Laemmli UK (2003) A two-step scaffolding model for mitotic chromosome assembly. *Dev Cell* 4: 467–480.
25. Hirano T, Kobayashi R, Hirano M (1997) Condensins, chromosome condensation protein complexes containing XCAP-C, XCAP-E and a *Xenopus* homolog of the *Drosophila* Barren protein. *Cell* 89: 511–521.
26. Kimura K, Hirano T (1997) ATP-dependent positive supercoiling of DNA by 13S condensin: a biochemical implication for chromosome condensation. *Cell* 90: 625–634.
27. Wang JC (2002) Cellular roles of DNA topoisomerases: a molecular perspective. *Nat Rev Mol Cell Biol* 3: 430–440.
28. Becker PB, Wu C (1992) Cell-free system for assembly of transcriptionally repressed chromatin from *Drosophila* embryos. *Mol Cell Biol* 12: 2241–2249.
29. Ito T, Bulger M, Pazin MJ, Kobayashi R, Kadonaga JT (1997) ACF, an ISWI-containing and ATP-utilizing chromatin assembly and remodeling factor. *Cell* 90: 145–155.
30. Li Q, Wrange O (1997) Assays for transcription factors access to nucleosomal DNA. *Methods* 12: 96–104.
31. Woodcock CL, Dimitrov S (2001) Higher-order structure of chromatin and chromosomes. *Curr Opin Genet Dev* 11: 130–135.
32. Willard HF (1998) Centromeres: the missing link in the development of human artificial chromosomes. *Curr Opin Genet Dev* 8: 219–225.
33. Vissel B, Choo KH (1991) Four distinct alpha satellite subfamilies shared by human chromosomes 13, 14 and 21. *Nucleic Acids Res* 19: 271–277.
34. Shizuya H, Birren B, Kim UJ, Mancino V, Slepak T, Tachiiri Y, Simon M (1992) Cloning and stable maintenance of 300-kilobase-pair fragments of human DNA in *Escherichia coli* using an F-factor-based vector. *Proc Natl Acad Sci USA* 89: 8794–8797.
35. Hizume K, Yoshimura SH, Maruyama H, Kim J, Wada H, Takeyasu K (2002) Chromatin reconstitution: development of a salt-dialysis method monitored by nano-technology. *Arch Histol Cytol* 65: 405–413.
36. Yoshimura SH, Ohniwa RL, Sato MH, Matsunaga F, Kobayashi G, Uga H, Wada C, Takeyasu K (2000) DNA phase transition promoted by replication initiator. *Biochemistry* 39: 9139–9145.
37. Opel ML, Arfin SM, Hatfield GW (2001) The effects of DNA supercoiling on the expression of operons of the ilv regulon of *Escherichia coli* suggest a physiological rationale for divergently transcribed operons. *Mol Microbiol* 39: 1109–1115.
38. Hizume K, Yoshimura SH, Takeyasu K (2004) Atomic force microscopy demonstrates a critical role of DNA superhelicity in nucleosome dynamics. *Cell Biochem Biophys* 40: 249–262.
39. Garcia-Ramirez M, Dong F, Ausio J (1992) Role of the histone "tails" in the folding of oligonucleosomes depleted of histone H1. *J Biol Chem* 267: 19587–19595.
40. Bates DL, Thomas JO (1981) Histones H1 and H5: one or two molecules per nucleosome? *Nucleic Acids Res* 9: 5883–5894.

41. Yoshimura SH, Kim J, Takeyasu K (2003) On-substrate lysis treatment combined with scanning probe microscopy revealed chromosome structures in eukaryotes and prokaryotes. *J Electron Microsc (Tokyo)* 52: 415–423.
42. Barboro P, D'Arrigo C, Mormino M, Coradeghini R, Parodi S, Patrone E, Balbi C (2003) An intranuclear frame for chromatin compartmentalization and higher-order folding. *J Cell Biochem* 88: 113–120.
43. Zhang C, Hutchins JR, Muhlhausser P, Kutay U, Clarke PR (2002) Role of importin-beta in the control of nuclear envelope assembly by Ran. *Curr Biol* 12: 498–502.
44. Takano M, Takeuchi M, Ito H, Furukawa K, Sugimoto K, Omata S, Horigome T (2002) The binding of lamin B receptor to chromatin is regulated by phosphorylation in the RS region. *Eur J Biochem* 269: 943–953.
45. Zhang C, Clarke PR (2000) Chromatin-independent nuclear envelope assembly induced by Ran GTPase in *Xenopus* egg extracts. *Science* 288: 1429–1432.
46. Newport J, Dunphy W (1992) Characterization of the membrane binding and fusion events during nuclear envelope assembly using purified components. *J Cell Biol* 116: 295–306.
47. Ge H, Zhao Y, Chait BT, Roeder RG (1994) Phosphorylation negatively regulates the function of coactivator PC4. *Proc Natl Acad Sci USA* 91: 12691–12695.
48. Kumar BR, Swaminathan V, Banerjee S, Kundu TK (2001) p300-mediated acetylation of human transcriptional coactivator PC4 is inhibited by phosphorylation. *J Biol Chem* 276: 16804–16809.

11 Scanning Near-Field Optical/Atomic Force Microscopy as a Tool for Simultaneous Specification of Chromosome Topography and Particular Gene Location on the Nanometer Scale

Motoharu Shichiri, Tomoyuki Yoshino, Daisuke Fukushi, Shoji Hagiwara, Kohei Akazawa, Toshio Ohtani and Shigeru Sugiyama*

CONTENTS

11.1 Introduction 138
11.2 Instrumentations and Techniques 139
11.2.1 SNOM/AFM and AFM 139
11.2.2 Chromosome Preparation 139
11.2.3 FISH and Probe 140
11.2.3.1 FISH for Barley Chromosomes 140
11.2.3.2 FISH for Human Chromosomes 141

*To whom correspondence should be addressed.

11.2.3.3 Observation and Image Analysis 141
11.2.3.4 Positional Analysis of Two Gene Loci 142
11.3. High-Resolution Detection of Telomere FISH Signals by SNOM/AFM 142
11.3.1 Chromosome Preparation for SPM Observation 142
11.3.2 Detection of Telomere FISH Signals on Barley Chromosomes 143
11.4 Single-Copy Gene Detection on Human Chromosomes Using SNOM/AFM 145
11.5 Multicolor FISH Detection Using SNOM/AFM 147
11.6 Discussion and Conclusion 150
Acknowledgment 151
References 152

11.1 INTRODUCTION

Fluorescence *in situ* hybridization (FISH) is a technique used to visualize defined nucleic acid sequences in cellular preparations by hybridization of complementary probe sequences, and is widely applied to the detection of a specific gene on the chromosome by fluorescence light microscopy. However, the resolution of conventional FISH by fluorescence light microscopy is in practice at the level of about half of a micrometer, due to optical limitations. Thus, there is need for a novel technique in order to visualize a specific gene on a chromosome at the nanometer scale.

Atomic force microscopy (AFM), on the other hand, has been used for studies of the three-dimensional structure of the chromosome (see Chapter 9) [1–4]. Some reports [5,6] further indicate the usefulness of scanning near-field optical microscopy (SNOM) in studies involving DNA visualization; this microscopy was derived from AFM, and can reveal a single DNA fiber at 100 nm resolution, although it could not be used in these studies to simultaneously collect topographic and fluorescent DNA images. Other researchers have also applied SNOM to chromosomal research and have succeeded in simultaneously obtaining topographic and fluorescent images of FISH-treated samples [7,8]. However, the resolution of the topographic images in those studies was insufficient, probably partly because the tip motion was controlled by the shear force. To overcome this problem, Iwabuchi et al. [9] and Yoshino et al. [10] applied SNOM/AFM to the study of chromosomes. The SNOM/AFM uses a bent optical fiber as a cantilever, which operates in a dynamic force mode by normal AFM [11]. We have applied SNOM/AFM to the study of FISH-treated chromosome samples because it can provide more detailed information on the chromosomal structure and fluorescent intensity than previously described techniques.

Thus, in this chapter, we will introduce a novel "chromosome nano-FISH" method to directly define the location of a specific gene on a chromosome at high resolution using SNOM/AFM. This method is theoretically expected to exceed the limited resolution of conventional FISH by fluorescent light microscopy. We will show some examples of high-resolution FISH images of chromosomes obtained by SNOM/AFM, and discuss the applicability of the chromosome nano-FISH method for analyzing metaphase chromosome structure on the nanometer scale.

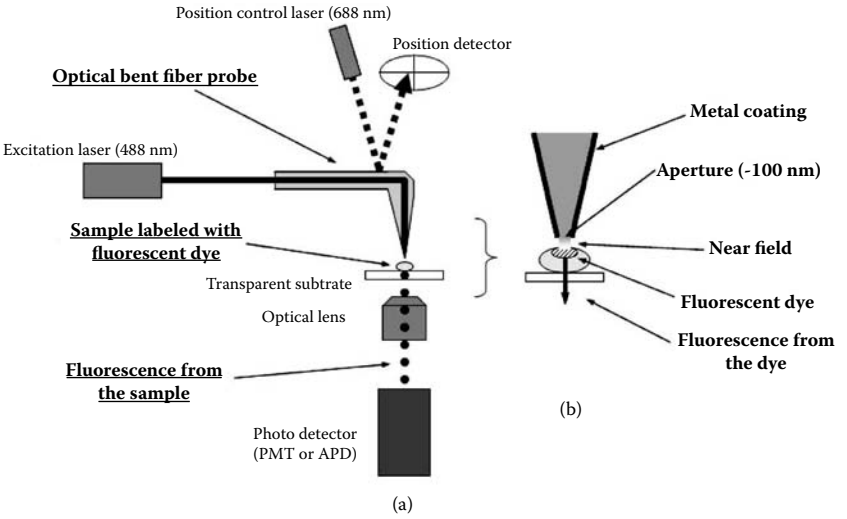

FIGURE 11.1 Schematic representation of the SNOM/AFM system.

11.2 INSTRUMENTATIONS AND TECHNIQUES

11.2.1 SNOM/AFM AND AFM

A schematic representation of the SNOM/AFM system is shown in Figure 11.1. The SNOM/AFM instrument is equipped on a conventional inverted optical microscope, and has an optical bent fiber probe with an aperture of less than 100 nm in diameter. A laser beam that is reflected on the surface of an optical bent fiber probe (broken line) is detected by a photodiode detector in order to control the probe (Figure 11.1a). A topographic image is obtained by analyzing the vibration amplitude of the optical bent fiber probe with an SPI 3800N probe station (SII NanoTechnology, Inc.). The spring constant of the fiber probe is usually about 20 N/m, and the resonance frequency is 10 to 20 kHz. An argon ion laser beam passes through the optical bent fiber probe, resulting in the generation of an optical near-field at the aperture of the probe. The fluorescence from the sample (dotted line in Figure 11.1[a] and arrow in Figure 11.1[b]) is collected by a ×100 objective lens, and the fluorescent intensity is detected by an avalanche photodiode or photo multiplier tube. The fluorescent image is generated by the SPI 3800N probe station (Figure 11.1[b]).

11.2.2 CHROMOSOME PREPARATION

Barley (*Hordeum vulgare,* cv. Minorimugi) chromosomes in the early stage were used in our study because these chromosomes are relatively large in size and small in number (2n = 14). The samples were prepared on glass slides according to the method of Liu et al. [12] for structural observation of the chromosomes.

Briefly, barley root tips from 3-day-old seedlings germinated at 25°C were excised, treated with distilled water (DW) or colchicine solution (final concentration, 5 μg/mL) at 0°C for 24 h, and fixed with methanol/acetic acid (1:1) solution. The root tips were placed on glass slides and treated with an aliquot of enzyme solution composed of 2% cellulase Onozuka RS (Yakult Honsha Co., Ltd., Tokyo, Japan), 1% pectolyase Y-23 (Kikkoman Corp., Noda, Japan), 7.5 m*M* KCl and 7.5 m*M* EDTA (pH 4.0). The root tips were then crushed with tweezers in Carnoy's fixative (methanol/acetic acid = 3:1 v/v) solution and rinsed briefly with 45% acetic acid (10 to 30 min). The specimens were then washed in 1× SSC and DW and air-dried.

The chromosome samples were prepared for FISH analysis by SNOM/AFM by a modification of Dillé's method [13]. Approximately 100 pieces of the cut-off barley root tips were digested with 1 mL of enzyme solution, and the meristem cells were collected. After hypotonic treatment and fixation with Carnoy's fixative, the samples were stored at –20°C until the following experiments were performed. Further details are described in previous reports [14,15]. The stored samples were defrosted and warmed to room temperature just before use. A droplet of the fixed-cell suspension was spread on a cover slip for SNOM/AFM or on a glass slide for light microscopy and AFM observations; the spread sample was immediately washed with a few drops of Carnoy's fixative and air-dried.

Human chromosomes were also used for the FISH experiments to detect single-copy genes. Normal human peripheral blood (0.5 mL) was cultured in 10 mL RPMI 1640 medium (Gibco) supplemented with 10% calf serum (Gibco) and 1% PHA (Murex) in a plastic disposable tissue-culture flask at 37°C for 72 h. Two hours prior to harvest, 0.1 mL of colcemid solution (1 μg/mL) was added (final concentration 10 ng/mL) to each culture flask. The cells were harvested by centrifugation, resuspended in hypotonic solution (0.075 *M* KCl) for 30 min at room temperature, and fixed with Carnoy's fixative. The samples were stored at –20°C until observation. They were spread over the substrates and dried as described above.

When we performed double fixation with formaldehyde, the prepared chromosome samples on the substrates were immediately immersed in formaldehyde solution for 10 min at room temperature and then washed with 2× SSC for 5 min three times. After washing with SSC, the chromosome samples were dehydrated by an ethanol series (70% 5 min and 100% 5 min).

11.2.3 FISH and Probe

11.2.3.1 FISH for Barley Chromosomes

The telomeric sequences amplified by PCR were used as FISH probes. The plant telomeric sequence $(5'\text{-TTTAGGG-}3')_n$ was amplified using a primer pair [$(5'\text{-AGG GTT T-}3')_5$ and $(5'\text{-AAA CCC T-}3')_5$] in the absence of template DNA. We labeled the PCR-amplified DNA with biotin-16-dUTP (Roche Molecular Systems, Inc., NJ, U.S.A.) using a Nick Translation Kit (Roche), and the standard FISH protocol was applied. The PCR conditions and FISH procedures are described in full detail in our papers [15,16].

11.2.3.2 FISH for Human Chromosomes

Three sequences were selected as FISH probes targeting the region within the myosin IIIB (MYO3B) and histone acetyltransferase (HAT1) genes (two probes within MYO3B and one probe within HAT1), which are located at the center of the long arm of human chromosome 2, for single gene detection by SNOM/AFM. These three sequences were amplified by PCR. Human genomic DNA isolated from blood cells using a QIAamp DNA Blood Mini Kit (Qiagen) was used as template. We used shuttle PCR (two-temperature PCR) combined with autosegment extension PCR. All PCR products were confirmed for molecular size and quantity by agarose gel electrophoresis and then purified using a QIAquick PCR purification kit (Qiagen). We named the probes HATp, MYOp-1 and MYOp-2 (Figure 11.2). They were labeled with two different reagents, biotin and digoxigenin (DIG), using biotin and DIG translation mix (Roche) to enable detection by different fluorochromes. The probes were fluorescence-labeled with Alexa Fluor® 488 and Alexa Fluor® 546 (Molecular Probes) after normal FISH treatment.

11.2.3.3 Observation and Image Analysis

We first located the metaphase nuclei using phase contrast microscopy after FISH treatment. The area including chromosome 2 was defined by incident-light

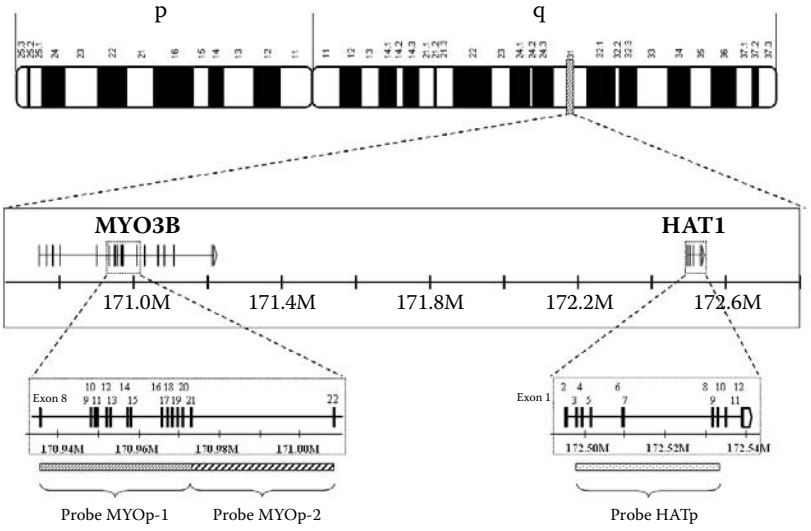

FIGURE 11.2 Gene structure of myosin IIIB (MYO3B) and histone acetyltransferase (HAT1) on chromosome 2. These genes are located 1.5 Mb apart on human chromosome 2q31. The MYO3B (HAT1) gene is constructed of 36 (12) exons with a total length of about 455 kb (70 kb). We used a portion of these gene sequences as FISH probes, which we named MYOp-1 (38.6 kb), MYOp-2 (35.2 kb) and HATp (38.0 kb). The scales in the schemes of the gene structure indicate the loci of the genes.

fluorescent microscopy with filter sets for Alexa488 (EX: HQ470/40x, BS: Q497LP, EM: HQ522/40m) and Alexa546 (EX: HQ545/30x, BS: Q570LP, EM: HQ610/75m) (Chroma) and was photographed using a digital camera (Nikon). Chromosomes with clear FISH signals were employed for the observation by SNOM/AFM (SNOAM; SII NanoTechnology Inc.) in air, in dynamic force mode. The images were 256×256 pixels and were analyzed using the SPI 3800N probe station. The chromosome area with FISH signals was scanned twice using the appropriate excitation light sources and filter sets to obtain a multicolor image. The obtained fluorescent images were processed with a 3×3 mean filter. The same chromosomes were scanned again using a silicon tip for the AFM, an SI-DF 40 (SII Nano Technology Inc.), for more detailed topographic analysis. The images obtained by SNOM/AFM and AFM were then superimposed and FISH signals were mapped on the chromosome structure.

11.2.3.4 Positional Analysis of Two Gene Loci

We analyzed the relative positions of the two probes (MYOp-1 and HATp) located 1.5 Mb apart. The MYOp-1 and HATp probes were fluorescence-labeled with Alexa 546 and Alexa 488, respectively. The metaphase chromosomes spread on the substrate that had clear multicolor FISH signals were imaged by fluorescence microscopy, and the chromosome images were aligned with the chromosome axis by rotating the image. The chromosome images with FISH signals were oriented with the short arm at the top and the long arm at the bottom. The center of balance (brightness-weighted average of the x and y coordinates of all pixels) of each signal was calculated by Image J (National Institutes of Health). The relative positions of two signals were plotted on the X–Y plane when one of the signals was fixed at the zero point. The 90, 95 and 99% confidence limits were calculated and are indicated by an oval in the figure.

11.3 HIGH-RESOLUTION DETECTION OF TELOMERE FISH SIGNALS BY SNOM/AFM

11.3.1 Chromosome Preparation for SPM Observation

It is very important to completely liberate the chromosome from the cytosol in order to visualize the true surface of the chromosome by scanning probe microscopy (SPM), because frequently film-like structures originating from the cytosol cover the chromosomal surfaces and interfere with the AFM observations. This is particularly serious for plant materials. In order to prepare clean chromosome samples, chromosomes are usually treated with hot 45% acetic acid, although the influence of this highly concentrated acetic acid treatment on the chromosome structure has not been evaluated in detail. Thus we first examined, using AFM, the effect of various concentrations of acetic acid on the chromosome structure. As a result, we propose two sample preparation methods suitable for the AFM observation of barley chromosomes that do not result in any major

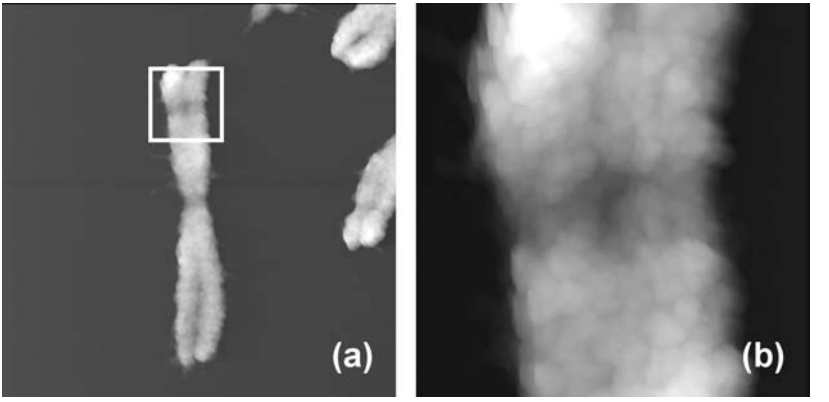

FIGURE 11.3 Topographic image of a barley chromosome observed by AFM. (a) Topographic image of barley chromosome 6. The sample was prepared by crushing in Carnoy's fixative, followed by a brief 45% acetic acid rinse. Scan range is $11 \times 11\ \mu m^2$. (b) High-magnification image of the secondary constriction of the chromosome (the region indicated by a white box in [a]). Scan range is $2 \times 2\ \mu m^2$.

cytosol contaminants or severe structural damage to the chromosome surface [12,14,17]: one is a method consisting of root tips crushed in 30% acetic acid followed by 30% acetic acid overnight treatment, and the other consists of crushing of the root tip in Carnoy's fixative followed by a brief 45% acetic acid rinse (30 min to 2 h). A typical example of a topographic image obtained by AFM of a barley chromosome using one of the recommended methods is shown in Figure 11.3.

11.3.2 Detection of Telomere FISH Signals on Barley Chromosomes

In order to develop SNOM/AFM suitable for the detection of FISH signals on chromosomes, we carried out FISH with barley chromosomes using barley telomeric DNA as probe, and observed the chromosomes using SNOM/AFM as well as fluorescence light microscopy. We detected telomeric signals on all chromosomes in images obtained by fluorescent light microscopy; the fluorescent signals were observed at the distal periphery of the chromosomes, where the telomeric regions were expected to be localized. After the FISH signals were confirmed by fluorescent light microscopy, we obtained simultaneous topographic images (Figure 11.4[a]) and fluorescent images of the same region of the chromosomes (Figure 11.4[b]) using SNOM/AFM (scan range $15 \times 15\ \mu m^2$), as shown in Figure 11.4. The three-dimensional structure of the barley chromosomes was altered during the FISH treatment, as described by Shichiri et al. [15], in that the width of the chromosome increased by twofold and the height of the chromosome arms decreased after the FISH treatment. We superimposed the fluorescent images on gray-scale topographic images with higher magnification (scan range

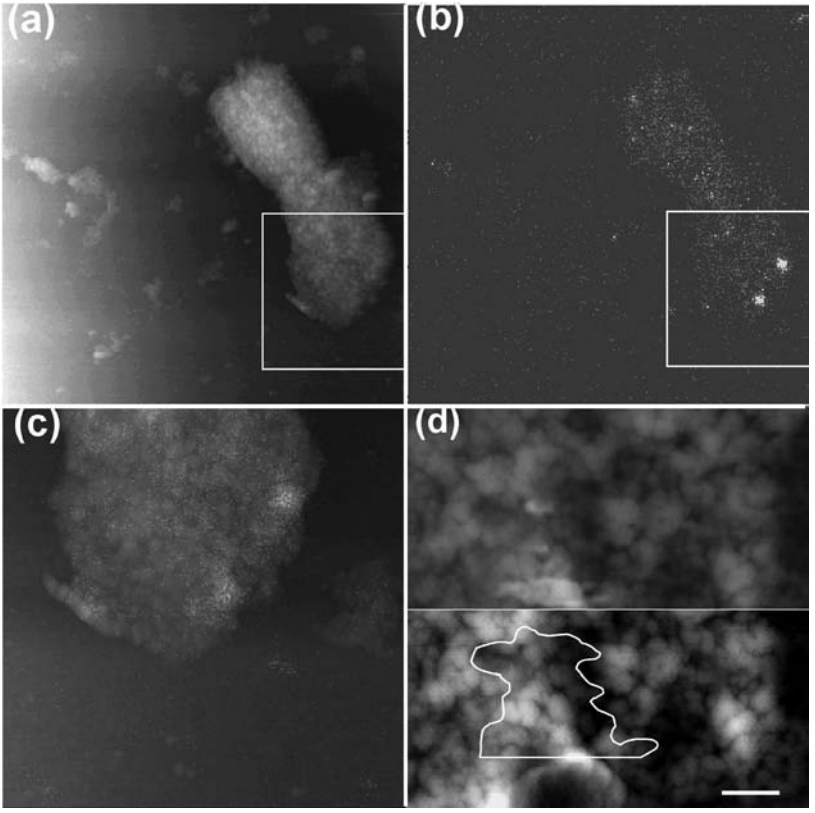

FIGURE 11.4 (See color insert following page 110) SNOM/AFM images of a FISH-treated barley chromosome using telomere repeat sequence as the probe. (a) Topographic and (b) fluorescent images simultaneously obtained by SNOM/AFM. Scan range is 15×15 μm^2. (c) Superimposed SNOM/AFM image of the region indicated by white boxes in (a) and (b). The fluorescent image was superimposed onto the topographic image. Scan range is 6×6 μm^2. (d) Higher magnification of the SNOM/AFM image. Upper panel: a superimposed image of a SNOM/AFM fluorescent image and AFM topographic image of the same region. Lower panel: the outline of the telomere FISH region is indicated as a white line on the AFM image. Bar = 200 nm.

6×6 μm^2) to identify the position of these fluorescent signals on the chromosome structure (Figure 11.4[c]). Fluorescent signals were detected at the distal periphery of the chromosomes, as were those detected by fluorescent light microscopy. The sizes of the two telomeric signals were also similar (approximately 500 nm) to those in the light microscopic images.

One problem is that topographic images obtained using SNOM/AFM do not have sufficient spatial resolution to precisely analyze the correlation between the chromosome ultrastructure and the FISH signal region, because the tip radius of the optical bent fiber probe of SNOM/AFM is much larger than that of the silicon

cantilever used for conventional AFM. Thus, we obtained a topographic image of the same portion using a conventional silicon cantilever after the SNOM/AFM observation. The fluorescent image with one FISH signal (lower left) obtained by SNOM/AFM was then superimposed onto the topographic image of the corresponding region obtained by AFM (Figure 11.4[d]) to investigate the relationship between the higher-order chromosome structure and the distribution of the telomeric region.

In Figure 11.4(d), the FISH signals were distributed over a region approximately 500 nm in diameter. The fluorescence intensity was not uniform and two high-intensity sub-regions were observed in the fluorescence image (Figure 11.4[d], upper panel). The two sub-regions were approximately 250 nm apart. We then investigated the relationship between the granular structures on the chromosome and the fluorescent signals. The topographic image acquired by the conventional AFM tip indicated that the granular structures on the chromosome were approximately 60 to 100 nm in diameter (Figure 11.4[d], lower panel), a size undetectable by the optical bent fiber probe. The granular structures are speculated to be 30-nm chromatin fibers based on their dimensions, when the effect of the tip radius of the silicon cantilever is considered. Thus, the distribution of telomere FISH signals on the chromatin fiber can be estimated by comparison of the SNOM/AFM fluorescent images with the AFM topographic images. In Figure 11.4(d), the chromatin fibers in the region surrounded by a white line in the lower panel are thought to contain telomeric repeat sequences. The topographic features of the chromatin fibers in the telomeric region were not significantly different at this resolution.

These results indicated that SNOM/AFM is useful for detecting fluorescent signals beyond the light microscopy optical limit. The combination of SNOM/AFM fluorescent images and AFM topographic images is also effective in determining the precise distribution of the region containing specific nucleotide sequences in relation to chromatin fiber folding.

11.4 SINGLE-COPY GENE DETECTION ON HUMAN CHROMOSOMES USING SNOM/AFM

We next attempted to detect FISH signals from a single-copy gene in a human chromosome by SNOM/AFM (Figure 11.5[d–i]) as well as by conventional light microscopy (Figure 11.5[a–c]). The FISH probe used in this experiment was an MYOp-1 sequence fluorescently labeled with Alexa 546. Circular or elliptical FISH signals were detected on both sister chromatids of a chromosome when observed by conventional light microscopy (Figure 11.5[b,c]). SNOM/AFM observation of the same chromosomes was then performed with magnification similar to that of the fluorescent microscope images (scan size $12 \times 12\ \mu m^2$) (Figure 11.5[d–f]) to demonstrate the advantage of this system in comparison with light microscopy. The topographic image (Figure 11.5[d]) suggested that the higher-order chromosomal structure collapsed during the FISH treatment,

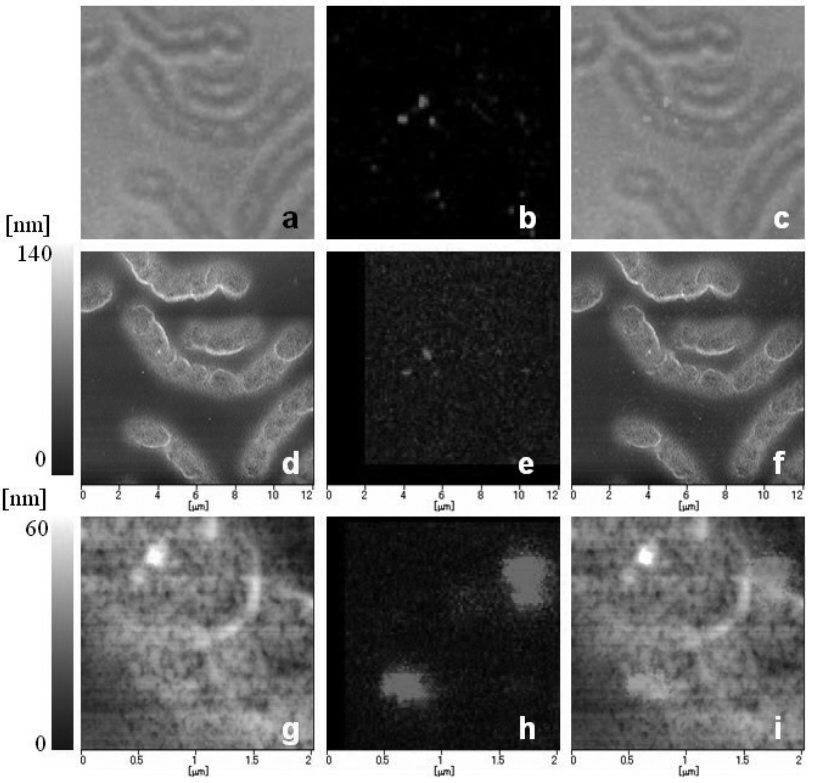

FIGURE 11.5 Conventional light microscopic and SNOM/AFM images of a human chromosome with FISH signals. The FISH probe used was the MYOp-1 sequence, which was fluorescence-labeled with Alexa 546. (a) Phase contrast and (b) fluorescent light microscopic image of human chromosomes. (c) Superimposed image of (a) and (b). (d, g) Topographic and (e, h) fluorescent images obtained by SNOM/AFM. (f, i) Superimposed images. (d–f) Scan range is 12×12 μm^2 and (g, h) 2×2 μm^2. Bars at left represent the height ranges of the samples.

because its height, which had originally been more than 100 nm, was decreased to a few tens of nanometers, as previously described [15,16]. The shape and outline of the signals were clearer in the fluorescent image obtained with SNOM/AFM (Figures 11.5[e,f]) than in the conventional fluorescent microscopic image (Figure 11.5[b]). We then observed a part of the chromosome arm, including the region with the fluorescent signals, by SNOM/AFM with greater magnification (Figures 11.5[g–i], scan size 5×5 μm^2). The chromosome surface in the topographic image (Figure 11.5[g]) was composed of granular structures similar to those observed in barley chromosomes (Figure 11.3). The FISH signal observed by SNOM/AFM was clear (Figures 11.5[h,i]), and its outline was rather complicated in contrast with the simple elliptical outline obtained by fluorescence microscopy.

11.5 MULTICOLOR FISH DETECTION USING SNOM/AFM

We further obtained images of multicolor FISH signals using two adjacent FISH probes (MYOp-1 and MYOp-2) by SNOM/AFM and compared their resolution with that of conventional fluorescent light microscopy. The two FISH signals — one being green fluorescence from Alexa 488 and the other red fluorescence from Alexa 546 — were observed with circular or elliptical forms of 300 to 500 nm diameter under a conventional fluorescent microscope. Moreover, the two fluorescent signals on the same sister chromatid were often overlapped to some degree (in some cases to a considerable degree) and it was impossible to identify the exact shape and location of each color signal (Figure 11.6[a–d]). After observation by fluorescent light microscopy, the same chromosome was observed by SNOM/AFM at low (Figure 11.6[e–h]) and higher (Figure 11.6[i–l]) magnification. In the fluorescence images obtained using SNOM/AFM, the outline of each signal was very complex, in contrast with the simple round shape that was observed with the conventional light microscope. These results indicate that high-resolution gene mapping beyond the optical limit is possible using SNOM/AFM.

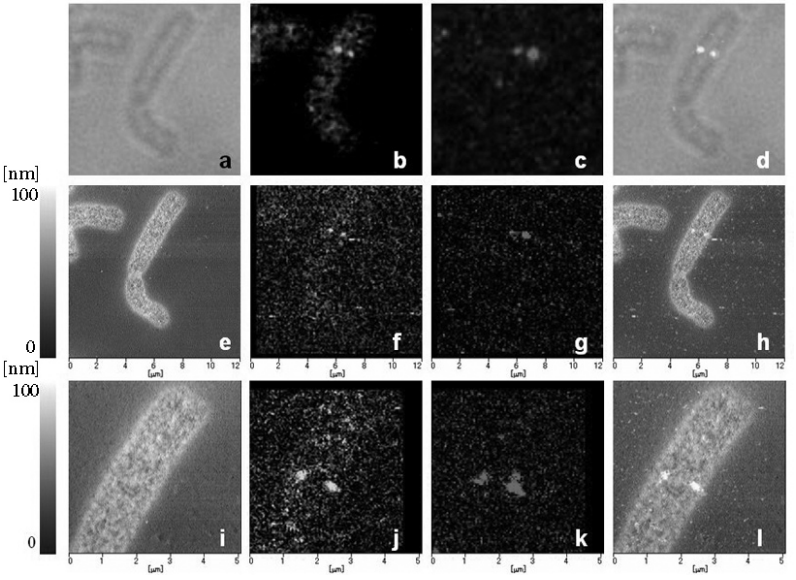

FIGURE 11.6 (See color insert following page 110) Conventional light microscopic and SNOM/AFM images of a chromosome with multicolor FISH signals. The adjacent MYOp-1 and MYOp-2 probes were used and detected by Alexa 546 (red) and Alexa 488 (green). (a–d) Conventional light microscopic images and (e–l) SNOM/AFM images. (a) Phase contrast image and (b) Alexa 488 and (c) Alexa 546 fluorescent images. (d) Superimposed images of (a–c). (e, i) Topographic images. (f, j) Alexa 488 and (g, k) Alexa 546 fluorescent images obtained by SNOM/AFM. (e–h) (h,l) Superimposed images of (e–g) and (i–k). Scan range is 12×12 μm^2 and (i–l) 5×5 μm^2.

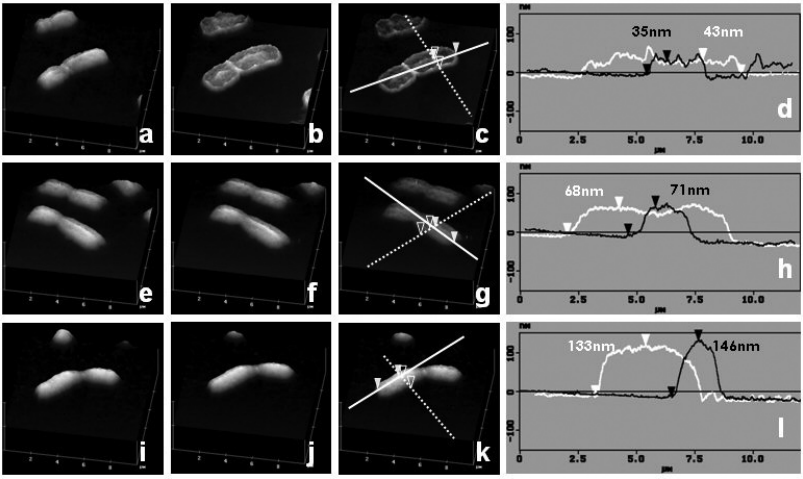

FIGURE 11.7 AFM images and their section profiles of formaldehyde-fixed/unfixed human chromosomes. (a–d) Fixed with Carnoy's fixative only. (e–h) Re-fixed with 1% formaldehyde before FISH treatment. (i–l) Re-fixed with 4% formaldehyde. (a, e, i) Untreated chromosomes. (b, f, j) Chromosomes after RNase treatment. (c, g, k) Chromosomes after heat denaturation. (d, h, l) Section profiles along solid and dotted lines in c, g and k are indicated by white and black lines, respectively.

For high-resolution gene mapping, it is important to make a precise evaluation of how FISH treatment influences the chromosomal structures, because the structural changes and chromosome damage during FISH treatment have not been well characterized. Thus, using AFM we observed the shape of human chromosomes during the FISH process. Figure 11.7(a–d) illustrates typical examples of AFM images showing the change in structure of chromosomes during the FISH treatment process. This result clearly shows that the structure of the chromosome changes significantly during FISH treatment, because the chromosomes after FISH treatment were increased in width by about twofold and their height was decreased to a few tens of nanometers (Figure 11.7[c]), as compared with untreated chromosomes (Figure 11.7[a]). These findings were almost the same as those previously reported for barley chromosomes [15].

We then performed multicolor FISH using two probes (MYOp-1 and HATp) located 1.5 Mb apart (Figure 11.2), and analyzed their geographical relationship to investigate chromosome damage during FISH treatment (Figure 11.8[a]). Positional analysis of the two gene loci revealed that the relative positions of the signals were dispersed in the direction of the *x*-axis (outer–inner direction) rather than the *y*-axis (centromere–telomere direction) and the distance between them reached over 1 μm, which is approximately the full width of a chromatid. These results indicate that the chromosomes were severely damaged and lost their three-dimensional structure after standard FISH treatment, in which chromosome samples are generally fixed with Carnoy's fixative only.

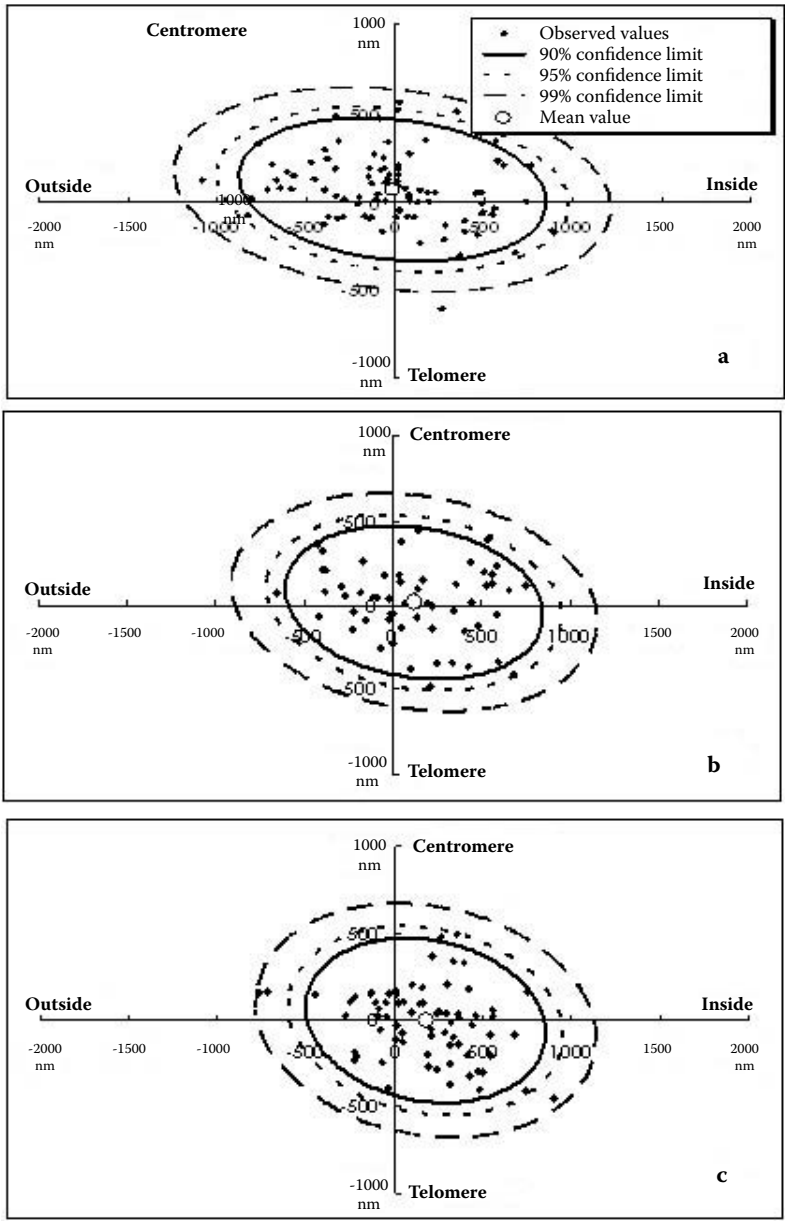

FIGURE 11.8 Plotted relative location of the green signals (HATp signals) based on the red signals (MYOp-L signals) as shown in Figure 11.6. The dots are observed values, and the small white circles on the graphs are the mean values. The dashed, dotted and solid oval lines indicate 90, 95 and 99% confidence limits. (a) Fixed with Carnoy's fixative only. (b, c) Re-fixed with 1 and 2% formaldehyde before FISH treatment. The numbers on the *x* and *y* axes indicate the distances between green and red signals.

In order to avoid destruction of the chromosome structures by FISH treatment, we attempted re-fixation of the chromosomes with various concentrations (0.5 to 4.0%) of formaldehyde after fixation with Carnoy's solution. We evaluated the effect of this double fixation using AFM (Figure 11.7[e–l]) and multicolor FISH (Figure 11.8[b,c]). The chromosomes fixed with 1% formaldehyde (Figure 11.7[e–g]) exhibited good durability against structural destruction by FISH processing, and maintained a height of about 70 nm after heat denaturation (Figure 11.7[h]). Moreover, the three-dimensional appearance of 4% formaldehyde-fixed chromosomes changed little before and after treatment (Figure 11.7[i–k]) and the height remained at over 100 nm even after FISH treatment (Figure 11.7[l]).

In the analysis of the relative positions of the two genes by multicolor FISH, there was a tendency to disperse the two signals in the *x*-direction rather than the *y*-direction, regardless of the fixation method of the chromosomes (Figure 11.8). However, this *x*-axis dispersion had a tendency to converge in double fixation with Carnoy's fixative and formaldehyde solution (Figure 11.8[b,c]). In addition, the mean value shifted to the inner side of the chromosome when formaldehyde fixation was performed, indicating that the HATp signal (green signal) has a tendency to appear on the inner side of MYOp-1 (red signal).

11.6 DISCUSSION AND CONCLUSION

Higher-resolution FISH protocols have been required in the last decade for mapping the increasing number of genes identified by the human genome project and other related studies. However, conventional light microscopy is unable to provide the resolution required in nanometer-scale studies, because its spatial resolution is fundamentally restricted to 300 nm by the diffraction limit of light.

Thus, in the present study, we applied SNOM/AFM to the mapping of genes and specific nucleotide sequences (such as a telomere sequence repeat) and succeeded in detecting the FISH signals on a chromosome with a resolution that exceeds conventional light microscopy.

In the present study, we used a SNOM/AFM instrument that operates in the dynamic-force mode. This instrument enabled us to analyze not only the positions of the genes but also their distributions in relation to higher-order chromosome structures (e.g., chromatin fiber folding) at nanometer-scale resolution. Using this instrument, we first observed barley chromosomes with the FISH signals of telomere repeats. The superimposition of the fluorescent image onto the topographic image obtained by SNOM/AFM was useful for analyzing the relationship between higher-order chromatin fiber folding and the FISH signal region. The results showed that no significant difference in structure is found between the chromatin fibers in the telomeric region and those in the non-telomeric region [18–20].

We also succeeded in SNOM/AFM detection of the FISH signal from a single gene. The shape of the FISH signal obtained by SNOM/AFM was irregular,

in contrast with the simply round or elliptical shape of the signal observed under conventional microscopy. From the signal outline information, the results of the present study indicate the possibility of gene mapping at the chromatin fiber level through superimposition of the fluorescent signal image by SNOM/AFM onto the topographic chromosome image obtained by AFM. We further succeeded in detecting multicolor FISH signals using SNOM/AFM, at a resolution beyond that of conventional fluorescent microscopy. Multicolor FISH is an essential technique for analyzing the relative location of a gene. Our results indicate that SNOM/AFM is a potential nanoscale gene mapping tool that is expected to be used for construction of high-density genetic maps.

We also showed that the three-dimensional higher-order structures of chromosomes fixed with conventional Carnoy's fixative were severely damaged during FISH treatment (Figure 11.7[a–c]). Thus, we introduced a novel technique consisting of a combination of Carnoy's fixative and formaldehyde re-fixation, which was effective in preserving the natural gene loci on the chromosome for nanoscale gene mapping studies. We also performed multicolor FISH analyses of two genes by light microscopy and AFM to further confirm the effect of the FISH treatment in relation to the structure of the chromosome. The results showed that the variance in distance between the two signals became somewhat smaller, irrespective of the fixation method of the chromosome. There are several possible explanations for these results: (1) the folding of the chromatin fiber may not be strictly controlled at the nanometer scale, although it determines the localization of each gene in relation to the chromosomal higher-order structure; (2) formaldehyde fixation can maintain the height and width of the chromosome, but it does not fix the internal structure of the chromosome (i.e., the chromatin fiber folding); and (3) gene location is altered from its original position by the initial Carnoy's fixation, before re-fixation with formaldehyde. Further examination and development of the FISH method including fixation are required to clarify the basis of this phenomenon and to establish a novel FISH method that does not damage the original gene loci. A FISH method using chromosome samples without any fixation is another potential approach.

In conclusion, we have introduced SNOM/AFM for the study of chromosomes labeled using the FISH method, and have demonstrated the usefulness of this technique for identifying particular gene locations on chromosomes in relation to the structure of the chromosome at a resolution higher than that of light microscopy. Thus, this novel "Chromosome nano-FISH method" is expected to become an important tool for the implementation of actual high-resolution gene mapping by SNOM/AFM.

ACKNOWLEDGMENT

This study was supported by Special Coordination Funds of the Ministry of Education, Culture, Sports, Science and Technology of the Japanese government.

REFERENCES

1. Ushiki T, Hitomi J, Ogura S, Umemoto T, Shigeno M (1996) Atomic force microscopy in histology and cytology. *Arch Histol Cytol* 59: 421–431.
2. Tamayo J, Miles M (2000) Human chromosome structure studied by scanning force microscopy after an enzymatic digestion of the covering cell material. *Ultramicroscopy* 82: 245–251.
3. Tamayo J, Miles M, Thein A, Soothill P (2000) Selective cleaning of the cell debris in human chromosome preparations studied by scanning force microscopy. *J Struct Biol* 128: 200–210.
4. Hausmann M, Bperner B, Rapp A, Scherthan H, Breulich K (2001) NSOM imaging of labelled mitotic and meiotic chromosomes. *Asia/Pacific Micro Anal* 3: 13–15.
5. Deckert V, Zeisel D, Zenobi R, Vo-Dinh T (1998) Near-field surface enhanced Raman imaging of dye labeled DNA with 100 nm resolution. *Anal Chem* 70: 2646–2650.
6. Garcia-Parajo MF, Veerman JA, Ruiter AG, van Hulst NF (1998) Near-field optical and shear-force microscopy of single fluorophores and DNA molecules. *Ultramicroscopy* 71: 311–319.
7. Moers MH, Ruiter AG, Jalocha A, van Hulst NF (1995) Detection of fluorescence in situ hybridization on human metaphase chromosomes by near-field scanning optical microscopy. *Ultramicroscopy* 61: 279–283.
8. Moers MH, Kalle WH, Ruiter AG, Wiegant JC, Raap AK, Greve J, de Grooth BG, van Hulst NF (1996) Fluorescence in situ hybridization on human metaphase chromosomes detected by near-field scanning optical microscopy. *J Microsc* 182: 40–45.
9. Iwabuchi S, Muramatsu H, Chiba N, Kinjo Y, Murakami Y, Sakaguchi T, Yokoyama K, Tamiya E (1997) Simultaneous detection of near-field topographic and fluorescence images of human chromosomes via scanning near-field optical/atomic-force microscopy (SNOAM). *Nucleic Acids Res* 25: 1662–1663.
10. Yoshino T, Sugiyama S, Hagiwara S, Ushiki T, Ohtani T (2002) Simultaneous collection of topographic and fluorescent images of barley chromosomes by scanning near-field optical/atomic force microscopy. *J Electron Microsc* 51: 199–203.
11. Muramatsu H, Homma K, Yamamoto N, Wang J, Sakata-Sogawa K, Shimamoto N (2000) Imaging of DNA molecules by scanning near-field microscope. *Mater Sci Eng C* 12, 29–32.
12. Liu XQ, Sugiyama S, Xu QY, Kobori T, Hagiwara S, Ohtani T (2003) Atomic force microscopy study of chromosome surface structure changed by protein extraction. *Ultramicroscopy* 94: 217–223.
13. Dillé JE, Bittel DC, Ross K, Gustafson JP (1990) Preparing plant chromosomes for scanning electron microscopy. *Genome* 33: 333–339.
14. Sugiyama S, Yoshino T, Kanahara H, Shichiri M, Fukushi D, Ohtani T (2004) Effects of acetic acid treatment on plant chromosome structures analyzed by atomic force microscopy. *Anal Biochem* 324: 39–44.
15. Shichiri M, Fukushi D, Sugiyama S, Yoshino T, Ohtani T (2003) Analysis of morphological changes of barley chromosome during FISH treatments by atomic force microscopy. *Chromosome Res* 11: 65–71.
16. Fukushi D, Shichiri M, Sugiyama S, Yoshino T, Hagiwara S, Ohtani T (2003) Scanning near-field optical/atomic force microscopy detection of fluorescence in situ hybridization signals beyond the optical limit. *Exp Cell Res* 289: 237–244.

17. Sugiyama S, Yoshino T, Kanahara H, Kobori T, Ohtani T (2003) Atomic force microscopic imaging of 30 nm chromatin fiber from partially relaxed plant chromosomes. *Scanning* 25: 132–136.
18. Zentgraf U (1995) Telomere-binding proteins of *Arabidopsis thaliana*. *Plant Mol Biol* 27: 467–475.
19. Kim JH, Kim WT, Chung IK (1998) Rice proteins that bind single stranded G-rich telomere DNA. *Plant Mol Biol* 36: 661–672.
20. Lee JH, Kim JH, Kim WT, Kang BG, Chung IK (2000) Characterization and developmental expression of single-stranded telomeric DNA-binding proteins from mung bean (*Vigna radiata*). *Plant Mol Biol* 42: 547–557.

12 Isolation of Human and Plant Chromosomes as Nanomaterials

Susumu Uchiyama, Tomoyuki Doi and Kiichi Fukui*

CONTENTS

12.1 Introduction 155
12.2 Isolation, Purification and Handling of Chromosomes 157
12.3 Mass Isolation of Human Chromosomes 158
12.3.1 Human Cell Culture 159
12.3.2 Isolation of PA Chromosomes by Multi-Step Centrifugation 161
12.3.3 Isolation of PA Chromosomes by Glycerol Density Gradient Centrifugation 161
12.3.4 Isolation of CA Chromosomes 162
12.4 Isolation of Specific Chromosomes 163
12.5 Mass Isolation of Plant Chromosomes 165
12.6 Conclusion 165
Acknowledgment 166
References 166

12.1 INTRODUCTION

In higher eukaryotes, when cells enter mitosis the chromosomes start to condense and at metaphase they take on their most condensed structure. Their characteristic X-shaped structure is common to all higher eukaryotes despite the differences in DNA sequence among species, and the formation of this structure is essential to cell viability. From the early stages of chromosome research in the late 19th century until recently, chromosomes have been mainly studied from morphological and genetic points of view. There are two main reasons for this. One is the fascinating structure of chromosomes visible under the light microscope with or without

*To whom correspondence should be addressed.

dye staining, thus rendering them well suitable for morphological study. The second reason is that DNA has been a primary research interest until the completion of sequencing of the human genome, and therefore preparation and handling techniques for chromosomes as large macromolecular complexes have been left behind the study of the genome. Difficulties in isolation of chromosomes in large quantities and their inherently fragile nature are also reasons for the current lack of information on chromosomal material. In the case of human chromosomes, each chromatid has dimensions of several micrometers in length and about 1 μm in width, which makes them suitable targets for on-chip devices produced using recent nanotechnology (see Chapter 4). Chromosomes of some plants such as barley and rye are larger in size than those of human chromosomes. Furthermore, the plant *Crepis*

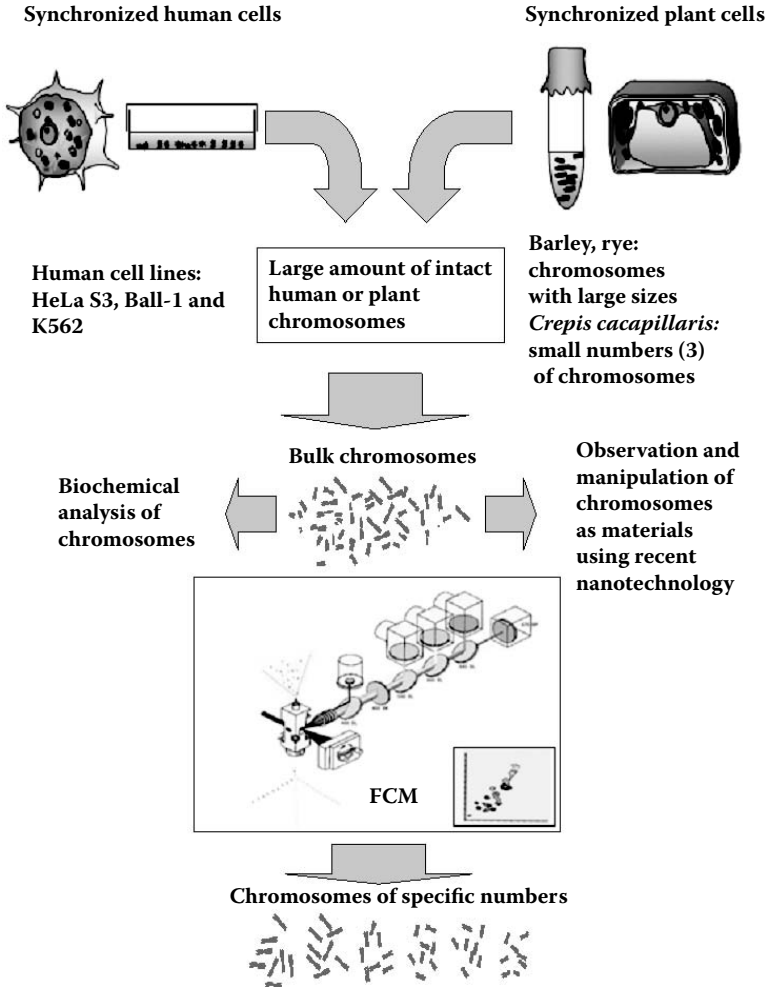

FIGURE 12.1 An outline summary of "chromosomes as nanomaterials."

capillaries, for example, has only three chromosomes. These plant chromosomes are therefore easily distinguished and handled under optical microscopy. Hence, as summarized in Figure 12.1, chromosomes from different sources can be chosen depending on the purpose of the experiment. In this chapter, the isolation, purification and handling of human and plant chromosomes as nanomaterials for differing purposes are described, based on our recent studies.

12.2 ISOLATION, PURIFICATION AND HANDLING OF CHROMOSOMES

Formation of the highly condensed structure of chromosomes occurs during only a short period of the whole cell cycle. In the case of human cells, the population of mitotic cells is only a small percentage of the total number of cells, which makes it difficult to prepare chromosomal material. Cell cycle synchronization is therefore required and can be attained by the addition of chemicals and/or by temperature control, which basically interfere with spindle polymerization or its attachment to kinetochores. Cell cycle synchronization to S phase is effective in raising the synchronization rate. In the case of isolation of plant chromosomes, a combination of different synchronization techniques are necessary for chromosome isolation, while more than 50% of human cells are arrested in metaphase (mitotic index: 50%) by a single chemical treatment [1], and at best, a synchronization rate of more than 90% has also been reported [2]. It should be noted that metaphase chromosomes prepared by the addition of chemical inhibitors related to spindle formation or attachment are generally hypercondensed, because chromosome condensation continues without spindle attachment and segregation [3]. Although the nuclear envelope is already broken down at metaphase, the cell membrane encapsulating the cytoplasm and chromosomes needs to be disrupted for isolation. For this purpose, hypotonic treatment following mechanical and/or chemical disruption is carried out. In plants, removal of the cell wall is also required. Chromosome structure is stabilized in the presence of divalent cations such as Mg^{2+} and Ca^{2+}; otherwise they change to a dispersed structure. However, at the same time these divalent cations unexpectedly activate nucleases and proteases, which leads to the degradation of chromosomes. Thus, instead of divalent cations, polyamines are used for the stabilization of chromosomes. Polyamines are highly positively charged molecules that are primarily used to stabilize the conformation of nucleic acids by shielding repulsive negative charges of the phosphate backbone, and are also used in ribosome preparation. Isolation of chromosomes from the heterogeneous mixture containing cytoplasmic materials and other subcellular constituents as well as chromosomes is generally attained by the use of centrifugation. Chromosomes are highly sticky materials and once bound to each other, their re-dispersion is almost impossible. Concentration or collection of chromosomes thus has to be carried out by low speed centrifugation to avoid aggregation. A glycerol cushion is effective in protecting from aggregation of chromosomes during the concentration by centrifugation. Stabilization of isolated chromosomes is enhanced by chemical, alcohol and acid fixations.

In the case of chromosomes without fixation, their stability depends on solution conditions. Generally, chromosome structure is maintained for a long period in acidic conditions, such as citric acid solution, and isolated chromosomes can be stored in citric acid solution at 4°C for more than 2 months. However, the protein composition of chromosomes is also influenced by the solution conditions [1]. For example, some chromosomal proteins such as linker histone H1 are stripped off in citric acid solution [1]. So far, the relationship between chromosome morphology and its protein composition has not been established. Alternatively, isolated chromosomes can be stored at –20°C in solution containing 60% glycerol. Glycerol prevents the solution from freezing and chromosomes from aggregating.

12.3 MASS ISOLATION OF HUMAN CHROMOSOMES

Chromosome isolation was mainly performed using two different methods, the polyamine (PA) and citric acid (CA) methods, according to the requirements of the subsequent experiment. Both methods provided isolated chromosomes in large quantities and the morphologies were well preserved (Figure 12.2[a–c]). At a synchronization rate of 50%, 400 mL of cell culture at 0.7×10^6 cells/mL typically

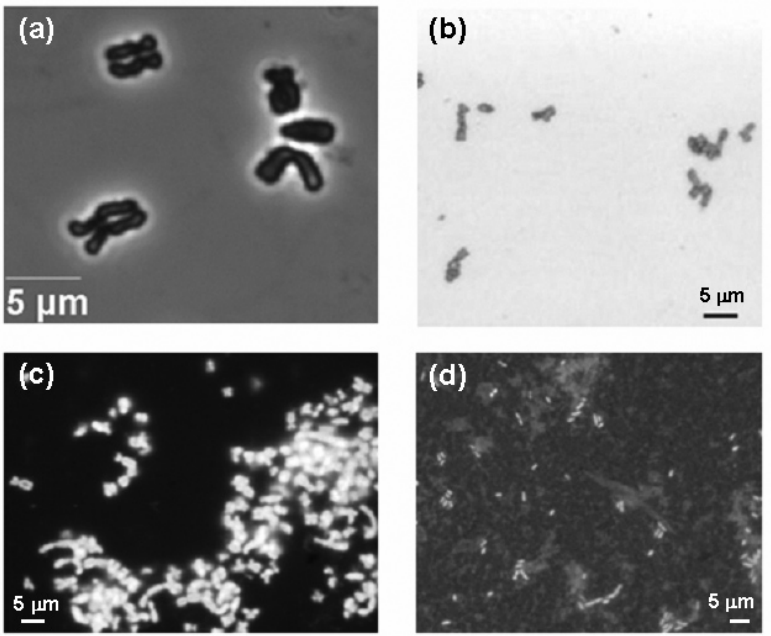

FIGURE 12.2 Isolated human and plant chromosomes. (a) Human chromosomes isolated using glycerol density gradient centrifugation (PA chromosomes), (b) human chromosomes isolated using the citric acid method (CA chromosomes), (c) CA chromosomes 2 weeks after isolation, (d) isolated barley chromosomes. In (a) and (b) chromosomes were stained with DAPI, while in (c) and (d) chromosomes were stained with YOYO-1.

produced approximately 5×10^9 PA chromosomes using these methods. Recently, however, our proteomic analysis of PA chromosomes revealed disruption of the cell membrane by the detergent used for chromosome isolation, causing release of proteins from mitochondria and the endoplasmic reticulum and consequent non-specific binding to isolated chromosomes. Thus, PA chromosomes are not suitable for biochemical or biophysical studies. Chromosome structure is known to be maintained at acidic pH or in ethanol/acetic acid (3:1) solution. Chemical fixation of chromosomes by glutaraldehyde or formaldehyde also allows the preservation of condensed structure. These fixation techniques have mainly been used for genetic studies. However, under these nonphysiological conditions, the interactions of proteins with other proteins or nucleic acids differ from those under physiological conditions. In general, chemical fixation causes almost irreversible cross-linking of proteins to each other, which interferes considerably with further biochemical analyses. A recent report on a procedure which enables proteomic analysis of organs after formaldehyde fixation might be useful for analysis of fixed chromosomes [4].

The isolation of metaphase chromosome was completed by either multistep centrifugation or glycerol density gradient centrifugation in the presence of PAs. Both methods produce chromosomes with a similar structure under optical microscopy, and similar protein constituents. Cytoskeletal proteins, such as actin and keratin, were strongly attached to PA chromosomes. Isolation and handling of chromosomes on ice minimizes non-specific binding of cytoskeletal protein to chromosomes [5,6]. PA chromosomes can be used for light-microscopy studies, such as protein localization analyses after immunochemical labeling and on-chip sorting of chromosomes. On the other hand, structural studies by SPM and EM and manipulation of chromosomes with SPM require further-purified chromosomes, because the impurities in PA chromosome solution frequently cover the surface of chromosomes (Figure 12.3). PA chromosomes can be stored at 4°C for 1 to 2 weeks or at –20°C in the presence of glycerol for a considerably longer period, and can be applied to purification by sucrose density gradient centrifugation or Percoll density gradient centrifugation, which removes chromosome coating proteins.

12.3.1 Human Cell Culture

HeLa S3 cells (ATCC CCL-2, RCB0007, RCB0191), K562 lymphocytes (RCB0027) and Ball-1 cells (RCB02561) were mainly used for human chromosome isolation. HeLa S3 cells are cells transformed to a floating version from the original adherent HeLa cells derived from glandular cervical cancer, while the latter two cell lines are derived from floating-type lymphoma cells. Although many cell biology studies have already been carried out using HeLa cells, the number of their chromosomes is anomalous. The number of chromosomes of K562 cells is also anomalous. Ball-1 cells are known to have 46 chromosomes. Cells were treated with 0.02 μg/mL colcemid for 13 to 16 h for cell cycle synchronization.

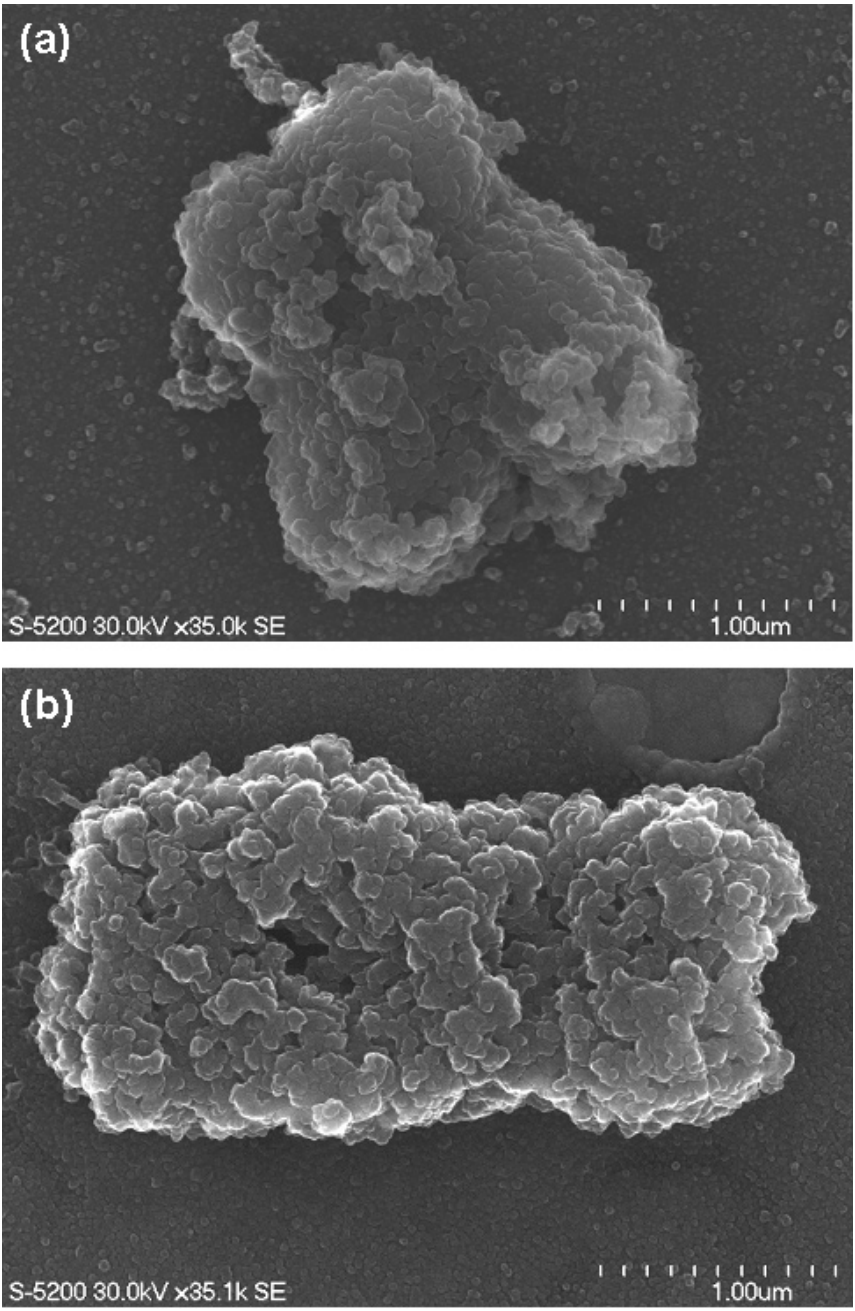

FIGURE 12.3 Scanning electron microscopy (SEM) images of isolated human chromosomes. (a) PA chromosomes, (b) PA chromosomes after purification by the Percoll density gradient centrifugation method.

12.3.2 Isolation of PA Chromosomes by Multi-Step Centrifugation

Isolation of PA chromosomes was performed according to the previously described method, with slight modifications [5,7–9].

1. Four liters of synchronized cells was harvested by centrifugation at 1500 *g* for 10 min.
2. The cells were resuspended in 100 mL of 75 m*M* KCl and the solution was transferred into two 50-mL tubes. Hypotonic treatment was performed for 15 min at room temperature (RT), then the cells were gently mixed and a further hypotonic treatment was performed for 15 min at RT, followed by centrifugation at 780 *g* at 4°C for 10 min. The cells were resuspended in 80 mL of ice-cold PA buffer (15 m*M* Tris–HCl pH 7.4, 2 m*M* EDTA, 80 m*M* KCl, 20 m*M* NaCl, 0.5 m*M* EGTA, 0.2 m*M* spermine, 0.5 m*M* spermidine and 0.1 m*M* PMSF) containing 0.1% Digitonin or 0.05% Empigen.
3. Forty milliliters of the solution was taken, and the cell membranes were disrupted on ice using a 40-mL capacity Dounce homogenizer with a loose type (B type) pestle. The same procedure was repeated with another 40 mL of solution.
4. The solutions were mixed and PA buffer was added to the mixed solution to a final volume of 90 mL. Fifteen-milliliter aliquots of the solution were transferred into six 50-mL tubes and centrifuged at 190 *g* at 4°C for 3 min. Approximately 10 mL of supernatant containing chromosomes was usually recovered.
5. PA buffer was added to the pellets up to a final volume of 15 mL after mixing and the solution was centrifuged at 190 *g* at 4°C for 3 min. The supernatant was then collected.
6. Solutions containing chromosomes were mixed (4 and 5, total of 120 mL), the mixture was gently overlaid into four 50-mL tubes each containing a 10-mL cushion of 70% glycerol in PA buffer, and the tubes were centrifuged at 1750 *g* at 4°C for 20 min. Most of the chromosomes were recovered as a white band at the boundary region between the supernatant and the cushion.
7. The supernatant (30 mL) was discarded and chromosomes were collected and stored at −20°C. Chromosome morphology is maintained for at least 1 month under these conditions. However, aggregation of chromosomes proceeds during preservation.

12.3.3 Isolation of PA Chromosomes by Glycerol Density Gradient Centrifugation

The glycerol density gradient centrifugation method was developed by Laemmli and colleagues [6,7] and is rather complicated compared to the multi-step centrifugation method. However, in this method, chromosomes are treated in a

dispersed state in solution until the final concentration step, thereby minimizing chromosome aggregation:

1. Four exponential glycerol density gradients (5 to 70% in LS buffer, 15 m*M* Tris, pH 7.4, 80 m*M* KCl, 2 m*M* EDTA, 0.2 m*M* spermine, 0.5 m*M* spermidine, 1% thiodiglycol, 0.1 m*M* PMSF and 0.05% Empigen) were prepared in separate centrifuge tubes (4 × 38.5 mL), and the gradient solution was kept at 4°C in a cold room or on ice.
2. Four hundred milliliters of synchronized cells was harvested by centrifugation at 1500 *g* at RT for 10 min.
3. Gently, but completely, the pellet was washed with 20 mL of HP buffer and the solution was centrifuged at 1200 *g* at RT for 5 min. The cell pellet was then transferred to a 50-mL tube, and the cell washing was repeated twice. The suspension was centrifuged at 1200 *g* for 5 min.
4. The pellet was resuspended in 20 mL of ice-cold LS buffer. From this step on, all the procedures were carried out at 4°C.
5. The cell membranes were disrupted using a 40-mL capacity Dounce homogenizer with a loose-type (B-type) pestle.
6. Separated aliquots of the solution were transferred onto the four exponential glycerol density gradients, and centrifuged at 200 *g* for 5 min using a SW24.38 swing rotor and then at 700 *g* for 15 min.
7. Three milliliter fractions were collected from the top to the bottom of the gradient. The fractions containing chromosomes were checked by optical microscopy for authentic morphology. Fractions containing chromosomes were layered onto a 5-mL cushion of 70% glycerol in ST (3.75 m*M* Tris pH 7.4, 20 m*M* KCl, 0.5 m*M* EDTA, 0.05 m*M* spermine, 0.125 m*M* spermidine, 1% thiodiglycol and 0.1 m*M* PMSF) buffer and centrifuged at 3000 *g* for 15 min. Chromosomes were recovered as a slightly white band at the boundary region between the supernatant and the cushion.
8. Chromosomes were collected and stored at −20°C.

12.3.4 Isolation of CA Chromosomes

CA methods provide well-shaped isolated chromosomes that can be stored for relatively long periods, such as 3 months, and are suitable for chromosome chip development because of their stability [1].

1. Four hundred milliliters of synchronized cells was harvested by centrifugation at 1500 *g* for 10 min.
2. The cells were resuspended in 40 mL of 75 m*M* KCl and the solution was transferred into two 50-mL tubes for hypotonic treatment for 30 min at RT. The cells were collected by centrifugation at 780 *g* at 4°C for 10 min. The cells were resuspended in 1.5 mL of CA solution (100 m*M* citric solution, 100 m*M* sucrose, and 0.5% Tween20, pH 2.7), followed by agitation by vortexing for cell membrane disruption.

3. Large materials including nuclei were removed by centrifugation at 190 *g* at 4°C for 3 min, and this centrifugation was repeated. Chromosomes were contained in the supernatant.
4. The supernatant was further centrifuged at 1750 *g* at 4°C for 10 min in order to remove cytoplasmic large complexes.
5. Chromosomes were homogenized in 1.5 mL of CA solution and subsequently recovered as sediment.

12.4 ISOLATION OF SPECIFIC CHROMOSOMES

Isolation of specific-number chromosomes can be performed by double staining chromosomes with two different types of dyes, Hoechst and chromycin A3, followed by two-dimensional separation using flow cytometry (FCM). Hoechst and chromomycin A3 are fluorescent dyes and stain the AT-rich regions and GC-rich regions of chromosomes, respectively. Flow sorting uses sheath solution that contains neither divalent cation nor polyamines for the separation, which causes collapse of chromosome structure. Chromosomes therefore need to be fixed immediately after flow sorting.

As indicated in Figure 12.4(a), chromosomes were separated into three groups based on DNA content, i.e., large, medium and small chromosomes. Disruption of the authentic shapes of chromosomes was avoided by collecting separated chromosomes in 70% ethanol. A well-maintained authentic shape of the chromosomes in group L was confirmed, as shown in Figure 12.4(b).

1. The cells at $2 \sim 3 \times 10^5$ cells/mL were cultured in RPMI 1640 containing 15% FCS and 0.25% Nutridoma hydroxyurea.
2. The cells at $6 \sim 8 \times 10^5$ cells/mL were cultured in the medium containing 0.2 μg/mL colcemid for 16 to 18 h.
3. The cells were suspended in PBS and centrifuged at 1500 *g* for 10 min at 4°C. Ten milliliters of 75 m*M* KCl was added to the pellet containing 10^7 cells.
4. The cells were suspended with PBS and centrifuged at 1500 *g* for 10 min at 4°C.
5. One milliliter of polyamine buffer containing digitonin was added to pellet containing 10^7 cells and agitated by vortexing.
6. The cells were disrupted by five strokes through a 22G needle.
7. Polyamine buffer (1.5 mL) and 15 μL of 1 *M* $MgCl_2$ were added to 20 μL of solution containing chromosomes followed by filtration with 20 μm mesh.
8. Chromomycin A3 was added to the solution containing chromosomes to a final concentration of 0.1 m*M*, and the solution was stored in the dark overnight at 4°C.
9. Six microliters of Hoechst 33342 solution was added to 1.5 mL of solution containing chromosomes and the solution was stored for 30 min at 4°C.
10. Chromosomes were separated using EPICS ALTRA FCM (Beckman-Coulter Inc.).

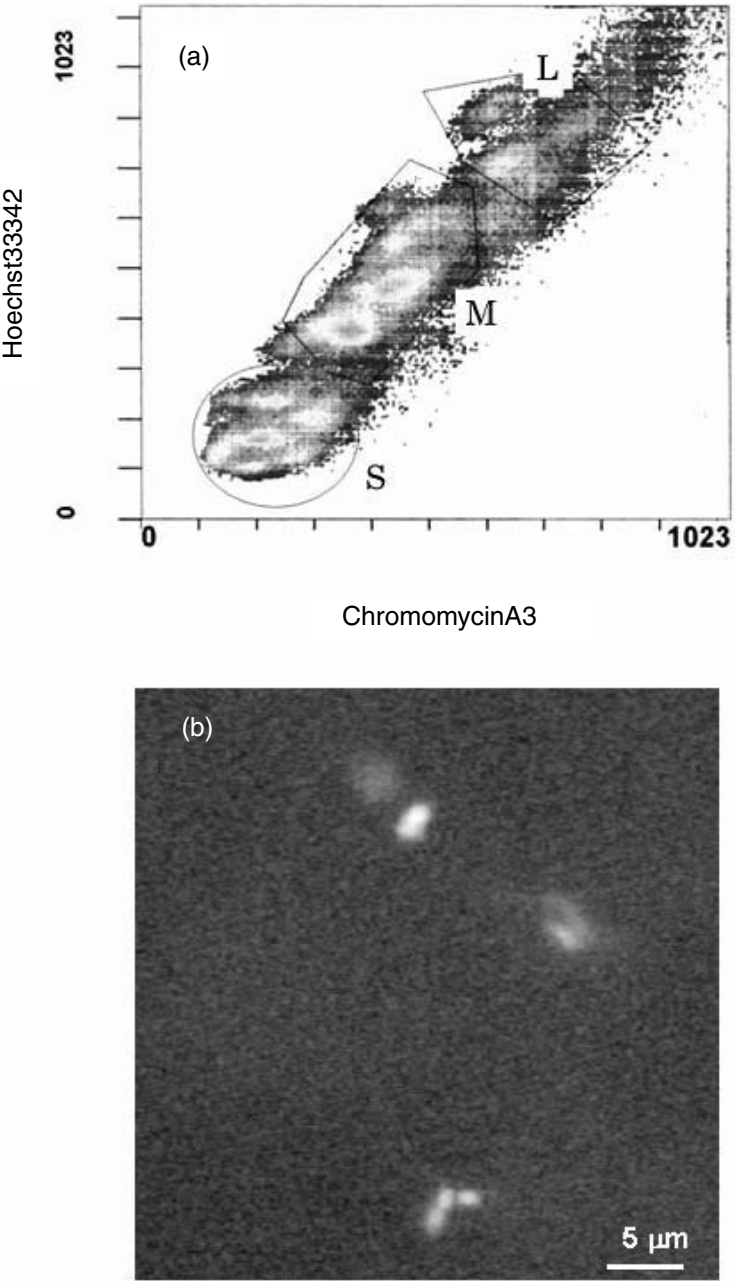

FIGURE 12.4 Flow cytometry separation of human chromosomes. (a) Chromosomes are separated into large (L), medium (M) and small (S) chromosomes using the double staining method. (b) The authentic shape of the separated chromosomes belonging to group L is confirmed under fluorescence microscopy.

12.5 MASS ISOLATION OF PLANT CHROMOSOMES

Generally, the synchronization rate of plant cells is low compared to those from animal species, thus studies using isolated chromosomes have been limited to a few plant species [10]. Here, three-step synchronization was applied to isolation of metaphase chromosomes from barley (*Hordeum vulgare* L.) or rye (*Secale cereale* L.) [11,12]. It should be noted that it is necessary to check the synchronization rate for each plant species. A mitotic index of more than 60% is attained for both barley and rye using the three-step synchronization method where the time and concentration of the treatment with HU and trifluralin are optimized, which enables chromosome isolation from the root meristem cells. As shown in Figure 12.2(d), isolated barley chromosomes are approximately 5 μm in length, which is larger than human chromosomes and makes them suitable for structural analysis.

1. Seedlings (about 1-cm-long primary roots) of barley or rye were incubated in Hoagland solution (Sigma) containing 1.25 m*M* hydroxyurea in the dark at room temperature for 14 h.
2. The seedlings were rinsed in distilled water and incubated in hydroxyurea-free Hoagland solution for 2 h.
3. The seedlings were treated with 1 m*M* trifluralin for 3 h. After accumulation of metaphase chromosomes, seedlings were transferred into ice-cold water and stored overnight.
4. The roots were cut 1 cm from the root tip and fixed with 2% paraformaldehyde in Tris buffer (10 m*M* Tris, 10 m*M* Na_2EDTA, 100 m*M* NaCl, 0.1% Triton X-100, pH 7.5) for 20 min [11,12]. Subsequently, metaphase chromosome solution was prepared in chromosome isolation buffer (50 m*M* KCl, 10 m*M* $MgSO_4$, 5 m*M* K_2HPO_4, 5 m*M* HEPES, 2 m*M* dithiothreitol, 0.2% Triton X-100, 25 μg/mL PI).
5. Twenty root tips were used to prepare one chromosome solution. Chromosomes were isolated from the terminal 1.5 mm of the root tip using a Polytron PT1300D homogenizer (Kinematica AG, Littau, Switzerland) at 9000 rpm for 15 s [12].
6. Homogenized solution was passed through 50-μm mesh to remove large contaminants, and centrifuged at 1000 *g* for 20 min. Sediment materials in 100 mL solution were resuspended to obtain a solution of isolated chromosomes, which can be stored for 1 week at 4°C.

12.6 CONCLUSION

The isolation, purification and storage methods of chromosomes from humans and plants described in this chapter were developed for different purposes, such as the development of a chromosome-chip and on-chip sorter. This study enabled us for the first time to handle chromosomes as nanomaterials in substantial quantities.

ACKNOWLEDGMENT

This study was supported by Special Coordination Funds of the Ministry of Education, Culture, Sports, Sciences and Technology of the Japanese government.

REFERENCES

1. Sone T, Iwano M, Kobayashi S, Ishihara T, Hori N, Takata H, Ushiki T, Uchiyama S, Fukui K (2002) Changes in chromosomal surface structure by different isolation conditions. *Arch Histol Cytol* 65: 445–455.
2. Gassmann R, Henzing AJ, Earnshaw WC (2004) Novel components of human mitotic chromosomes identified by proteomic analysis of the chromosome scaffold fraction. *Chromosoma* 113: 385–397.
3. Ushiki T, Hoshi O, Iwai K, Kimura E, Shigeno M (2002) The structure of human metaphase chromosomes: its histological perspective and new horizons by atomic force microscopy. *Arch Histol Cytol* 65: 377–390.
4 Palmer-Toy DE, Krastins B, Sarracino DA, Nadol JB Jr, Merchant SN (2005) Efficient method for the proteomic analysis of fixed and embedded tissues. *J Proteome Res* 4: 2404–2411.
5. Uchiyama S, Kobayashi S, Takata H, Ishihara T, Hori N, Higashi T, Hayashihara K, Sone T, Higo D, Nirasawa T, Takao T, Matsunaga S, Fukui K (2005) Proteome analysis of human metaphase chromosomes. *J Biol Chem* 280: 16994–17004.
6. Gasser S, Laemmli U (1987) Improved methods for the isolation of individual and clustered mitotic chromosomes. *Exp Cell Res* 173: 85–98.
7. Lewis C, Laemmli U (1982) Higher order metaphase chromosome structure: evidence for metalloprotein interactions. *Cell* 29: 171–181.
8. Spector D, Goldman R, Leinwamd L (1998) *Chromosome isolation for biochemical and morphological analysis in cells: a laboratory manual*, Janssen K., Ed. Cold Springer Harbor Laboratory Press, New York: 49.1.
9. Uchiyama S, Kobayashi S, Takata H, Ishihara T, Sone T, Matsunaga S, Fukui K (2004) Protein composition of human metaphase chromosomes analyzed by two-dimensional electrophoreses. *Cytogenet Genome Res* 107: 49–54.
10. Dolezel J, Cihalikova J, Weiserova J, Lucretti S (1999) Cell cycle synchronization in plant root meristems. *Methods Cell Sci* 21: 95–107.
11. Ma YZ, Lee JH, Li LC, Uchiyama S, Ohmido N, Fukui K (2005) Fluorescent labeling of plant chromosomes in suspension by FISH. *Genes Genet Syst* 80: 35–39.
12. Lee JH, Ma Y, Wako T, Li LC, Kim KY, Park SW, Uchiyama S, Fukui K (2004) Flow karyotypes and chromosomal DNA contents of genus *Triticum* species and rye (*Secale cereale*). *Chromosome Res* 12: 93–102.

13 Proteome Analysis of Human Metaphase Chromosomes

Kiichi Fukui and Susumu Uchiyama*

CONTENTS

13.1 Introduction 167
13.1.1 Historical Perspective 167
13.1.2 Implications of the Higher-Order Structure of a Chromosome... 168
13.1.3 Models of Chromosomal Higher-Order Structure 168
13.2 Identification of Chromosomal Proteins 170
13.2.1 Isolation of Human Metaphase Chromosomes 170
13.2.2 Protein Extraction from Isolated Chromosomes 171
13.2.3 Protein Separation by Four Different Electrophoresis Techniques 171
13.2.4 Protein Identification by Mass Spectrometry 172
13.3 Comparative Proteome Analysis of Human Chromosomes 173
13.3.1 Proteins Identified from Three Different Isolation Methods ... 173
13.3.2 Proteins Identified from Two Different Cell Lines 178
13.4 The Four-Layer Model, a Protein Framework of Human Chromosomes 180
13.4.1 Localization of Chromosomal Proteins 180
13.4.2 Chromosomal Proteins Are Classified into Four Groups 180
13.4.3 Four-Layer Model 185
13.5 Conclusion 186
Acknowledgments 187
References 187

13.1 INTRODUCTION

13.1.1 Historical Perspective

Chromosomes were first discovered by Karl Wilhelm von Nägeli in 1842 and were thus named "chromosomes" by Heinrich Wilhelm Gottfried von Waldeyer-Hartz in 1888. Chromosomes are now understood to be "super molecules" consisting of DNA

*To whom correspondence should be addressed.

proteins, and appearing at the M phase in mitosis and meiosis. The chromosomal higher-order structure is established during the M phase and is completed at the metaphase stage (see Chapter 9). The overall higher-order structure of chromosomes remains an enigma in spite of the efforts of numerous researchers, and dozens of different models have been presented. One of the main obstacles in characterizing the chromosomal higher-order structure model lies in the fact that the chromosome constituent proteins have not fully been identified or analyzed, although it is well known that each chromosome contains two DNA molecules, five major histone proteins, and nonhistone proteins. In this chapter, we describe a human metaphase chromosome protein framework, defined using the results of proteome analysis of human metaphase chromosomes. We present a "four-layer model" of human metaphase chromosomes— the first chromosome structural model based on information of the chromosomal constituent proteins and their localization.

13.1.2 Implications of the Higher-Order Structure of a Chromosome

The construction of the higher-order structure of a chromosome has biological implications such as packaging of long chromatin fibers with single DNA molecules into two small carrier chromatids of limited volume; facilitating transportation of DNA fibers to two new daughter cells without damage; equal distribution of essential proteins to the daughter cells; preserving epigenetic marking on both DNA molecules; and preventing histone proteins from modification during dynamic movement of chromatin fibers through the cell cycle. It has long been known that the nucleolar proteins attached to the surface of chromosomes are transported evenly to the two daughter cells. They protect the chromosomal surface structure from friction with cytoplasmic substances during movement to the fixed position in the daughter cells.

It is also important to point out that in both plants and animals, chromosomes have the common basic structure of the centromere, two arms, telomeres, and so on, despite proceeding along different evolutional pathways for billions of years from the point when the symbiosis of cyano-bacteria was established in a plant ancestor. This implies that the importance of the functional role of the chromosome rigidly restricts structural divergence, as demonstrated, for example, in the similarity in structure of human and octopus eyes, even though vertebrates and mollusks have passed through very different evolutional histories [1]. Thus the common structure of chromosomes among evolutionally different organisms indicates, in itself, their functional importance to the organisms [2].

13.1.3 Models of Chromosomal Higher-Order Structure

The basic structure of a chromosome has been elucidated as being a nucleosome, where the DNA strand and histone octamer form a complex of 11 nm diameter [3,4]. Chromosomal structure higher than the nucleosome level, however, has not yet been elucidated, although several models have been proposed. Even for the 30-nm fiber structure, there are tens of different models including the solenoid

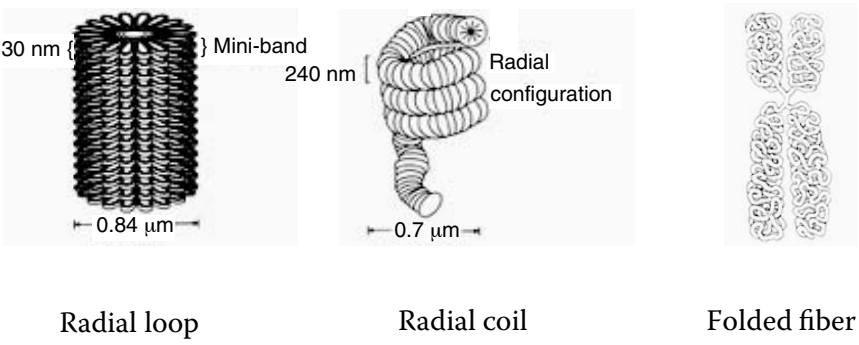

FIGURE 13.1 Three schematic models for human chromosomes from Fukui and Uchiyama [2]. With permission.

model, zigzag model, cross-link model, etc. [5–8]. For the structure of metaphase chromosomes, these can be classified into three basic patterns, i.e., the radial loop model with chromosome scaffold, the radial coil model, and the folded fiber model [9–12], as depicted in Figure 13.1.

Each hypothesis has both strengths and weaknesses. For example, the radial loop model requires a central pole referred to as the "chromosome scaffold," where the chromatin loop attaches. Its latest incarnation is the "barber pole model," where the alternating localization of topoisomerase IIα and 13S condensin characterizes a barber pole-like scaffold [13]. Immuno-detection of topoisomerase IIα, however, often shows a broader distribution of the signals from condensin than that expected from the axial location of the scaffold model [14–16]. Chromosome stretching experiments indicate much elasticity of the chromosome, which would suggest the absence of rigid structure at the axis of the chromatids [17,18]. These recent results do not fully support any single model. Moreover, no model has referred to the protein constituents, because analysis of constituent chromosomal proteins has only recently become possible.

On the other hand, it is known that chromosome morphology varies substantially in different buffer conditions. We also observed a conspicuous difference in the surface structure of two chromosomes, respectively, prepared with either polyamine buffer (PA) or citric acid solution (CA), as demonstrated in Figure 13.2 [20]. PA chromosomes have a rather smooth surface covered by flattish scaly structures of different sizes and shapes. This structure appears to be a dense covering of the inner structure with a particular matrix. CA chromosomes have a quite different appearance, of dense fibrous structures of rather uniform diameter (50 to 70 nm). Moreover, CA chromosomes show a more relaxed morphology with the emergence of two sister chromatids.

Comparison of protein composition using 1-D SDS-PAGE further reveals the key role of protein composition in the chromosome surface structure. Most of the linker histone, H1, was removed from the CA chromosomes, although the core histones remained almost the same between PA and CA chromosomes [20].

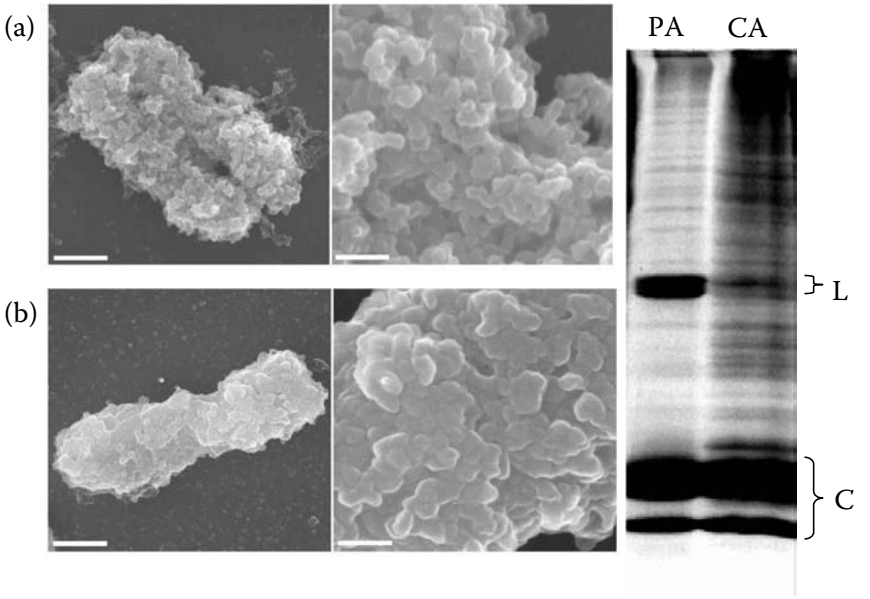

FIGURE 13.2 Comparison of chromosome surface morphology in different isolation methods. (a) CA chromosomes isolated in citric acid solution and (b) PA chromosomes isolated in polyamine buffer. 1-D SDS-PAGE pattern of PA and CA chromosomes is shown in the right panel. C and L correspond to the core and linker histones, respectively. (From Sone et al. [20]. With permission.)

Moreover, the surface structure of the human metaphase chromosomes was of a completely different structural pattern, as shown in Figure 13.2. This fact enables us to propose that chromosomal proteins play important roles in the structure of chromosomes. Therefore, we began to analyze, identify and quantify the chromosomal proteins using isolated chromosomes under different buffer conditions.

13.2 IDENTIFICATION OF CHROMOSOMAL PROTEINS

13.2.1 Isolation of Human Metaphase Chromosomes

The cell lines used in our study are epithelial-like cells, HeLa and HeLa S3, and lymphoma-type cells, BALL-1 and K562. A detailed description of the culture of these cells, synchronization conditions and isolation procedures of metaphase chromosomes is given in our previous paper [21–23] and a separate chapter of this book. For the protein analyses, we isolated PA chromosomes using the polyamine method, SG chromosomes using the sucrose density gradient centrifugation (SDGC) method, CA chromosomes using the citric acid solution method and PG chromosomes using the Percoll density gradient centrifugation (PDGC) method. Three isolation methods developed for chromosome preparation are shown in Figure 13.3.

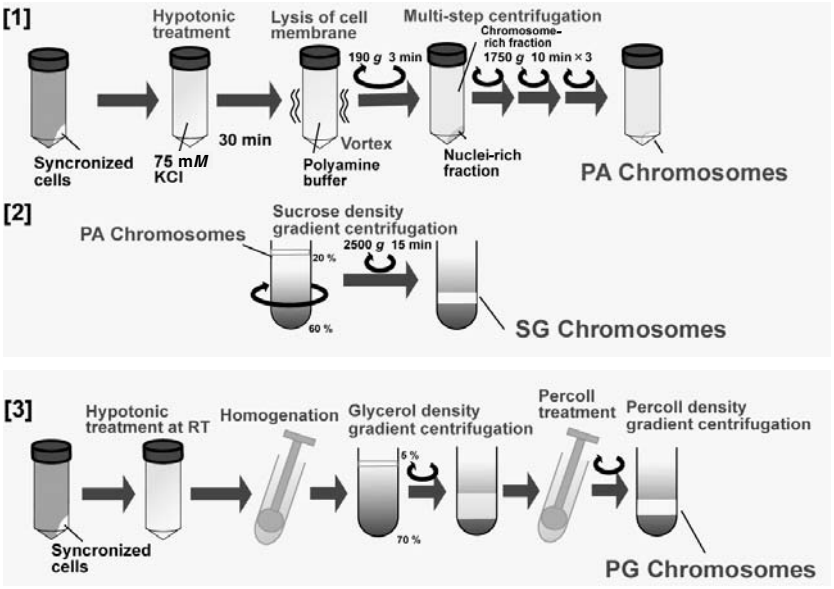

FIGURE 13.3 Three isolation methods developed for PA, SG, and PG chromosomes.

13.2.2 Protein Extraction from Isolated Chromosomes

Highly efficient protein extraction from isolated metaphase chromosomes is an important step for proteome analysis with high reproducibility and sensitivity. Additionally, the extracted protein needs to be highly buffer-soluble for separation using electrophoresis. After examining different conditions for protein extraction, the following procedures were established. For 1-D SDS-PAGE analysis, isolated chromosomes were directly suspended and dissolved in the SDS sample buffer (62.5 m*M* Tris–HCl, pH 6.8; 5% 2-mercaptoethanol; 20% glycerol; 2% SDS; and 0.005% BPB). For two-dimensional electrophoresis (2-DE), proteins were extracted from isolated chromosomes using an acetic acid extraction method. Typically, a single extraction experiment using PA chromosomes isolated from 2.8×10^8 BALL-1 cells yields 500 μg of proteins, whereas PG chromosomes isolated from 2.8×10^8 HeLa S3 cells yield 44 μg of proteins. The lower quantities of proteins extracted from PG chromosomes was mainly a result of the decrease in the amount of chromosomes at each purification step. Protein aliquots were lyophilized and stored at −80°C until further analysis.

13.2.3 Protein Separation by Four Different Electrophoresis Techniques

Protein separation was performed employing four different electrophoresis techniques in order to obtain comprehensive proteome information on metaphase chromosomes. Conventional SDS-PAGE gives an overall view of protein composition except for in the ultrahigh molecular weight (MW) range, where

proteins have a MW higher than 1 MDa. In order to separate ultrahigh MW proteins, 2 to 6% gradient SDS-PAGE was used, which is frequently used for the separation of the giant protein titin. Titin T1 (MW: ~3000 kDa), titin T2 (MW: ~2000 kDa) and nebulin (MW: ~800 kDa) from rabbit skeletal muscle were applied as positive controls to check for efficient separation, and as size markers. For 2-DE, in addition to conventional isoelectric focusing (IEF) 2-DE, radical-free and highly reducing (RFHR) 2-DE was also used for the separation of chromosomal proteins covering a wide range of isoelectric points. RFHR 2-DE provides excellent separation of highly basic proteins. The detailed procedures involved in IEF and RFHR 2-DE are described in our previous paper. Proteins separated by 1-D SDS-PAGE were stained with Coomassie Brilliant Blue (CBB) and then quantified using ImageQuant (GE Healthcare). In addition, quantitative information on proteins with a molecular weight lower than approximately 100 kDa was mainly obtained from 2-DE analysis. Proteins separated by 2-DE were analyzed with ImageMaster 2-D Elite (GE Healthcare). The amount of each protein was determined as a ratio of the amount of core histone H4, which was well separated from the other core histones. The molar ratio of each protein in relation to histone H4 was calculated from the results obtained with the smallest possible starting amounts of protein, in order to avoid artifactual underestimation resulting from stain saturation of the bands or spots in 1-D SDS-PAGE or 2-DE, respectively. Thus, in these conditions, the amount of protein has a linear relationship with the intensity of the corresponding band or spot. The relative amount of each protein was determined by averaging more than six 2-DE results obtained under the same conditions. In the case that several proteins were identified from a single band, the band intensity was divided by the averaged molecular weight of the identified proteins, which provided a summation of the relative molar ratio of the identified proteins.

13.2.4 Protein Identification by Mass Spectrometry

First, pieces of the gel containing proteins of interest were excised for digestion with trypsin, lysylendopeptidase (Lys-C) or endoproteinase (Glu-C) using the following procedures. Gel pieces obtained from 1-DE or 2-DE were destained by incubation in 1 mL of 50 m*M* ammonium bicarbonate in 50% methanol. For reductive alkylation, gels dehydrated with 100% acetonitrile (AcN) for 10 min at room temperature were incubated for 30 min at 56°C in 25 μL of 100 m*M* dithiothreitol (DTT) in 100 m*M* ammonium bicarbonate, followed by replacement of DTT solution with 25 μL of 100 m*M* iodoacetamide in 100 m*M* ammonium bicarbonate, and incubation for 30 min at 37°C in the dark. Gel pieces were then dehydrated in 100% AcN and dried for 30 min in a SpeedVac. Dried pieces were rehydrated for 45 min at 4°C in 5 to 30 μL of a solution of 50 m*M* ammonium bicarbonate containing 2 to 3 pmol of trypsin, Lys-C or Glu-C. After incubation for 16 h at 37°C, peptides were eluted with 20 μL of 0.1% TFA in 50% AcN for 10 min at room temperature with sonication. The second and third elutions of the

peptides were performed under the same conditions. The first, second and third TFA solutions were mixed together, followed by reduction of the volume to 5 μL using the SpeedVac. Desalting of the peptides was performed with a Ziptip C18. After equilibration with 0.1% TFA, peptides were adsorbed to the Ziptip C18, followed by washing with 0.1% TFA and elution with 5 μL of 50% AcN containing 0.1% TFA.

Protein identification was subsequently carried out by mass spectrometry (MS) measurement combined with a database search. For identification using the peptide mass fingerprinting (PMF) method, 1-μL aliquots were deposited on an Anchor Chip 384-well target plate followed by deposition of 1 μL of matrix (10 mg/mL a-cyano-4-hydroxycinaamic acid in 50% AcN, 0.1% TFA). The drops were then air-dried. The identification of each protein after the enzymatic digestions was carried out by PMF analysis using a matrix-assisted laser desorption ionization/time of flight mass spectrometer (MALDI-TOF MS), Autoflex (Bruker Daltonics, Bremen, Germany) or Ultraflex (Bruker Daltonics) and by tandem MS analysis using MALDI-TOF/TOF, Ultraflex. In addition, Esquire ESI MS/MS (Bruker Daltonics) or micrOTOF-Q (Bruker Daltonics), both equipped with liquid chromatography (LC) apparatuses (Dionex, Sunnyvale, CA, U.S.A.), were employed for protein identification. Mass data extracted by the flex analysis for MALDI-TOF/TOF or by the Hystar 2.3 for ESI MS/MS were analyzed using Biotools 2.2 employing the MASCOT search engine. Most proteins were identified by matching the PMF results against an NCBInr database. Identification was considered positive when high scores were obtained from both trypsin and Lys-C or Glu-C endopeptidase digestions. In some cases, three to four proteins could be identified by PMF analysis of a single band. Several peptide peaks observed in MALDI-TOF MS were further analyzed by MALDI-TOF/TOF MS/MS for identification and/or confirmation of proteins.

13.3 COMPARATIVE PROTEOME ANALYSIS OF HUMAN CHROMOSOMES

13.3.1 Proteins Identified from Three Different Isolation Methods

1-D SDS-PAGE of PA chromosomes (Figure 13.4) revealed numerous protein bands spanning a broad MW range in addition to reasonably intense bands of the most abundant proteins, core and linker histones, while that of PG chromosomes revealed a lower number of proteins (Figure 13.5). The percentage by weight of histones in the total chromosomal protein is estimated at 60%, of which 48% and 12% correspond to the core and linker histones, respectively. RFHR 2-DE results for PA, SG and PG chromosomal proteins have also been provided in Figure 13.6. PA chromosomes had a larger number of proteins than the SG or PG chromosomes, especially in the weakly basic regions that are indicated by dashed circles in Figure 13.6. Over 200 and 150 spots were reproducibly detected for PA and SG chromosomes, respectively, while PG chromosomes gave approximately 120 spots. Most of the intense bands or spots observed after electrophoresis have been unambiguously

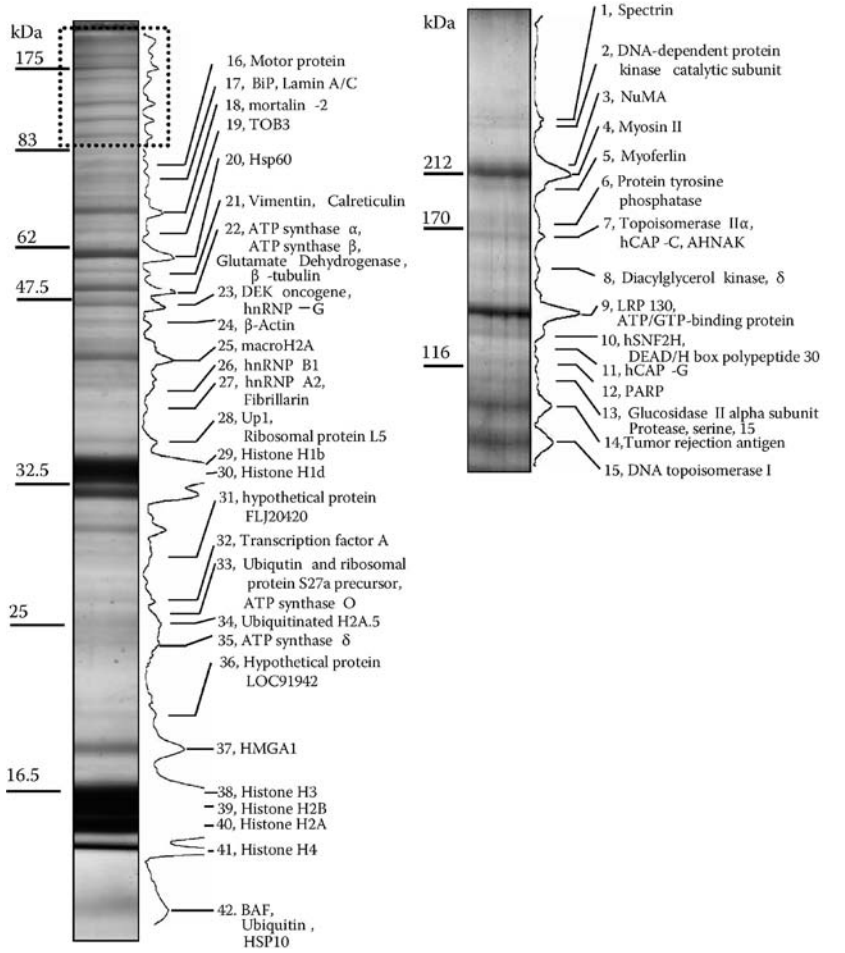

FIGURE 13.4 Detection of the proteins of PA chromosomes. A small gel image shows the protein distribution at high MW regions indicated by the broken lines at the top of the large gel image. (From Uchiyama et al. [22]. With permission.)

identified. Of the PA and SG chromosomes, 209 proteins were identified, of which only 51 proteins overlapped in 1-D SDS-PAGE and the two types of 2-DEs. Thus, 158 proteins were identified among the PA and SG chromosomes [22]. Generally, their amounts estimated from 1-D SDS-PAGE were similar to those obtained from 2-DE. As for 1-D SDS-PAGE and RFHR of PG chromosomes, 107 major proteins involved in the detected bands or spots were identified.

Proteome analysis of the metaphase chromosomes at the higher MW region were also carried out (Figure 13.7). The proteins identified in the >100-kDa region included cytoskeletal proteins (myosin, myoferlin and plectin), chromatin-remodeling proteins (SPT16 and SNF2h) and well-known chromosome proteins

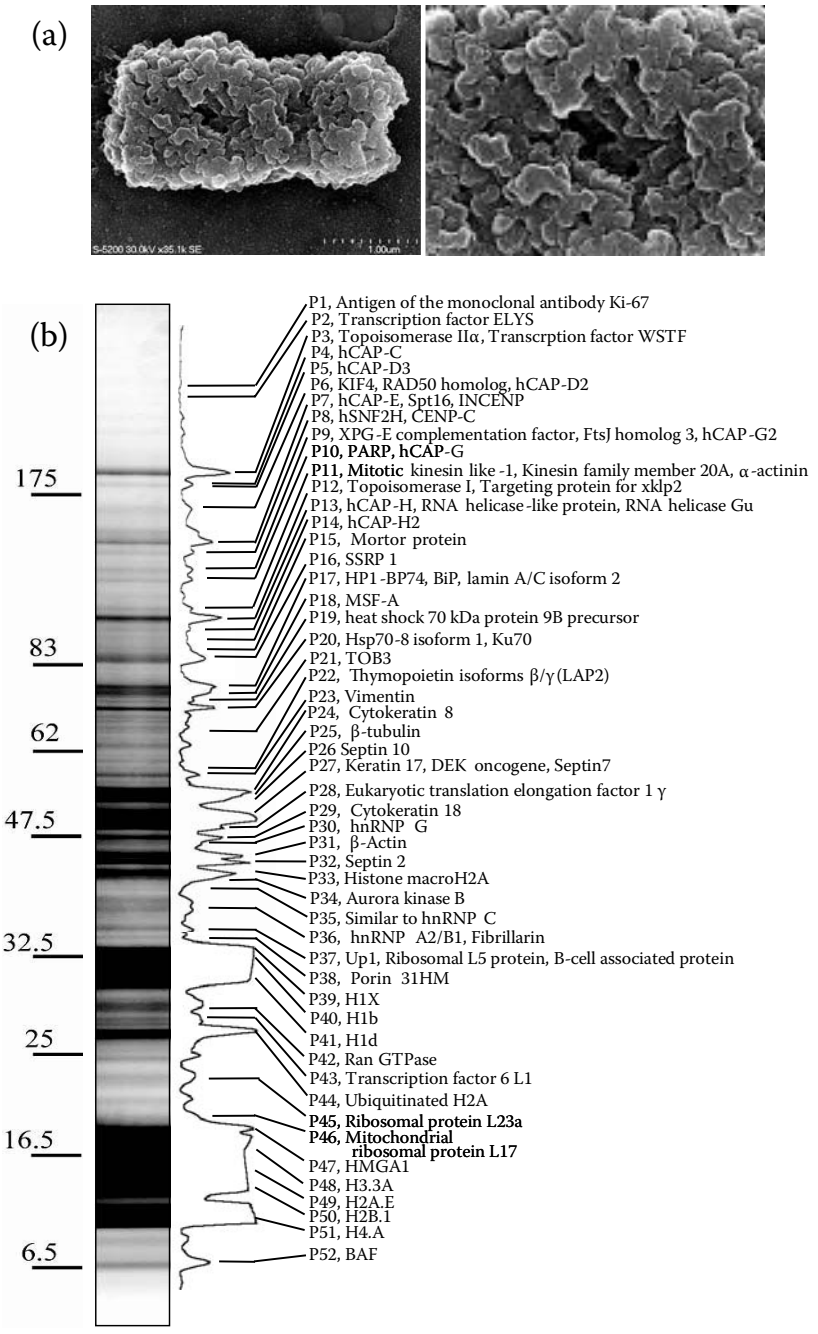

FIGURE 13.5 (a) A SEM image of PG chromosome. (b) Detection of the proteins of PG chromosomes by 1-D SDS-PAGE. (From Uchiyama et al. [22]. With permission.)

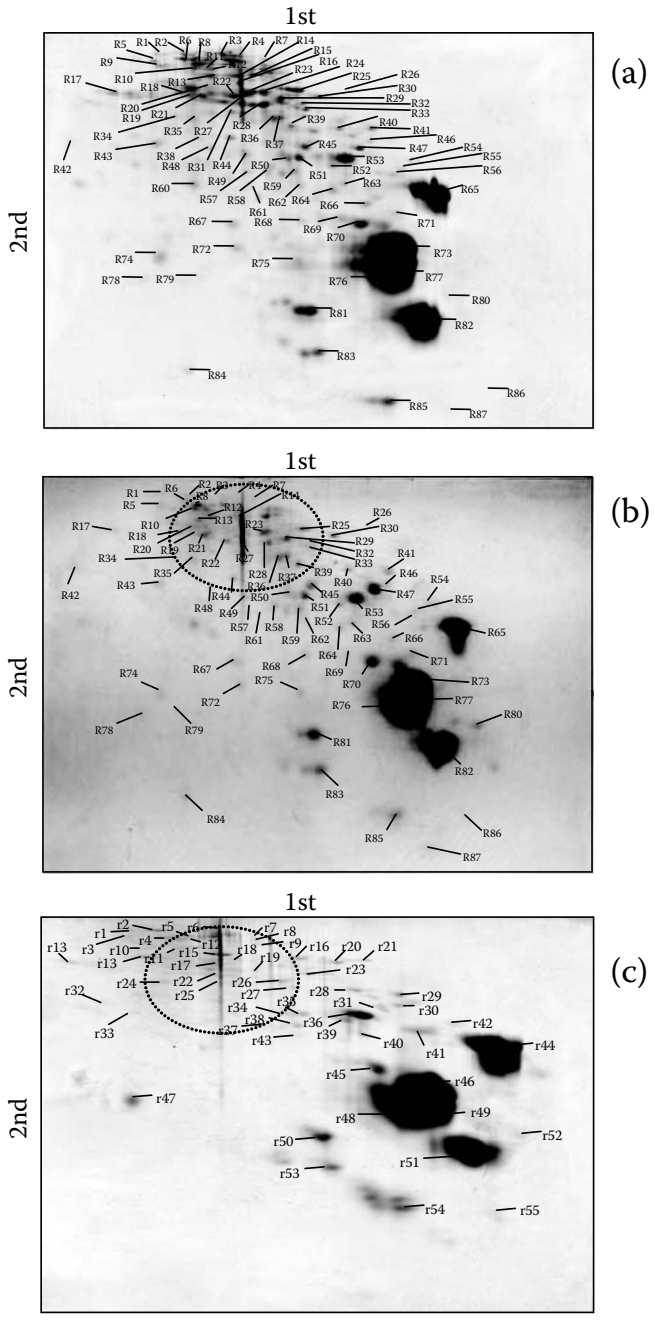

FIGURE 13.6 Comparison of protein constituents among PA, SG and PG chromosomes by RFHR 2-DE. (a) PA chromosomes, (b) SG chromosomes and (c) PG chromosomes. (From Uchiyama et al. [22]. With permission.)

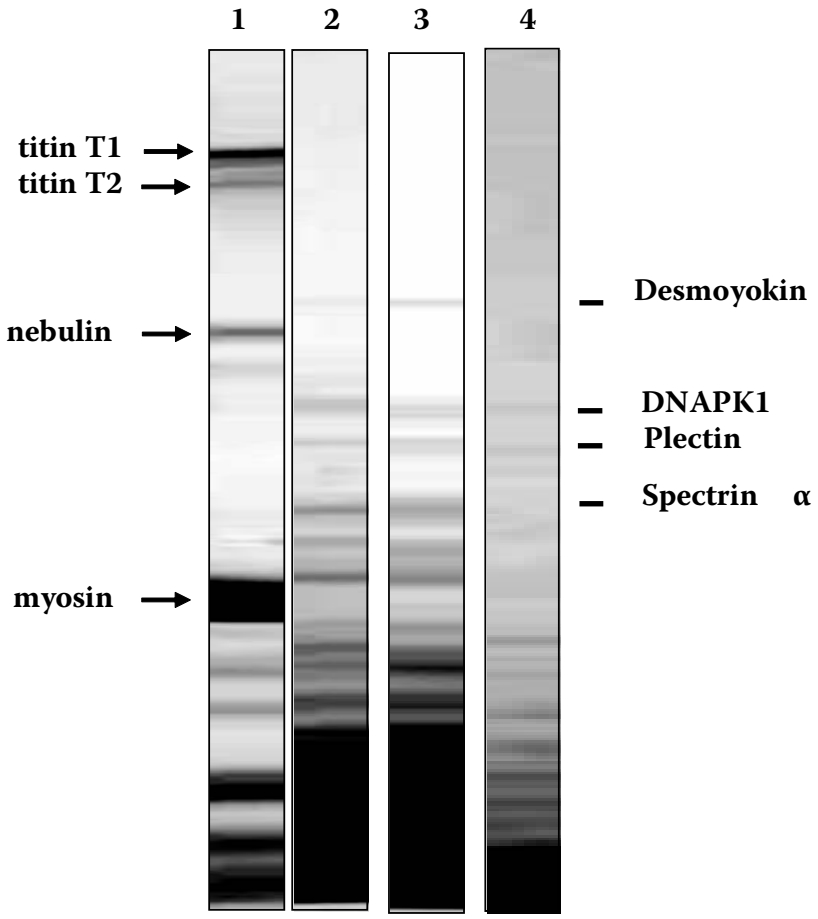

FIGURE 13.7 Identification of ultrahigh MW proteins using 2 to 6% gradient SDS-PAGE. Lane 1: rabbit skeletal muscle proteins used as MW markers [titin T1 (~3000 kDa), titin T2 (~2000 kDa), nebulin (~800 kDa) and myosin heavy chain (~220 kDa)] and confirmed by in-gel digestion followed by mass spectrometry; lane 2: HeLa cell extract; lane 3: HeLa S3 extract; lane 4: proteins extracted from HeLa PA chromosomes. Proteins were detected with CBB staining and the names of the identified proteins are shown. Desmoyokin is only identified in the cell extract. (From Takata et al. [23]. With permission.)

(topoisomerase II and SMC proteins). Furthermore, the involvement of titin (MW: 3300 to 3700 kDa; also called connectin), which had been considered to be one of the chromosomal proteins giving the chromosomes elasticity, was thoroughly examined. None of the current analyses, i.e., MS after electrophoretic separation, Western blotting or immunostaining using different antibodies, or titin microarray analyses, proved the presence of titin in isolated chromosomes or in HeLa cells. Overall, our results indicate that in the MW >3000 kDa, titin does not exist

in the chromosomes at levels high enough to be detected [23]. Thus our work supports a model in which the elastic nature of chromosomes is not generated from a scaffold composed of full-size titin molecules, but rather from other factors, such as a cross-linking network of chromatin.

13.3.2 Proteins Identified from Two Different Cell Lines

In order to distinguish common chromosomal proteins from cell line-specific chromosomal proteins, comparative proteomic analysis between PA chromosomes isolated from HeLa S3 cells and BALL-1 cells was carried out [23]. As a result, we could eliminate contaminating proteins and narrow down the chromosomal proteins by quantitative comparison of the identified proteins between the two cell lines. Most of the identified chromosomal proteins possessed features of the particular type of human cell line, while the mechanism for chromosome formation should be common to both cell lines. Several proteins present in large amounts were identified in the PA chromosomes from both cell lines. In addition, proteins commonly present in similar amounts are thought to contribute to chromosome structure.

Figure 13.8 shows the pI and MW distributions of the identified proteins. In addition to proteins identified in HeLa PA chromosomes, those previously identified in BALL PA and PG chromosomes are also shown. The identified proteins were distributed in the acidic ($4 < pI < 6$) and basic ($9 < pI < 12$) regions, and were especially concentrated in the basic and low MW (<30-kDa) region. In contrast, there were only a few neutral ($6 < pI < 8$) proteins. The distribution patterns of the identified proteins were similar between the BALL PA and HeLa PA chromosomes.

Histone variants and post-translationally modified histones were included in the identified histones. Among the cytoskeletal proteins, only β-actin (MW: 40 kDa) and vimentin (MW: 50 kDa) were identified in PA chromosomes from both cell lines. β-actin was previously reported to have a nuclear localization, and the actin network is required for chromosome congression in animal oocytes. In mitotic HeLa cells, vimentin was associated closely with the mitotic spindle. In addition, vimentin and tubulin were identified in Chinese hamster metaphase chromosomes isolated under physiological conditions.

The proteins which vary in quantity between HeLa PA chromosomes and BALL PA chromosomes are generally weakly bound to chromosomes. Considering that the chromosome morphologies of PA chromosomes between epithelial-like cells and lymphoma-type cells were indistinguishable, even under electron microscopy [23], these results indicate that PA chromosomes include proteins that are not essential for the maintenance of chromosome morphology. Keratins and septins were identified only in HeLa PA chromosomes. These results are consistent with a previous report stating that expression of these molecules was limited to specific tissues. Some of the mitochondrial and cytoplasmic proteins were identified in PA chromosomes from only one of the two cell lines.

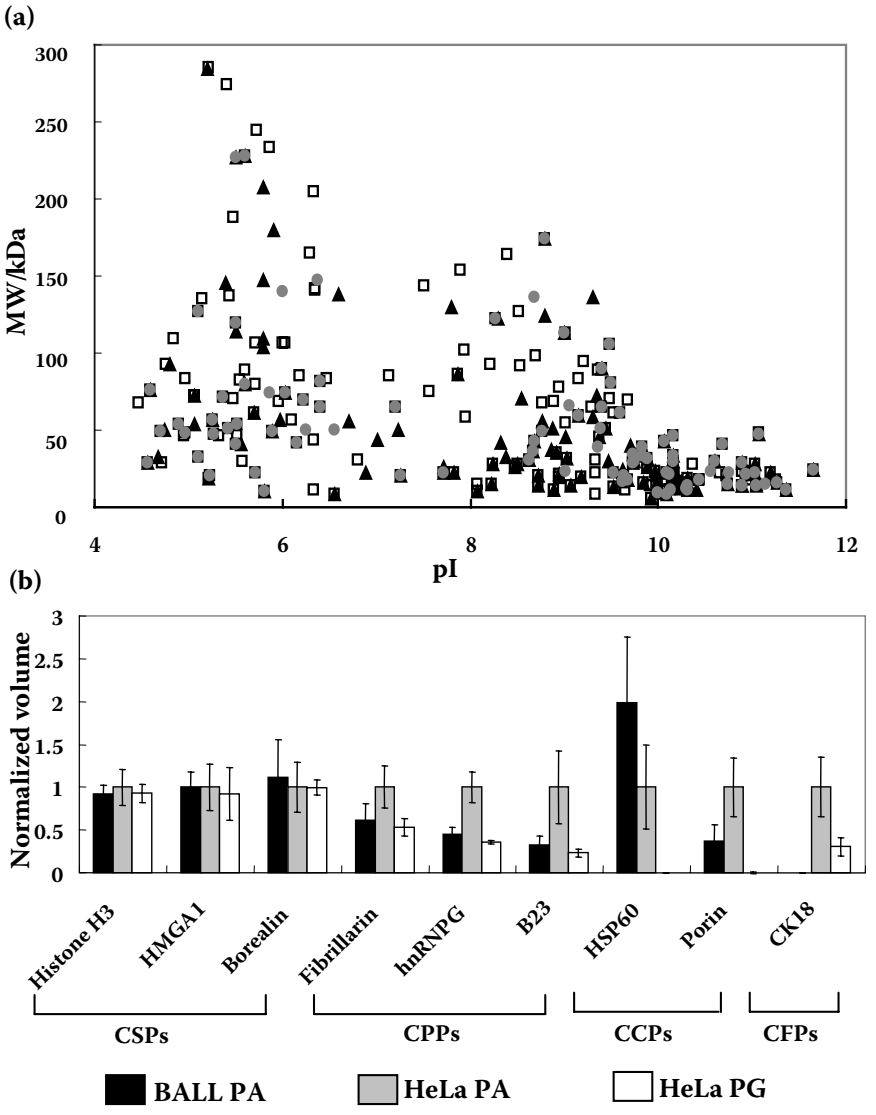

FIGURE 13.8 Quantitative analysis of the identified proteins. (a) MW vs. pI plot of the identified chromosome proteins (MW < 300 kDa). Triangles: proteins identified in BALL PA chromosomes (BALL PA); blank squares: proteins identified in HeLa PA chromosomes (HeLa PA); white circles: proteins identified in HeLa PG chromosomes (HeLa PG). (b) Protein volumes were obtained using image analysis software, and compared among BALL PA chromosomes, HeLa PA chromosomes and HeLa PG chromosomes. In this diagram, the protein volumes for BALL PA chromosomes and HeLa PG chromosomes were normalized against the protein volumes for HeLa PA chromosomes. (From Takata et al. [23]. With permission.)

13.4 THE FOUR-LAYER MODEL, A PROTEIN FRAMEWORK OF HUMAN CHROMOSOMES

13.4.1 Localization of the Chromosomal Proteins

The localization on the chromosomes of representative proteins identified in this study was visualized by indirect immunostaining under three different cytological conditions in chromosome preparations. The three cytological conditions of suspension chromosomes (Figure 13.9), chromosomes in cells and ordinary spread chromosome specimens would reflect isolated chromosomes, *in vivo* chromosomes and the cytological control, respectively. Some proteins were detected around isolated chromosomes and the cytological control but on *in vivo* chromosomes, in the current conditions. This group included BiP. The remaining proteins were all localized on the chromosomes prepared under the three different conditions. They were divided into two obviously different types. Ki-67 was visualized at the peripheral regions of two chromatids of all three types of chromosomes, and heteronuclear ribonucleoprotein (hnRNP) A2/B1 showed a similar distribution pattern. Histone H1 and hSNF2H exhibited a rather uniform localization on all the chromosomes, while hCAP-G displayed axial localization at the "mid-ribs" of both chromatids. β-actin was distributed unevenly on chromosomes, with speckled intense signals at the periphery. Based on the available information, mitochondrial and cytoplasmic proteins were all classified as one type of protein that was not localized on *in vivo* chromosomes and had low affinity for isolated chromosomes.

13.4.2 Chromosomal Proteins Are Classified into Four Groups

To better define the protein constitution of metaphase chromosomes, the identified proteins were individually compared based on the following four criteria: protein behavior during SDGC and PDGC, conservation across the two different cell lines, localization of each protein on metaphase chromosomes and information on functional and biochemical properties. Based on the present results, all the identified chromosomal proteins were newly classified into the following four groups [22,23]: (1) chromosome-coating proteins (CCPs), (2) chromosome peripheral proteins (CPPs), (3) chromosome structural proteins (CSPs) and (4) chromosome fibrous proteins (CFPs) (Table 13.1).

CCPs are proteins whose amounts decreased markedly in SG chromosomes or were low in PG chromosomes. They are mainly mitochondrial and cytoplasmic proteins found in small amounts (6.4%) but in a significant number (49.7%, 79/159) in the case of PA chromosomes. Mitochondrial proteins with basic pI appear to be nonspecifically and weakly bound to chromosome surfaces during the chromosome isolation process. The identified cytoplasmic proteins, including endoplasmic reticulum proteins, are mainly acidic. The acidic proteins in PA chromosomes are likely to interact with the basic histones in the chromosome suspension. It appears that these proteins are not part of the chromosomes in living cells, where the subcellular

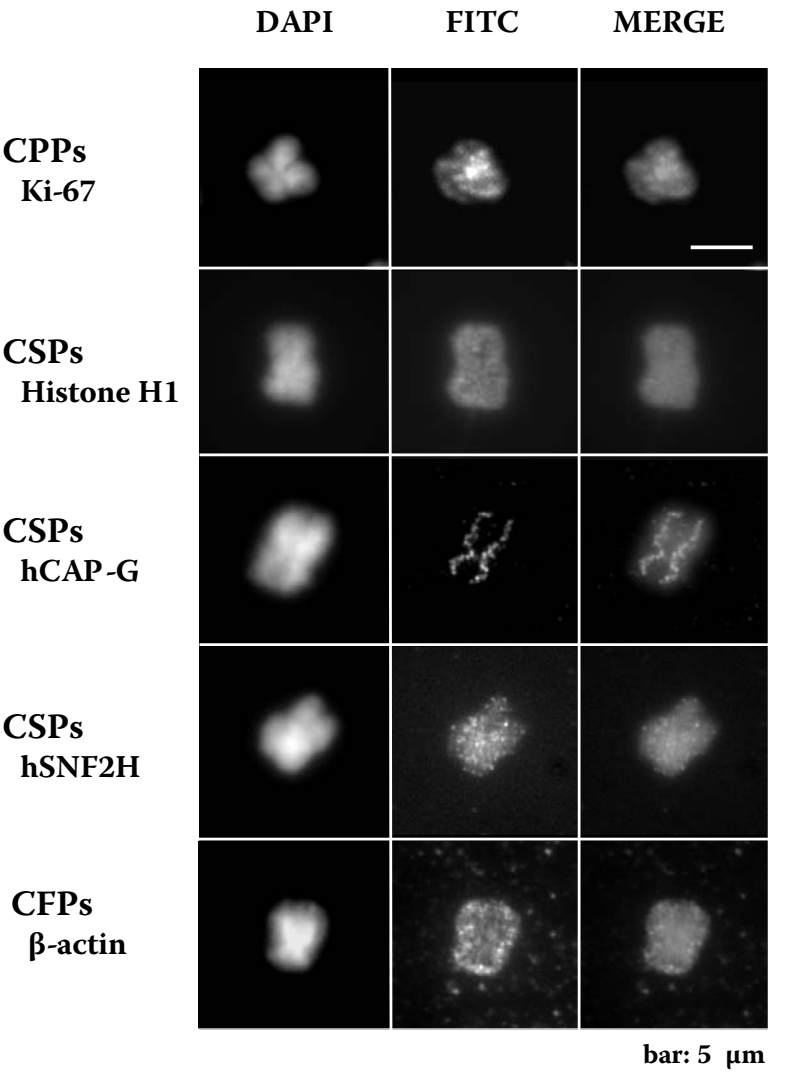

FIGURE 13.9 (**See color insert following page 110**) Indirect immunofluorescence microscopy of identified proteins. Staining patterns of isolated chromosomes are indicated. (left) DAPI staining, (middle) FITC and (right) merged. CPPs (chromosome peripheral proteins), CSPs (chromosome structural proteins), and CFPs (chromosome fibrous proteins) are the new classifications of chromosomal proteins introduced in this study. [22]

organelles are maintained in their intact forms. The detergent used in the chromosome isolation causes the release of organelle proteins, thereby leading to their nonspecific binding to the surface of isolated chromosomes. However, recently we reported chromosome localization of an endoplasmic reticulum protein, calreticulin; thus further investigation needs to be carried out [24].

TABLE 13.1
A Sample of Chromosome Proteins Identified from the Current Proteome Analysis

Protein	pI	Ms	New classification
130kDa leucine-rich protein (LRP130)	5.4	145109	CCPs
Heat shock 70kD protein 9B (mortalin-2)	6.0	73682	CCPs
Chaperonin 60, Hsp60	5.7	61016	CCPs
DNA dependent protein kinase	6.9	465266	CPPs
Nucleolin	4.59	76298	CPPs
Heterogeneous nuclear ribonucleoprotein H1 (hnRNP H1)	5.9	49198	CPPs
RNA binding motif protein, X chromosome (hnRNP G)	10.1	42306	CPPs
Fibrillarin	10.2	33407	CPPs
Ribosomal protein S6	10.9	28614	CPPs
Nucleophosmin/B23.2	4.56	28383	CPPs
Ran GTPase	7.0	24423	CPPs
Barier to autointegration factor 1	5.8	10052	CPPs
DNA Topoisomerase II α	8.8	174286	CSPs
Chromosome associated protein C (hCAP-C)	6.6	137978	CSPs
KIF4	6.0	139893	CSPs
hCAP-E	8.7	135696	CSPs
MTB protein (hCAP-G2)	6.4	130876	CSPs
Xeroderma pigmentosum group E complementation factor	5.1	126831	CSPs
hSNF2H	8.3	121828	CSPs
Poly(ADP-ribose) polymerase	9.0	113011	CSPs
INCENP	9.5	105500	CSPs
DNA topoisomerase I	9.4	90222	CSPs
KIAA0074 (hCAP-H)	4.9	82483	CSPs
SSRP1	6.4	81024	CSPs
Targeting protein for xklp2 (TPX2)	9.5	80939	CFPs
MacroH2A	9.8	39159	CSPs
HP1Hs-α	5.71	22080	CSPs
Histone H1 b	11.0	21852	CSPs
Histone H1 d	10.9	21352	CSPs
HP1 γ	5.23	20798	CSPs
H4 histone family, member A	11.7	11360	CSPs
HMGA1	10.3	10673	CSPs
Mitotic kinesin like-1	9.0	98044	CFPs
β-actin	5.5	40978	CFPs

Ms: Molecular mass of identified proteins. CCPs: chromosome coating proteins; CPPs: chromosome peripheral proteins; CSPs: chromosome structural proteins; CFPs: chromosome fibrous proteins (From Uchiyama et al. [22]. With permission.)

Proteins classified as CPPs were mainly nucleolar and nuclear envelope-related proteins. They were partly removed by SDGC. However, most of the CPPs that were identified in PA and SG chromosomes with significant amounts were also identified in PG chromosomes, thus indicating that they are essential proteins for metaphase chromosomes. Proteins in this group are the second-most frequently identified (28%) in PG chromosomes. From the beginning of chromosome research, the existence of the chromosome peripheral proteins was visually detected and was referred to as the "chromosome matrix" or "chromosome sheath" [25]. In the mitotic prometaphase, the nucleolus disappears after the breakdown of the nuclear

envelope. The existence of fibrillarin at the chromosome periphery has already been reported [26,27]. Other nucleolar proteins, such as hnRNPs, have also been detected. Proteins related to nucleolar formation, ribosome biogenesis, mRNA turnover and nuclear envelope formation may localize to the chromosome peripheral region during mitosis and function at the end of telophase and at the onset of interphase. Fibrillarin, hnRNPs, BAF, lamin A/C, Ki-67 and DNAPKcs are examples of CPPs. CPPs identified in PG chromosomes included proteins for telomere composition. Although hnRNP-A2/B1 is a component of the telomere complex and Ku70 is involved in telomere maintenance, their localization in metaphase is not only at the telomeric region but also includes the entire peripheral region of metaphase chromosomes. This fact points to an interesting dynamic feature of telomeric proteins in action. Presumably they are pooled at the peripheral region as CPPs and function at the telomeric region of metaphase chromosomes. Some ribosomal proteins were still found in SG and PG chromosomes, indicating the existence of certain ribosomal proteins that are different from the usual ribosomal proteins classified as CCPs. This view is supported by reports in which a ribosomal protein, S1, is localized to the chromosome peripheral region and a ribosomal protein, S6, is a component of RNP complexes.

Since CSPs form the body of chromosomes and play a role in the condensation/decondensation of chromosomes, they should be common to PA, SG and PG chromosomes. More than half (57.5%, 27/47) of the identified nuclear (N) proteins from PA chromosomes belonged to this group and CSPs comprised over 80% of the PA chromosomal proteins. CSPs were most frequently (40.2%) identified from PG chromosomes among the three chromosomes analyzed. Naturally, core and linker histones were identified; a histone variant, macro H2A, and a post-translationally modified histone (ubiquitinated H2A) were also identified in all three types of isolated chromosomes. HMGN2 and HMGA1 were the second and third most abundant proteins, respectively. These results suggest an important structural role of these particular HMG proteins, which is further supported by their high affinity for the chromatin fiber, when compared with other HMGs, such as, for instance, HMGB. Poly(ADP-ribosyl) polymerase (PARP) [28], hSNF2H and the DEK oncogene protein were identified. INCENP, Aurora B and borealin identified from PG chromosomes are known as chromosome passenger proteins and are localized to the centromeric region at metaphase. Localization of PARP on the centromere, neocentromere and chromosome arm has already been reported [27]. One of the features emerging from analyses using the three types of chromosomes was that not all the components of the centromere/kinetocore and telomere regions of the chromosome were detected, although several proteins that concentrate at the centromeric region during mitosis, such as chromosome passenger proteins and heterochromatin protein 1γ, were identified. Centromere protein C (CENP-C) was the only protein identified sporadically in this study among CENP proteins. These facts suggest that centromere/kinetocore and telomere proteins are present only in small amounts compared to the overall chromosomal proteins. In fact, the quantitative purification of CENP-A and TRF1 (telomeric repeat binding factor 1) from human cells revealed a markedly low molar ratio

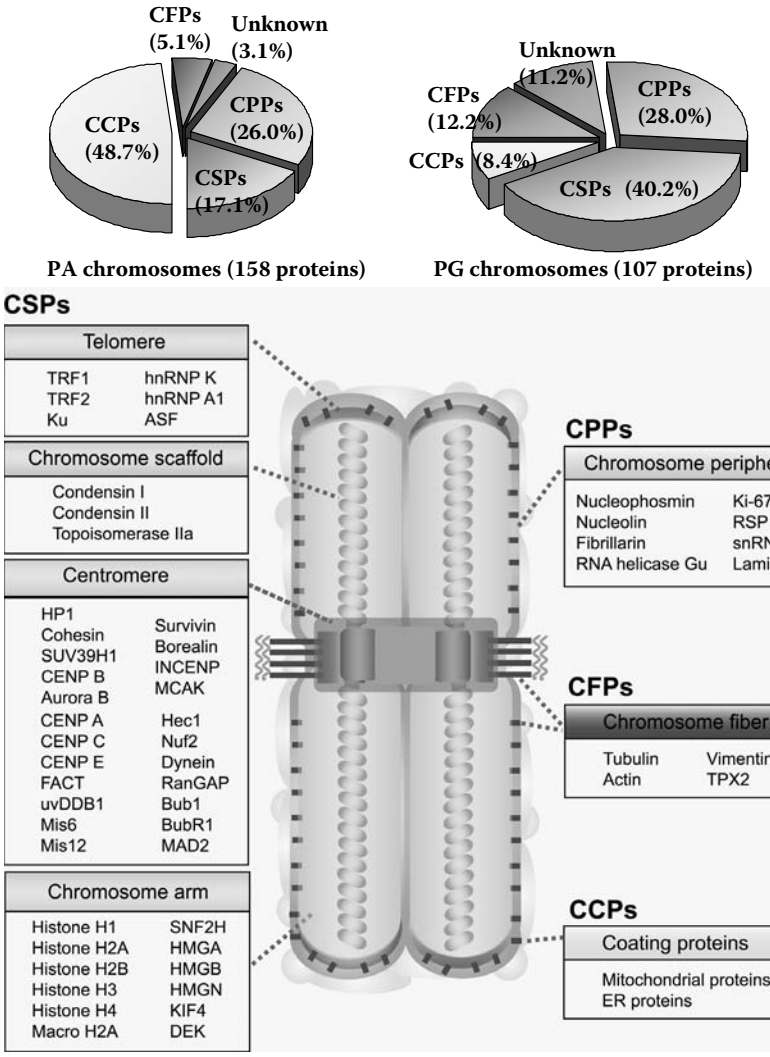

FIGURE 13.10 (**See color insert following page 110**) Upper panels show percentages of proteins classified into the four groups. They are based on the number of identified proteins for PA chromosomes (left) and PG chromosomes (right). Lower panel shows a schematic representation of the metaphase chromosome from the constituent protein perspective. The representative proteins from our studies and those previously reported are indicated in each group and are depicted on the corresponding chromosomal regions. Some proteins which have not been identified in our proteome analysis are the proteins with low amounts, although their functions on the chromosomes have already been reported in the previous studies. (From Uchiyama et al. [22] and Takata et al. [23]. With permission.)

of approximately 1/70,000 and 1/100,000, respectively, relative to histone H4 [29,30]. All eight subunits of the condensin I and II complexes were identified from PG chromosomes [31,32]. Assuming that one nucleosome is present in every 200 bp of DNA, the molar ratio of hCAP-C (138 kDa) to 100 molecules of histone H4 (11 kDa) based on their band intensities is 0.32 at the most, which means that they bind to chromatin fiber every 33 kbp on average.

CFPs were classified primarily as an independent group because they are fibrous in nature and their levels were not different between PA and SG chromosomes. Mitotic kinesin-like protein, which interacts with the mitotic spindle, was also classified into this group. The contribution of CFPs to chromosome structure is still ambiguous. Myosin II, tubulin and actin have been shown to be involved in chromosome segregation during mitosis [33]. Furthermore, β-actin is one of the components of the chromatin remodeling SWI/SNF-like BAF complex [34]. When all these facts are considered together, it can be assumed that β-actin would be tightly bound to metaphase chromosomes and would play a definite role in their structural aspects.

13.4.3 Four-Layer Model

We proposed here a four-layer model of metaphase chromosomes, as shown in Figure 13.10. In this model, in addition to presently identified proteins, known chromosomal proteins are also classified into each of four groups. It is naturally accepted that chromatin fibers composed of DNA and core and linker histones are the basis of chromosomes. Relatively abundant proteins, such as HMGs, might partly contribute to the bending of chromatin fibers to form a higher-order structure. In addition, specially localized proteins constitute a special region of chromosomes, such that centromeric or telomeric proteins constitute the centromere or telomere of chromosomes, respectively. These proteins relating to chromosome structure are CSPs involving chromosome scaffold proteins, topoisomerase IIα and the condensin complex. However, recent RNAi and knockout experiments of condensin subunits show that chromosomes are condensed even in the absence of condensin protein, although their overall morphology is apparently collapsed, suggesting that condensin itself contributes to determining the shape of metaphase chromosomes rather than condensation of chromatin fibers that are relaxed during interphase. It has recently been understood that topoisomerase IIα is required not for the chromosome condensation, but for the segregation, though its specific localization to the axis of two chromatids is still enigmatic. CPPs surround chromosomes at the peripheral region to form the outer layer of chromosomes, though their involvement in chromosome structure has not yet been clarified. CPPs seem to be delivered on the surface of chromosomes to daughter cells. Failure of alignment of chromosomes during mitosis is observed following RNAi treatment of a CPP protein. CCPs form the outer layer only in isolated chromosomes, and not in chromosomes *in vivo*, thus so far it appears unlikely that they make a structural contribution to metaphase chromosomes. Mandeville and Rieder [35] have reported that metaphase chromosomes are surrounded by a "cage" of keratin filaments that

restrict the dispersion of chromosomes during the breakdown of the nuclear envelope or microtubule penetration between and through the chromosomes. Thus, the CFPs that maintain the spatial organization of chromosomes within a mitotic cell are also likely to be bound to chromosomes *in vivo.*

13.5 CONCLUSION

Well over a century after their discovery in 1842, the enigma of the higher-order structure of chromosomes remains. We present here a "four-layer model" of human metaphase chromosomes, the first comprehensive chromosome protein framework based on identification of more than 200 chromosomal proteins by proteome analysis of isolated human metaphase chromosomes using MS.

The model consists of four layers, each with different chromosomal protein sets, i.e., CCPs, CPPs, CSPs and CFPs. More than 200 identified proteins have been classified and assigned into the four layers, with each layer occupying a distinct region of the chromosome. CCPs are localized at the most outer regions of the chromosomes and they attach to these regions tentatively and occasionally. CCPs include mainly mitochondrial and cytoplasmic proteins, e.g., 70-kDa heat shock protein 9B, and Hsp60. CPPs are also localized at the peripheral regions of the chromosomes, but as an essential part of the chromosomes. CPPs include nucleolin, lamin A/C, fibrillarin, etc. CSPs are the main chromosomal structure proteins, and include topoisomerase IIα, condensin subunits and histones. CFPs have a fibrous nature; e.g., β-actin, vimentin, myosin II and tubulin. A data set of these proteins that we developed contains essential chromosomal proteins with classified information based on this four-layer model, and provides useful leads for further studies on chromosomal structure and function.

Our four-layer chromosome model consisting of four distinct sets of specific proteins is the first chromosome model explaining overall chromosomal structure based on its protein constituent materials. The model has no known inconsistency with the previous chromosomal models and presents fixed positions for all the chromosomal proteins so far identified, although the reported elasticity of chromosomes is rather difficult to explain by the presence of rigid 13S condensin complexes and topoisomerase IIα existing alternately at the chromosome scaffold. This may, on the other hand, mean that scaffold proteins might not be important to chromosome structure. Even if condensin complexes and topoisomerase IIα are present at a chromosomal axis as its scaffold, they may not play important roles in forming and maintaining chromosome higher-order structure. Moreover, to date over 30 proteins identified have been examined using the RNAi method, but the overall chromosome structures are still apparently constructed, although several chromosome behavioral aberrations are repeatedly observed. It is likely that the functional aspects rather than the structural aspects are more important for most of the chromosomal proteins. This view of chromosome higher-order structure is obtained based on detailed consideration of the structural aspects of over a hundred identified proteins, and should open a new path to the construction of a model for chromosome higher-order structure based on DNA itself.

ACKNOWLEDGMENTS

The authors thank Prof. Takefumi Sone (Institute of Microbial Diseases, Osaka University, Osaka, Japan) for his efforts in developing the proteome project at the initial stages. The authors also thank Prof. Wada (Osaka Medical University, Osaka, Japan) and Prof. Takao (Institute for Protein Research, Osaka University) for their technical support in RFHR gel electrophoresis and mass spectrometry, respectively. This study was supported by Special Coordination Funds of the Ministry of Education, Culture, Sports, Sciences and Technology (MEXT) of the Japanese government to K.F.

REFERENCES

1. Darwin C (1872) The *Origin of Species*, 6th ed. John Murray, London.
2. Fukui K, Uchiyama S (2007) Chromosome protein framework from proteome analysis of isolated human metaphase chromosomes. *Chem Rec* 7:230–237.
3. Kornberg R, Thomas JO (1974) Chromatin structure; oligomers of the histones. *Science* 184: 865–868.
4. Luger K et al. (1997) Crystal structure of the nucleosome core particle at 2.8 A resolution. *Nature* 389: 251–260.
5. Finch JT, Klug A (1976) Solenoidal model for superstructure in chromatin. *Proc Natl Acad Sci USA* 73: 1897–1901.
6. Woodcock CL et al. (1993) A chromatin folding model that incorporates linker variability generates fibers resembling the native structures. *Proc Natl Acad Sci USA* 90: 9021–9025.
7. Sun J, Schlick T (2005) Electrostatic mechanism of nucleosomal array folding revealed by computer simulation. *Proc Natl Acad Sci USA* 102: 8180.
8. Schalch T et al. (2005) X-ray structure of a tetranucleosome and its implications for the chromatin fibre. *Nature* 436: 138–141.
9. Marseden MP, Laemmli UK (1979) Metaphase chromosome structure: evidence for a radial loop model. *Cell* 17: 849–858.
10. Lewis C, Laemmli UK (1982) Higher order metaphase chromosome structure: evidence for metalloprotein interactions. *Cell* 29: 171–181.
11. Gasser S et al. (1986) Metaphase chromosome structure. Involvement of topoisomerase II. *J Mol Biol* 188: 613–629.
12. Pienta KJ, Getzenberg RH, Coffey DS (1991) Cell structure and DNA organization. *Crit Rev Eukaryotic Gene Exp* 1: 355–385.
13. Dupraw EJ (1970) *DNA and Chromosomes*. Holt, Rinehart and Winston, Inc., New York: 154.
14. Maeshima K, Laemmli UK (2003) A two-step scaffolding model for mitotic chromosome assembly. *Dev Cell* 4: 467–480.
15. Kireeva N et al. (2004) Visualization of early chromosome condensation: a hierarchical folding, axial glue model of chromosome structure. *J Cell Biol* 166: 775–785.
16. Christensen M et al. (2002) Dynamics of human DNA topoisomerases IIalpha and IIβ in living cells. *J Cell Biol* 157: 31–44.
17. Tavormina P et al. (2002) Rapid exchange of mammalian topoisomerase II α at kinetochores and chromosome arms in mitosis. *J Cell Biol* 158: 23–29.

18. Poirier M, Marko J (2002) Mitotic chromosomes are chromatin networks without a mechanically contiguous protein scaffold. *Proc Natl Acad Sci USA* 99: 15393–15397.
19. Pope LH, Xiong C, Marko JF (2006) Proteolysis of mitotic chromosomes induces gradual and anisotropic decondensation correlated with a reduction of elastic modulus and structural sensitivity to rarely cutting restriction enzymes. *Mol Biol Cell* 17: 104–113
20. Sone T et al. (2002) Changes in chromosomal surface structure by different isolation conditions. *Arch Histol Cytol* 65: 445–455.
21. Uchiyama S et al. (2004) Protein composition of human metaphase chromosomes analyzed by two-dimensional electrophoreses. *Cytogenet Genome Res* 107: 49–54.
22. Uchiyama S et al. (2005) Proteome analysis of human metaphase chromosomes. *J Biol Chem* 280: 16994–17004.
23. Takata H et al. (2007) A comparative proteome analysis of human metaphase chromosomes isolated from two different cell lines reveals a set of conserved chromosome-associated proteins. *Genes Cells* 12: 269–284.
24. Kobayashi S et al. (2006) Calreticulin as a new histone binding protein in mitotic chromosomes. *Cytogenet Genome Res* 115*:* 10–15.
25. Sharp L (1929) Structure of large somatic chromosomes. *Bot Gaz* 88: 349.
26. Sumner A (2003) *Chromosome, Organization and Function*. Blackwell Science, Oxford: 5–142.
27. Hernandez-Verdun D, Gautier T (1994) The chromosome periphery during mitosis. *Bioessays* 16: 179–185.
28. Earle E et al. (2000) Poly(ADP-ribose) polymerase at active centromeres and neocentromeres at metaphase. *Hum Mol Genet* 22: 187–194.
29. Martinez A et al. (1998) Isolation and comparison of natural and recombinant human CENP-A autoantigen. *J Autoimmunity* 11: 611–619.
30. Chong L et al. (1995) A human telomeric protein. *Science* 270: 1663–1667.
31. Hirano T, Mitchison TJ (1994) A heterodimeric coiled-coil protein required for mitotic chromosome condensation in vitro. *Cell* 79: 449–458.
32. Ono T et al. (2003) Differential contributions of condensin I and condensin II to mitotic chromosome architecture in vertebrate cells. *Cell* 115: 109–121.
33. Scholey JM, Brust-Mascher I, Mogilner A (2003) Cell division. *Nature* 422: 746–752.
34. Zhao K, Wang W (1998) Rapid & phosphoinositol-dependent binding of the SWI/SNF-like BAF complex to chromatin after T lymphocyte receptor signaling. *Cell* 95: 625–636.
35. Mandeville EC, Rieder CL (1990) Keratin filaments restrict organelle migration into the forming spindle of newt pneumocytes. *Cell Motil Cytoskeleton* 15: 111–120.

14 Antipeptide Antibodies for Examining the Conformation and Molecular Assembly of an Intracellular Protein

*Masatoshi Nakagawa, Nobuko Ohmido, Katsumi Ishikawa, Susumu Uchiyama, Kiichi Fukui and Takachika Azuma**

CONTENTS

14.1 Introduction 190
14.2 Experimental Design 191
14.2.1 Preparation of Antigens 191
14.2.2 Mass Spectrometry 191
14.2.3 Preparation of Recombinant S6 Protein 191
14.2.4 Immunization and Ab Purification 192
14.2.5 ELISA 192
14.2.6 Immunostaining of S6 Protein in HeLa Cells 192
14.3 Results 193
14.3.1 Ag Preparation and Immunization 193
14.3.2 Preparation of rS6 Protein 193
14.3.3 Binding of Abs to rS6 195
14.3.4 Binding of Abs to S6 Protein in HeLa Cells 196
14.4 Discussion 196
14.5 Conclusion 199
Acknowledgments 200
References 200

*To whom correspondence should be addressed.

14.1 INTRODUCTION

Antibodies (Abs) have long been used for studying protein structure in solution because of their specificity in recognition of structure and conformation [1]. Abs recognize the antigenic determinant (epitope) that has structural complementarity to the Ab-combining site (paratope). Epitopes have been classified into two types: "linear or segmental" and "conformational or topographic" [2–6]. Linear epitopes are determined by their linear amino acid sequences, while conformational epitopes are related to the three-dimensional protein structure and are considered to be an assemblage of several amino acid segments. Abs prepared by immunization of animals with native proteins seem to largely recognize conformational epitopes and sometimes fail to react with denatured proteins or peptides [2]. These Abs, therefore, cannot be used for detection of proteins by Western blotting analysis after SDS-PAGE. On the other hand, Abs prepared by immunization with synthetic peptides are able to bind to both native and denatured proteins, and can be used for isolating and characterizing gene products.

Due to advances in the methodology of peptide synthesis, in addition to progress in the theoretical understanding of the immunochemistry of antigen (Ag)–Ab recognition [7], antipeptide Abs have been widely used for identification of proteins in cell extracts or living cells that contain corresponding peptide segments (see Chapters 7 and 16) [8]. Ab reactivity is considered to depend on two factors: the degree of epitope exposure on the protein surface and the secondary structure of the peptide segments in the target proteins. Although most peptides used as immunogens possess no obvious secondary structure, the rigid conformation of the corresponding segments in a folded protein was expected to affect Ab reactivity. However, Stanfield et al. [9] showed that the conformation of a peptide in complex with an antipeptide Ab was different from that in which the peptide was a portion of the intact protein, forming a type II β-turn in the former and an α-helix in the latter. It was also shown that antipeptide Abs were able to create combining sites for peptide accommodation by an induced fit mechanism [10]. Therefore, it is likely that the secondary structure of a peptide segment is less important in determining Ab reactivity than its degree of exposure on the surface. Peptide segments folded into the interior of a protein or buried in the protein interface would not be accessible to Abs. This suggests that the reactivity of an antipeptide Ab is a measure of the folding state of the recognized peptide sequence, in the case of purified protein, as well as of interactions with other macromolecules in the case of proteins present in cells.

In the present experiments, we prepared Abs by immunizing rabbits with synthetic peptides possessing amino acid sequences corresponding to human ribosomal S6 protein as a model, since this protein was detected as a component of chromosomal proteins in two-dimensional gel electrophoresis (see Chapter 13) [11]. S6 protein is a ribosome component that interacts with other ribosomal components, and its structure and assembly in *Thermus thermophilus* have been extensively investigated [12]. Since S6 is abundant in cells, the binding of Abs to this protein was expected to be easily visualized by immunostaining. First, we

compared the reactivity for the Abs between peptide and recombinant S6 protein (rS6) by the enzyme-linked immunosorbent assay (ELISA), in which peptide and rS6 were each coated onto plastic plates. This assay was expected to provide information on the extent of exposure of the peptide segments on the monomeric S6 protein. Next, we compared the reactivity of Abs with rS6 on plates, using ELISA, and S6 in HeLa cells by immunostaining and attempted to explain the observed differences in terms of accessibility of the epitopes.

14.2 EXPERIMENTAL DESIGN

14.2.1 Preparation of Antigens

Peptides were prepared corresponding to the following amino acid segments of S6 protein; Ser6-Asp20, Ile52-Gly66, Asp103-Gly117, Asn146-Lys160 and Arg178-Ile192. A Cys residue was added at the N or C terminus of these peptides for conjugation with carrier proteins. We used a solid phase Fmoc strategy for synthesizing the peptides. The synthesis was performed on NovaSyn-TGR resin (Novabiochem, Darmstadt, Germany) and the peptides were purified by high-performance liquid chromatography.

The synthetic peptides were conjugated to bovine serum albumin (BSA) using *m*-maleimidobenzoyl-*N*-hydroxysuccinimide ester (MBS; Pierce). MBS was first reacted with BSA at pH 8.5 (HEPES buffer containing 150 m*M* NaCl) for 2 h, followed by gel filtration with a PD-10 column equilibrated with HEPES buffer containing 1 m*M* EDTA. Peptides with a free Cys residue at either the N or C terminus were added to the MBS–BSA solution at a peptide-to-BSA ratio of 50:1, and reacted for 1 h. The unreacted peptides were removed on a PD-10 column.

14.2.2 Mass Spectrometry

Mass spectrometry (MS) analyses were performed by matrix-assisted laser desorption/ionization time-of-flight mass spectrometry (MALDI-TOF-MS) to identify the number of peptides conjugated to BSA. BSA and peptide-conjugated BSA were dissolved in water and mixed with matrix solution (2:1 (v/v) mixture of 0.1% trifluoroacetic acid/acetonitrile) saturated with sinapinic acid (Sigma) on respective sample plates, and then dried at room temperature. All MS experiments were carried out using a REFLEX III mass spectrometer (Bruker Daltonics) in the linear-positive ion mode. Sample ionization was performed by irradiation using a nitrogen laser with emission set at 337 nm.

14.2.3 Preparation of Recombinant S6 Protein

The S6 cDNA was prepared by reverse transcriptase PCR (RT-PCR) from mRNA of HeLa cells and cloned using the GATEWAY system (Invitrogen). The protein was expressed in *Escherichia coli* strain BL (DE3) (Stratagene). Cells were grown in LB medium containing 100 μg/mL ampicillin and induced with isopropyl-β-d(–)-thiogalactopyranoside at a final concentration of 0.1 m*M*. After

incubation at 4°C for 4 h, cells were harvested by centrifugation. The cell pellet was resuspended in the sonication buffer (20 m*M* Tris–HCl, pH 7.4, 130 m*M* NaCl, 1 m*M* PMSF) and cells were lysed by sonication. The precipitate was collected by centrifugation and dissolved in refolding buffer (20 m*M* Tris–HCl, pH 7.4, 130 m*M* NaCl, 8 *M* urea). This protein solution was dialyzed twice against a Ni column buffer (20 m*M* Na_2HPO_4, pH 7.4, 500 m*M* NaCl, 6 *M* urea) containing 50 m*M* imidazole, and applied to a Ni column. After washing, the target protein was eluted with Ni column buffer containing 500 m*M* imidazole. The urea-denatured purified protein was then folded by a stepwise dilution of urea concentration by dialysis against 20 m*M* Tris–HCl (pH 8.0), 1 m*M* EDTA solution containing respective concentrations of 4, 2, 1, and 0 *M* urea. The folded protein was purified using an anion exchange column, and the target protein was then concentrated and dialyzed against phosphate buffered saline (PBS).

14.2.4 Immunization and Ab Purification

Rabbits were purchased from Oriental Yeast Co., Ltd. (Japan). The peptide-BSA conjugates were emulsified with complete Freund's adjuvant and rabbits were immunized subcutaneously followed by booster immunizations on days 14, 28 and 56. They were bled at 9 weeks post-immunization. Anti-BSA Abs were removed by passing through a column of BSA-Sepharose, and flow-through fractions were used for further analysis.

14.2.5 ELISA

In order to estimate the amount of Ab capable of binding to the peptides or rS6 protein, microtiter plates were coated with either peptides or rS6 protein at 0.33 μ*M* (50 μL/well) at 4°C, followed by incubation with 5% skim milk (250 μL/well). Sera from the immunized rabbits were then applied to the plates, and IgG bound to Ags was detected using horseradish peroxidase-conjugated goat anti-rabbit IgG (MP Biomedicals, Inc.).

14.2.6 Immunostaining of S6 Protein in HeLa Cells

The immunostaining was carried out according to the procedure of Maeshima and Laemmli [13] with a small modification. HeLa S3 cells were grown on 18 × 18 mm poly-l-lysine-coated glass coverslips in RPMI1640 (Nacalai Tesque) supplemented with 10% fetal calf serum (Gibco BRL), 1% penicillin and streptomycin, at 37°C in a 5% CO_2 incubator for 3 days. After washing with PBS, the cells were incubated in 0.5 mg/mL $NaBH_2$ in XBE2 (10 m*M* HEPES, pH 7.6, 2 m*M* $MgCl_2$, 100 m*M* KCl, 5 m*M* EGTA) for 5 min. Permeabilization was carried out with 0.5% Triton X-100 in XBE2 at room temperature, and cells were then fixed with 2% paraformaldehyde/XBE2 for 15 min and incubated with 10 μg/μL of the purified antipeptide Abs (diluted 1:100 in XBE2 containing 1% BSA and 0.05% Tween 20) for 60 min. The bound antipeptide Abs were detected by FITC-

labeled goat anti-rabbit IgG Ab (Sigma) (1:200 in XBE2 containing 1% BSA and 0.05% Tween 20). The slides were embedded in Vectashield containing 1 μg/mL DAPI. Images were obtained using a fluorescence microscope, BX60 (Olympus), equipped with a sensitive cooled CCD camera (PXL 1400; Photometrics). The B- and UV-light excitation filters were used for excitation of FITC and DAPI, respectively. Captured images were digitally stored and analyzed using imaging software (Photoshop 7.0, Adobe).

14.3 RESULTS

14.3.1 Ag Preparation and Immunization

Table 14.1 shows the amino acid sequences of the peptides used in these experiments. Each peptide was coupled to BSA through a Cys residue introduced at either the N or C terminus for conjugation using MBS. The number of peptides conjugated to BSA was estimated by mass spectroscopy. Figure 14.1 shows a typical mass spectrum of a peptide-BSA conjugate (S6-4-BSA). This spectrum exhibits a single broad peak corresponding to a MW of 88 kDa, suggesting that approximately 13 peptides were BSA-conjugated.

The binding of antipeptide Abs to their respective peptides at various dilutions of antisera was examined by ELISA using peptide-coated plates and is shown in Figure 14.2. Each peptide-BSA conjugate provided a high Ab production except for S6-3. No significant difference was observed in Ab production between peptides conjugated through a Cys at the N vs. the C terminus (data not shown).

14.3.2 Preparation of rS6 Protein

The rS6 protein was prepared with a His-tag sequence at the N terminus for purification. The protein was recovered from transformed *E. coli* in the insoluble fraction and solubilized with 8 *M* urea. The purity of rS6 at each step of purification was examined by SDS-PAGE (Figure 14.3). Two bands with different MW are evident in the purified material. Since both components were capable of binding to the Ni column and the His-tag was attached to the N terminus of these proteins,

TABLE 14.1
Amino Acid Sequences of Synthesized Peptides and Location in Human S6 Protein

Peptide	Position	Amino Acid Sequence
S6-1	6–20	SFPATGCQKLIEVDD
S6-2	52–66	ISGGNDKQGFPMKQ
S6-3	103–117	DANLSVLNLVIVKKG
S6-4	146–160	NLSKEDDVRQYVVRK
S6-5	178–192	RLVTPRVLQHKRRRI

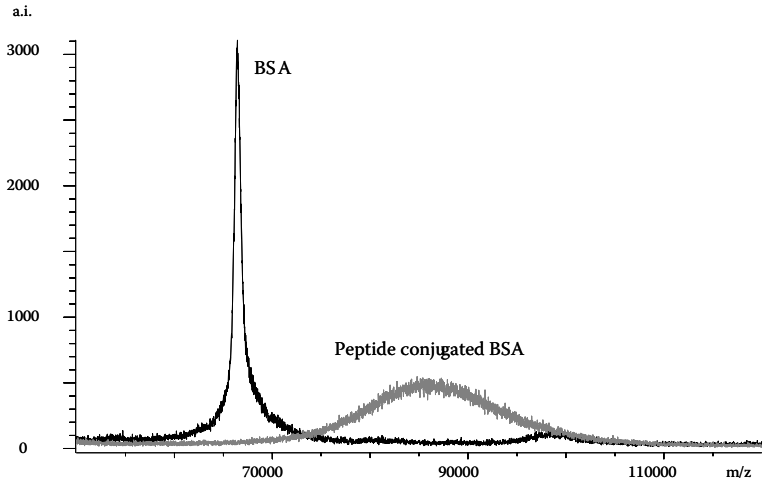

FIGURE 14.1 MALDI-TOF-MS spectra of BSA (black line) and S6-4-BSA conjugate (gray line). Absolute intensity (a.i.) was plotted against mass per charge (*m/z*).

it was considered that the molecular heterogeneity had not arisen from proteolysis at the N-terminal segment, and that either post-translational modification at the C terminus or digestion by proteases during preparation may have occurred. Post-translational modification has been shown in the S6 protein of *E. coli* [14]. Since no significant differences were observed in Ab reactivity with these components by Western blotting (data not shown), we used this mixture as the source of rS6 protein for further experiments.

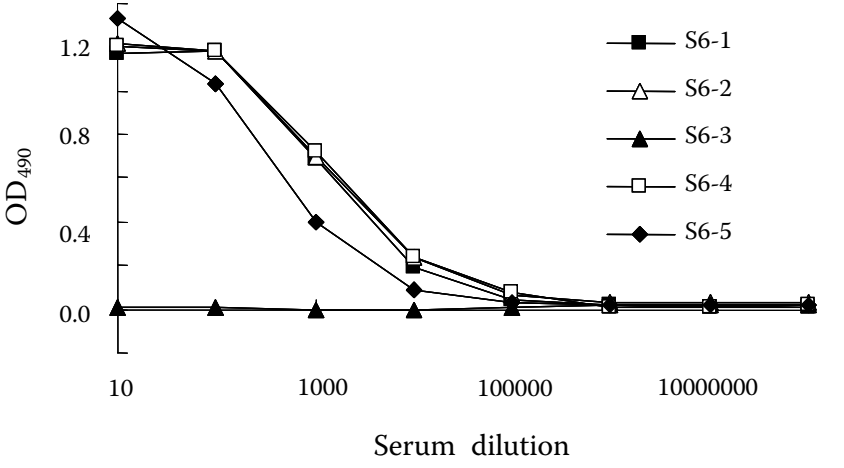

FIGURE 14.2 Binding of antipeptide Abs to respective peptides (0.33 μ*M*) coated on the ELISA plates. OD values at 490 nm were plotted against dilutions of antisera.

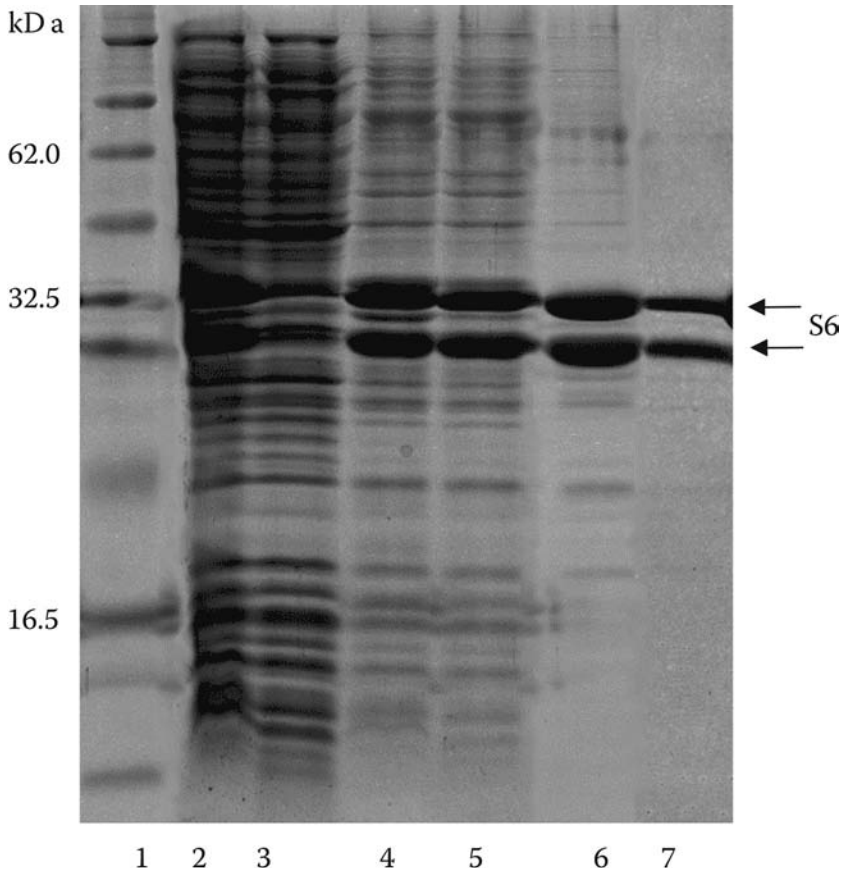

FIGURE 14.3 Analysis of rS6 at each step of purification by SDS-PAGE. 1, Molecular weight marker; 2, *E. coli* total lysate; 3, soluble fraction; 4, inclusion bodies dissolved in 8 *M* urea; 5, inclusion bodies dissolved in 6 *M* urea; 6, inclusion bodies purified on a Ni column; 7, rS6 protein purified on a Ni column and an anion exchange column.

14.3.3 Binding of Abs to rS6

The binding of antipeptide Abs was examined by ELISA using plates coated with rS6, and the results shown in Figure 14.4 indicated that reactivity varied greatly among Abs, in spite of the fact that they showed a similar capability of binding to the corresponding free peptides, except for S6-3. In order to eliminate the effect of Ab concentration-dependent variation, we calculated the binding ratio of rS6 relative to each peptide (*R*), representing a normalized capability of binding to rS6 (Figure 14.5[a]). As shown in Figure 14.5(a), anti-S6-5 Abs showed the most efficient binding to rS6. On the other hand, the weak binding of anti-S6-1 to rS6 suggested that the segment at the N-terminal region was buried in the protein interior and was less exposed, or that the His-tag introduced at the N terminus

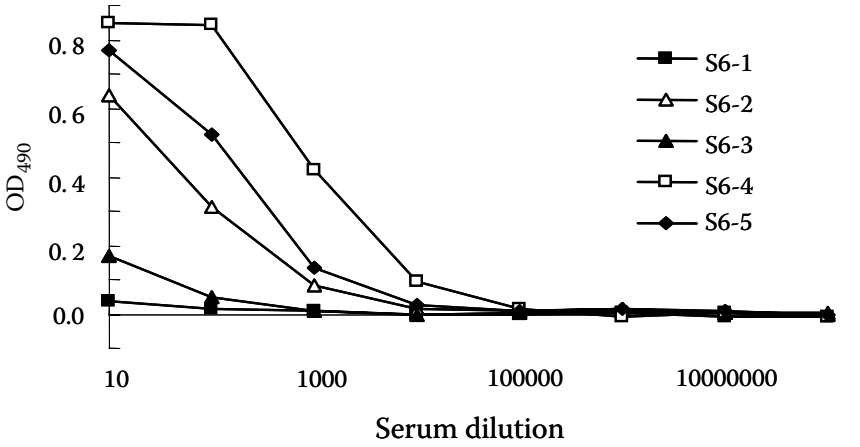

FIGURE 14.4 Binding of antipeptide Abs to rS6 coated on the ELISA plates. ODs at 490 nm were plotted against serum dilutions.

hindered Ab binding to the S6-1 epitope. The fact that the anti-S6-2, anti-S6-4 and anti-S6-5 Abs showed high reactivity to rS6 indicates that the corresponding epitopes were exposed on the rS6 surface.

14.3.4 Binding of Abs to S6 Protein in HeLa Cells

The binding of Abs to the proteins in HeLa cells was examined by immunostaining. Anti-S6-4 Abs showed strong reactivity to S6 proteins in the cytoplasm but not in the nucleus, as shown in Figure 14.5(b). The anti-S6-4 Abs reacted with particles in the cytoplasm, which corresponded to liposomes where S6 protein is found. In contrast to the reactivity of anti-S6-4, the anti-S6-5 Abs bound only at very low levels to S6 protein in HeLa cells, in spite of their strong reactivity with rS6 (Figure 14.5[a]). This suggests that S6 interacts with other macromolecules such as S18 or mRNA in the cell, and that anti-S6-5 could not therefore bind to the epitope. On the other hand, anti-S6-1 did show evidence of binding to S6 in HeLa cells (although rather weak), despite a minimal level of binding to rS6.

14.4 DISCUSSION

One of the goals in clarifying the structural biology of proteins is to understand the role of their quaternary structure in living cells. However, the structural aspects of protein function and interactions with various intracellular components in living cells are not yet well understood, although information is available on the three-dimensional structures of proteins as provided by x-ray crystallography and nuclear magnetic resonance. In this study, we attempted to deduce the configuration of peptide segments within the protein structure, i.e., whether they exist on the surface, or in the interior due to protein folding, or are

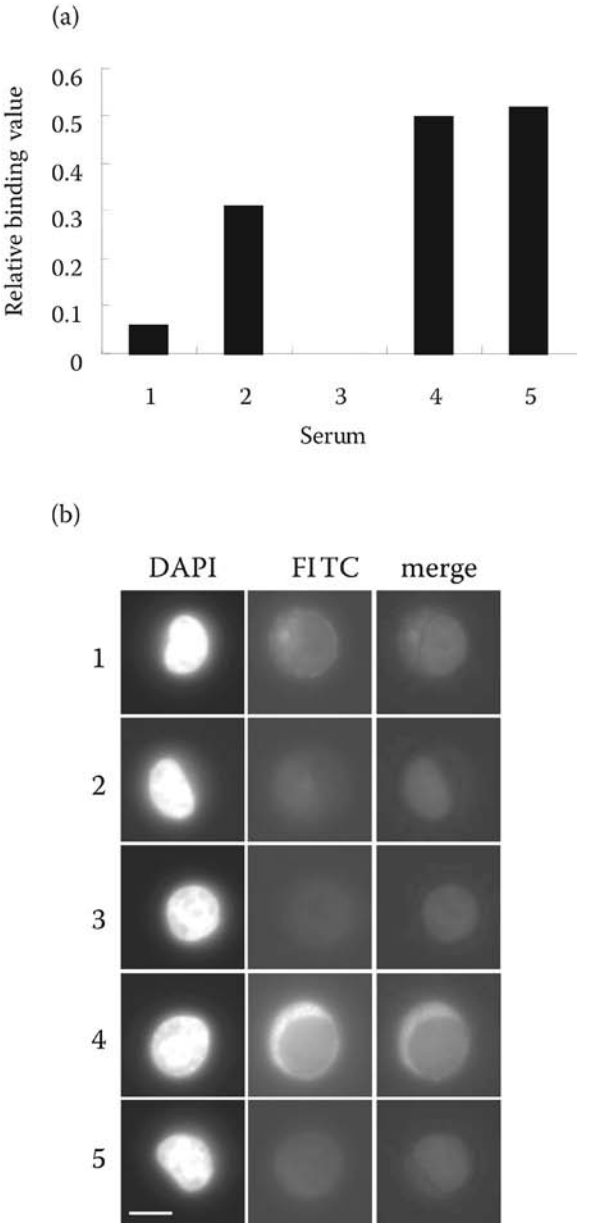

FIGURE 14.5 Relative binding of antipeptide Abs. (a) The ratio of binding of rS6 protein relative to the respective peptide was calculated using OD at 490 nm. *Due to low production, the relative binding of anti-S6-3 could not be obtained. (b) Immunostaining of HeLa cells for antipeptide Abs. 1, anti-S6-1; 2, anti-S6-2; 3, anti-S6-3; 4, anti-S6-4; 5, anti-S6-5. Nuclei were stained with DAPI. The bound antipeptide Abs were detected by FITC-labeled goat anti-rabbit IgG Abs (b).

located at the interface of protein–macromolecule cellular interactions. For this purpose, we prepared antipeptide Abs by immunizing rabbits with peptides of 15 amino acid residues and examined the relative Ab reactivity with the peptides vs. the intact protein.

We assumed that Ab reactivity is determined by accessibility to the epitopes. We considered that the peptides, whether free in solution or coated on the plates, were fully exposed and reactive with the antipeptide Abs. Since the peptide segments located on the surface of S6 protein might not be exposed completely, unlike the free peptide, it was expected that reactivity with S6 would be less than that with the peptide. In fact, in ELISA, rS6 was approximately 100-fold less reactive than the peptides (data not shown). However, it is worth considering that the relative binding of Abs is a measure of the exposure of the segment on the surface. In this context, we surmised that the secondary structure of the segments did not significantly affect the reactivity of antipeptide Ab, since Stanfield et al. [9] showed that the conformation of a peptide in complex with antipeptide Ab was different from that in the intact protein—the former forming a type II β-turn, while the latter an α-helix.

We chose ribosomal S6 protein as a model because it is abundant in ribosomes and exists as a complex with other proteins and RNA. An x-ray crystallographic study of S6 from *T. thermophilus* [12,14,15] showed that this protein contains four β-strands and two α-helices. The small (30S) subunit of the *E. coli* bacterial ribosome has been studied as a model for the ordered assembly of a large ribonucleoprotein complex [16]. According to this model, S6 forms a heterodimer with another ribosomal protein, S18, with a dissociation constant of less than 10 n*M* [17] and the S6-S18 heterodimer interacts with 16 S RNA [18]. It was expected that a large surface area was involved in these interactions [12].

S6-1 comprises the N-terminal region of S6 protein. Since this region does not exist in S6 from bacteria such as *T. thermophilus*, for which the tertiary structure was determined by x-ray crystallography [12], structural information was not yet available. We predicted that this region would be exposed on the protein surface *in vivo* on the basis of the reactivity of anti-S6-1 Abs using immunostaining of HeLa cells. However, anti-S6-1 Abs did not bind to rS6 at substantial levels, suggesting that the S6-1 epitope is not exposed on the surface of rS6. Such a disagreement between rS6 and S6 in HeLa cells in terms of reactivity with anti-S6-1 Ab can be explained in terms of a conformational change. We expect that the N-terminal region of S6 protein is less exposed when free, but is exposed in HeLa cells due to an allosteric effect from interaction with other macromolecules. It is also possible that the His-tag introduced at the N terminus causes steric hindrance in the reaction with anti-S6-1 Abs.

In *T. thermophilus*, S6-2 consists of a β-strand (β1) and an α-helix (α1). We expected that S6 in HeLa cells would bind to the anti-S6-2 Abs because the region containing the S6-2 epitope did not interact with other molecules such as RNA or S18 in *T. thermophilus* [18]. However, the finding that anti-S6-2 Ab bound to rS6 but not to S6 in HeLa cells suggested that human S6 interacts with other

macromolecules via the segment containing the S6-2 epitope, or that the conformation of this portion changed after interaction with other macromolecules, even if the interaction occurred through segments other than S6-2.

The region containing the S6-4 epitope is homologous with respect to the amino acid sequences of various species [14,15]. The corresponding region of *T. thermophilus* formed a β-strand (β4). The fact that the anti-S6-4 Abs reacted with both rS6 and S6 in HeLa cells suggested that this epitope is exposed on the protein surface without taking part in interactions with other macromolecules. Among the antipeptide Abs capable of reacting with rS6, only anti-S6-4 reacted strongly with HeLa cell S6. It is of interest that no reaction with cytoplasmic proteins was observed with anti-S6-5 Abs, in spite of their strong reactivity to rS6 (Figure 14.5[a]) (see Chapter 16). This was explicable in terms of steric hindrance resulting from interaction with macromolecules. We prepared Abs to S6-4 and S6-5 by immunization of three rabbits with the respective peptides and found that all anti-S6-4 Abs reacted with rS6 as well as with S6 in HeLa cells, while all anti-S6-5 Abs failed to react with HeLa cell S6 (data not shown). Therefore, the specificity of these Abs did not depend on differences among individual animals. Abs such as anti-S6-5 cannot be used for cytostaining or immunoprecipitation experiments.

As described above, we were able to prepare highly reactive anti-S6-4 Ab capable of binding to human ribosomal S6 protein. Although all Abs possessed a similar level of reactivity to the respective peptides, they behaved differently with S6 protein of HeLa cells. Such variation in reactivity to proteins in living cells could not be explained in terms of affinity for the peptide or for the purified proteins, and seemed to depend on the extent of epitope exposure on the protein surface. Steric hindrance caused by the other components would affect interactions between antipeptide Ab and epitope, suggesting that antipeptide Abs can be used as tools for predicting sites of protein–macromolecule interactions in living cells.

14.5 CONCLUSION

Structural aspects of a human ribosomal protein, S6, were examined in terms of folding and molecular assembly *in vivo* using Abs prepared by immunizing rabbits with synthetic peptides. Five peptides corresponding to the segments Ser6-Asp20 (S6-1), Ile52-Gly66 (S6-2), Asp103-Gly117 (S6-3), Asn146-Lys160 (S6-4) and Arg178-Ile192 (S6-5) were chosen as epitopes of human ribosomal S6 protein. Four of these peptides induced strong Ab production, and in an ELISA, three Abs, anti-S6-2, anti-S6-4 and anti-S6-5, showed high reactivity to rS6, while anti-S6-1 did not, suggesting that S6-2, S6-4 and S6-5 were exposed on the rS6 surface, while S6-1 was less exposed or possessed a different conformation. The immunostaining of HeLa cells with these Abs indicated that S6-4 was exposed on the protein surface but that S6-2 and S6-5 were not, suggesting that the latter peptide segments were buried by interaction with other macromolecules in HeLa cells, and that only anti-S6-4 Abs can be used for immunoprecipitation.

ACKNOWLEDGMENTS

This study was supported by Special Coordination Funds of the Ministry of Education, Culture Sports, Sciences and Technology of the Japanese government. The authors thank Dr. William Campbell for English editing of the manuscript.

REFERENCES

1. Benjamin DC, Berzofsky JA, East IJ, Gurd FR, Hannum C, Leach SJ, Margoliash E, Michael JG, Miller A, Prager EM, Reichlin M, Sercarz EE, Smith-Gill SJ, Todd PE, Wilson AC (1984) The antigenic structure of proteins: a reappraisal. *Ann Rev Immunol* 2: 67–101.
2. Sachs DH, Schechter AN, Eastlake A, Anfinsen CB (1972) An immunological approach to the conformational equilibria of polypeptides. *Proc Natl Acad Sci USA* 69: 3790–3794.
3. Berzofsky JA, Buckenmeyer GK, Hicks G, Gurd FR, Feldmann RJ, Minna J (1982) Topographic antigenic determinants recognized by monoclonal antibodies to sperm whale myoglobin. *J Biol Chem* 257: 3189–3198.
4. Geysen HM, Barteling SJ, Meloen RH (1985) Small peptides induce antibodies with a sequence and structural requirement for binding antigen comparable to antibodies raised against the native protein. *Proc Natl Acad Sci USA* 82: 178–182.
5. Tainer JA, Getzoff ED, Paterson Y, Olson AJ, Lerner RA (1985) The atomic mobility component of protein antigenicity. *Ann Rev Immunol* 3: 501–535.
6. Rodda SJ, Geysen HM, Mason TJ, Schoofs PG (1986) The antibody response to myoglobin. I. Systematic synthesis of myoglobin peptides reveals location and substructure of species-dependent continuous antigenic determinants. *Mol Immunol* 23: 603–610.
7. Berzofsky IA, Berkower IJ, Epstein SL (1993) Antigen-antibody interaction and monoclonal antibodies, in *Fundamental Immunology*, 3rd ed. Paul WE, Ed. Raven Press Ltd., New York: 421–425.
8. Getzoff ED, Tainer JA, Lerner RA, Geysen HM (1988) The chemistry and mechanism of antibody binding to protein antigens. *Adv Immunol* 43: 1–98.
9. Stanfield RL, Fieser TM, Lerner RA, Wilson IA (1990) Crystal structures of an antibody to a peptide and its complex with peptide antigen at 2.8 A. *Science* 248: 712–719.
10. Rini JM, Schulze-Gahmen U, Wilson IA (1992) Structural evidence for induced fit as a mechanism for antibody-antigen recognition. *Science* 255: 959–965.
11. Uchiyama S, Kobayashi S, Takata H, Ishihara T, Hori N, Higashi T, Hayashihara K, Sone T, Higo D, Nirasawa T, Takao T, Matsunaga S, Fukui K (2005) Proteome analysis of human metaphase chromosomes. *J Biol Chem* 280: 16994–17004.
12. Brodersen DE, Clemons WM, Carter AP, Wimberly BT, Ramakrishnan V (2002) Crystal structure of the 30S ribosomal subunit from *Thermus thermophilus*: structure of the proteins and their interactions with 16 S RNA. *J Mol Biol* 316: 725–768.
13. Maeshima K, Laemmli UK (2003) A two-step scaffolding model for mitotic chromosome assembly. *Dev Cell* 4: 467–480.
14. Sedelnikova SE, Agalarov SC, Eliseikina A (1991) Crystals of protein S6 from the 30 S ribosomal subunit of *Thermus thermophilus*. *J Mol Biol* 220: 549–550.
15. Lindahl M, Svensson LA, Liljas A, Sedelnikova SE, Eliseikina IA, Fomenkova NP, Nevskaya N, Nikonov SV, Garber MB, Muranova TA, Rykonova AI, Amons R (1994)

Crystal structure of the ribosomal protein S6 from *Thermus thermophilus*. *EMBO J* 13: 1249–1254.
16. Held WA, Ballou B, Mizushima S, Nomura M (1974) Assembly mapping of 30S ribosomal proteins from *Escherichia coli*. Further studies. *J Biol Chem* 249: 3103–3111.
17. Recht MI, Williamson JR (2001) Central domain assembly: thermodynamics and kinetics of S6 and S18 binding to an S15-RNA complex. *J Mol Biol* 313: 35–48.
18. Agalarov SC, Sridhar Prasad G, Funke PM, Stout CD, Williamson JR (2000) Structure of the S15, S6, S18-rRNA complex: assembly of the 30S ribosome central domain. *Science* 288: 107–113.

15 Structure and Interactions of the Imitation SWI-Type Chromatin-Remodeling Complex, ATP-Dependent Chromatin-Assembly Factor

Tadayasu Ohkubo, Mariana Petkova-Andonova, Yukiko Kojima, Shota Nakamura, Hiroko Fujita, Yoshinori Nishi, Hiroaki Nakano, Susumu Uchiyama, Kiichi Fukui and Yuji Kobayashi*

CONTENTS

15.1 Introduction 204
15.2 Classification of Chromatin-Remodeling Complexes 204
15.2.1 The Switch/Sucrose Non-Fermenting (SWI/SNF) and the Imitation SWI (ISWI) Families of SWI2/SNF2 Chromatin-Remodeling Complexes 204
15.2.2 Functions of SWI/SNF and ISWI 205
15.3 Mechanisms of Chromatin Remodeling 206
15.3.1 Chromatin-Remodeling Complexes and Helicase 206
15.3.2 Mechanism of DNA Translocation 206
15.4 Interactions of the ACF Chromatin-Remodeling Complex 208
15.4.1 Organization of the ACF Chromatin-Remodeling Complex 208
15.4.2 Quantitative Analysis of the Interaction between hSNF2H and hACF1 210

*To whom correspondence should be addressed.

15.5 Conclusion 212
Acknowledgment 213
References 213

15.1 INTRODUCTION

Chromatin is a nucleoprotein complex with a general role in DNA packaging, in order to protect the eukaryotic genome from damage and to repress gene expression [1]. The primary repeating unit of chromatin structure is the nucleosome, in which approximately 1.7 turns of DNA consisting of 147 base pairs (bp) are wrapped around a histone octamer composed of a histone H3–H4 tetramer and two histone H2A–H2B dimers (see Chapter 10) [2,3]. In chromatin, nucleosomes are separated by 20 to 30 bp of linker DNA. To efficiently stow DNA into the small nucleus of a eukaryotic cell, nucleosomes are aligned into an ordered array or chain, which is then folded into a highly compact arrangement, referred to as the higher-order chromatin structure [4]. However, the wrapping of DNA into nucleosomes inhibits access by a number of DNA-binding factors. Therefore, DNA-mediated processes such as transcription, replication and repair require flexibility of the chromatin structure. A number of chromatin-remodeling complexes in eukaryotic cells mediate the repositioning of nucleosomes in the regulation of this flexibility [5,6]. These complexes belong to the SWI2/SNF2 superfamily of ATPases, and use the energy provided by ATP hydrolysis to disrupt histone–DNA interactions and move the nucleosomes [7]. This chapter focuses on the mechanisms of the chromatin-remodeling process and the interactions of chromatin-remodeling complexes, based on recent structural studies and our results derived from quantitative analysis of the binding affinities among the domains of these complexes.

15.2 CLASSIFICATION OF CHROMATIN-REMODELING COMPLEXES

15.2.1 The Switch/Sucrose Non-Fermenting (SWI/SNF) and the Imitation SWI (ISWI) Families of SWI2/SNF2 Chromatin-Remodeling Complexes

The SWI2/SNF2 superfamily of ATP-dependent chromatin-remodeling complexes comprises at least five distinct subfamilies: SWI/SNF, ISWI, INO80, SWR1 and Mi-2/NURD. SWI/SNF and ISWI are the best studied of these subfamilies [7,8]. Although several remodeling complexes are known to have specific biological functions, all remodeling complexes change the position of the DNA on the nucleosome, resulting in an alteration in DNA accessibility. All remodeling complexes investigated to date contain a conserved DNA-dependent ATPase subunit and require ATP hydrolysis for remodeling [7]. The isolated ATPase subunit has limited nucleosome remodeling activity *in vitro* and

acts as the catalytic subunit [9,10]. The similarity of the ATPase subunit between chromatin-remodeling complexes indicates that these complexes all use the energy of ATP hydrolysis in a similar manner to alter the architecture of chromatin at the nucleosomal level. Remodeling complexes of the SWI/SNF subfamily contain an ATPase subunit and a set of conserved additional core members. For example, the yeast remodeling complex RSC has the ATPase subunit Sth1 and the core proteins Rsc8, Rsc6, Sfh1, Arp7 and Arp9 [11]. Remodeling complexes of the ISWI subfamily such as nucleosome-remodeling factor (NURF), chromatin-accessibility complex (CHRAC) and ATP-dependent chromatin-assembly factor (ACF) contain a conserved ATPase subunit, ISWI, and specialized, associated proteins that are unique to each complex [12]. For example, the ACF complex has the ISWI ATPase subunit and the associated protein ACF1 [13]. Since the ATPase domain of SWI/SNF ATPases is similar to the ATPase domain of ISWI, these ATPase domains are considered to have a similar action in translocating the DNA on the nucleosome [14,15]. Several SWI/SNF remodeling complexes have multiple bromodomains and specifically bind to a particular region on the nucleosome, through contact between the bromodomain and acetylated lysines within the N-terminal histone tail of H4 [16]. Although ISWI lacks a bromodomain, it can still interact with acetylated histones. The C terminus of ISWI has two unique domains, known as SANT and SLIDE. These two domains bind to the histone tails and to the linker DNA that emerges from the nucleosome, respectively [17]. *In vivo* and *in vitro* studies have shown that ISWI complexes have central roles in clustering, assembly and spacing of nucleosomes during DNA replication, and in repression of transcription, resulting in a dense, relatively inaccessible and highly compact arrangement, known as the higher-order chromatin structure [7]. SWI/SNF remodeling complexes, in contrast, lack this function. SWI/SNF remodeling complexes are involved in disordering of the higher-order chromatin structure and reorganization of the nucleosome array in order to promote access of transcription factors, and to regulate gene expression.

15.2.2 Functions of SWI/SNF and ISWI

ISWI complexes generally consist of a small number of subunits (2 to 5 subunits) compared with SWI/SNF complexes which contain in the order of 8 to 15 subunits. There are two fundamental differences between the ISWI and SWI/SNF subfamilies of ATP-dependent remodeling complexes: differences in the diversity of function and in the targets [8]. Most SWI/SNF ATP-dependent remodeling complexes function in transcriptional activation or repression. Different compositions of additional subunits may be responsible for positioning of the catalytic ATPase subunit to its specific site of action, and for interaction with different transcription factors. Therefore, different SWI/SNF remodeling complexes regulate different sets of genes. In contrast, many of the functions performed by ISWI remodeling complexes do not require site-specific interaction [18,19]. During replication, nucleosome clustering, assembly and spacing occur. Site-directed interactions of ISWI are not likely to be needed for formation of higher-order

chromatin structure, and ISWI presumably recognizes structural features of the DNA rather than specific DNA sequences [8].

15.3 MECHANISMS OF CHROMATIN REMODELING

15.3.1 Chromatin-Remodeling Complexes and Helicase

Recent structural and biochemical studies have addressed the question of how chromatin-remodeling complexes alter nucleosomes, and have raised the suggestion that they function as specialized DNA translocases. These complexes have been found to track along the nucleosomal DNA, while remaining anchored at the core histone of the nucleosome [20]. The results of a large number of biochemical experiments have suggested that nucleosome sliding is a process common to both SWI/SNF and ISWI remodeling complexes. These complexes use ATP hydrolysis to achieve nucleosome sliding through disruption of DNA–histone interactions. In the nucleosome, the DNA duplex contacts the surface of the core histone octamer at 14 sites to form a stable complex through approximately 140 hydrogen bonds [2,3]. Since DNA–histone interactions mainly involve the DNA backbone, the histone octamer binds DNA in a relatively nonsequence-specific manner.

The ATPase subunits of remodeling complexes belong to the superfamily II (SF2) of DEAD/H-box helicases and translocases [21,22]. SF2 helicases have two domains: a wedge-like domain and a DNA-translocating domain, and the helicase activity is provided by their combined and coupled actions. The wedge-like domain destabilizes and separates the translocating DNA duplex, however, sequence alignments have shown that the chromatin-remodeling ATPases contain the translocation domain but lack a wedge-like domain [23]. Therefore, SWI/SNF and ISWI remodeling complexes lack helicase activity and act as DNA translocases, without separating the DNA duplex.

15.3.2 Mechanism of DNA Translocation

Recent structural studies have revealed the mode of binding of remodeling complexes to the nucleosome [20]. The crystal structure of the SWI2/SNF2 ATPase core of *Sulfolobus solfataricus* Rad54 homolog reveals that it consists of two domains with a deep central cleft separating the two domains, and it is in this cleft that the DNA binds [24]. Biochemical studies have shown that SWI/SNF remodeling complexes interact with the nucleosome at a fixed site deep within the nucleosome [25], with a contact site located about two DNA helical turns from the dyad of the nucleosome. At this site, the histone H4 tail emerges from the nucleosome, and this region of H4 is important for activating ATPase activity [26,27]. After binding to the nucleosome, the SWI/SNF remodeling complex lifts the DNA around the contact site off the histone surface to form a DNA bulge or loop [20,23]. In contrast, ISWI remodeling complexes interact with the nucleosome at two separate sites: an internal site, and an external site [17] that involves a DNA linker that is near the nucleosome-entry site as shown in Figure 15.1.

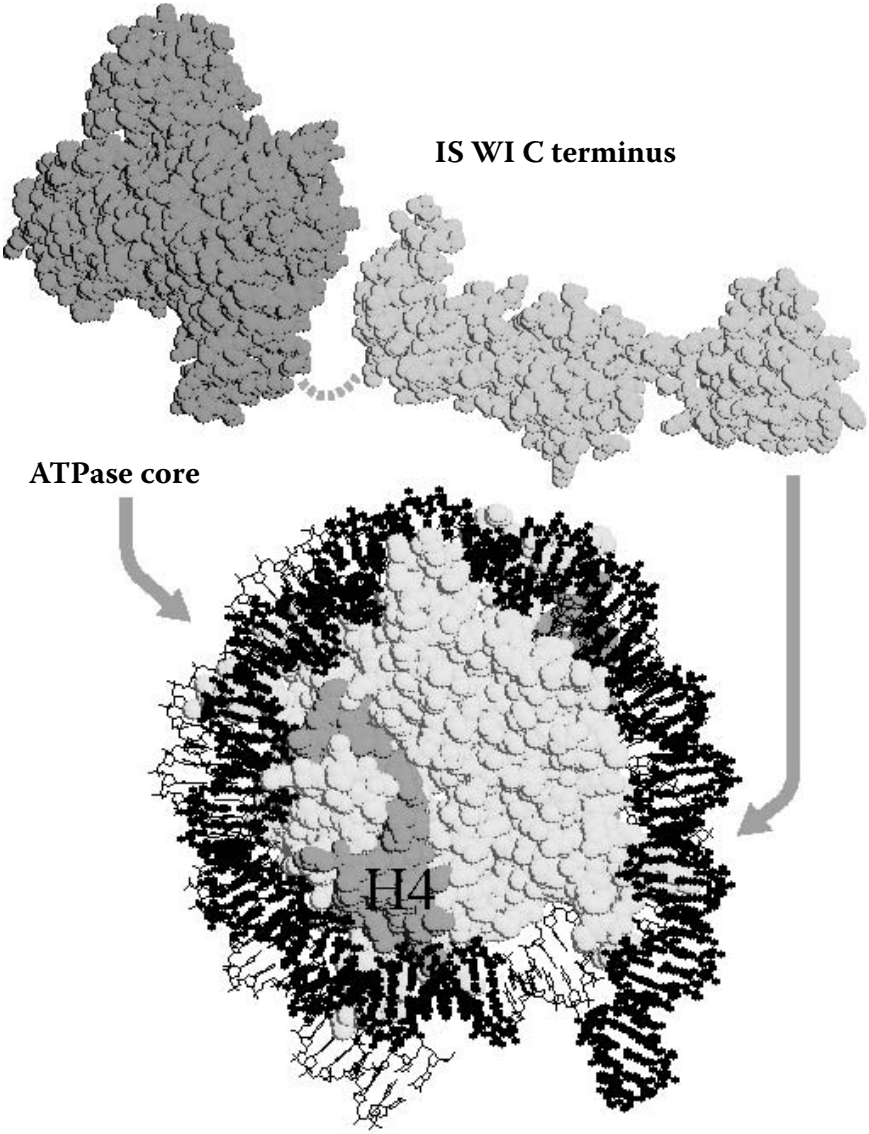

FIGURE 15.1 Model explaining the interaction of the ISWI subunit of the chromatin remodeling complex with the nucleosome. The crystal structures of the SWI2/SNF2 ATPase core of *Sulfolobus solfataricus* Rad54 homolog (PDB accession code 1Z63), the C terminus of ISWI (PDB accession code 10FC), and the nucleosome core (PDB accession code 1AOI) are depicted in a space-filling representation.

At the entry site, DNA can be easily lifted off the histone surface and the DNA bulge or loop is formed. Therefore, SWI/SNF or ISWI remodeling complexes disrupt only a subset of the histone–DNA interactions in the nucleosome. Then, adjacent histone–DNA contacts are broken and histone–DNA contacts are reformed at the other edge of this bulge or loop. Propagation of this distortion over the surface of the histone octamer leads to nucleosome relocation. Since most of the contacts are maintained during the propagation step, the total energy required for translational repositioning is lowered. The energy needed for the disruption of histone–DNA interactions is compensated for by the formation of new, equivalent interactions.

15.4 INTERACTIONS OF THE ACF CHROMATIN-REMODELING COMPLEX

15.4.1 Organization of the ACF Chromatin-Remodeling Complex

To regulate replication and transcription and to repair DNA, ATP-dependent chromatin-remodeling complexes mobilize nucleosomes and increase the accessibility of condensed chromatin. The nucleosome-dependent ATPase, SNF2H, is a constituent of these complexes and various functionally different complexes are formed, reflecting differing subunit compositions. ACF1 associates with SNF2H and enhances SNF2H-induced nucleosome mobilization by an order of magnitude. Furthermore, through their nucleosome-mobilizing activity, ACF1/SNF2H complexes promote chromatin assembly by transforming a disordered array of nucleosomes into an evenly spaced nucleosome array.

Recent genetic and biochemical studies in human cells have revealed several multi-protein complexes having ATP-dependent chromatin-remodeling activities: William's syndrome transcription factor-related chromatin-remodeling factor (hWCRF)/ACF [28], hCHRAC [29], hACF [30,31] and hNURF [32]. These remodeling complexes are conserved among other species such as *Drosophila, Xenopus* and yeast [33–35], and use energy to increase the general accessibility of DNA in chromatin. Unlike the other known remodeling complexes, hCHRAC can also function during chromatin assembly, using the energy in ATP to convert randomly distributed nucleosome arrays into a regular array of nucleosomes with even spacing [30,31]. hCHRAC also differs from hWCRF/ACF and hACF in possessing two small histone fold factors, p15 and p17. The DNA-binding properties of p15 and p17 are responsible for incorporation of the nucleosomes into chromatin, enhancing the nucleosome-remodeling activity of this complex [29]. In these complexes, the core subunit is the 185-kDa subunit ACF1, associated with the 125-kDa SNF2H subunit [33]. ACF1 has a similar domain organization to WSTF, the gene of which is lacking in the genome of Williams–Beuren syndrome patients [36].

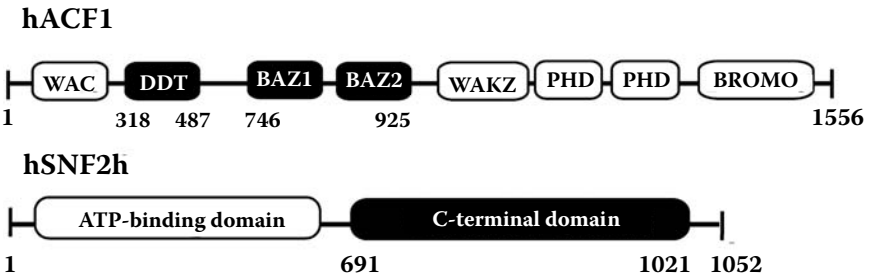

FIGURE 15.2 The domain organization of hACF1 and hSNF2H.

ACF1 contains a putative WAC heterochromatin-targeting domain [37], DDT, BAZ and WAKZ domains, two PHD domains and a bromodomain (Figure 15.2), all of which are conserved in ACF-related proteins. The bromodomain was first found in the *Drosophila* Brahma protein and functions as a histone acetyltransferase [38–41]. Deletion of a bromodomain in human HBRM, a protein constituent of the SWI/SNF remodeling complex, causes both decreased stability and loss of nuclear localization [41]. Meanwhile, an analog of hSNF2H, ISWI from *Drosophila*, has been extensively studied. ISWI is a member of the subfamily of ATPases that hydrolyze ATP only in the presence of nucleosomes. According to the amino acid sequence, ISWI contains HAND, SLIDE and SANT-like domains in the C-terminal region, but no bromodomain which is a hallmark of ACF1-type proteins. The function of the SANT and SLIDE domains is predicted by sequence alignments and crystal structure analysis of the ISWI-C domain [17,42]. The SANT domain contains a number of highly conserved residues that are also found in the c-Myb DNA-binding domain [43]. The DNA-binding unit of Myb is a helix-turn-helix–related motif with a conserved tryptophan that forms a hydrophobic core. In contrast to the positively charged c-Myb repeats R2 and R3, most of the corresponding residues in the SANT domain are acidic [42]. On the other hand, the SLIDE domain appears compatible with a role in DNA-binding, since it displays an overall positive charge and contains residues corresponding to the DNA-binding residues of repeat R3 of c-Myb. ISWI is a remodeling factor by itself, while association with other proteins enhances its activity. For example, ACF1 enhances the nucleosome-remodeling activity of ISWI and changes the direction of ISWI-catalyzed nucleosome sliding on a DNA fragment [18]. In the presence of ATP, ISWI alone can move an entry-positioned nucleosome to the opposite end of a DNA fragment, whereas the ACF1-ISWI complex catalyzes the reverse reaction and moves the nucleosomes to the center position of the DNA fragment. Thus, the interaction partner of ACF1 in chromatin-remodeling complexes is SNF2H [44–46], and in our studies we have thus far investigated the interaction between them.

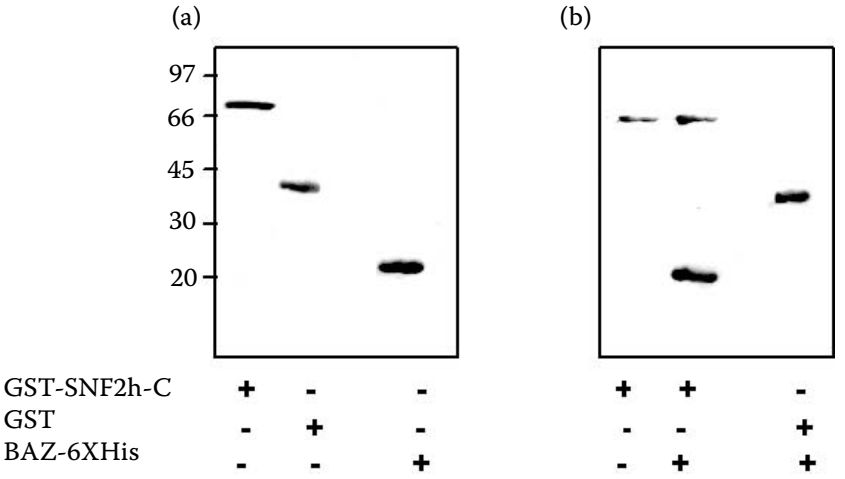

FIGURE 15.3 GST-pulldown assay of hSNF2H-C protein with hACF and its domain, ACF1-BAZ. (a) As input control, an equivalent amount of analyzed protein was electrophoresed for comparison. (b) Bacterially expressed recombinant GST and GST-SNF2H-C were immobilized on glutathione-Sepharose 4B resin and assayed for interaction with ACF1-BAZ-6×His. Protein complexes were identified by Western blotting using anti-6×His antibody.

15.4.2 Quantitative Analysis of the Interaction between hSNF2H and hACF1

Human ACF1 and SNF2H were expressed in baculovirus and their domains were expressed in *Escherichia coli*. The binding affinities among these proteins and their subunits were examined by GST-pulldown (Figure 15.3) and BIAcore assays (Figure 15.4). From these results, we identified a region within ACF1, called the BAZ domain, as being essential for interaction with SNF2H. This domain of ACF1 showed high affinity for the SNF2H C-terminal domain with an apparent dissociation constant of 15 μ*M*. This value is slightly higher than the dissociation constant of wild-type ACF1 with the SNF2H C-terminal domain, 8.3 μ*M*. Inhibition of binding of the SNF2H C-terminal domain to wild-type ACF1 through the BAZ domain, by the addition of SNF2H C-terminal domain, was also observed. Ultracentrifugation analyses of this association–dissociation system showed that the BAZ domain and the SNF2H C-terminal domain form a 1:1 complex. These data clearly demonstrated that the major contact site of ACF1 and SNF2H is via the BAZ domain of ACF1 and the C-terminal domain of SNF2H (Figure 15.5). Previous biochemical experiments have shown that the PHD domain of ACF1 interacts with nucleosome core histones [39,45]. Based on

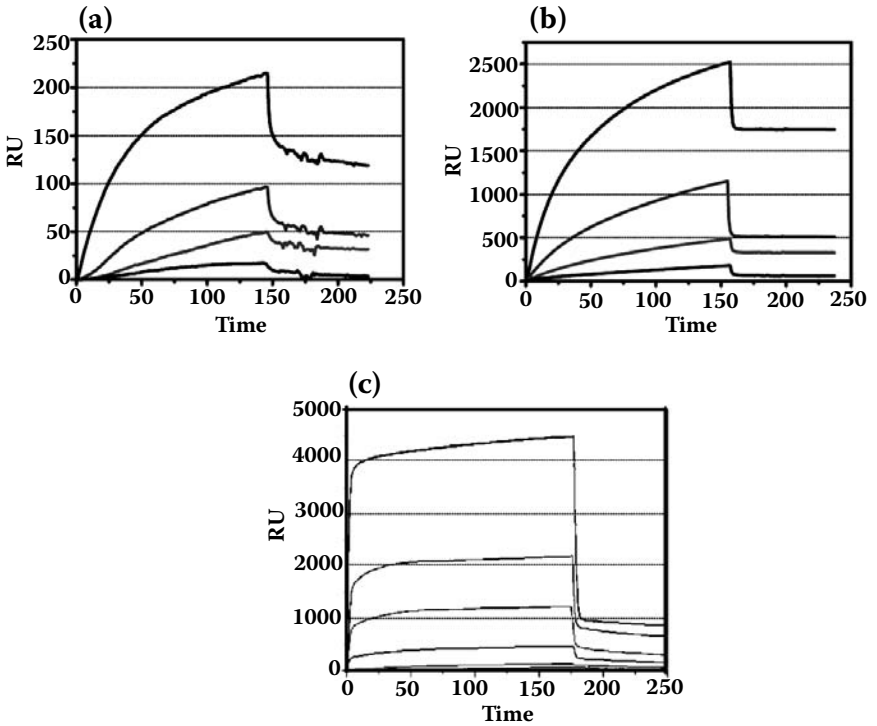

FIGURE 15.4 Surface plasmon resonance (SPR) sensorgrams of the interaction between hACF1 and its BAZ domain, with hSNF2H-C. The sensorgrams show the interactions for 1 min and with four concentrations of binding partner with immobilized ligand on a CM5 sensor chip, recorded on a BIAcore 2000 system. (a) SPR sensorgram showing binding of hACF1-FL-Flag to immobilized hSNF2H-C. Various concentrations (17, 35, 70 and 140 μ*M*) of hACF1-FL-Flag were injected over the surface having immobilized hSNF2H-C. (b) SPR sensorgram of the interaction of hACF1-BAZ as ligand and with four different concentrations (3.7, 7.5, 15 and 31 μ*M*) of hSNF2H-C as analyte. (c) SPR sensorgram of the concentration-dependent inhibition of interaction between hSNF2H-C and hACF1-BAZ by hSNF2H-C. hSNF2H-C was fixed on the sensor chip and hACF1-BAZ was used as analyte. Various ratios — 1:1, 1:2, 1:5 and 1:10 — of both hSNF2H-C and hACF1-BAZ were used.

these results, we propose that ACF1 plays a role in enforcing the binding of the SNF2H C-terminal domain to linker DNA, and provides the anchoring point. SNF2H alone binds to nucleosomes mainly through interaction of its C-terminal SLIDE domain with nucleosomal DNA. SNF2H may be an inefficient remodeling enzyme because it lacks a stable anchoring point on the nucleosome, and the BAZ and PHD domains of ACF1 may provide the anchoring point for effective translocation.

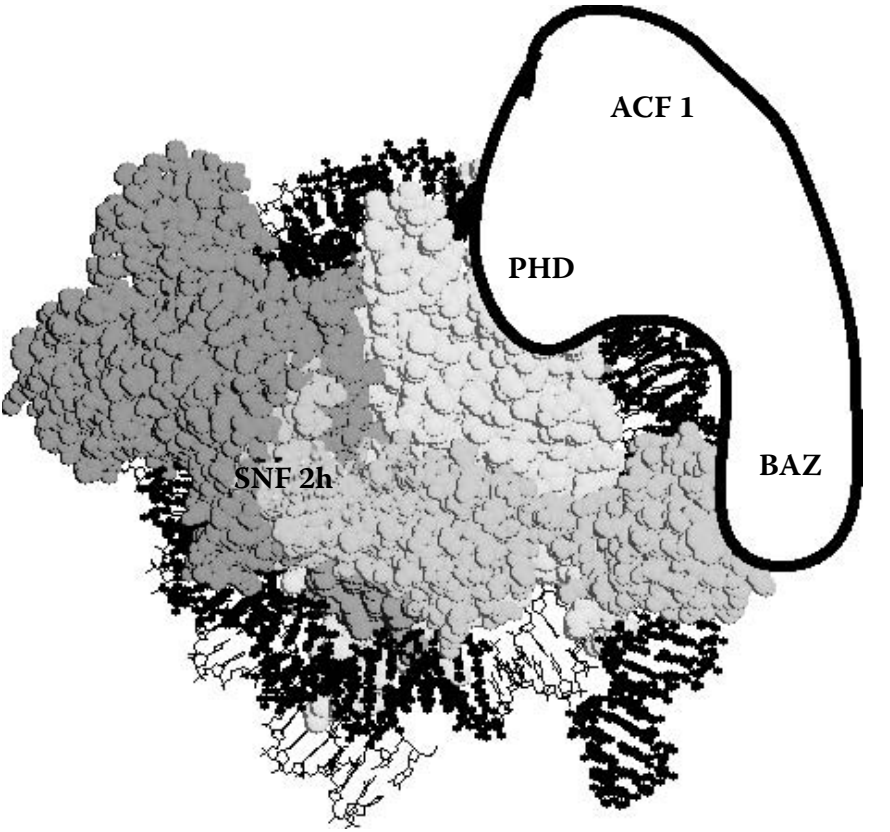

FIGURE 15.5 Schematic representation of the proposed model for the ACF-nucleosome complex. A space-filling representation of the SNF2H-nucleosome complex was constructed from the ISWI-nucleosome model shown in Figure 15.1. In this model, SNF2H can cover the nucleosome core particle. The BAZ domain of ACF1 binds to the C-terminal domain of SNF2H.

15.5 CONCLUSION

In this chapter, we reviewed the classification of ATP-dependent chromatin-remodeling complexes, the mechanism of the chromatin-remodeling process, and the interactions of the ACF chromatin-remodeling complex. Recent structural and biochemical data have shown that chromatin-remodeling complexes function as specialized DNA translocases. Based on our results, the major contact site between ACF1 and SNF2H is via the BAZ domain of ACF1 and the C-terminal domain of SNF2H, as shown in Figure 15.5. ACF1 may play a role in enforcing the binding of the SNF2H C-terminal domain to linker DNA for effective nucleosome translocation.

ACKNOWLEDGMENT

This study was supported by Special Coordination Funds of the Ministry of Education, Culture Sports, Sciences and Technology of the Japanese government.

REFERENCES

1. Cairns BR (1998) Chromatin remodeling machines: similar motors, ulterior motives. *Trends Biochem Sci* 23: 20–25.
2. Luger K, Mader AW, Richmond RK, Sargent DF, Richmond TJ (1997) Crystal structure of the nucleosome core particle at 2.8 A resolution. *Nature* 389: 251–260.
3. Richmond TJ, Davey CA (2003) The structure of DNA in the nucleosome core. *Nature* 423: 145–150.
4. Felsenfeld G, Groudine M (2003) Controlling the double helix. *Nature* 421: 448–453.
5. Peterson CL, Logie C (2000) Recruitment of chromatin remodeling machines. *J Cell Biochem* 78: 179–185.
6. Strahl BD, Allis CD (2000) The language of covalent histone modifications. *Nature* 403: 41–45.
7. Johnson CN, Adkins NL, Georgel P (2005) Chromatin remodeling complexes: ATP-dependent machines in action. *Biochem Cell Biol* 83: 405–417.
8. Dirscherl SS, Krebs JE (2004) Functional diversity of ISWI complexes. *Biochem Cell Biol* 82: 482–489.
9. Phelan ML, Sif S, Narlikar GJ, Kingston RE (1999) Reconstitution of a core chromatin remodeling complex from SWI/SNF subunits. *Mol Cell* 3: 247–253.
10. Corona DF, Langst G, Clapier CR, Bonte EJ, Ferrari S, Tamkun JW, Becker PB (1999) ISWI is an ATP-dependent nucleosome remodeling factor. *Mol Cell* 3: 239–245.
11. Cairns BR, Lorch Y, Li Y, Zhang M, Lacomis L, Erdjument-Bromage H, Tempst P, Du J, Laurent B, Kornberg RD (1996) RSC, an essential, abundant chromatin-remodeling complex. *Cell* 87: 1249–1260.
12. Vignali M, Hassan AH, Neely KE, Workman JL (2000) ATP-dependent chromatin-remodeling complexes. *Mol Cell Biol* 20: 1899–1910.
13. Ito T, Bulger M, Pazin MJ, Kobayashi R, Kadonaga JT (1997) ACF, an ISWI-containing and ATP-utilizing chromatin assembly and remodeling factor. *Cell* 90: 145–155.
14. Laurent BC, Yang X, Carlson M (1992) An essential *Saccharomyces cerevisiae* gene homologous to SNF2 encodes a helicase-related protein in a new family. *Mol Cell Biol* 12: 1893–1902.
15. Eisen JA, Sweder KS, Hanawalt PC (1995) Evolution of the SNF2 family of proteins: subfamilies with distinct sequences and functions. *Nucleic Acids Res* 23: 2715–2723.
16. Winston F, Allis CD (1999) The bromodomain: a chromatin-targeting module? *Nat Struct Biol* 6: 601–604.
17. Grune T, Brzeski J, Eberharter A, Clapier CR, Corona DF, Becker PB, Muller CW (2003) Crystal structure and functional analysis of a nucleosome recognition module of the remodeling factor ISWI. *Mol Cell* 12: 449–460.
18. Langst G, Becker PB (2001) ISWI induces nucleosome sliding on nicked DNA. *Mol Cell* 8: 1085–1092.
19. Langst G, Becker PB (2001) Nucleosome mobilization and positioning by ISWI-containing chromatin-remodeling factors. *J Cell Sci* 114: 2561–2568.

20. Becker PB (2005) Nucleosome remodelers on track. *Nat Struct Mol Biol* 12: 732–733.
21. Singleton MR, Wigley DB (2002) Modularity and specialization in superfamily 1 and 2 helicases. *J Bacteriol* 184: 1819–1826.
22. Murray NE (2000) Type I restriction systems: sophisticated molecular machines (a legacy of Bertani and Weigle). *Microbiol Mol Biol Rev* 64: 412–434.
23. Saha A, Wittmeyer J, Cairns BR (2006) Chromatin remodelling: the industrial revolution of DNA around histones. *Nat Rev Mol Cell Biol* 7: 437–447.
24. Durr H, Korner C, Muller M, Hickmann V, Hopfner KP (2005) X-ray structures of the *Sulfolobus solfataricus* SWI2/SNF2 ATPase core and its complex with DNA. *Cell* 121: 363–373.
25. Saha A, Wittmeyer J, Cairns BR (2005) Chromatin remodeling through directional DNA translocation from an internal nucleosomal site. *Nat Struct Mol Biol* 12: 747–755.
26. Clapier CR, Langst G, Corona DF, Becker PB, Nightingale KP (2001) Critical role for the histone H4 N terminus in nucleosome remodeling by ISWI. *Mol Cell Biol* 21: 875–883.
27. Corona DF, Clapier CR, Becker PB, Tamkun JW (2002) Modulation of ISWI function by site-specific histone acetylation. *EMBO Rep* 3: 242–247.
28. Bochar DA, Savard J, Wang W, Lafleur DW, Moore P, Cote J, Shiekhattar R (2000) A family of chromatin remodeling factors related to Williams syndrome transcription factor. *Proc Natl Acad Sci USA* 97: 1038–1043.
29. Poot RA, Dellaire G, Hulsmann BB, Grimaldi MA, Corona DF, Becker PB, Bickmore WA, Varga-Weisz PD (2000) HuCHRAC, a human ISWI chromatin remodelling complex contains hACF1 and two novel histone-fold proteins. *EMBO J* 19: 3377–3387.
30. LeRoy G, Loyola A, Lane WS, Reinberg D (2000) Purification and characterization of a human factor that assembles and remodels chromatin. *J Biol Chem* 275: 14787–14790.
31. Ito T, Levenstein ME, Fyodorov DV, Kutach AK, Kobayashi R, Kadonaga JT (1999) ACF consists of two subunits, Acf1 and ISWI, that function cooperatively in the ATP-dependent catalysis of chromatin assembly. *Genes Dev* 13: 1529–1539.
32. Barak O, Lazzaro MA, Lane WS, Speicher DW, Picketts DJ, Shiekhattar R (2003) Isolation of human NURF: a regulator of Engrailed gene expression. *EMBO J* 22: 6089–6100.
33. Varga-Weisz PD, Wilm M, Bonte E, Dumas K, Mann M, Becker PB (1997) Chromatin-remodelling factor CHRAC contains the ATPases ISWI and topoisomerase II. *Nature* 388: 598–602.
34. Guschin D, Geiman TM, Kikyo N, Tremethick DJ, Wolffe AP, Wade PA (2000) Multiple ISWI ATPase complexes from *Xenopus laevis*. Functional conservation of an ACF/CHRAC homolog. *J Biol Chem* 275: 35248–35255.
35. Tsukiyama T, Palmer J, Landel CC, Shiloach J, Wu C (1999) Characterization of the imitation switch subfamily of ATP-dependent chromatin-remodeling factors in *Saccharomyces cerevisiae*. *Genes Dev* 13: 686–697.
36. Lu X, Meng X, Morris CA, Keating MT (1998) A novel human gene, WSTF, is deleted in Williams syndrome. *Genomics* 54: 241–249.
37. Fyodorov DV, Kadonaga JT (2002) Binding of Acf1 to DNA involves a WAC motif and is important for ACF-mediated chromatin assembly. *Mol Cell Biol* 22: 6344–6353.

38. Tamkun JW, Deuring R, Scott MP, Kissinger M, Pattatucci AM, Kaufman TC, Kennison JA (1992) Brahma: a regulator of *Drosophila* homeotic genes structurally related to the yeast transcriptional activator SNF2/SWI2. *Cell* 68: 561–572.
39. Eberharter A, Vetter I, Ferreira R, Becker PB (2004) ACF1 improves the effectiveness of nucleosome mobilization by ISWI through PHD-histone contacts. *EMBO J* 23: 4029–4039.
40. Doerks T, Copley R, Bork P (2001) DDT — a novel domain in different transcription and chromosome remodeling factors. *Trends Biochem Sci* 26: 145–146.
41. Jones MH, Hamana N, Nezu J, Shimane M (2000) A novel family of bromodomain genes. *Genomics* 63: 40–45.
42. Boyer LA, Langer MR, Crowley KA, Tan S, Denu JM, Peterson CL (2002) Essential role for the SANT domain in the functioning of multiple chromatin remodeling enzymes. *Mol Cell* 10: 935–942.
43. Ogata K, Hojo H, Aimoto S, Nakai T, Nakamura H, Sarai A, Ishii S, Nishimura Y (1992) Solution structure of a DNA-binding unit of Myb: a helix-turn-helix-related motif with conserved tryptophans forming a hydrophobic core. *Proc Natl Acad Sci USA* 89: 6428–6432.
44. Eberharter A, Ferrari S, Langst G, Straub T, Imhof A, Varga-Weisz P, Wilm M, Becker PB (2001) Acf1, the largest subunit of CHRAC, regulates ISWI-induced nucleosome remodelling. *EMBO J* 20: 3781–3788.
45. Collins N, Poot RA, Kukimoto I, Garcia-Jimenez C, Dellaire G, Varga-Weisz PD (2002) An ACF1-ISWI chromatin-remodeling complex is required for DNA replication through heterochromatin. *Nat Genet* 32: 627–632.
46. Nakano H, Yoshida T, Uchiyama S, Kawachi M, Matsuo H, Kato T, Ohshima A, Yamaichi Y, Honda T, Kato H, Yamagata Y, Ohkubo T, Kobayashi Y (2003) Structure and binding mode of a ribosome recycling factor (RRF) from mesophilic bacterium. *J Biol Chem* 278: 3427–3436.

16 Dynamic and Functional Analysis of Chromosomal Proteins

Nobuko Ohmido, Susumu Uchiyama, Sachihiro Matsunaga, Masatoshi Nakagawa, Takachika Azuma and Kiichi Fukui*

CONTENTS

16.1 Introduction 217
16.2 Development of the Screening Methods for Chromosomal Proteins 218
16.2.1 Localization Analysis Using Human Fixed Cells, Chromosome Spreads and Isolated Chromosomes 218
16.2.2 Comparison of the Three Methods Using Chromosome Scaffold Proteins 219
16.2.3 Production of Polyclonal Antibodies against Ribosomal Protein S6 221
16.2.4 Characterization of the Antibodies against Ribosomal Protein S6 222
16.3 Localization of Chromosomal Proteins 223
16.4 Dynamics of the Chromosomal Protein FtsJ Homolog 3 224
16.4.1 Immunodetection of FtsJ Homolog 3 226
16.4.2 Function of FtsJ Homolog 3 226
16.5 Conclusions 227
Acknowledgment 228
References 228

16.1 INTRODUCTION

Chromosome formation during mitosis ensures the equal and appropriate segregation of genomic information provided by DNA, with modifications, into two daughter cells. Chromosomes are highly compacted and the component chromosomal proteins are mainly composed of histone (H1, 2A, 2B, 3, 4) and nonhistone protein

*To whom correspondence should be addressed.

(topoisomerase IIα and structural maintenance of chromosome) [1,2]. The organization of chromosome requires harmony between efficient compaction and accessibility of its genetic information. Chromosomes both of histone and nonhistone proteins contribute to mitotic chromosome formation and its dynamics. For years, biochemical and morphological studies have been extensively performed to elucidate chromosome function and structure. Since human genome analysis and mass spectrometry techniques for protein identification are now both well advanced, proteome analysis has become a powerful tool for discovery-driven research. Furthermore, chromosomes are the repositories of the genetic information and biochemical machinery; many researchers have great interest in chromosomes as source material for proteomic studies.

To identify the functional components of human chromosome condensation, dynamic and localization analyses are carried on proteins that have been newly revealed as chromosomal proteins by proteome analysis of human metaphase chromosomes. It is still not well understood which proteins really contribute to the higher-order structure and actual function of human chromosomes. To understand which proteins are significant in chromosome higher-order structure, proteome analyses of isolated human chromosomes were carried out [3,4]. Gassmann et al. [4] initiated a proteomic screening of the chromosome scaffold fraction. Their screening identified 79 proteins, 30 of which had not previously been described as components of mitotic chromosomes. Uchiyama et al. [3] had analyzed isolated human metaphase chromosomes using the proteomic method in order to examine the protein framework and thereby understand the higher-order structure. As a result, a list of 107 proteins was obtained which were considered to be related to chromosome structure. In this study, we have obtained polyclonal antibodies against the candidate proteins and performed localization and dynamic analyses to identify the contribution of these specific proteins in forming the higher-order chromosomal structure in human cells.

16.2 DEVELOPMENT OF THE SCREENING METHODS FOR CHROMOSOMAL PROTEINS

16.2.1 Localization Analysis Using Human Fixed Cells, Chromosome Spreads and Isolated Chromosomes

To analyze the localization of proteins identified in the proteome study using human metaphase chromosomes [3], we have examined three immunolocalization methods using three different preparation methods: fixed cells, spread chromosomes and isolated chromosomes. HeLa S3 cells were grown on poly-l-lysine–coated glass coverslips in RPMI1640 (Nacalai Tesque) supplemented with 10% fetal calf serum (Gibco BRL) and 1% penicillin-streptomycin (Gibco BRL), at 37°C in a 5% CO_2 incubator for 3 days. Then, after washing with PBS, the cells were fixed with 2% PFA/XBE2 (paraformaldehyde/10 m*M* HEPES, pH 7.6, 2 m*M* $MgCl_2$, 100 m*M* KCl, 5 m*M* EGTA). The spread chromosomes were prepared using the method described by Ono et al. [2]. Spread chromosomes prepared from cells cultured

for 3 days, with high cell-proliferating activity, were synchronized by 0.1 μg/mL colcemid at 37°C for 3 h to induce accumulation in metaphase. Cells were treated with hypotonic 75 m*M* KCl for 15 min and were centrifuged. Isolated mitotic chromosomes were prepared from a synchronized human cell line (BALL-1) using the polyamine procedure, and metaphase chromosomes were purified using the glycerol and Percoll density gradient method described by Uchiyama et al. [3].

The indirect-immunofluorescence method using HeLa cells was applied following the procedure of Maeshima and Laemmli [5], with minor modifications. After washing the coverslips with PBS, the cell/chromosome samples were incubated in 0.5 mg/mL $NaBH_2$ in XBE2 for 5 min and washed in XBE2 (two times for 5 min each wash). Permeabilization was carried out by the addition of 0.5% Triton X-100 in XBE2 buffer at room temperature. After washing in XBE2 (two times for 5 min each wash), cell samples were fixed with 2% PFA/XBE2 for 15 min. The HeLa cells on the coverslips were then incubated for 60 min with 10 μg/μL in 3% BSA/XBE2 of the purified antipeptide antibodies (Abs; diluted 1:100 in XBE2 containing 1% BSA, 0.05% Tween 20). After washing five times with XBE2, the coverslips were incubated for 60 min with FITC-labeled secondary goat anti-rabbit IgG Abs (Sigma) (1:200 in XBE2 containing 1% BSA, 0.05% Tween 20) to detect bound rabbit Abs. The coverslips were again washed in XBE2 (six times for 5 min each wash) and the slides were then embedded in Vectashield containing 1 μg/mL DAPI.

The fluorescent images were obtained using a fluorescence microscope, BX60 (Olympus) equipped with a CCD camera (PXL 1400, Photometrics). The B- or UV-light excitation filters were used for the excitation of FITC and DAPI, respectively. Captured images were digitally stored on a Macintosh computer and analyzed using imaging software (Photoshop 7.0, Adobe).

16.2.2 Comparison of the Three Methods Using Chromosome Scaffold Proteins

Immunolocalization of Topoisomerase IIα (TopoIIα, monoclonal antibody from TopoGEN) was employed to characterize the three different methods of preparation of the HeLa S3 cells (Figure 16.1). Topo II catalyzes transient breakage and reunion of double-stranded DNA, and was the first protein shown to be essential for mitotic chromosome condensation [6]. A role for Topo II in the structural maintenance of mitotic chromosomes has been suggested on the basis of the finding that Topo II is a major protein constituent of the chromosome scaffold [7,8]. In previous reports on the immunolocalization of anti-Topo IIα antibodies, Topo IIα was described as being enriched in an axial structure within uncondensed and condensed chromatin [9]. Topo IIα and condensin are both required for mitotic chromosome assembly [5], and they constitute the two main components of the chromosomal scaffold on histone-depleted chromosomes.

In this study, anti-Topo IIα antibody was found to be localized in a "beads on a string"-like distribution in the axial region of the spread and isolated chromosomes (Figure 16.1). The axial localization is, however, not clear in the case of intact cells, because the chromosomes are not well elongated in the cell. The results here of the

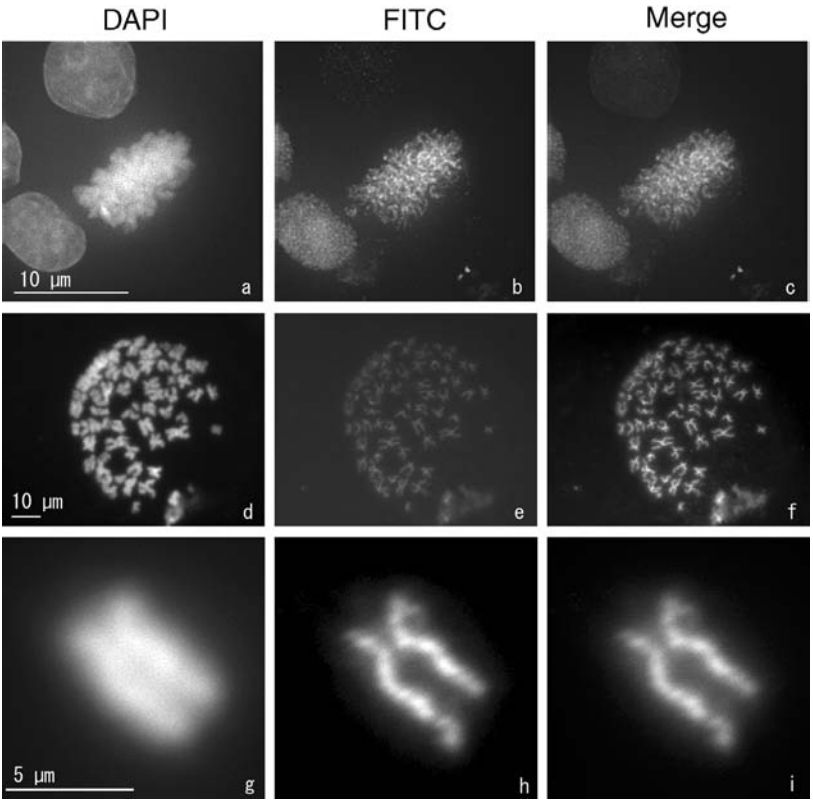

FIGURE 16.1 (**See color insert following page 110**) Immunofluorescence signals of a chromosome structural protein, Topoisomerase IIα, using three different preparation methods. The DAPI and FITC images show counterstain and immunofluorescent signals in the left and middle columns, respectively, and the right column is a merged image of the two images. (a–c) Fixed cells, (d–f) chromosome spreads, (g–i) isolated chromosome.

chromosomal localization of Topo IIα, using the preparation methods of spread chromosomes and isolated chromosomes, are consistent with those of previous reports. Strong fluorescence signals were detected with both of these methods.

These three preparation methods are efficient for the examination of protein localization, and immunostaining of antibodies in fixed HeLa cells can be representative of *in vivo* conditions. However, if the antigen exists both in the nucleus and cytoplasm, and if its localization is ambiguous or if the affinity of the antigen for the antibody is weak, cytoplasmic components can seriously interfere with detection of the signals. Immunolocalization using isolated chromosomes would therefore provide more precise positioning of the protein. In this study, we generally used fixed cells as well as spread and isolated chromosomes for immunolocalization of antibodies; the signals thus detected should provide precise evidence for protein localization on chromosomes and/or in cells.

16.2.3 Production of Polyclonal Antibodies against Ribosomal Protein S6

Antipeptide antibodies (Abs) made by immunizing with peptides consisting of 15 amino acid residues were prepared and were examined for their relative reactivity between peptide and protein. Human S6 ribosomal protein was thus examined on the basis of its reactivity with Abs prepared by immunizing rabbits with synthetic peptides. Five peptides corresponding to the segments Ser6-Asp20 (S6-1), Ile52-Gly66 (S6-2), Asp103-Gly117 (S6-3), Asn146-Lys160 (S6-4) and Arg178-Ile192 (S6-5) were chosen as epitopes of human ribosomal S6 protein. The characteristics of the peptides are shown in Table 16.1. These Abs were bound with cysteine at N- and/or C-terminal domains. For immunization and purification, the peptide-BSA conjugates were emulsified with complete Freund's adjuvant and administered to the rabbits by subcutaneous injection, and this was followed by booster immunizations on days 14, 28 and 56. At 9 weeks post-immunization, the anti-BSA Abs were isolated using a BSA-bound Sepharose column and the flow-through fractions were used for analysis.

To select the most effective epitopes for the anti-S6 polyclonal antibodies, immunostaining was carried for the three types of preparations. When S6-4 antibody was used in fixed cells, bright immunofluorescent signals were observed in the cytoplasm. In addition, immunofluorescence signals of S6-4N and S6-4C were detected in cell nucleoli (Figure 16.2). Immunolocalization with the S6-1, S6-2, S6-3 and S6-5 antibodies was difficult to determine due to the weak signals obtained (data not shown). Characteristics of the anti-S6 antibodies differed according to the different terminal-labeling methods used, i.e., immunofluorescent signals from S6-4N, S6-4C and S6-4NC antibodies used in fixed cells were observed in the cytoplasm. The signals from S6-4 antibody were the brightest, and those from the other antibodies were very weak. S6-4NC antibody signal was as bright as S6-4C antibody (Figure 16.2[e,f,h,i]) and also was comparable in fluorescence intensity to S6-4NC. The immunofluorescent intensities in fixed cells were quantified as values relative to the average value of S6-4C. The fluorescence intensity of S6-4N antibody was comparatively low (Figure 16.2[b,c]); however, the fluorescence intensity of S6-4N in fixed cells at mitosis was similar

TABLE 16.1
Epitope Sequences for the Antipeptide Antibodies against S6 Ribosomal Protein

ID	Characterization	Amino Acid Sequence
S6-1	Eukaryotic-specific regions	SFPATGCQKLIEVDD
S6-2	S6 ribosomal protein-specific region	ISGGNDKQGFPMKQG
S6-3	Loop structure	DANLSVLNLVIVKKG
S6-4	Homologous region among species	NLSKEDDVRQYVVRK
S6-5	Nucleotransportation signal-specific region	RLVTPRVLQHKRRRI

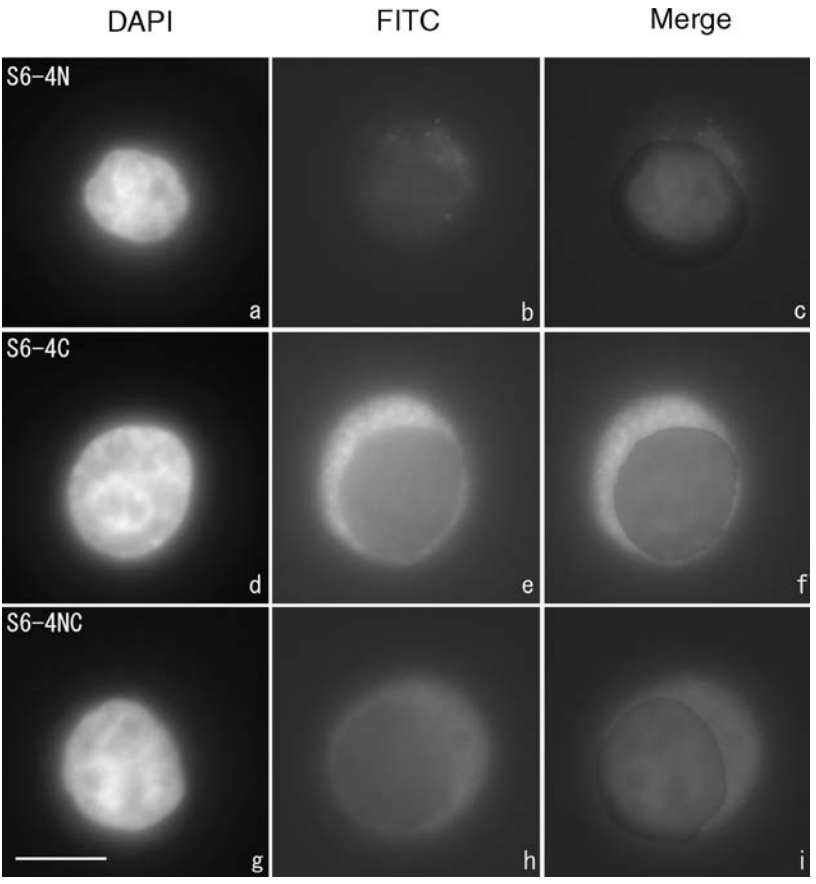

FIGURE 16.2 (**See color insert following page 110**) Immunofluorescence signals in the fixed cells using antibodies against S6-4 ribosomal protein. C and N indicate the position of the cysteine. Bright signals were detected in the cytoplasm. Bar = 10 μm.

to that of S6-4NC. The S6-4 antibodies, especially S6-4C, have highest affinity for the antigen. Therefore, it is concluded that the selection of epitope would be important as well as the site of the cysteine conjugation residue. Weak signals were also observed in the cytoplasm after immunostaining with S6-1, S6-2, S6-3, S6-4 and S6-5 antibodies using the spread chromosomes (data not shown).

16.2.4 Characterization of the Antibodies against Ribosomal Protein S6

Intense fluorescent signals were observed in the cytoplasm of intact HeLa cells immunostained with S6-4 of NLSKEDDVRQYVVRK (Table 16.1, Figure 16.2). In the fixed cells, the fluorescence intensity level of S6-4 antibodies as measured

by CCD camera was high. These results suggested that selection of appropriate peptide as epitope is the most important aspect in developing an effective monoclonal antibody. Thus, sequence of S6 ribosomal protein that is homologous across species is appropriate to use for antibodies for immunostaining. The homologous sequences of S6 ribosomal protein were localized on the surface of the calculated three-dimensional structure. The peptides of the homologous sequences would also be significant epitopes and would be important for the function of S6 ribosomal protein.

Jimenez-Garcia et al. [10] reported that S6 protein localized in the nucleoli, cytoplasm and coiled body at the interphase stage. The cytoplasmic localization of S6 protein is observed from prophase to anaphase. In this study, S6 localization in the chromosomal spreads was consistent with that in the previous report; however, in interphase cells, S6 localization was different from that in the previous study (Figure 16.2). The eukaryotic ribosome consists of 60S and 40S subunits, and S6 ribosomal protein contributes to protein synthesis as a component of the 40S subunit [11,12]. Since S6 protein is abundant in the cell, the binding of Abs to this protein was expected to be easily visualized by immunostaining. These data suggest that no localization was observed in nucleoli in the fixed cells because of lower affinity arising from the effects of the cytoplasm.

16.3 LOCALIZATION OF CHROMOSOMAL PROTEINS

The localization in the cell of proteins previously identified in metaphase chromosomes by proteome analysis [3] was investigated. We produced polyclonal antibodies against these proteins and performed immunofluorescent staining using the three types of chromosome samples from HeLa S3 cells. The primary antibodies and antiserum used were anti-RBMX, hSNF2H, Ki-67, HMGN, HMGA1, nucleophosmin (B23), BIP, AAA-ATPase TOB3, HP, RRS1, SSRP1, RNA helicase like-1 and transcription factor 6 (TCF6L) (Santa Cruz Biotechnology, Inc., Santa Cruz, CA, U.S.A.) 1:1000. Anti-hCAP-E and FtsJ homolog 3 antibodies were also prepared, as described in the procedure for S6 ribosomal proteins.

Anti-hCAP-E, anti-hSNF2H and anti-human kinesin superfamily protein member 4 (KIF4) antibodies, which were the antibodies against the proteins classified as chromosome structural proteins [3], were examined for their localization using isolated human metaphase chromosomes (KIF4; Figure 16.3). In the previous study [13], it was revealed that KIF4 is a chromokinesin that binds to chromosomes. Since several kinds of kinesin localize at the midzone (also known as the central spindle), and/or the midbody that connects two daughter cells, this suggests their involvement in cell division. Anti-hCAP-E as well as anti-TopoIIα localized on the axis of chromatids. Although anti-hSNF2H (H) showed dot-like signals, anti-hSNF2H (C) was not detected on the chromosome.

B23 (nucleophosmin), Ki-67 and RBMX are classified as chromosome peripheral proteins. B23 and Ki-67 were localized in perichromosomal regions. B23 is a nucleolar phosphoprotein [14,15], and has been shown to bind to nucleic acids, to digest pre-rRNA and to be localized in nucleolar granular components from which

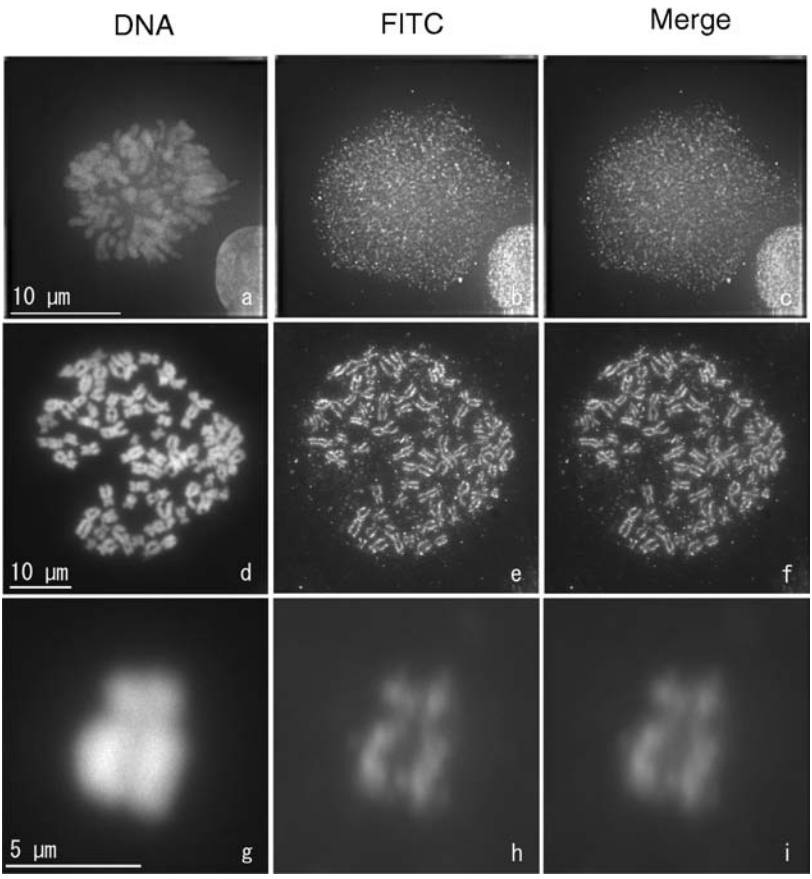

FIGURE 16.3 (**See color insert following page 110**) Immunofluorescence signals from antibody against KIF4 protein, using the three types of chromosomal preparation. Bright signals were detected on the chromosome. (a–c) Fixed cell, (d–f) chromosome spreads, (g–i) isolated chromosome.

preribosomal particles are transported to the cytoplasm. The intracellular localization of B23 changes significantly during the cell cycle. In this study, immunofluorescent signals of RBMX and FtsJ homolog 3 were localized at the peripheral regions of the sister chromatids and isolated metaphase chromosomes.

16.4 DYNAMICS OF THE CHROMOSOMAL PROTEIN FTSJ HOMOLOG 3

FtsJ homolog 3, known to be associated with chromosomes [3], is shown to localize at a peripheral region of the chromosomes, and strong signals on the isolated chromosomes were detected by immunostaining. To study the function of FtsJ

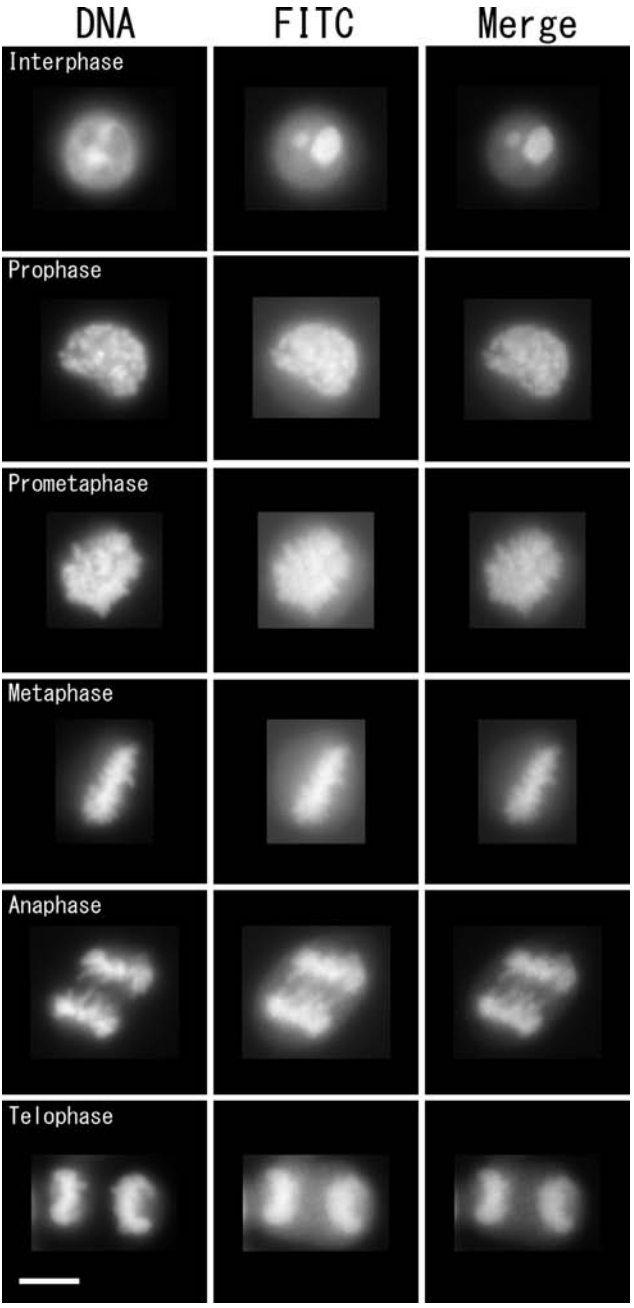

FIGURE 16.4 Differences in localization of immunofluorescence signals from FtsJ homolog 3 through the mitotic stages, using antibodies against FtsJ homolog 3, Lys579-Lys593 (peptide no. 3) and fixed HeLa S3 cells. Bar = 5 μm.

homolog 3 in human cells, we examined its localization at each cell stage and carried out RNA interference assays. Ftsj is a well-conserved protein from bacteria through to humans [16], and Ftsj methylates 23S rRNA within 50S ribosomal subunits, both *in vitro* and *in vivo*. The *ftsj* gene encoding the 209 amino acid protein was originally identified by Ogura et al. [17]. Null mutations of *ftsj* result in a dramatically altered ribosome profile, a severe growth disadvantage, and a temperature-sensitive phenotype [18].

16.4.1 Immunodetection of FtsJ Homolog 3

We generated polyclonal antibodies against FtsJ homolog 3 and performed immunofluorescent staining according to the protocol described above. Anti-FtsJ homolog 3 rabbit polyclonal antibodies and secondary antibody, anti-rabbit IgG FITC (Sigma), were used for detection.

Immunolocalization of FtsJ homolog 3 after indirect immunofluorescent staining for a whole cell cycle (Figure 16.4) showed that the localization of FtsJ homolog 3 changed during mitosis. Fluorescent signals were particularly observed in the nucleoli in interphase, and the localization moved to chromosomes from prophase to telophase. FtsJ homolog 3 was localized to chromosome peripheral regions in the isolated chromosomes and spread chromosome samples (Figure 16.5a–c). Our data for FtsJ homolog 3 regarding chromosomal localization and aberration of siRNA suggest that FtsJ homolog 3 might also have certain functions related to chromosomes during the cell cycle.

16.4.2 Function of FtsJ Homolog 3

Ftsj encodes a ribosomal RNA methyltransferase and its sequence is largely conserved from bacteria to humans. It is also known to be related to cell growth and the ribosome profile in *Escherichia coli*. Ching et al. [16] reported the cloning of human FtsJ homolog 2 (*ftsj2*), a human gene encoding a putative RNA methyltransferase. Northern blot analysis revealed that FTSJ2 transcripts are abundant in skeletal muscle, placenta, and heart, as well as in cancer cells. Immunofluorescence staining demonstrated that FTSJ2 protein localized at the nucleolus. They suggested that FTSJ2 is likely to be a nucleolar RNA methyltransferase involved in eukaryotic RNA processing and modification.

The siRNA sequence for FtsJ homolog 3 was designed as 5'-UCAUAGAUAACUCCUUCAATT-3'. HeLa cells were transfected with siRNA for FtsJ homolog 3, and 48 h later were fixed with 4% PFA and counterstained with Hoechst 33342. Knockdown of FtsJ homolog 3 induced unsuccessful chromosome alignment (Figure 16.5d), and the mitotic index of FtsJ homolog 3-knockdown cells increased by 1% compared with that of the control. The metaphase cells among the mitotic cells in the control comprised 6%, but the ratio in the knockdown cells was increased to approximately 60%. Misaligned chromosomes were also observed in approximately 8% of mitotic cells, whereas almost no misaligned chromosomes were observed in the control cells. FtsJ deletion was found to result in a growth

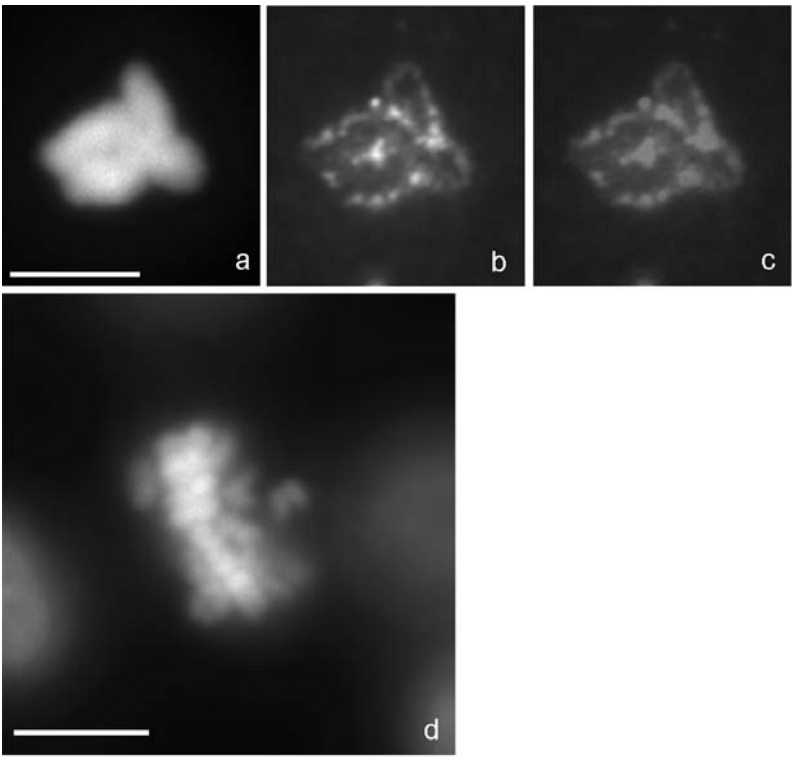

FIGURE 16.5 (**See color insert following page 110**) Immunolocalization of FtsJ homolog 3 on the isolated metaphase chromosomes. (a–c) The antibodies for FtsJ homolog 3 showed that FtsJ homolog 3 localized at the peripheral regions of the chromosome. Bar = 5 μm. (d) Chromosomes stained with Hoechst 33342 after treatment with small interfering RNAs (siRNAs). Knockdown of FtsJ homolog 3 induced "misaligned chromosomes" in mitosis. Bar = 10 μm.

defect and altered ribosome profile in *E. coli* [18,19]. The localization of FtsJ homolog 3 at nucleoli is consistent with the previous report that FtsJ homolog 3 might also be related to the functions of precise chromosomal division and ribosomal RNA methylation [18].

16.5 CONCLUSIONS

In this research, various Abs were prepared from rabbits using synthetic peptides possessing amino acid sequences of a human S6 ribosomal protein. Comparison of their reactivity based on the peptide sequences by immunostaining using the three preparation methods (fixed cell, chromosome spread by conventional hypotonic treatments, and isolated chromosomes) revealed that the three preparation methods are efficient for the localization of new chromosomal proteins.

We surveyed the various antibodies against the candidate proteins for their localization throughout the cell cycle, via indirect immunofluorescence analysis. Several proteins were identified as chromosomal proteins using the specific peptide antibodies and siRNA. As a result, down-regulation of FtsJ homolog 3 localized on chromosomes in the mitotic stages was performed, and promoted chromosomal aberration. Therefore, our study suggests that FtsJ homolog 3 might be a functional protein for chromosome organization and segregation through the human cell cycle.

ACKNOWLEDGMENT

This study was supported by Special Coordination Funds of the Ministry of Education, Culture Sports, Sciences and Technology of the Japanese government.

REFERENCES

1. Sumner AT (1996) The distribution of topoisomerase II on mammalian chromosomes. *Chromosome Res* 4: 5–14.
2. Ono T, Losada A, Hirano M, Myers MP, Neuwald AF, Hirano T (2003) Differential contributions of Condensin I and Condensin II to mitotic chromosome architecture in vertebrate cells. *Cell* 115: 109–121.
3. Uchiyama S, Kobayashi S, Takata H, Ishihara T, Hori N, Higashi T, Hayashihara K, Sone T, Higo D, Nirasawa T, Takao T, Matsunaga S, Fukui K (2005) Proteome analysis of human metaphase chromosomes. *J Biol Chem* 280: 16994–17004.
4 Gassmann R, Henzing AJ, Earnshaw WC (2005) Novel components of human mitotic chromosomes identified by proteomic analysis of the chromosome scaffold fraction. *Chromosoma* 113: 385–397.
5. Maeshima K, Laemmli UK (2003) A two-step scaffolding model for mitotic chromosome assembly. *Dev Cell* 4: 467–480.
6. Uemura T, Ohkura H, Adachi Y, Morino K, Shiozaki K, Yanagida M (1987) DNA topoisomerase II is required for condensation and separation of mitotic chromosomes in *S. pombe*. *Cell* 50: 917–925.
7. Earnshaw WC, Halligan B, Cooke CA, Heck MMS, Liu LF (1985) Topoisomerase II is a structural component of mitotic chromosome scaffolds. *J Cell Biol* 100: 1706–1715.
8. Gasser SM, Laroche T, Falquet J, Boy de la Tour E, Laemmli UK (1986) Metaphase chromosome structure. Involvement of topoisomerase II. *J Mol Biol* 188: 613–629.
9. Cuvier O, Hirano T (2003) A role of topoisomerase II in linking DNA replication to chromosome condensation. *J Cell Biol* 160: 645–655.
10. Jimenez-Garcia LF, Segura-Valdez ML, Ochs RL, Rothblum LI, Hannan R, Spector DL (1994) Nucleologenesis: U3 snRNA-containing prenucleolar bodies move to sites of active pre-rRNA transcription after mitosis. *Mol Cell Biol* 5: 955–966.
11. Schmidt C, Lipsius E, Kruppa J (1995) Nuclear and nucleolar targeting of human ribosomal protein S6. *Mol Cell Biol* 6: 1875–1885.
12. Brodersen DE, Clemons WM Jr, Carter AP, Wimberly BT, Ramakrishnan V (2002) Crystal structure of the 30 S ribosomal subunit from *Thermus thermophilus*: structure of the proteins and their interactions with 16 S RNA. *J Mol Biol* 316: 725–768.

13. Lee YM, Kim W (2004) Kinesin superfamily protein member 4 (KIF4) is localized to midzone and midbody in dividing cells. *Exp Mol Med* 36:93–97.
14. Dundr M, Misteli T, Olson MO (2000) The dynamics of postmitotic reassembly of the nucleolus. *J Cell Biol* 150: 433–446.
15. Okuwaki M, Tsujimoto M, Nagata K (2002) The RNA binding activity of a ribosome biogenesis factor, nucleophosmin/B23, is modulated by phosphorylation with a cell cycle-dependent kinase and by association with its subtype. *Mol Biol Cell* 13: 2016–2030.
16. Ching YP, Zhou HJ, Yuan JG, Qiang BQ, Kung HF, Jin DY (2002) Identification and characterization of FTSJ2, a novel human nucleolar protein homologous to bacterial ribosomal RNA methyltransferase. *Genomics* 79: 2–6.
17. Ogura T, Tomoyasu T, Yuki T, Morimura S, Begg KJ, Donachie WD, Mori H, Niki H, Hiraga S (1991) Structure and function of the ftsH gene in *Escherichia coli*. *Res Microbiol* 142: 279–282.
18. Bügl H, Fauman EB, Staker BL, Zheng F, Kushner SR, Saper MA, Bardwell JC, Jakob U (2000) RNA methylation under heat shock control. *Mol Cell* 6: 349–360.
19. Caldas T, Binet E, Bouloc P, Costa A, Desgres J, Richarme G (2000) The FtsJ/RrmJ heat shock protein of *Escherichia coli* is a 23 S ribosomal RNA methyltransferase. *J Biol Chem* 275: 16414–16419.

17 Development of a Sustainable Chromosome Imaging Database

Kenji Taniguchi, Chiharu Mitsueda, Naho Okumura and Wakako Miyazaki*

CONTENTS

17.1 Introduction 231
17.2 A New Chromosome Image Database 232
17.2.1 Principle 232
17.2.2 Architecture 234
17.2.3 Registration of Images 235
17.3 Features of the Image Database 236
17.3.1 Features of the Database 237
17.3.2 Registration of Images 240
17.3.2.1 Uploading Images 240
17.3.2.2 Annotation to Upload Image 240
17.3.2.3 Search 241
17.3.2.4 Contacting "CILib" 241
17.4 Future Prospects 242
17.5 Conclusion 242
Acknowledgments 242
References 243

17.1 INTRODUCTION

Various databases are constructed according to desired purposes, or due to necessity, in all biological fields. In the life sciences, there are many databases [1–3] for DNA, proteins, or for the chemical structures and classification of various biomolecules. For the chromosomes, containing many genes, advanced databases

* To whom correspondence should be addressed.

for mapping the genes of chromosomes of various species (e.g., humans [4], nematode [5], *Arabidopsis* [6]) have already been created. On the other hand, for a large number of species, only limited information such as the chromosome number has been released [7,8]. For this reason, we have now designed a chromosome imaging database system in order to assist chromosome researchers as well as researchers in other biological fields.

17.2 A NEW CHROMOSOME IMAGE DATABASE

We have developed an imaging database that we named the "Chromosome Image Library" (or CILib). Recently, the application of genetic information has become increasingly necessary in the life sciences. The necessity for information with regard to these chromosomes as a storage box of genes is also increasing rapidly. As an example, if information is available on whether a target plant is polyploid, autopolyploid, or allopolyploid, or where the target gene is located on the chromosome, then this is of great benefit to the researchers utilizing these genes. However, due to the inadequacies of current chromosome databases, researchers from other fields face difficulties in systematically or easily acquiring information regarding chromosomes. Thus, we have designed a database system for collecting images from a broad range, and in large quantities, in a short period of time.

17.2.1 Principle

There are three types of systems for collecting information in an image database (Figure 17.1). The contents of the database are assembled by the administrator alone in System A, by both the administrator and the designated users in System

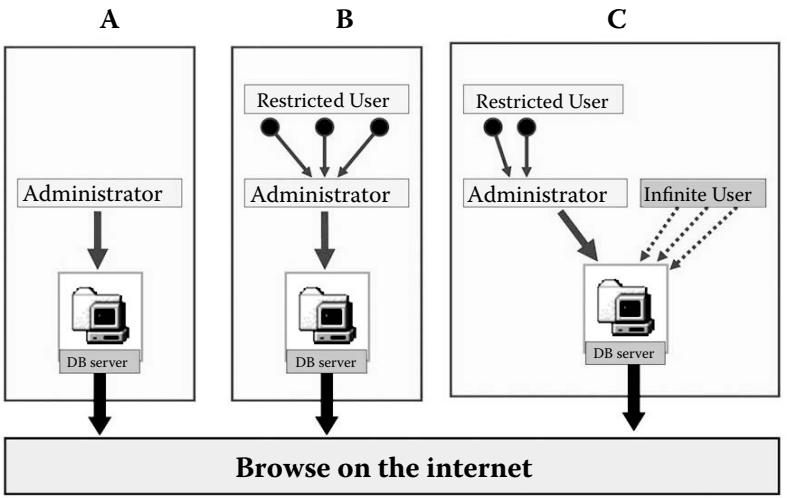

FIGURE 17.1 Three types (A, B, C) of systems in image databases for collecting information. These types are characterized by registration of "Infinite Users" or "Restricted User(s)."

B, and by both the administrator and the general public users in System C. Most scientific image databases are either of the type of System A or B, while System C is rarely used in a scientific setting. The goal of a database is to collect more, exact information, and over a wider range. Systems A and B are very effective for collecting exact information, while they are not the most effective for collecting more information or a wider range of information. On the other hand, System C has a low capacity for collecting exact information, while it is capable of effectively collecting more information and a wider range of information. Examples of the scientific success of System C are remarkably restricted to only the database on DNA sequences [1–3] and the free encyclopedia *Wikipedia* [9], because the C-type database has the defects of including much information, both useful and non-useful or even incorrect, from a diverse group of unspecified users. However, since we gave priority to System C due to the advantage of being able to collect extraordinary amounts of information, we decided to adopt System C and to design a new overall system that could compensate for such faults of System C.

The citation of papers is usually performed through the noting of copyright, but the citation of an image requires the author's permission. The release of images on the Web is therefore faced with a substantial barrier. Original images registered by the administrators of Systems A and B are released with copyright. However, registration of other images is accompanied by very large copyright problems, requiring the permission of the author and/or the publishing company. These processes call for a lot of work.

On the other hand, our system has three kinds of image sources (Figure 17.2): the original images registered by the user, images obtained from our e-journal and images from other journals that had been previously published. In the first two

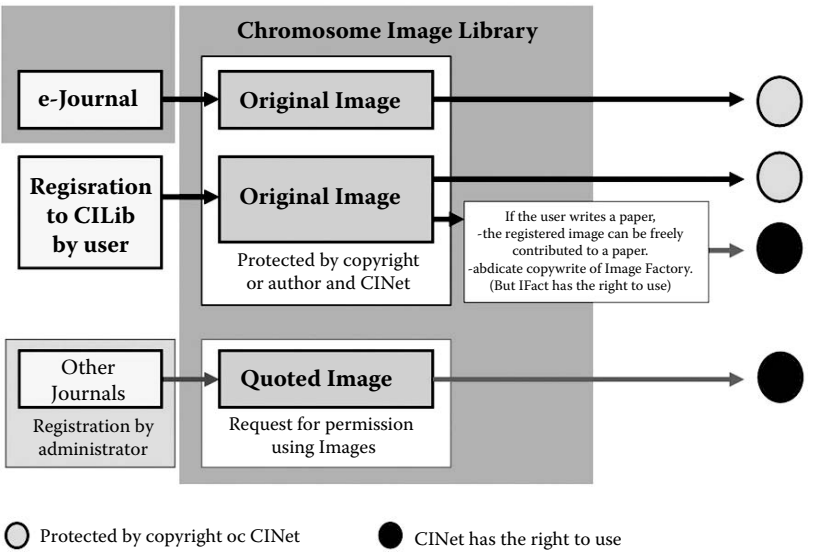

FIGURE 17.2 Solution for the copyright problems incorporated into CILib.

cases, because the users or administrators own the copyrights for all the images collected by them, we are released from this problem. On the other hand, the last case requires permission for registration; but this registration will not impose a substantial problem for us because the proportion of occurrences of images from this group is relatively low. If the user wishes to contribute the registered image to other journals, so far as the right to continue publishing the image in our system is protected, our system will abandon copyright.

17.2.2 Architecture

The device for a user to be able to positively participate and further improve the quality of registered images was designed during the construction of the database system (Chromosome Information Network [CINet] [10]) based on the C-type system shown in Figure 17.1. It will correct a fault of the chromosome image database (the CILib) by organically correlating the four Web sites of (1) the technical manual on chromosomes (Chromosome Techniques), (2) the link of chromosomes and genes (Chromosome and Gene Link), (3) the e-journal (Chromosome Letters) and (4) the personal databases (Figure 17.3). The features of the CINet are as follows.

Chromosome Image Library: The contents of the database are created by the general public users and our administrators. It consists of both personal Web sites as well as search Web sites. The former is a private site only used by the personal user that includes three sub-sites: an upload site for the user's images, an input site for annotating the user's images and a personal viewer site for the user's personal images and information. Each sub-site except for the upload site then includes three thumbnail

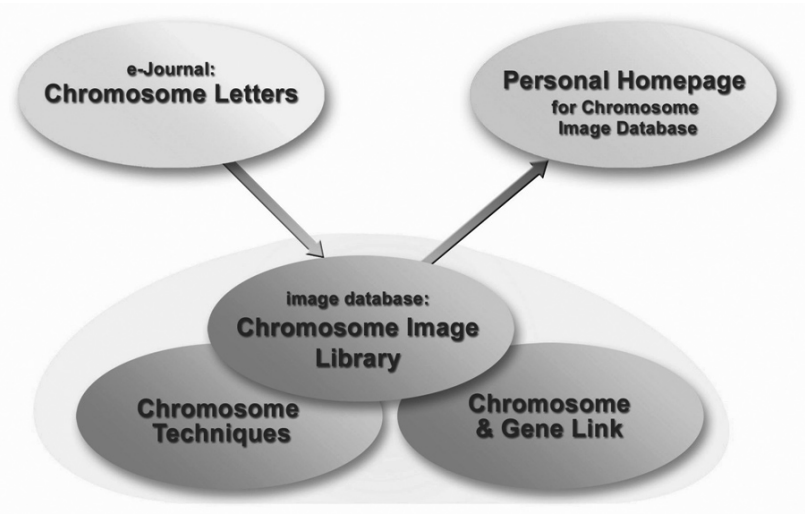

FIGURE 17.3 Component of the Chromosome Information Network (CINet) system to which the registration of high-definition image by as many users as possible is urged. CINet can be accessed at the following URL: http://cilib.sci.hiroshima-u.ac.jp/hiroshima.

pages, a handy entry page, and a full entry page. For the handy entry page, the question of how to effectively annotate multiple images was taken into consideration, and it was subsequently designed so that the user would fill in the annotation with a table style.

Chromosome and Gene Link (CGLink): The contents of this Web site are created by the administrator. The representative chromosomes in each species are chosen from the chromosome images stained with Orcein, Giemsa, etc., which had been registered in the CILib, and the selected image is set as a standard karyotype. Next, the chromosome arms of the image are measured and the chromosome information is recorded onto the CSV file. Finally, based on the record, an idiogram is framed [11]; furthermore, other new idiograms mapping various banding patterns, protein information, and gene information on the idiogram of this standard karyotype are added. These idiograms are also measured from the images registered in the CILib as for the case of the standard karyotype, and these records are registered as the CSV file. The instructions for drawing the idiogram to the CGLink site are under registration now.

Chromosome Techniques (CTech): The contents of this Web site are created by the administrator alone, and various types of staining methods [11] are included. The manuscripts are submitted by the chromosome researchers and commissioned by the administrator. Preparations and staining methods for the chromosomes registered on CILib will be submitted with text and image files, and they will be displayed on the Web screen.

Publication of e-Journals (Chromosome Letters; CLet): The Web site performs an important role in collecting original chromosome images of high quality. A manuscript is submitted electronically via the Web or with the use of compact disks. The manuscript and electronic files are reviewed by the editor and, if correct and complete, are displayed on the Web site for Chromosome Letters. If incorrect and incomplete, then it will be revised by the reviser on the Web site. In addition, the chromosome images displayed on CLet will be automatically registered to CILib.

Personal Homepage: When the user has a lot of image data, the user may hope to open his/her images or request to open them. However, if the user attempts to open his/her own database, he/she will have to go through a lot of effort. If user wishes to open his/her own image collection on the Web site, then CILib will support in opening a personal home page. The personal database is a system that is appropriated from the CILib system, and is made by the user for opening public images except for private images.

17.2.3 Registration of Images

Types of chromosome images that chromosome investigators possess are film images, digital images and images from paper. CILib has ways of implementing the following four techniques:

1. Direct registration by the user on the Web
2. Trust Data Registration Support (to convert the film images into digital images: a large number of the unpublished analog images)

3. Registration of the images of previously published journals, which are permitted for our publication
4. Automatic registration from Chromosome Letters, which will be published as an electronic journal for chromosomes

Chromosome images that have been recently published are being digitalized, while a large number of images (the majority) still remain on film. For adding film images to the database, they must first be converted to digital images. As this digitization work requires considerable effort by the investigators, we have begun to support the digitalization of film images, promotion of the registration of this database and annotation of the images registered in the database. So far, we have received the permission and cooperation for participating in imaging registration from Japanese investigators who possess many analog images of chromosomes, five investigators who have retired from active services and five investigators from the U.S., Britain and China. These five investigators had been requesting the digitization of films. The registration of 84,000 images across 5500 taxa has now been successfully completed to date. We will continue digitizing films and registering their images to CILib and, for the time being, much of our time will be taken up by this work.

17.3 FEATURES OF THE IMAGE DATABASE

The CILib will be at the center of our database system (CINet) when we have completed the program and are in opening or in testing. A site map of the programmed CINet is shown in Figure 17.4. The CILib is already complete and has been open to the public since April 2006, as a beta version [10].

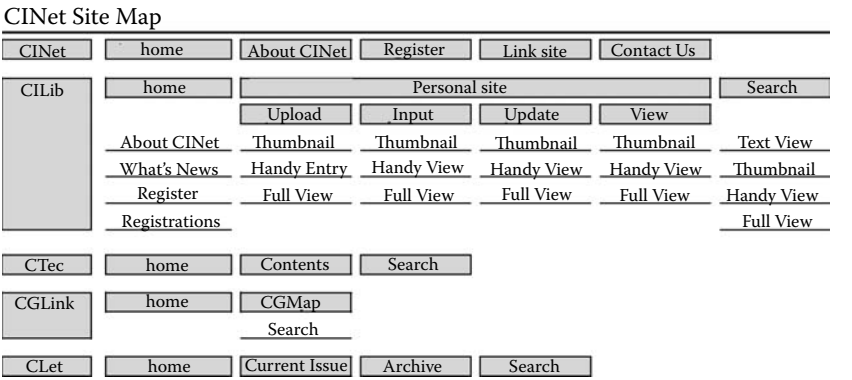

FIGURE 17.4 Site map of the Chromosome Information Network (CINet) system. Black letters indicate open sites, and gray letters indicate those sites currently in the process of online testing.

17.3.1 Features of the Database

In the CILib, character information is annotated to all images of chromosomes. For the uploaded chromosome images, annotation of the information on the reporter, publication, category, experiment, images and genome is executed. Recorded articles for the respective information are as follows:

Reporter information: reporter, date and title
Publication information: author, title, journal (meeting) and year
Classification information: family, genus, species, species author, variety, variety author, Japanese name, English name, source and strain
Experiment information: experimental number, tissue, pretreatment, fixation, staining and probe(s)
Imaging information: accession number, image name, image-created date, figure size (pixels) and scale (pixels/μm)
Genome information: n, 2n, phase, genome information (karyotype, genome formula) and remarks.

CILib has the following Personal and Search sites.

Personal site: This site can be used only by input of a password. It is composed of the annotated site and the View site of the user. These consist of

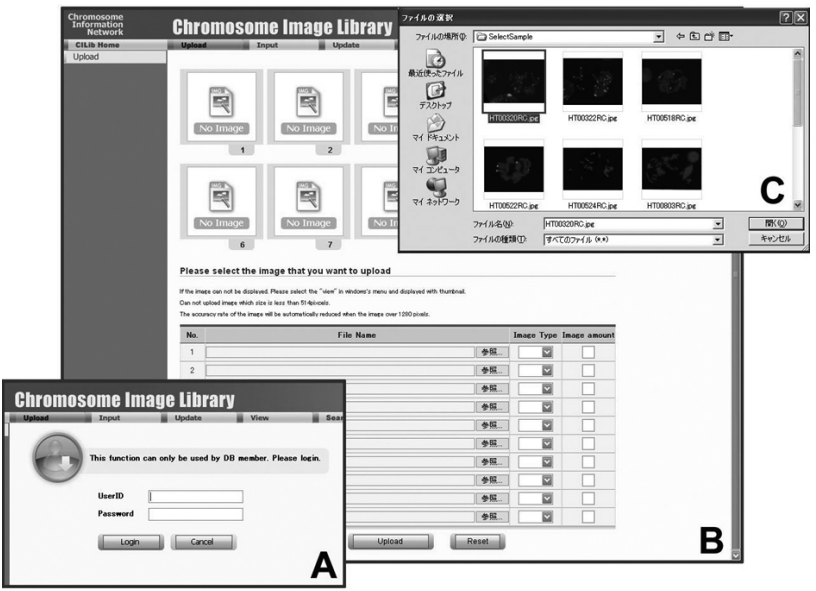

FIGURE 17.5. Upload site of images on the Personal site. The user directly inputs the password and logs into the Upload site (a) and uploads 10 or less images (b). After checking the uploaded images (c), the registration is complete.

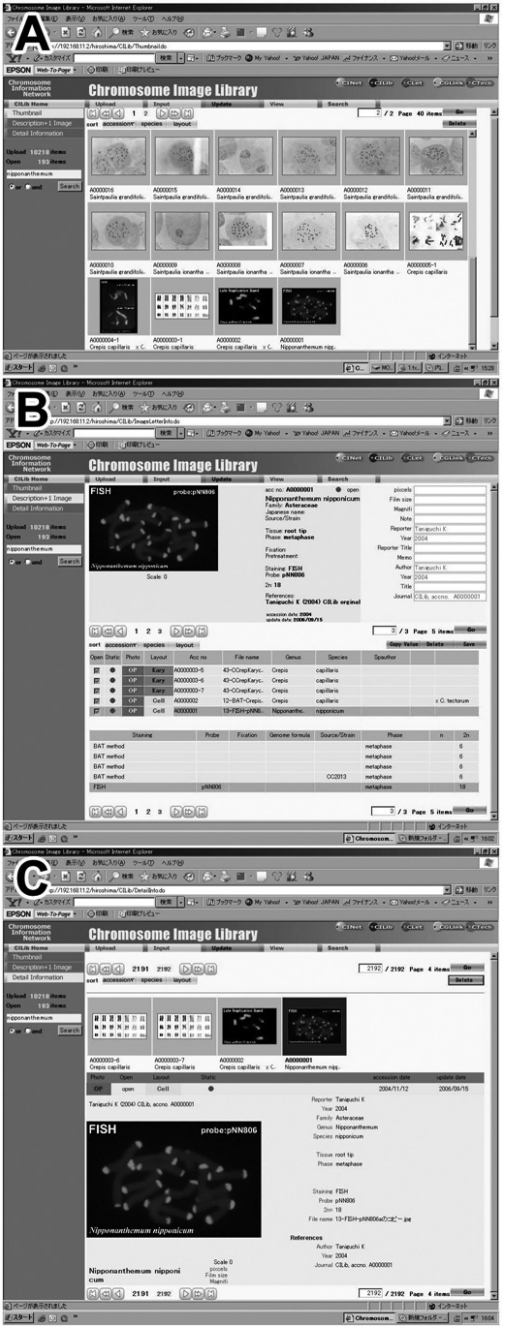

FIGURE 17.6 Three pages of the Personal site. (a) Thumbnail page, (b) Handy Entry page on the Personal site, (c) Full Entry page on the Personal site.

the following four sites: the Upload site for uploading images (Figure 17.5), the Input site for registering new information, the Update site for correcting, updating or deleting the registered information, and the View site to be used as a personal database. Each site includes the following three Web pages: Thumbnail page, Handy Entry page and Full Registry page (Figure 17.6). The Thumbnail page contains small data images or text. The Handy Entry page is useful for continuously filling in information on multiple images simultaneously. The Full Entry page is used for showing one image and every annotation of the image.

Search site: This site can be accessed without member registration, but the Handy and Full View pages can only be accessed by entering the password. They consist of three pages in the same manner as the Personal site mentioned above, and an additional page is displayed only in the form of text data (Figure 17.7).

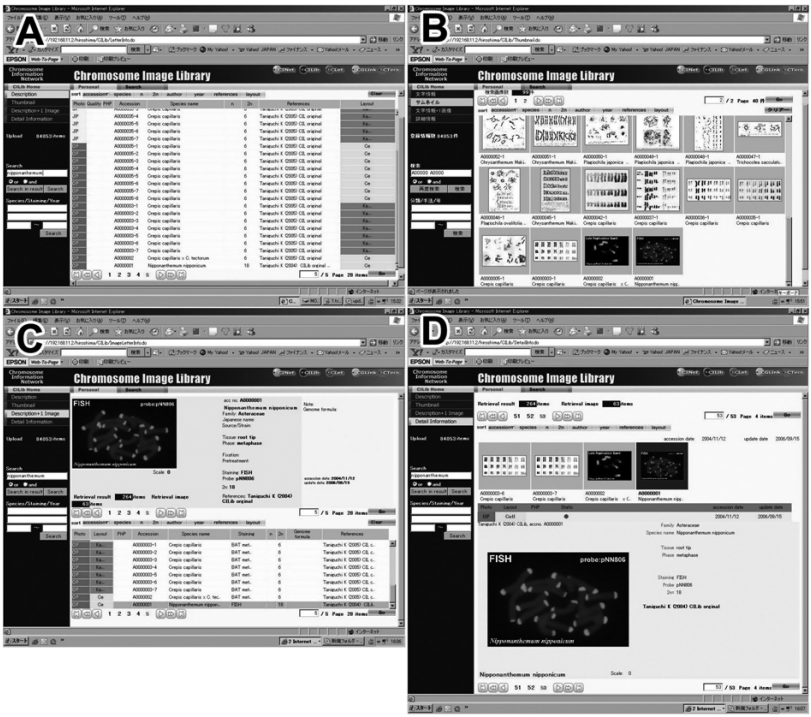

FIGURE 17.7 Four pages of the Search site. (a) Text View page with text only and no images, (b) Thumbnail page, (c) Handy View page on the Search site, (d) Full View page.

17.3.2 Registration of Images

CILib database consists of administrator registration, user registration, and user search. It can be used when all the users register as members. For the registration of images and their annotations, there are three methods: automatic registration of the original images from our e-journal registration by the administrator from other sources except our e-journal and general registration by the user. For the last method of registration by the user, the information of how to actually use the CILib is introduced as follows.

17.3.2.1 Uploading Images

There are two methods for uploading images: the user can directly execute the function on the Web site (Figure 17.5), or the user can entrust registration to the administrator. Generally, the former method is chosen. The user directly inputs the password and logs into the Upload site (Figure 17.5[a]) and uploads 10 or less images (Figure 17.5[b]). After checking the uploaded images (Figure 17.5[c]), the registration is complete. In the case of this method, we also provide support for the user to be able to register a larger number of images, and a JPG file and an Excel file recording annotation of images in a fixed style are indirectly registered by us (the administrator). The contact address for registering via the administrator is noted in Section 17.3.2.4.

17.3.2.2 Annotation to Upload Image

Only a CILib member can enter and operate the site. As mentioned above, it includes three classes: the Input site, Update site and View site, and then each site includes the following three subordinate sites: Thumbnail site, Handy Entry site and Full Entry site. The general public presentation or secret restriction can be selected according to the user's own judgments.

1. *Registration of New Information*: The first information registration is enforced on the uploaded images. After clicking on "Update," the Thumbnail page in the Update site first appears (Figure 17.6[a]). By clicking on the "Handy Entry" or "Full Entry" button, the user can fill in the information regarding the above-mentioned articles. If the user wants to simultaneously fill in the information on a larger number of images, then the user should select the Handy Entry page (Figure 17.6[b]). If the user wishes to fill in the detailed information on a few images only, the user should select the Full Entry page (Figure 17.6[c]).
2. *Correction, Updating and Deletion*: This site is similar to the Input site. If needed, the user can always correct, update or delete the annotation that has been filled in at the Input site. The registered images can be opened on the CILib site. If the user does not plan on opening the image, the user can use it privately by selecting "Personal."

3. *Personal View Site*: This is the personal database site used only by the registrant. The images registered can be searched and, in addition, sorted by access number, species name and layout. As nobody except the registrant can browse the private images on the Web, this site is suitable to be used as a private database.

17.3.2.3 Search

The database of CILib includes two types of annotated information with and without the images. The former is the page with text only and no images (hence called Text View) (Figure 17.7[a]) and the site searched mainly with regard to the chromosome number. The Text View page can be freely accessed. For example, if you would like to know the chromosome number of a *Dendranthema* species, a search box is filled in as "Dendranthema." As a result, 50 of the references on the chromosome number in *Dendranthema* species have been found as of September 2006.

The latter type of page (with images) has three pages including the Thumbnail, Handy View and Full View. The Thumbnail page can be freely accessed, while the Handy and Full View pages can only be accessed by members. If the "Search" icon is clicked, the input of key words is required. The Text View page is initially displayed, and by clicking the buttons on the left frame, each page with images is displayed. If Thumbnail is clicked, then the user can see the image list of some selected small photos (Figure 17.7[b]). If Handy View is clicked, then the user will be able to see the annotated text list (table formula) of selected images and one image prompted by the cursor (Figure 17.7[c]). The text information is more frequently displayed for some of the articles, i.e., layout, accession number, species name, staining, n and 2n of the chromosome number, and reference. If Full View is clicked on, then the user can see one large selected image and its full articles (Figure 17.7[d]).

The search service includes simple search and compound search according to the author name, year of publication, species name and keyword. In simple search, switching between and/or is possible. For example, if you would like to search FISH images of humans, "and" in the radio box is checked and the search box is filled in as "Homo FISH." As a result, nine images are currently displayed, as in September 2006. Moreover, sorting by registration number, species name, author, year of publication and layout of images can be used to further classify the searched information.

17.3.2.4 Contacting "CILib"

As the fundamental system registering to CILib has been developed, many users will now be able to access our chromosome information. We would like that a large number of chromosome researchers participate, because this system can only be completed with the participation of many users. Anyone is immediately welcome to enter into the following sites and to register their chromosome images.

Inquiry
URL: http://cilibrary.sci.hiroshima-u.ac.jp/hiroshima
Laboratory of Plant Chromosome and Gene Stock, Graduate School of Sciences, Hiroshima University, Kagamiyama 1-3-1, Higashi-Hiroshima 739-8526, Japan
Tel./Fax: +81-82-424-2471, E-mail: imagefac@hiroshima-u.ac.jp

17.4 FUTURE PROSPECTS

The chromosome image database, "CILib," started operation in April 2006. CILib is, however, only one database of the overall system (the CINet) mentioned in this paper. Other sites are almost complete in programming and are currently undergoing the process of online testing. The contents of Chromosome Techniques and Chromosome and Gene Link are currently quite empty. The e-journal, Chromosome Letters, is now in preparation for publishing.

Finally, five databases of the CINet will be created. If this system succeeds, then we will be able to contribute to the research of a large number of users studying the subjects of chromosomes, molecular genetics, breeding, environment and education. Because the amount of information in this system will increase rapidly with time, the prospective value in the future should be extensive, as has been the case with the databases of DNA and protein sequences.

17.5 CONCLUSION

The device for a user to be able to positively participate and for further improving the quality of the registered images was designed during the construction of the database system (the CINet). This system has five Web sites, namely, (1) the chromosome image database (Chromosome Image Library), (2) the technical manual on chromosomes (Chromosome Techniques), (3) the link of chromosomes and genes (Chromosome and Gene Link), (4) the e-journal (Chromosome Letters) and (5) the personal databases. The Chromosome Image Library is the core of the Chromosome Information Network, while the other four Web sites combine effectively with the Chromosome Image Library. The Chromosome Image Library started operation in April 2006. Other sites are currently in the process of online testing.

ACKNOWLEDGMENTS

We would like to thank Drs. R.-Y. Chen, K. Fukui, K. Watanabe, S. Masumori (deceased), T. Sera and T. Hoshino for contributing chromosome images. This study was supported by Special Coordination Funds of the Ministry of Education, Culture Sports, Sciences and Technology of the Japanese government.

REFERENCES

1. National Center for Biotechnology Information. GenBank, retrieved from http://www.ncbi.nlm.nih.gov/Genbank/.
2. DNA Data Bank of Japan (DDBJ), retrieved from http://www.ddbj.nig.ac.jp/.
3. European Molecular Biology Laboratory (EMBL), retrieved from http://www.embl.org/.
4. Human Genome Resources (served by NCBI's Web site), retrieved from http://www.ncbi.nlm.nih.gov/genome/guide/human/.
5. *Caenorhabditis elegans* (nematodes) genome view, retrieved from http://www.ncbi.nlm.nih.gov/mapview/map_search.cgi?taxid=6239.
6. *Arabidopsis thaliana* (mouse-ear cress) genome view, retrieved from http://www.ncbi.nlm.nih.gov/mapview/map_search.cgi?taxid=6239.
7. Missouri Botanical Garden, Index to chromosome numbers, retrieved from http://mobot.mobot.org/W3T/Search/ipcn.html.
8. Watanabe K, Index to chromosome numbers in Asteraceae, retrieved from http://www.asteraceae.cla.kobe-u.ac.jp/index.html.
9. Wikipedia, the free encyclopedia, retrieved from http://en.wikipedia.org/wiki/.
10. Chromosome Information Network, retrieved from http://cilibrary.sci.hiroshima-u.ac.jp/hiroshima.
11. Fukui K, Mukai Y, Taniguchi K, Eds. (2006) *Chromosome: Handbook of Plant Chromosome*. Yokendo Co., Tokyo: 251.

18 Image Database and Image Analysis of Chromosome Information

Shin-ichi Toyabe, Takayuki Matsuto, Tatsuo Ushiki and Kohei Akazawa*

CONTENTS

18.1 Introduction 245
18.2 CHRONIS as a Chromosome Image Database 246
18.2.1 History of CHRONIS 246
18.2.2 Hardware and Software Used for CHRONIS 247
18.2.3 Accessing CHRONIS 247
18.2.4 Bibliographic Search in CHRONIS 248
18.2.5 Contents of the Image Database 249
18.2.6 How to Search for Images Using the Image Database 250
18.2.7 Registered Users 251
18.3 A New Method of Image Analysis for SNOM/AFM 252
18.3.1 Problems in Denoising FISH Images Obtained Using SNOM/AFM 252
18.3.2 Development of a New Denoising Method 253
18.3.3 Performance of the New Denoising Method 254
18.3.4 Merits of the New Denoising Method 255
18.4 Conclusions and Future Directions 256
Acknowledgment 256
References 256

18.1 INTRODUCTION

Why do we study chromosomes? We study chromosomes because their behavior at fertilization and cell division determines the nature of inheritance, and their organization controls the activity of genes [1]. Microscopic observation of chromosomes is important for the study of chromosomes. There are various types of microscopes

*To whom correspondence should be addressed.

and a wide range of techniques for observing chromosomes by microscopy. Recent advances in microscopic technology such as scanning near-field optical microscopy (SNOM) and atomic force microscopy (AFM) have enabled researchers to observe chromosomes on the nanometer scale (see also Chapters 9 to 11) [2–6]. The use of fluorescence-labeled DNA probes in comparative genomic hybridization and fluorescence *in situ* hybridization (FISH) has made it possible to observe the localization of specific DNA on chromosomes (see also Chapter 6) [7–11]. The diverse range of techniques has provided us with large numbers of chromosome images, processed by various methods at various magnifications. Systematic accumulation of these chromosome images and access to the images using an easy search tool would be beneficial for researchers. There are some text-based databases of chromosomal information [12,13] but no databases of animal chromosome images. We have therefore constructed a database of images of animal chromosomes and bibliographic information on chromosomes and nanotechnologies related to handling, analyzing and sorting of chromosomes. The constructed database, named CHRONIS (CHROmosome and Nano-Information System), is now open to the public on the Web. The database contains a large number of images of animal chromosomes as well as bibliographic information on chromosomes.

During the process of collecting chromosome images for CHRONIS, problems regarding image quality have arisen. The quality of many images is not sufficient for use in our database, because of image noise derived not only from poor quality of the photographs but also from the microscopic observation system itself. As a typical example of the latter case, FISH images obtained using SNOM and AFM have background noises that inevitably arise from the low signal-to-noise (S/N) ratio of the system. Several methods for denoising FISH images obtained using SNOM/AFM have been developed [14], but these methods are not satisfactory. We developed a new method to denoise FISH images using statistical estimation of the true distribution of signals from the observed distribution of signals on the image. Using this new denoising method, we were able to obtain images of satisfactory quality for use in the image database of CHRONIS.

In this chapter, we will first introduce a newly constructed database for a chromosome image library, or CHRONIS, and second, describe a method for the image analysis for SNOM/AFM, especially suitable for denoising FISH images. Last, brief comments on the future directions for the chromosome image database are added.

18.2 CHRONIS AS A CHROMOSOME IMAGE DATABASE

18.2.1 History of CHRONIS

The database server was first installed in Niigata University, Japan, in 2001. At first, we collected only bibliographic information on chromosomes and nanotechnologies related to the handling, analyzing and sorting of chromosomes. The bibliographic information includes books, manuscripts from scientific journals and contents on the Web. We then developed various search engines to improve

convenience for users of the database. Collection of animal chromosome images was started in 2003, and we opened CHRONIS to the public on the Web in 2004.

18.2.2 Hardware and Software Used for CHRONIS

The database server and a Web server are incorporated in one unit, a Compac Proliant ML 570 Tower computer with a 700-MHz Intel Pentium III Xeon processor, 1024 megabytes of RAM and four 18.2-gigabyte RAID5 (redundant array of independent disks) disk arrays. It is implemented with Miracle Linux Standard Edition (Miracle Linux Co. Ltd., Tokyo, Japan) as the operating system. The search server is in another unit, a DELL PowerEdge 600SC computer with a 1.8-GHz Pentium IV processor, 512 megabytes of RAM and two 80 gigabyte RAID1 disk arrays. It is implemented with Windows 2000 Server SP2 (Microsoft Co., WA, U.S.A.).

The minimum requirements for the client unit are a 100-MHz Pentium processor, 64 megabytes of RAM, an operating system of Windows 95 (or more recent versions), a Web browser of Internet Explorer 4.01 (Microsoft Co.) or Netscape Communicator 4.5 (Netscape Communications Co., CA, U.S.A.) (or more recent versions) and Java 2 Runtime Environment 1.3.1 for Microsoft Windows (or more recent versions).

Software Oracle 8i enterprise edition for Linux (Oracle Co., NY, U.S.A.) is used as the database management system implemented on the Linux server unit. GNU (GNU is Not Unix) wget is used to retrieve files from the given URLs of the Internet using HyperText Transfer Protocols (HTTP) [15]. GNU wget is distributed under the GNU General Public License. At first, we collected certain URLs concerning information on chromosomes and related nanotechnologies, and we assigned these URLs as starting points to collect other URLs. Information on these URLs is collected at regular intervals using GNU wget. The information collected from these URLs is indexed using Namazu in order to be able to search easily for necessary information. Namazu is also used to index and search the image database. Namazu is a full-text search engine for a wide range of types of documents and is distributed by Namazu Project under the GNU Public License [16]. Apache is used as a Web server and Jakarta Tomcat is used as a Java servlet container to construct the CHRONIS web page [17,18]. Software itBASE (Access System Co. Ltd., Tokyo, Japan) is used for construction of the database of chromosome images, and dbMAGIC Enterprise Server for Linux (Magic Software Japan Co. Ltd., Tokyo, Japan) is used as a Rapid Application Development and Deployment tool to make Web applications.

18.2.3 Accessing CHRONIS

CHRONIS is now open to the public at the following URL: http://chromosome.med.niigata-u.ac.jp/chronis/servlet/chronis.ChronisServlet.

When the URL is accessed, the initial screen of CHRONIS appears. In the initial screen, there are search tools for bibliographic information in the upper part of the screen, and six icons corresponding to six fields of contents of the database

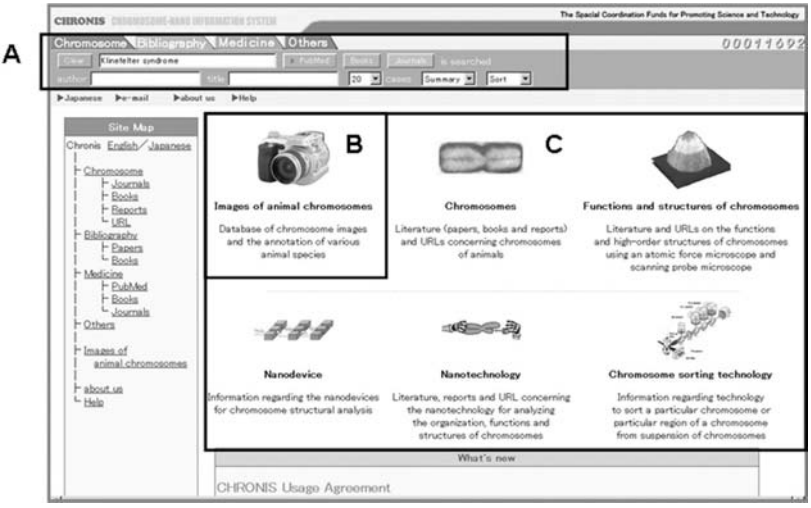

FIGURE 18.1 Initial screen of CHRONIS. CHRONIS can be accessed at the following URL: http://chromosome.med.niigata-u.ac.jp/chronis/servlet/chronis.ChronisServlet. In the initial screen of CHRONIS, there are search boxes for bibliography in the upper part of the Web page (A) and six icons corresponding to fields of interest in research of chromosomes. The upper-left camera icon (B) is linked with the image database, and the other five icons (C) are linked with the bibliographic database.

in the lower part of the screen (Figure 18.1). The icons are entitled "images of animal chromosomes," "chromosomes," "functions and structure of chromosomes," "nanodevice," "nanotechnology" and "chromosome sorting technology." The "images of animal chromosomes" icon is linked to the image database of animal chromosomes. By clicking icons other than the image database, the user can select a field of interest of bibliographic data.

18.2.4 Bibliographic Search in CHRONIS

CHRONIS contains enormous amounts of bibliographic data collected automatically from the Web by using GNU wget at regular intervals. Starting point URLs for this automatic retrieval were specified manually at first. The collected information was indexed and categorized into five fields containing information on animal chromosomes, function and structure of chromosomes, nanodevices to handle chromosomes, nanotechnology to handle chromosomes and technology to sort chromosomes. By clicking one of the five icons, we can narrow the range of data to the specified field. We can search data with particular keywords and with specified types of bibliography such as journals, books, reports and URLs.

As an example, consider a search for information on Klinefelter's syndrome (Figure 18.2). We input the term into the text search box and click on the button labeled "books." The database shows a list of books that contain information on

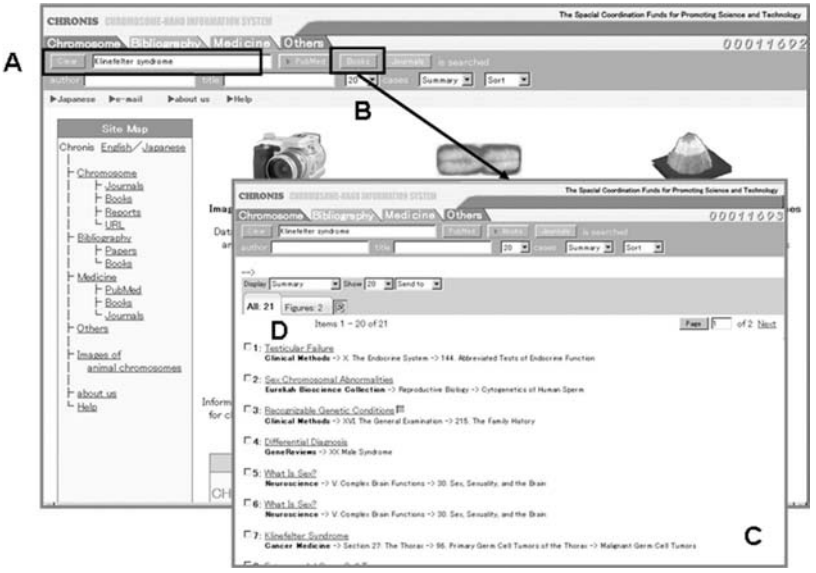

FIGURE 18.2 An example of a bibliographic search. If the user wants to find information on books that contain information on "Klinefelter syndrome," the user inputs the term into the text search box (A) and clicks on the "Books" button (B). The database shows a list of books about this syndrome (C). The titles of books in the list are hyperlinked with the Web page where information on the book is shown (D).

Klinefelter's syndrome. We have also added an option to search for a particular manuscript in medical journals using the PubMed database and an option to search for a particular URL using the Yahoo and Google search engines. The search results using these search engines are displayed in a single Web page, being categorized by the results found using each type of search engine.

18.2.5 Contents of the Image Database

The microscopic images of animal chromosomes were manually collected from the literature with permission from the copyright owner and from the authors of the literature. Other images were kindly provided by researchers who studied animal chromosomes or those who dealt with animal chromosomes during their investigations. Not only researchers in universities or institutes in Japan, but also researchers from all over the world, cooperated with us. These images were scanned with a digital scanner at 300 dpi resolution using the moiré pattern reduction method in the case of printed materials. In the case of portable document files in electronic journals, we used Adobe Acrobat (Adobe Systems Inc., San Jose, CA, U.S.A.) to extract the image we wanted. The images were saved in JPEG format at the highest resolution and the lowest compression setting and processed using Adobe Photoshop (Adobe Systems Inc.). As of August 2006, we

TABLE 18.1
Database Fields for the Image Database

Category	Field	Description
Classification of the animal	**Order**	**Order name of the animal**
	Family	Family name of the animal
	Genus	Genus name of the animal
	Species	Species name of the animal
	Strain	Strain of the animal
	Japanese name	Japanese name of the animal
	English name	English name of the animal
Materials	**Tissue**	**Tissue specimen**
	Source	Place where the animal was obtained
Methods	**Staining**	**Staining method of the specimen**
	Probe	Probes used for *in situ* hybridization
Information on chromosome	**2n**	**Chromosome number**
	Phase	Cell phase
Source of information	**Journal**	**Journal name**
	Title	Title of the manuscript
	Author	Author of the journal or provider of the image

have collected 4800 images for general users and 9200 images for registered users covering 1900 species of animal. The latter images are not open to the public because permission from the copyright owner has not yet been obtained.

To each image, we added text-based information on the image such as information on the animal, tissue specimen and methods used for microscopic examination, karyotype and reference of the image (Table 18.1). We can find images we want by using keywords that search these data fields.

18.2.6 How to Search for Images Using the Image Database

We can access the image database by clicking on the "images of animal chromosomes" icon on the initial screen of the database. In the upper part of the screen, there are five search boxes, including search boxes for general keywords, the common name of an animal we wish to search for, the genus name of the animal, species name of the animal and methods of microscopic examination (Figure 18.3). The general keywords cover all of the data fields attached to image data. The staining method is selected from pull-down lists of various kinds of microscopic examinations and staining methods of specimens. The number of images matching the specified search is shown in the lower part of the screen together with lists of thumbnails of the matched images. When we click on a

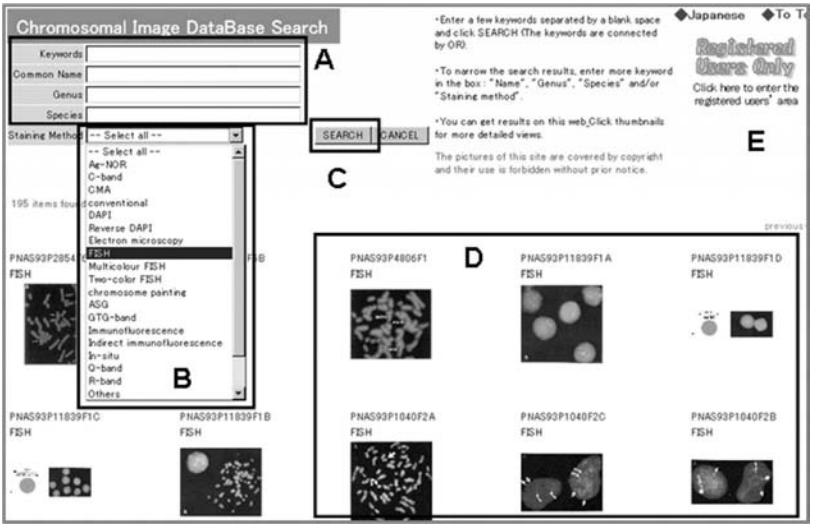

FIGURE 18.3 Accessing the image database. By clicking the camera icon, the user can enter the image database. In the upper part of the screen, there is a search panel consisting of five kinds of search boxes in which keywords are entered (A). The search boxes are for keyword, common name, genus name, species name of the animal and staining method used in the image. The "keywords" box covers all 19 fields concerning an image, shown in Table 18.1. The staining method is selected from pull-down lists (B). When the user clicks on the search button (C) after inputting keywords, the search results are shown as thumbnail images in the lower part of the screen (D). In the upper right corner of the screen, there is a button to specify authority of user (E).

thumbnail image, an enlarged image and information on the image are displayed in an independent window (Figure 18.4).

As an example, consider a search for images related to human metaphase chromosomes. We input the term “metaphase” into the keyword box and “human” into the common name box. The database provides 164 images related to human metaphase chromosomes, including images of various specimens and tissues processed by various techniques with a wide range of magnifications.

18.2.7 Registered Users

Images in the image database of CHRONIS for which permission for use has been obtained from their copyright owners are open to the public. Images for which permission for use from their copyright owners has not been obtained can be accessed only by registered users. To become a registered user, users must send a registration form by e-mail or FAX to the administrator of the Web site. The registration form can be obtained from the following URL: http://chromosome.med.niigata-u.ac.jp/chronis/file/RegistrationForm.pdf. After a careful review by

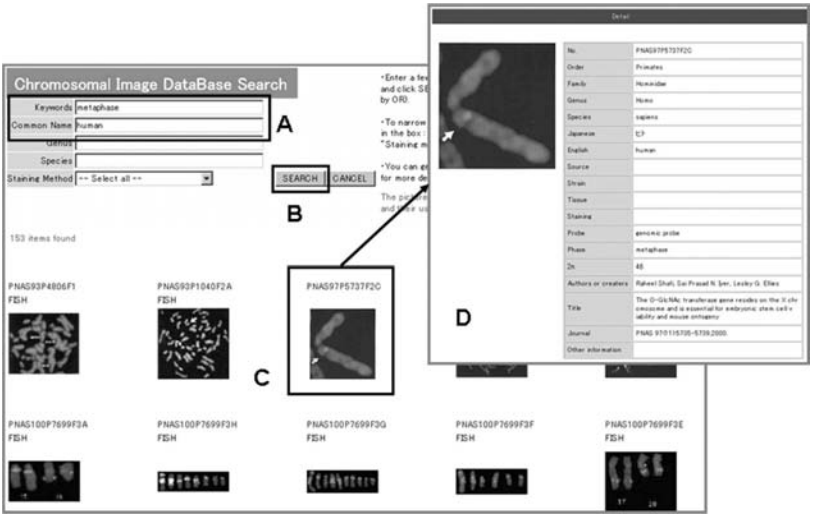

FIGURE 18.4 Annotation box of the image database. To obtain detailed information on the searched image, the user clicks on the thumbnail image. The database shows the annotation of the image in the newly opened window with an enlarged image (A).

our committee, a user ID and password are provided to the approved user. The registration is free of charge in principle.

18.3 A NEW METHOD OF IMAGE ANALYSIS FOR SNOM/AFM

18.3.1 Problems in Denoising FISH Images Obtained Using SNOM/AFM

FISH is a technique used to detect target genes on chromosomes using fluorescence microscopy, by binding of specific DNA probes labeled with fluorescent compounds. Combined use of the FISH technique with SNOM/AFM reveals the distribution of genes on a chromosome on the nanoscale (see also Chapter 11). SNOM/AFM provides fluorescent images by detecting photons generated from fluorescently labeled DNA [5,19–21]. The signals detected by SNOM/AFM are discrete because they depend on the number of photons counted by the microscopy. The main problem in using SNOM/AFM to observe FISH images is low S/N ratio. There are several reasons for the low S/N ratio, including low optical throughput of the probe, non-specific binding of probes, small number of generated photons, weakening of signals located far from the detector and stochastic detection of signals. Prolongation of observation time or repeated observation of the same area might be effective for improving the S/N ratio. However, this is not realistic because long-term exposure to the excitation light would rapidly attenuate the signals of the observed area, as well as signals around areas that have not yet been observed.

There are several methods for denoising FISH images obtained by SNOM/AFM and improving the S/N ratio, i.e., the moving average method and the use of filters such as Gaussian, median and low-pass filters [14]. Although these methods improve the S/N ratio and make clearer the images, there are still problems. The margins of figures on images often become unclear after the averaging procedure and noises might be resident on the background of the image. Moreover, the denoising parameters in these methods are arbitrary and there are no established criteria to determine the optimal value of these parameters.

To resolve the problems associated with these methods, we have developed a new method to obtain a clear image of FISH observed using SNOM/AFM.

18.3.2 Development of a New Denoising Method

The new denoising method is based on statistical estimation of the true distribution of fluorescent signals from the observed distribution of signals on FISH images.

A FISH image observed by SNOM/AFM is an aggregation of signals. Each signal originates from photons detected per pixel. The intensity of each signal is discrete and its generation stochastically fluctuates with very low frequency. Therefore, the distribution of signal intensities should follow a Poisson distribution. If we assume that n photons were observed with p frequency in a pixel during an observation time lasting a few milliseconds, the distribution of signal intensities np follows a Poisson distribution. Next, we focus on the neighboring pixels around the first pixel. The number of pixels that we focus on is initially 4, and then the number of pixels we focus on is gradually increased. The final number of neighboring pixels k is determined as an area within which the homogeneity test for a Poisson distribution is accepted. If every pixel within the area follows the distribution with the same Poisson distribution, these pixels are considered as having the same Poisson parameter λ. To test this hypothesis, a likelihood test using statistic $-2 \log \Lambda$ is used [22]. The statistic $-2 \log \Lambda$ is defined by a comparison of the likelihood scores between a model where each pixel has its own λ and a model where every pixel has the same parameter λ. If we denote the number of neighboring pixels around the first pixel by n, and the number of photons in each pixel by $x_1, x_2, \ldots, x_n$, then,

$$-2 \log \Lambda = 2\left[\sum^{n} x_i \log x_i - t \log (t/n)\right],$$

$$t = \sum_{i=1}^{n} x_i \cdot$$

When t/n was large ($t/n > 5$), the statistic $-2 \log \Lambda$ followed a chi-square distribution with $(n - 1)$ degrees of freedom. In the case where t/n was small, we used the exact distribution of the statistic $-2 \log \Lambda$ instead of the chi-square distribution. The exact distribution of the statistic $-2 \log \Lambda$ was developed using

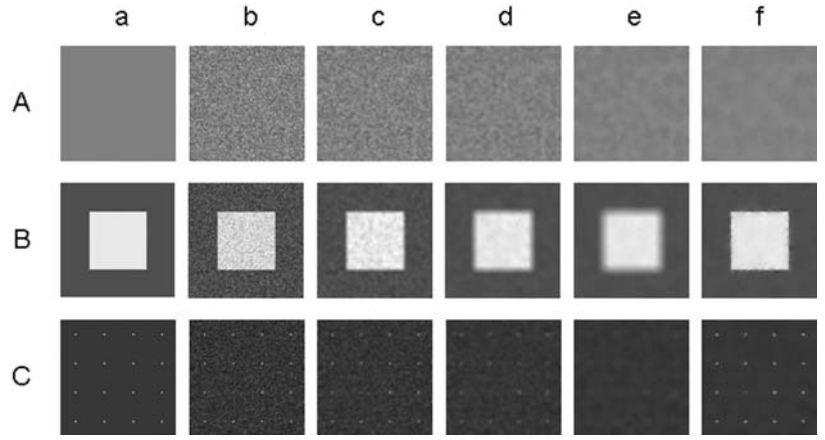

FIGURE 18.5 Denoising of artificial images by the moving average method and the new method. Three types (A, B, C) of artificial images (b) were made from original images (a) by adding artificial Poisson noise. The noise was reduced by the moving average method (c–e) and the new method (f). In the moving average method, the radius of each averaging area was set at 5 pixels (c), 10 pixels (d) and 15 pixels (e). (From Dr. Toshio Ohtani, National Food Research Institute, Japan. With permission.)

Fisher's exact method [23]. The homogeneity test using the exact distribution for the statistic is repeated while increasing the number of neighboring pixels n until the test fails. The signal intensity of pixels within the area where the homogeneity test is accepted is considered as having the same parameter λ and the true intensity of the first pixel can be estimated as the average of the signal values of these pixels. The same procedure is applied to every pixel in the image.

18.3.3 Performance of the New Denoising Method

We applied the new denoising method to artificial images and compared the results with those obtained using the conventional moving average method (Figure 18.5). We made artificial images from original images by adding noise that was sampled from a Poisson distribution with a parameter λ. Moving average methods with various ranges of averaging area and the new method were applied to the flat image (A-a). When the moving average method was used, an irregular pattern of signals was observed within the image when the averaging area was small (A-c). On the other hand, the new method faithfully reproduced the flat image from the original (A-f). The new method gave satisfactory results also in reproduction of figures such as a bright square (B-a) and small bright points (C-a) compared with the moving average method. The signals within the square became uneven by reducing the size of the averaging area in the moving average method, although the edges of the square were sharpened (B,C). In the same way, the background of the small bright points became uneven as the bright points became clearer in

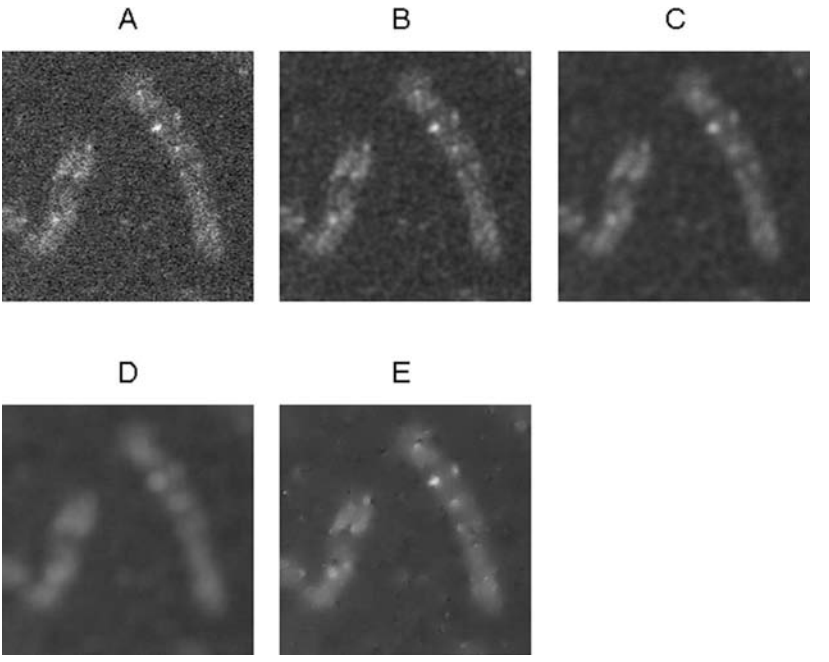

FIGURE 18.6 Denoising of a FISH image of a chromosome observed by SNOM/AFM. A FISH image of a chromosome (A) was denoised using the moving average method (B–D) and the new method (E). In the moving average method, the radius of each averaging area was set at 5 pixels (B), 10 pixels (C) and 15 pixels (D). The SNOM/AFM images were kindly supplied by Dr. Toshio Ohtani, National Food Research Institute, Japan.

the moving average method (B-c). On the other hand, these figures were clearly reproduced using the new method (B-f, C-f).

Next, we applied the methods to a FISH image of a chromosome observed by SNOM/AFM (Figure 18.6). When the size of averaging area was small, granular signals were distributed over the chromosome in spite of clear positive signals for FISH (B). By increasing the size of the averaging area, the surface of the chromosome became smooth, but positive signals on it disappeared (C, D). Specific signals became more obvious when using the new method, while non-specific signals were smoothed (E).

18.3.4 Merits of the New Denoising Method

The most important merit of the new method is that the method has a clear criterion for denoising. The moving average method has no criterion for determining the averaging area, and determination of the size of the averaging area is arbitrary. Another merit of the new method is that the size of the averaging area varies from one locality to another, which allows more minute smoothing than the moving average method. In the moving average method, a uniform criterion

for the size of the averaging area is applied for all points of the image. Based on these advantages of the new method, we can obtain clear FISH images that have satisfactory sharpness and brightness of figures and appropriate suppression of background noises. These images are of sufficient quality to use in the image database of CHRONIS.

18.4 CONCLUSIONS AND FUTURE DIRECTIONS

CHRONIS is the first trial for construction of an integrated database of animal chromosomes. The database contains a large quantity of chromosome images as well as bibliographic information. To improve the quality of the images in the database, we developed a new statistical method to reduce noise in the images. Our database system provides a powerful tool for research of animal chromosomes.

We plan to improve the usability of the image database. First, we plan that researchers will be able to register their image data directly into the database over the Web. This will be achieved by authorization of users to edit data of CHRONIS. This plan will extend the contents of the image database and compensate for a lack of image data for some animal species. Second, we plan to link CHRONIS to other databases of molecular and cell biology after obtaining permission to make a link [24–26]. The databases that we plan to link to CHRONIS include databases of gene mapping, functions of genes, sequences of genes, primers used for polymerase chain reaction, probes used for *in situ* hybridization and information on corresponding amino acids. Users will be able to obtain various types of information on a gene and FISH images of the gene simultaneously. The linkage to these databases will enable users to gain an overall understanding of the gene.

ACKNOWLEDGMENT

This study was supported by Special Coordination Funds of the Ministry of Education, Culture Sports, Sciences and Technology of the Japanese government.

REFERENCES

1. Sumner A (2003) *Chromosomes: Organization and Function*. Blackwell, Oxford.
2. Kimura E, Hitomi J, Ushiki T (2002) Scanning near field optical/atomic force microscopy of bromodeoxyuridine-incorporated human chromosomes. *Arch Histol Cytol* 65: 435–444.
3. De Grooth BG, Putman CA (1992) High-resolution imaging of chromosome-related structures by atomic force microscopy. *J Microsc* 168: 239–247.
4. Fritzsche W, Schaper A, Jovin TM (1994) Probing chromatin with the scanning force microscope. *Chromosoma* 103: 231–236.
5. Ohtani T, Shichirii M, Fukushi D, Sugiyama S, Yoshino T, Kobori T, Hagiwara S, Ushiki T (2002) Imaging of chromosomes at nano-meter scale resolution using scanning near-field optical/atomic force microscopy. *Arch Histol Cytol* 65: 425–434.

6. Kimura E, Hoshi O, Ushiki T (2004) Atomic force microscopy of human metaphase chromosomes after differential staining of sister chromatids. *Arch Histol Cytol* 67: 171–177.
7. Brandriff BF, Gordon LA, Trask BJ (1991) DNA sequence mapping by fluorescence in situ hybridization. *Environ Mol Mutagen* 18: 259–262.
8. Cheung SW, Tishler PV, Atkins L, Sengupta SK, Modest EJ, Forget BG (1997) Gene mapping by fluorescent in situ hybridization. *Cell Biol Int Rep* 1: 255–262.
9. Gray JW, Lucas J, Kallioniemi O, Kallioniemi A, Kuo WL, Straume T, Tkachuk D, Tenjin T, Weier HU, Pinkel D (1991) Applications of fluorescence in situ hybridization in biological dosimetry and detection of disease-specific chromosome aberrations. *Prog Clin Biol Res* 372: 399–411.
10. Liehr T, Starke H, Weise A, Lehrer H, Claussen U (2004) Multicolor FISH probe sets and their applications. *Histol Histopathol* 19: 229–237.
11. Hoshi O, Shigeno M, Ushiki T (2006) Atomic force microscopy of native human metaphase chromosomes in a liquid. *Arch Histol Cytol* 69: 73–78.
12. Nadkarni PM, Reeders ST, Shifman MA, Miller PL (1992) CHROMINFO: a database for viewing and editing top-level chromosome data. *Proc Annu Symp Comput Appl Med Care*: 366–370.
13. Jones RN, Diez M (2004) The B chromosome database. *Cytogenet Genome Res* 106: 149–150.
14. Mather P (1999) *Computer Processing of Remotely-Sensed Images: An Introduction*, 2nd ed. John Wiley & Sons, West Sussex.
15. The GNU Operating System. Retrieved from http://www.gnu.org/.
16. The Namazu Project. Retrieved from http://www.namazu.org/.
17. The Apache Software Foundation. Retrieved from http://www.apache.org/licenses/.
18. The Apache Jakarta Project. Retrieved from http://jakarta.apache.org/.
19. Fukushi D, Shichiri M, Sugiyama S, Yoshino T, Hagiwara S, Ohtani T (2003) Scanning near-field optical/atomic force microscopy detection of fluorescence in situ hybridization signals beyond the optical limit. *Exp Cell Res* 289: 237–244.
20. Oberringer M, Englisch A, Heinz B, Gao H, Martin T, Hartmann U (2003) Atomic force microscopy and scanning near-field optical microscopy studies on the characterization of human metaphase chromosomes. *Eur Biophys J* 32: 620–627.
21. Yoshino T, Sugiyama S, Hagiwara S, Fukushi D, Shichiri M, Nakao H, Kim JM, Hirose T, Muramatsu H, Ohtani T (2003) Nano-scale imaging of chromosomes and DNA by scanning near-field optical/atomic force microscopy. *Ultramicroscopy* 97: 81–87.
22. Severini T (2000) *Likelihood Methods in Statistics*. Oxford University Press, Oxford.
23. Armitage P, Berry G, Matthews JNS, *Statistical Methods in Medical Research*, 4th ed., Blackwell Science, Oxford, 2002.
24. National Center for Biotechnology Information. Genbank. Retrieved from http://www.ncbi.nlm.nih.gov/Genbank/.
25. DNA Data Bank of Japan (DDBJ). Retrieved from http://www.ddbj.nig.ac.jp/.
26. European Molecular Biology Laboratory (EMBL). Retrieved from http://www.embl.org/.

Index

A

Ancestral karyotypes, chromosome rearrangements, delineation of process, 71–73
Antipeptide antibodies, conformation/molecular assembly, intracellular protein, 189–202
  amino acid sequences, synthesized peptides, 193
  antigen preparation, immunization, 193
  binding of antibodies to rS6, 195–196
  binding of antibodies to S6 protein in HeLa cells, 196
  ELISA, 192
  experimental design, 191–193
  immunization, purification, 192
  immunostaining S6 protein, in HeLa cells, 192–193
  mass spectrometry, 191
  preparation of antigens, 191
  preparation of rS6 protein, 193–195
  recombinant S6 protein, preparation of, 191–192
  results, 193–196
  reverse transcriptase PCR, 191
Atomic force microscopy, 246
  higher-order chromosome structure, 105–118
    air-dried chromosomes, atomic force microscopy images, 109
    cell division, dynamic structural changes during, 115
    chromosome spreads, 108
    critical-point dried chromosomes, atomic force microscopy images, 110
    dried chromosomes, 109–110
    fixed chromosomes in liquid condition, atomic force microscopy images, 111
    human metaphase chromosomes, mitotic stages, atomic force microscopy images, 115
    isolated chromosomes, 108–109
    model, higher-order structure of human metaphase chromosomes, 113–114
    sample preparation, 108–109
    unfixed chromosomes, liquid condition, atomic force microscopy images, 112
    wet chromosomes, 111–113
  scanning near-field optical, chromosome topography, gene location, 137–154
    atomic force microscopy, 139
    chromosome preparation, 139–140
    fluorescence *in situ* hybridization, probe, 140–142
      barley chromosomes, 140
      human chromosomes, 141
      image analysis, 141–142
      positional analysis, two gene loci, 142
    instrumentations, 139–142
    multicolor fluorescence *in situ* hybridization detection using scanning near-field optical microscopy/atomic force microscopy, 147–150
    single-copy gene detection on human chromosomes using scanning near-field optical microscopy/atomic force microscopy, 145–146
    telomere fluorescence *in situ* hybridization signals, scanning near-field optical microscopy/atomic force microscopy, high-resolution detection, 142–145
      chromosome preparation for scanning probe microscopy observation, 142–143
      detection of telomere fluorescence *in situ* hybridization signals on barley chromosomes, 143–145
  in vitro reconstituted chromatin, higher-order chromatin folding, 119–136
    atomic force microscopy observation, nucleosomes, 123–124
    chromatin reconstitution
      linker histone H1, 128
      materials for, 124
    chromatin salt-dependent conformational changes, 127
    contribution of matrix/scaffold proteins, 131–132
    DNA negative supercoiling, nucleosome formation, 126–127

linker histone H1, nucleosome compaction, 128–130
addition to reconstituted 100-kb chromatin, 128–129
dose-dependency of linker histone H1, formation of thicker fibers, 129
physiological ionic strength, formation of 30-nm fibers, 129–130
linker histones, 121–122
long nucleosome array, establishment of *in vitro* reconstitution system, 123–127
nonhistone chromosomal protein PC4 induced chromatin compaction by mechanism different from histone H1 induced compaction, 133
nonhistone chromosome proteins, 130–133
nonhistone proteins, 121–122
nucleosome, 121
plasmid length, frequency of nucleosomes in relation to, 124–126
reconstituted chromatin fibers, atomic force microscopy images, 125
reconstitution materials, 123
salt, effect on reconstituted chromatin, 127
salt-dialysis-reconstitution, nucleosomes, 123–124
superhelical strain of template DNA, chromatin reconstitution, effects, 126
in vitro chromatin reconstitution system, 122
Atomic force microscopy probes, 15–30
atomic force microscopy imaging, manipulation, 22–28
knife-edged atomic force microscopy probe design, fabrication, 17–18
sample preparation for manipulation experiments, 20–22
tweezers atomic force microscopy probe, design, fabrication, 18–20
ATP-dependent chromatin-assembly factor, imitation SWI-type chromatin-remodeling complex, 203–216
chromatin remodeling, mechanisms of, 206–208
chromatin-remodeling complexes
classification, 204–206
helicase, 206
DNA translocation, mechanism of, 206–208
functions, 205–206
interactions of ATP-dependent chromatin-assembly factor chromatin-remodeling complex, 208–212
organization of ATP-dependent chromatin-assembly factor chromatin-remodeling complex, 208–210
quantitative analysis of interaction between hSNF2H and hATP-dependent chromatin-assembly factor1, 210
switch/sucrose non-fermenting, imitation SWI families, SW12/SNF2 chromatin-remodeling complexes, 204–205
Aurora kinase fused with GFP, analysis of chromosome dynamics using, 58–60

B

Base, microchamber array sequence-specific DNA detection, single chromosome via trace volume PCR, 31–42
chromosome-1 using tweezers-type probe, collection, rearrangement, 39
microchamber array, 33
microchamber array, design, fabrication, 32–33
microchamber array PCR amplification, whole human chromosomes, 38
nanoliter dispenser, sample loading into microchamber array, 35
on-chip DNA amplification, single chromosome-1, 40
on-chip quantitation, initial DNA concentration, 35–38
reagents, 33–35
sample preparation, 33–35
specific sequence detection from single human chromosome-1, nanoliter-volume PCR, 38–40
thermal cycling, fluorescence detection, 35

C

CGLink. *See* Chromosome and Gene Link
Chromatin folding, higher-order, atomic force microscopy, *in vitro* reconstituted chromatin, 119–136
atomic force microscopy observation, nucleosomes, 123–124
chromatin reconstitution
linker histone H1, 128
materials for, 124
chromatin salt-dependent conformational changes, 127
contribution of matrix/scaffold proteins, 131–132
DNA negative supercoiling, nucleosome formation, 126–127

linker histone H1, nucleosome compaction, 128–130
addition to reconstituted 100-kb chromatin, 128–129
dose-dependency of linker histone H1, formation of thicker fibers, 129
physiological ionic strength, formation of 30-nm fibers, 129–130
linker histones, 121–122
long nucleosome array, establishment of *in vitro* reconstitution system, 123–127
nonhistone chromosomal protein PC4 induced chromatin compaction by mechanism different from histone H1 induced compaction, 133
nonhistone chromosome proteins, 130–133
nonhistone proteins, 121–122
nucleosome, 121
plasmid length, frequency of nucleosomes in relation to, 124–126
reconstituted chromatin fibers, atomic force microscopy images, 125
reconstitution materials, 123
salt, effect on reconstituted chromatin, 127
salt-dialysis-reconstitution, nucleosomes, 123–124
superhelical strain of template DNA, chromatin reconstitution, effects, 126
in vitro chromatin reconstitution system, 122
Chromatin salt-dependent conformational changes, *in vitro* reconstituted chromatin, atomic force microscopy, higher-order chromatin folding, 127
Chromosome and Gene Link, 235
CHROmosome and Nano-Information System. *See* CHRONIS
Chromosome Image Library, 232, 234–235, 241–242
copyright problem solution, 233
Chromosome Information Network system, 234
site map, 236
Chromosome spreads, higher-order chromosome structure, atomic force microscopy, 108
Chromosome Techniques, 235
CHRONIS, 246
accessing, 247–248
bibliographic search in, 248–249
as chromosome image database, 246–252
hardware, software, 247
history of, 246–247
CILib. *See* Chromosome Image Library
CINet. *See* Chromosome Information Network
Citric acid chromosomes, isolation, 162–163
Citric acid method, isolation, human, plant chromosomes as nanomaterials, 158
Comparative chromosome painting, 69–71
Comparative cytogenetic maps
construction, with EST clones in map-poor animals, 65–69
GC heterogeneity, genome compartmentalization investigation, 73–75
Condensation mechanisms, nano-microlevels, mechanical approaches, 1–14
chromosome preparation, 3–4
elongating chromosomes, setup for observation of morphology, 6
elongating process, time-serial optical phase contrast images, unfixed human chromosomes, 11
experimental design, 3–6
finite thickness model, force curve, data set calculated from, 8
mechanical elongation, chromosomes, 9
mechanical scanning probe microscopy, 4
mechanical stretching of chromosomes, 5–6
scanning probe microscopy, 4–5
evaluation of chromosome elasticity, 7–8
topography, elasticity mapping, human chromosomes, 8–9
CTech. *See* Chromosome Techniques

D

Database imaging, 231–258
annotation to upload image, 240–241
architecture
atomic force microscopy, 246
Chromosome and Gene Link, 235
Chromosome Image Library, 232, 234–235
copyright problem solution, 233
Chromosome Information Network system, 234
site map, 236
Chromosome Techniques, 235
CHRONIS, 246
accessing, 247–248
bibliographic search in, 248–249
as chromosome image database, 246–252
hardware, software, 247
history of, 246–247
contacting Chromosome Image Library, 241–242
contents, 249–250

denoising fluorescence *in situ* hybridization images, 252–253
e-journal publication, 235
features, 236–242
future prospects, 242
image database, accessing, 251
image databases for collecting information, systems, 232
personal homepage, 235
registered users, 251–252
registration of images, 235–236, 240–242
scanning near-field optical microscopy, 246
search, 241, 250–251
uploading images, 240
Denoising fluorescence *in situ* hybridization images, 252–253
Direct R-banding fluorescence *in situ* hybridization, chromosome mapping, 64–65
Dried chromosomes, higher-order chromosome structure, atomic force microscopy, 109–110
Dynamic, functional analysis, chromosomal proteins, 217–230
chromosome scaffold proteins, methods using, comparison of, 219–220
localization, chromosomal proteins, 223–224
localization analysis using human fixed cells, chromosome spreads, isolated chromosomes, 218–219
screening methods, 218–223

E

Elasticity mapping, topography, human chromosomes, 8–9
Electric, magnetic fields, on-chip chromosome sorter using, 43–52
chemical treatment of chromosomes, 45
device fabrication, 41
experimental design, 44–46
human chromosome isolation, 44–45
instrumentation, 46
magnetic beads, 45
magnetic field
chromosome sorting using, 49–50
chromosomes sorted via, distribution ratio, 50
magnets, 45
on-chip chromosome sorter, using magnetic field, 49
voltage modulation, chromosome sorting using, 46–49
voltage modulation technique, on-chip chromosome sorting apparatus using, 46
Elongating chromosomes, setup for observation of morphology, 6

F

Finite thickness model, force curve, data set calculated from, 8
FISH. *See* Fluorescence *in situ* hybridization
Fluorescence *in situ* hybridization, 63–80
chromosome rearrangements, ancestral karyotypes, delineation of process, 71–73
comparative chromosome painting, identification of chromosomal homology between different species, 69–71
comparative cytogenetic map construction, with EST clones in map-poor animals, 65–69
comparative cytogenetic maps, GC heterogeneity, genome compartmentalization investigation, 73–75
direct R-banding fluorescence *in situ* hybridization, chromosome mapping, 64–65
phylogenetic relationships, karyotypes, amniotes, 67
Fluorescence microscopy, chromosome dynamics analysis, 53–62
aurora kinase fused with GFP, analysis of chromosome dynamics using, 58–60
fluorescence microscopy
dynamic analysis of human mitotic chromosomes, 57
dynamic analysis of mitotic chromosomes of plant cells, 58
histone H1 fused with GFP, analysis of chromosome dynamics using, 55–58
microscopic chamber, for dynamic analyses, 55
microscopic systems, 54–55
FtsJ homolog
dynamics of, 224–227
function of, 226–227
immunodetection of, 226

G

Glycerol density gradient centrifugation, polyamine chromosome isolation, 161–162

H

High-resolution scanning electron microscopy of, dried, metal-coated chromosomes, 97–100
Higher-order chromatin folding, atomic force microscopy, *in vitro* reconstituted chromatin, 119–136
  atomic force microscopy observation, nucleosomes, 123–124
  chromatin reconstitution
    linker histone H1, 128
    materials for, 124
  chromatin salt-dependent conformational changes, 127
  contribution of matrix/scaffold proteins, 131–132
  DNA negative supercoiling, nucleosome formation, 126–127
  linker histone H1, nucleosome compaction, 128–130
    addition to reconstituted 100-kb chromatin, 128–129
    dose-dependency of linker histone H1, formation of thicker fibers, 129
    physiological ionic strength, formation of 30-nm fibers, 129–130
  linker histones, 121–122
  long nucleosome array, establishment of *in vitro* reconstitution system, 123–127
  nonhistone chromosomal protein PC4 induced chromatin compaction by mechanism different from histone H1 induced compaction, 133
  nonhistone chromosome proteins, 130–133
  nonhistone proteins, 121–122
  nucleosome, 121
  plasmid length, frequency of nucleosomes in relation to, 124–126
  reconstituted chromatin fibers, atomic force microscopy images, 125
  reconstitution materials, 123
  salt, effect on reconstituted chromatin, 127
  salt-dialysis-reconstitution, nucleosomes, 123–124
  superhelical strain of template DNA, chromatin reconstitution, effects, 126
  in vitro chromatin reconstitution system, 122
Higher-order chromosome structure, atomic force microscopy, 105–118
  air-dried chromosomes, atomic force microscopy images, 109
  cell division, dynamic structural changes during, 115
  chromosome spreads, 108
  critical-point dried chromosomes, atomic force microscopy images, 110
  dried chromosomes, 109–110
  fixed chromosomes in liquid condition, atomic force microscopy images, 111
  human metaphase chromosomes, mitotic stages, atomic force microscopy images, 115
  isolated chromosomes, 108–109
  model, 113–114
  sample preparation, 108–109
  unfixed chromosomes, liquid condition, atomic force microscopy images, 112
  wet chromosomes, 111–113
Histone H1 fused with GFP, analysis of chromosome dynamics using, 55–58

I

Imaging databases, 231–258
  accessing, 251
  annotation to upload image, 240–241
  architecture
  atomic force microscopy, 246
  Chromosome and Gene Link, 235
  Chromosome Image Library, 232, 234–235
    copyright problem solution, 233
  Chromosome Information Network system, 234
    site map, 236
  Chromosome Techniques, 235
  CHRONIS, 246
    accessing, 247–248
    bibliographic search in, 248–249
    as chromosome image database, 246–252
    hardware, software, 247
    history of, 246–247
  contacting Chromosome Image Library, 241–242
  contents, 249–250
  denoising fluorescence *in situ* hybridization images, 252–253
  e-journal publication, 235
  features, 236–242
  future prospects, 242
  image database, accessing, 251
  image databases for collecting information, systems, 232
  personal homepage, 235
  registered users, 251–252
  registration of images, 235–236, 240–242

scanning near-field optical microscopy, 246
search, 241, 250–251
uploading images, 240
Imitation SWI-type chromatin-remodeling complex, ATP-dependent chromatin-assembly factor, 203–216
chromatin remodeling, mechanisms of, 206–208
chromatin-remodeling complexes
classification, 204–206
helicase, 206
DNA translocation, mechanism of, 206–208
functions, 205–206
interactions of ATP-dependent chromatin-assembly factor chromatin-remodeling complex, 208–212
organization of ATP-dependent chromatin-assembly factor chromatin-remodeling complex, 208–210
quantitative analysis of interaction between hSNF2H and hATP-dependent chromatin-assembly factor1, 210
switch/sucrose non-fermenting, imitation SWI families of SW12/SNF2 chromatin-remodeling complexes, 204–205
Immunocytochemistry, 81–92
cells, 82
chromosomal proteins, study of, 83–84
chromosome spreading, 83
differential staining, chromosomes, 86–88
histone modifications, study of, 84–86
immunocytochemistry, 83
methodology, 82–83
In vitro reconstituted chromatin, atomic force microscopy, higher-order chromatin folding, 119–136
atomic force microscopy observation, nucleosomes, 123–124
chromatin reconstitution
linker histone H1, 128
materials for, 124
DNA negative supercoiling, nucleosome formation, 126–127
linker histones, 121–122
long nucleosome array, establishment of *in vitro* reconstitution system, 123–127
nonhistone chromosomal protein PC4 induced chromatin compaction by mechanism different from histone H1 induced compaction, 133
nonhistone proteins, 121–122
nucleosome, 121
plasmid length, frequency of nucleosomes in relation to, 124–126
reconstituted chromatin fibers, atomic force microscopy images, 125
reconstitution materials, 123
salt, effect on reconstituted chromatin, 127
salt-dialysis-reconstitution, nucleosomes, 123–124
superhelical strain of template DNA, chromatin reconstitution, effects, 126
in vitro chromatin reconstitution system, 122
Isolation, human, plant chromosomes as nanomaterials, 155–166
citric acid chromosomes, 162–163
citric acid method, 158
flow cytometry separation, human chromosomes, 164
human cell culture, 159–160
mass isolation, 158–163
plant chromosomes, 165
polyamine chromosomes
glycerol density gradient centrifugation, 161–162
multi-step centrifugation, 161
polyamine method, 158
purification, handling of chromosomes, 157–158
scanning electron microscopy, isolated human chromosomes, 160
specific chromosomes, 163–164

K

Knife-edged atomic force microscopy probe design, fabrication, 17–18

L

Linker histone H1, nucleosome compaction, *in vitro* reconstituted chromatin, atomic force microscopy, higher-order chromatin folding, 128–130
addition to reconstituted 100-kb chromatin, 128–129
dose-dependency of linker histone H1, formation of thicker fibers, 129
physiological ionic strength, formation of 30-nm fibers, 129–130
Long nucleosome array, establishment of *in vitro* reconstitution system, 123–127
Low-vacuum scanning electron microscopy, hydrous chromosomes observed by, 100–102

M

Magnetic, electric fields, on-chip chromosome sorter using, 43–52
chemical treatment of chromosomes, 45
device fabrication, 41
experimental design, 44–46
human chromosome isolation, 44–45
instrumentation, 46
magnetic beads, 45
magnetic field
chromosome sorting using, 49–50
chromosomes sorted via, distribution ratio, 50
magnets, 45
on-chip chromosome sorter, using magnetic field, 49
voltage modulation, chromosome sorting using, 46–49
voltage modulation technique, on-chip chromosome sorting apparatus using, 46
Matrix/scaffold proteins, *in vitro* reconstituted chromatin, atomic force microscopy, higher-order chromatin folding, 131–132
Mechanical approaches, chromosome condensation mechanisms, nano-microlevels, 1–14
chromosome preparation, 3–4
elongating chromosomes, setup for observation of morphology, 6
elongating process, time-serial optical phase contrast images, unfixed human chromosomes, 11
experimental design, 3–6
finite thickness model, force curve, data set calculated from, 8
mechanical elongation, chromosomes, 9
mechanical scanning probe microscopy, 4
mechanical stretching of chromosomes, 5–6
scanning probe microscopy, 4–5
evaluation of chromosome elasticity, 7–8
topography, elasticity mapping, human chromosomes, 8–9
Mechanical elongation, chromosomes, 9
Mechanical scanning probe microscopy, 4
Mechanical stretching of chromosomes, 5–6
Metaphase chromosomes
scanning electron microscopy, 97–102
high-resolution scanning electron microscopy of, dried, metal-coated chromosomes, 97–100
low-vacuum scanning electron microscopy, hydrous chromosomes observed by, 100–102
transmission electron microscopy, 94–97
ultrathin sections, 94–95
whole-mount preparation of chromosomes, 96–97
Multi-step centrifugation, polyamine chromosome isolation, 161

N

Nonhistone chromosome proteins, chromatin compaction, *in vitro* reconstituted chromatin, atomic force microscopy, higher-order chromatin folding, 130–133
Nucleosome, atomic force microscopy, *in vitro* reconstituted chromatin, higher-order chromatin folding, 121
Nucleosome compaction, linker histone H1, atomic force microscopy, *in vitro* reconstituted chromatin, higher-order chromatin folding, 128–130
addition to reconstituted 100-kb chromatin, 128–129
dose-dependency of linker histone H1, formation of thicker fibers, 129
physiological ionic strength, formation of 30-nm fibers, 129–130
Nucleosome formation, atomic force microscopy, *in vitro* reconstituted chromatin, higher-order chromatin folding, DNA negative supercoiling, 126–127
Nucleosomes, atomic force microscopy, *in vitro* reconstituted chromatin, higher-order chromatin folding
atomic force microscopy observation, 123–124
salt-dialysis-reconstitution, 123–124

O

On-chip chromosome sorter, using magnetic, electric fields, 43–52
chemical treatment of chromosomes, 45
device fabrication, 41
experimental design, 44–46
human chromosome isolation, 44–45
instrumentation, 46
magnetic beads, 45
magnetic field
chromosome sorting using, 49–50
chromosomes sorted via, distribution ratio, 50
magnets, 45

on-chip chromosome sorter, using magnetic field, 49
voltage modulation, chromosome sorting using, 46–49
voltage modulation technique, on-chip chromosome sorting apparatus using, 46
On-chip chromosome sorter using electric fields, 43–52
chemical treatment of chromosomes, 45
device fabrication, 41
experimental design, 44–46
human chromosome isolation, 44–45
instrumentation, 46
magnetic beads, 45
magnetic field
chromosome sorting using, 49–50
chromosomes sorted via, distribution ratio, 50
magnets, 45
on-chip chromosome sorter, using magnetic field, 49
voltage modulation, chromosome sorting using, 46–49
voltage modulation technique, on-chip chromosome sorting apparatus using, 46

P

Phylogenetic relationships, karyotypes, amniotes, 67
Polyamine method, isolation, human, plant chromosomes as nanomaterials, 158
Polyclonal antibodies against ribosomal protein S6, production, 221–222
Proteins, chromosomal, dynamic, functional analysis, 217–230
chromosome scaffold proteins, methods using, comparison of, 219–220
FtsJ homolog, dynamics of, 224–227
FtsJ homolog 3
function of, 226–227
immunodetection of, 226
localization, chromosomal proteins, 223–224
localization analysis using human fixed cells, chromosome spreads, isolated chromosomes, 218–219
polyclonal antibodies against ribosomal protein S6, production, 221–222
ribosomal protein S6, characterization of antibodies against, 222–223
screening methods, 218–223
Proteome analysis, human metaphase chromosomes, 167–188
chromosomal protein identification, 170–173
isolation, human metaphase chromosomes, 170
isolation methods, chromosome preparation, 171
protein extraction, isolated chromosomes, 171
protein identification, mass spectrometry, 172–173
protein separation, electrophoresis techniques, 171–172
chromosome surface morphology, various isolation methods, 170
comparative proteome analysis, human chromosomes, 173–179
proteins identified from different cell lines, 178–179
proteins identified from isolation methods, 173–178
four-layer model, protein framework of human chromosomes, 180–186
chromosomal proteins, classification, 180–185
localization, chromosomal proteins, 180
higher-order structure of chromosome, 168
historical perspective, 167–168
models, chromosomal higher-order structure, 168–170
scanning electron microscopy, cell cycle model, 169

R

Ribosomal protein S6, characterization of antibodies against, 222–223

S

Salt-dialysis-reconstitution, nucleosomes, 123–124
Scanning electron microscopy, metaphase chromosomes, 97–102
high-resolution scanning electron microscopy of, dried, metal-coated chromosomes, 97–100
low-vacuum scanning electron microscopy, hydrous chromosomes observed by, 100–102
Scanning near-field optical/atomic force microscopy, chromosome topography, gene location, 137–154
chromosome preparation, 139–140

fluorescence *in situ* hybridization, probe, 140–142
barley chromosomes, 140
human chromosomes, 141
image analysis, 141–142
positional analysis, two gene loci, 142
instrumentations, 139–142
multicolor fluorescence *in situ* hybridization detection using scanning near-field optical microscopy/atomic force microscopy, 147–150
single-copy gene detection on human chromosomes using scanning near-field optical microscopy/atomic force microscopy, 145–146
telomere fluorescence *in situ* hybridization signals, scanning near-field optical microscopy/atomic force microscopy, high-resolution detection, 142–145
chromosome preparation for scanning probe microscopy observation, 142–143
detection of telomere fluorescence *in situ* hybridization signals on barley chromosomes, 143–145
Scanning near-field optical microscopy, 246
Scanning probe microscopy, 4–5
evaluation of chromosome elasticity, 7–8
SEM. *See* Scanning electron microscopy
Sequence-specific DNA detection, microchamber array-based, single chromosome via trace volume PCR, 31–42
chromosome-1 using tweezers-type probe, collection, rearrangement, 39
microchamber array, 33
microchamber array, design, fabrication, 32–33
microchamber array PCR amplification, whole human chromosomes, 38
nanoliter dispenser, sample loading into microchamber array, 35
on-chip DNA amplification, single chromosome-1, 40
on-chip quantitation, initial DNA concentration, 35–38
reagents, 33–35
sample preparation, 33–35
specific sequence detection from single human chromosome-1, nanoliter-volume PCR, 38–40
thermal cycling, fluorescence detection, 35
SNOM. *See* Scanning near-field optical microscopy
SPM. *See* Scanning probe microscopy

T

TEM. *See* Transmission electron microscopy
Time-serial optical phase contrast images, unfixed human chromosomes, 11
Transmission electron microscopy, metaphase chromosomes, 94–97
ultrathin sections, 94–95
whole-mount preparation of chromosomes, 96–97
Tweezers atomic force microscopy probe, design, fabrication, 18–20

U

Ultrathin sections, transmission electron microscopy, metaphase chromosomes, 94–95

V

Voltage modulation, chromosome sorting using, 46–49

W

Wet chromosomes, higher-order chromosome structure, atomic force microscopy, 111–113
Whole-mount chromosome preparation, metaphase chromosomes, transmission electron microscopy, 96–97

Z

ZOO-FISH, 69–71. *See also* comparative chromosome painting
identification of chromosomal homology between different species, 69–71

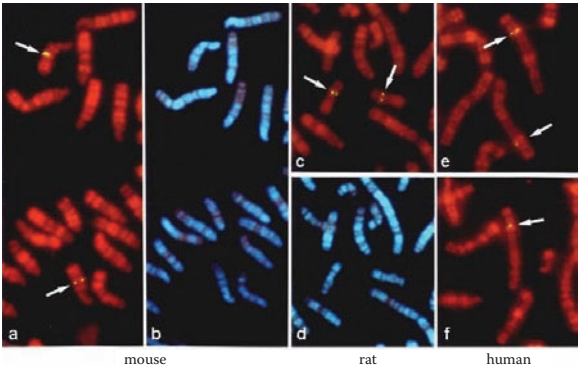

FIGURE 6.1

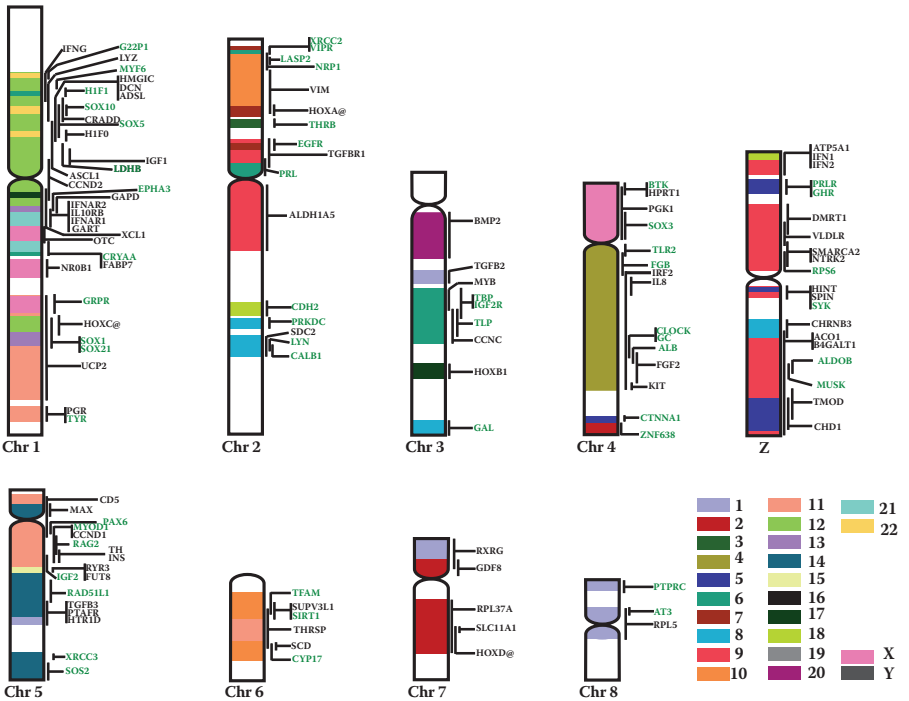

FIGURE 6.2

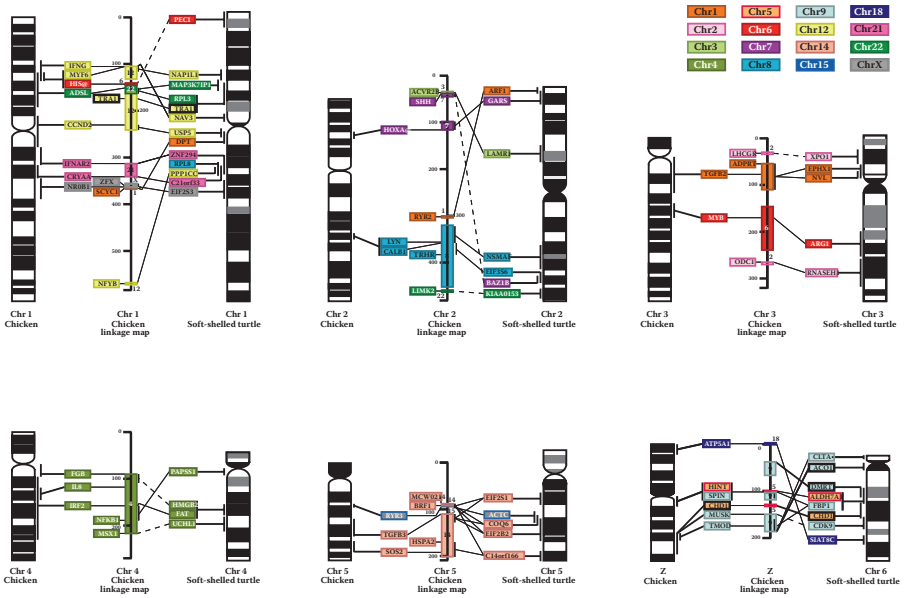

FIGURE 6.4

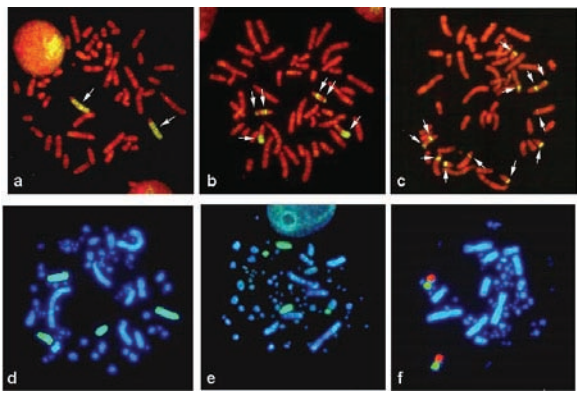

FIGURE 6.5

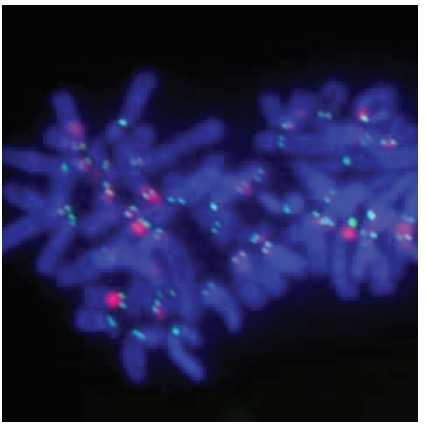

FIGURE 7.2

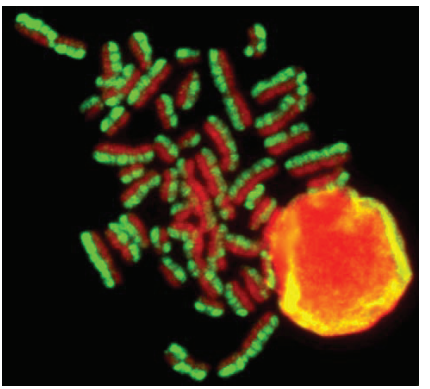

FIGURE 7.3

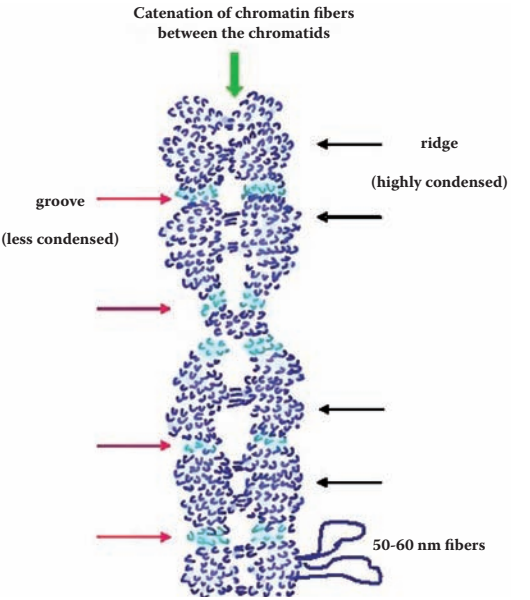

FIGURE 9.6

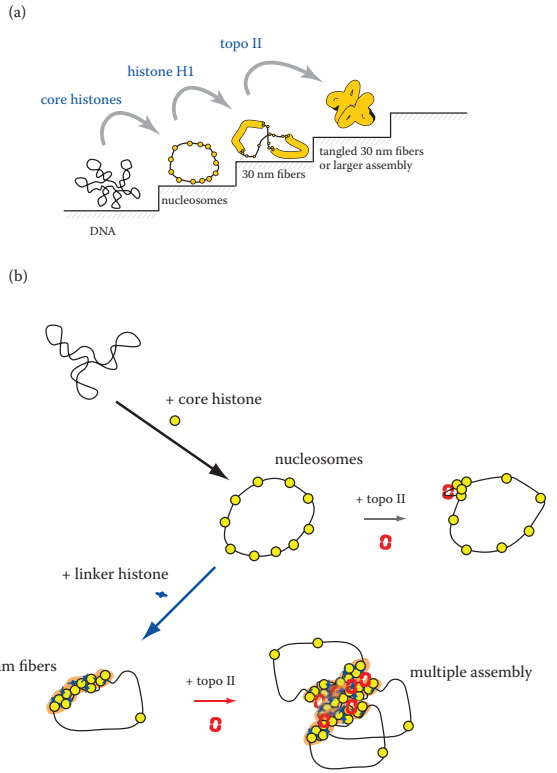

FIGURE 10.7

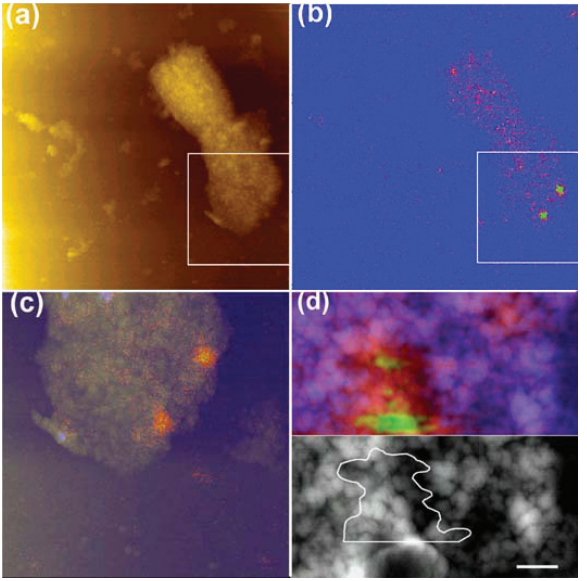

FIGURE 11.4

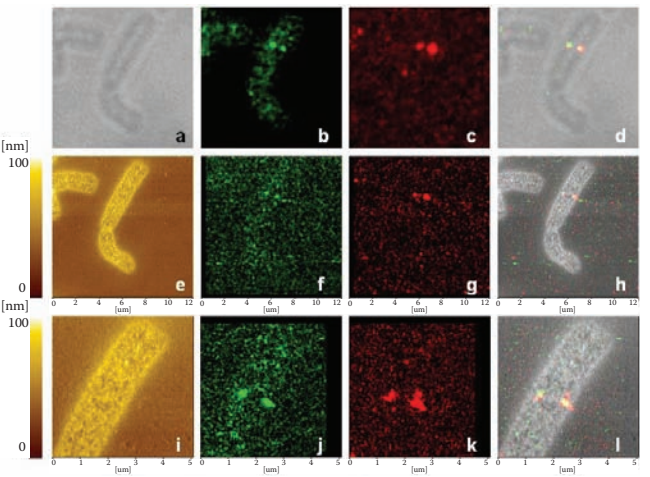

FIGURE 11.6

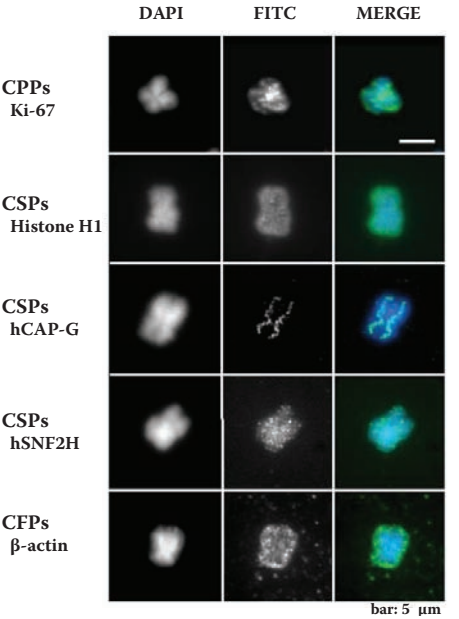

FIGURE 13.9

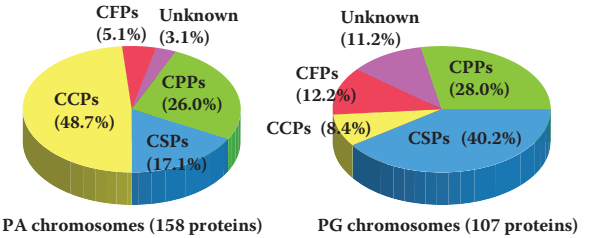

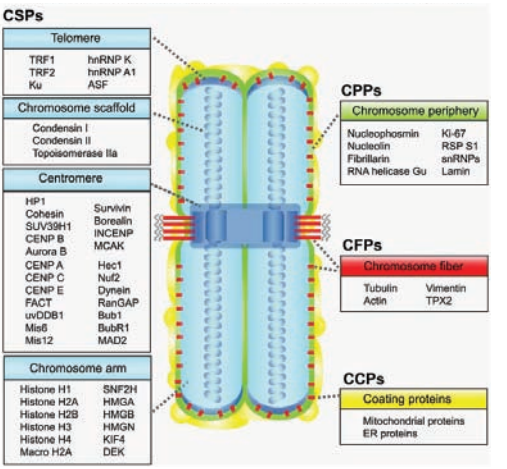

FIGURE 13.10

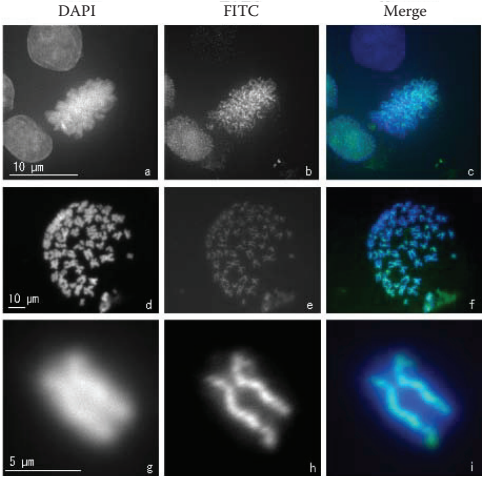

FIGURE 16.1

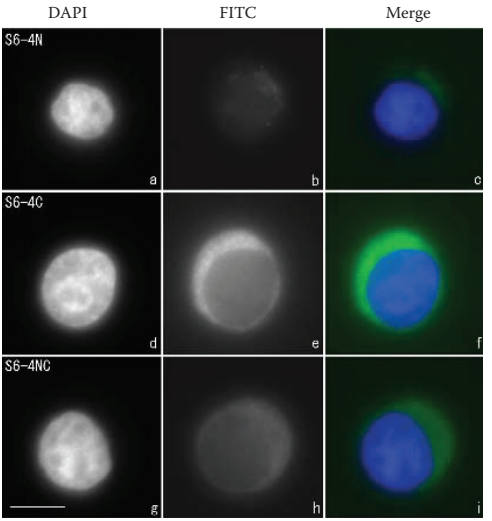

FIGURE 16.2

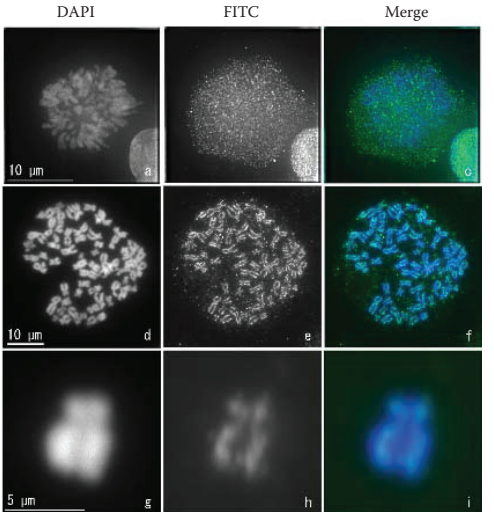

FIGURE 16.3

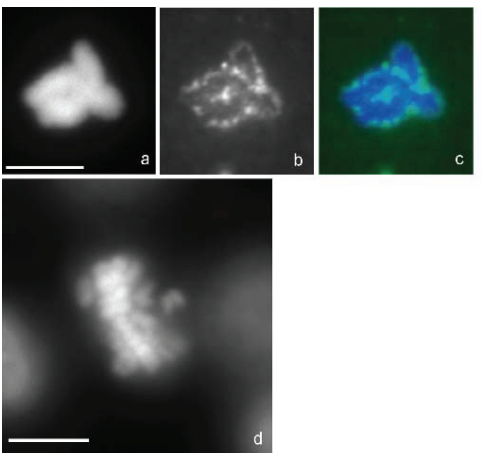

FIGURE 16.5

Chromosome Nanoscience and Technology

COPY TO COME

44915

www.crcpress.com

CRC Press
Taylor & Francis Group
an informa business
www.taylorandfrancisgroup.com

6000 Broken Sound Parkway, NW
Suite 300, Boca Raton, FL 33487
270 Madison Avenue
New York, NY 10016
2 Park Square, Milton Park
Abingdon, Oxon OX14 4RN, UK